Exceptional points in atomic spectra and Bose-Einstein condensates

Von der Fakultät Mathematik und Physik der Universität Stuttgart
zur Erlangung der Würde eines Doktors der Naturwissenschaften
(Dr. rer. nat.) genehmigte Abhandlung

Vorgelegt von

Holger Cartarius

aus Böblingen

Hauptberichter:	Prof. Dr. Jörg Main
Mitberichter:	Prof. Dr. Hans-Rainer Trebin
Tag der mündlichen Prüfung:	8. Dezember 2008

1. Institut für Theoretische Physik der Universität Stuttgart

2008

Inhaltsangabe

„Exceptional points“ oder „Ausnahmepunkte“ stellen eine besondere Art einer Entartung dar. Sie kann bei Resonanzen in parameterabhängigen Quantensystemen, die durch einen nicht-hermiteschen Hamiltonoperator beschrieben werden, auftreten. Ausnahmepunkte sind Orte im Parameterraum, an denen zwei oder sogar mehr Resonanzen eine Verzweigungssingularität durchlaufen. An den kritischen Parameterwerten sind die Energien, die Breiten und die Wellenfunktionen, die die Resonanzen beschreiben, identisch. Die zwei mit der Verzweigung verbundenen Zustände weisen für eine Umrundung der Verzweigungssingularität eine geometrische Phase auf.

In der vorliegenden Arbeit werden Ausnahmepunkte in zwei wichtigen Quantensystemen untersucht. Das erste System ist das Wasserstoffatom in gekreuzten, externen elektrischen und magnetischen Feldern. Es vertritt die Klasse der Atome in statischen äußeren Feldern, die als fundamentale Quantensysteme sowohl experimentell als auch mit theoretischen Methoden zugänglich sind und ideal geeignet sind, um den Einfluss der Ausnahmepunkte zu studieren. Die Resonanzen des Wasserstoffatoms werden numerisch unter Zuhilfenahme der Methode der komplexen Rotation berechnet. Eine Vorgehensweise, Ausnahmepunkte gezielt aufzuspüren, wird ausgearbeitet und die Existenz von Ausnahmepunkten wird nachgewiesen. Der Einfluss der Verzweigungssingularitäten auf die Energien der Resonanzen, die Wellenfunktionen und den Photoionisationswirkungsquerschnitt wird analysiert. Darüber hinaus wird eine Möglichkeit vorgeschlagen, Ausnahmepunkte in einem Experiment mit Atomen in äußeren Feldern zu beobachten.

Die Untersuchung der Resonanzen in Spektren des Wasserstoffatoms, die in dieser Arbeit durchgeführt wird, deckt weiterhin Strukturen auf, die einen Einblick in den Ionisationsmechanismus erlauben. Die Ionisation des Wasserstoffatoms in gekreuzten elektrischen und magnetischen Feldern wurde z.B. unter Anwendung der klassischen Theorie der Übergangszustände untersucht. Die hier vorgestellten Rechnungen zeigen eindeutige Hinweise auf einen wichtigen Einfluss des klassischen Übergangszustands auf Quantenspektren.

Eine zweite Klasse von Quantensystemen, in denen Ausnahmepunkte auftreten, stellen die stationären Zustände von Bose-Einstein-Kondensaten dar. Diese lassen sich durch die nichtlineare Gross-Pitaevskii-Gleichung beschreiben. Es ist bekannt, dass gemeinsam mit dem Grundzustand bei Variation der Systemparameter ein zweiter stationärer Zustand der Gross-Pitaevskii-Gleichung aus einer Tangentenbifurkation heraus entsteht. In der vorliegenden Arbeit wird aufgezeigt, dass die Gesamtenergien, die chemischen Potentiale und die Wellenfunktionen dieser beiden Zustände am Bifurkationspunkt das Verhalten eines Ausnahmepunkts aufweisen. Die Ergebnisse erlauben es, das Konzept des Ausnah-

mepunkts auf nichtlineare Quantensysteme auszuweiten. Zwei Arten von Kondensaten werden zu diesem Zweck untersucht. Bose-Einstein-Kondensate mit einer laserinduzierten, gravitationsartigen $1/r$-Wechselwirkung liefern durch analytisch darstellbare Lösungen einen direkten Beweis für die Existenz der Ausnahmepunkte. Die in diesem System erhaltenen Ergebnisse lassen sich dann nutzen, um Ausnahmepunkte auch im experimentell besonders interessanten und bereits realisierten Fall der Bose-Einstein-Kondensation dipolarer Gase zu identifizieren und zu beschreiben.

Abstract

Exceptional points are a special type of degeneracy which can appear for the resonances of parameter-dependent quantum spectra described by non-Hermitian Hamiltonians. They represent positions in the parameter space at which two or even more resonances pass through a branch point singularity. At the critical parameter values, the energies, the widths, and the wave functions describing the resonances are identical. The branching eigenstates show a geometric phase for a parameter space loop around the branch point.

In this thesis exceptional points are investigated in two important quantum systems. The first system is the hydrogen atom in crossed external electric and magnetic fields. It is a representative for the class of atoms in static external fields, which are as fundamental quantum system accessible both with experimental and theoretical methods and are ideally suited to study the influence of exceptional points. The resonance spectra of the hydrogen atom are numerically calculated with the complex rotation method. A procedure to systematically search for exceptional points is elaborated and the existence of exceptional points is proven. The influence of the branch point singularities on the resonance energies, the wave functions, and the photoionization cross section is analyzed. In addition, a possibility for the observation of exceptional points in an experiment with atoms is proposed.

The investigation of the resonances in spectra of the hydrogen atom in this thesis furthermore reveals structures which can provide an insight into the ionization mechanism. The ionization mechanism of the hydrogen atom in crossed electric and magnetic fields has been investigated, e.g., by application of the transition state theory. Here, calculations are performed which give clear evidence for an important influence of the classical transition state in the quantum spectrum.

A second class of quantum systems in which exceptional points appear are the stationary states of Bose-Einstein condensates. They are described by the nonlinear Gross-Pitaevskii equation and it is known that by a variation of the system's parameters the ground state and a second stationary solution are born together in a tangent bifurcation. It is pointed out in this thesis that the mean field energies, the chemical potentials, and the wave functions show at the point of bifurcation the behavior of an exceptional point. The results allow for the extension of the concept of exceptional points to nonlinear quantum systems. Two types of condensates are investigated for this purpose. Bose-Einstein condensates with a laser-induced gravity-like $1/r$ interaction exhibit analytic solutions which directly prove the existence of exceptional points. The results obtained in this system are used to identify and describe exceptional points in the Bose-Einstein

condensation of dipolar gases which is of high experimental interest and has already been realized.

Contents

List of abbreviations

BEC Bose-Einstein condensate, Bose-Einstein-Kondensat

cf. confer, compare

e.g. for example

EP exceptional point

i.e. that is

IRAM implicitly restarted Arnoldi method

STLM spectral transformation Lanczos method

viz. videlicet, namely

z.B. zum Beispiel

1 Introduction

1.1 Motivation

It is a common fact of quantum systems that above the ionization threshold resonances exist among the continuum of unbound states. Resonances are long-lived or quasi bound states. In the energy spectrum, they are normally described by their shape, their energy (or position), and their width. As for the bound states of a quantum system resonances can also show the effect of a degeneracy, where for a resonance a degeneracy means that the energies and the widths of both states are identical. A special type of such a coalescence, so-called "exceptional points" [1, 2], recently has attracted growing interest theoretically [3–7] as well as experimentally [8–13]. Exceptional points can be found in systems which depend on at least two real valued parameters. They are positions in the parameter space at which (normally) two energy eigenvalues pass through a branch point singularity, i.e., the two eigenvalues can mathematically be described by two branches of the same analytic function and the exceptional point is the branch point singularity. If this is the case, also the eigenvectors (or wave functions) pass through a branch point singularity and, hence, are identical at the exceptional point. Within the framework of the linear Schrödinger equation, the existence of resonances is important for the occurrence of exceptional points because the coalescence of two eigenstates with identical eigenvectors is not possible in the spectra of Hermitian Hamiltonians, which describe bound states. Here, always a set of orthogonal eigenstates, which never can become identical, exists. For resonances, the situation is different. They are not in the Hermitian domain of the Hamilton operator [14] and require a different description. The complex rotation method [14–16] constructs *non*-Hermitian Hamiltonians, in whose spectra resonances are uncovered as complex eigenvalues. For non-Hermitian Hamiltonians a condition which prohibits the coalescence of two eigenvectors does not exist and the occurrence of exceptional points is possible.

The physical meaning of an exceptional point in a quantum system is that two quantum mechanical eigenstates become completely identical at the critical parameter value, i.e., the energies, the widths, and the wave functions are the same for two eigenstates which are different at other parameter values. An important consequence of the existence of exceptional points in quantum systems is the occurrence of geometric phases [17], which are the result of nontrivial topological structures in the parameter space. Geometric phases can be observed if the parameters of the system are varied continuously on a closed curve around the critical value. After the return to the initial parameter

values the physical conditions are the same as in the beginning but the quantum mechanical eigenstates or wave functions can differ in the phase. The geometric phase which appears in connection with exceptional points is rather complicated and deserves a detailed analysis. If an exceptional point is encircled in its parameter space, one of the two eigenfunctions which coalesce at the critical parameter value changes its phase by the value of π and the phase of the other remains unchanged [2].

Physical systems in which exceptional points can appear have to depend on at least a two-dimensional parameter space. Normally, the physical parameters which influence the system are real and, thus, two real parameters are required. If exceptional points shall be observable it must be possible to adjust these parameters in a sufficiently wide range of the parameter space. Furthermore, the complex energy eigenvalues, typically the positions (frequencies or energies) and widths of resonances, must be accessible with a high precision. Examples are discussed, e.g., for complex atoms in laser fields [18], a double δ well [19], the scattering of a beam of particles by a double barrier potential [20], or models used in nuclear physics [21]. Furthermore, the resonant behavior of atom waves in optical lattices [22] shows structures of exceptional points [5]. But the phenomenon of exceptional points in physics is not restricted to quantum mechanics. Acoustic modes in absorptive media [23] represent a mechanical system, in which branch point singularities appear. The occurrence of coalescing modes in the light propagation in absorptive media [24, 25] and branch points in $\mathcal{PT}$-symmetric waveguides [7] are manifestations of the same effect. The most detailed experimental analysis of exceptional points has been done for the resonances of microwave cavities [8, 10, 12], which open the possibility to study the properties of the complex resonance frequencies and the wave functions. In particular, the geometric phase has been demonstrated experimentally [9, 11].

Despite the broad variety of physical systems in which exceptional points have been verified, up to now they have not been found in atoms in static external fields. The main reason is that there is only one parameter in the cases studied most intensely, viz. atoms either in an electric *or* in a magnetic field. For the occurrence of exceptional points, the parameter space has to be at least two-dimensional, i.e., at least two real parameters are required, which can be represented by crossed electric *and* magnetic fields. Atoms in static external electric and magnetic fields are fundamental physical systems. As real quantum systems they are accessible both with experimental and theoretical methods and have, e.g., very successfully been used for comparisons with semiclassical theories [26–29]. The occurrence of phenomena like Ericson fluctuations in photoionization spectra has been demonstrated both in numerical studies [30, 31] and experiments [32]. Therefore, atoms in external fields are ideally suited to study the influence of exceptional points on quantum systems.

In this thesis, the resonances of the hydrogen atom in static electric and magnetic fields are investigated numerically and the first detection of exceptional points in this system is reported. The confirmation of the existence of exceptional points supplements the richness of phenomena which have been found in the spectra of atoms in static external fields. Furthermore, a method which can be used to verify the existence of exceptional

points in experiments with atoms is proposed.

The resonances of the hydrogen atom in external fields reveal a further phenomenon of the ionization mechanism. A classical description of this process is provided by the transition state theory [33–36], which uses the classical electron motion near the Stark saddle point, in whose vicinity the transition state is located, to distinguish between ionizing and non-ionizing situations. It will be shown in this thesis that the classical electron motion near the transition state described with a power series expansion of the potential [37] leads to clear signatures in quantum resonance spectra.

The calculation of resonance spectra of the hydrogen atom in crossed electric and magnetic fields requires the diagonalization of large matrices. Due to the application of the complex rotation method these matrices are non-Hermitian but complex symmetric. While for real symmetric and Hermitian matrices effective numerical algorithms exist, this is not the case for complex symmetric eigenvalue problems. However, it is conceivable that algorithms for real symmetric problems can be extended to the complex symmetric case. It is one purpose of this thesis to fathom the possibilities to perform such extensions.

While the main focus in the investigation of exceptional points so far has been on open, linear quantum systems, it is possible to extend the concept to nonlinear quantum systems. In particular, it is a known property of the nonlinear Gross-Pitaevskii equation [38, 39] describing Bose-Einstein condensates that stationary solutions exist only in certain regions of the parameter space governing the physics of the condensates. Normally, in all types of Bose-Einstein condensates, the s-wave scattering length and the number of particles belong to the parameters, and for the case of an attractive s-wave contact interaction it was theoretically predicted (see, e.g., [40–42]), and experimentally confirmed, that the condensate collapses when, for given negative scattering length, the number of particles becomes too large [43–45] or the s-wave scattering length is tuned below a critical value [46] via Feshbach resonances. Stationary solutions exist only above the critical value of the scattering length. At that critical value not one but *two* stationary solutions are born in a tangent bifurcation [47, 48]. It can be shown that the point of bifurcation corresponds to an exceptional point, where the eigenenergies as well as the wave functions are identical and pass through a branch point singularity and, thus, can be understood as a "nonlinear version" of an exceptional point.

Quite recently it was proven [49, 50] that a similar bifurcation behavior persists in Bose-Einstein condensates where, in addition to the short-range (van der Waals-like) interaction a long-range "gravity-like," attractive $1/r$ interaction is present [51]. There, too, the ground state and a second, excited, state of the condensate are born in a tangent bifurcation, when crossing the borderlines in the parameter space spanned by particle number, scattering length and trap frequency. The system stands out due to the possibility of a self-trapped condensate, i.e., a stable condensate without external harmonic trap. In the case of self-trapping, the investigation of exceptional points is especially suitable because simple approximate analytic solutions exist, which directly reveal the branch point singularity structure, i.e., it can be shown analytically that the

nonlinear extended Gross-Pitaevskii equation exhibits exceptional points.

In contrast to "monopolar" condensates, where the experimental realization has not been achieved yet, dipolar Bose-Einstein condensates [52–57] are of high experimental interest. In particular, the achievement of Bose-Einstein condensation in a gas of chromium atoms [58], with a large dipole moment, has opened the way to promising experiments on dipolar quantum gases [59, 60]. For example, the experimental observation of the dipolar collapse of a quantum gas, which means the experimental realization of a nonlinear quantum system close to an exceptional point, has been reported [61, 62]. With the experience gained in the consideration of "monopolar" condensates it is straightforward to search for exceptional points in the Bose-Einstein condensation of dipolar gases. The appearance of a long-range interaction alongside the short-range contact interaction is similar to the gravity-like "monopolar" case.

1.2 Outline

Chapter 2 gives an introduction to the basic concepts of exceptional points. Branch point singularities are considered and their appearance in parameter dependent eigenvalue problems are discussed. The properties of the eigenvalues which pass through a branch point singularity at an exceptional point are pointed out, the geometric phase connected with exceptional points is presented, and the occurrence of chiral states is mentioned. All aspects are demonstrated with a simple two-dimensional matrix model and some results obtained in experiments with microwave cavities are cited. A brief introduction to the complex rotation method used for the calculation of the resonances of the hydrogen atom is given in chapter 3. The use of complex scaled variables and their influence on the energy spectrum are discussed as well as the need to take special care of complex scaled variables in inner products of vectors. Chapter 4 is devoted to large scale eigenvalue problems. The possibility to perform extensions of algorithms for real symmetric matrices to complex symmetric problems is discussed for direct approaches as well as for iterative methods used in particular for the diagonalization of large matrices with several thousand basis states. After the fundamental concepts have been covered in the previous chapters, chapter 5 presents the verification of exceptional points in spectra of the hydrogen atom. It is shown how it is possible to detect exceptional points in numerical calculations by exploiting their properties and examples for exceptional points are presented. In addition, a proposal for an experiment with atoms capable to confirm exceptional points is given. The properties of exceptional points in spectra of atoms are analyzed in chapter 6. In particular, the local structure of the energy eigenvalues near the branch point singularities, and the paths of the complex energies for variations of the external fields are discussed. Furthermore, the connection with avoided level crossings, the geometric phase of the wave functions, and the influence of exceptional points on dipole matrix elements and the photoionization cross section are investigated. Chapter 7 highlights the influence of the classical transition state on atomic spectra and analyzes

the existence of signatures of the classical electron motion near the transition state on exact quantum resonances. The concept of exceptional points is generalized to nonlinear quantum systems in chapter 8, where the Gross-Pitaevskii equation for Bose-Einstein condensates with attractive $1/r$ interaction is investigated. Here, it is shown that the bifurcation point of the system corresponds to a "nonlinear version" of an exceptional point both with a variational approach and numerically exact wave functions. The properties of exceptional points in the nonlinear system and the stability properties of the two condensate wave functions emerging at the branch point are elaborated in detail. In chapter 9 the methods developed in the previous chapter are extended to investigate the experimentally relevant case of dipolar Bose-Einstein condensates. Conclusions are drawn in chapter 10.

2 Exceptional points

The term "exceptional point" is used in literature for the occurrence of branch point singularities in the eigenspectra of linear maps [1] and has been extended to the discussion of coalescing eigenstates in physical quantum systems [2]. In this chapter exceptional points are introduced and their properties are discussed.

First, a description of branch point singularities is given in section 2.1. Then their influence on the eigenspectra of linear maps is described in section 2.2 and a brief discussion of a simple example is added in section 2.3. Afterwards two of the consequences of exceptional points in quantum systems, viz. the occurrence of geometric phases and chiral states are discussed in section 2.4 and section 2.5, respectively. The last section of this chapter covers a brief comparison of exceptional and diabolical points.

2.1 Branch point singularities

It is a common fact of analytic functions that one can distinguish between single-valued and multiple-valued functions [63]. For example, one can consider an analytic function $f(z)$ which depends on one complex variable z. It is called a *single-valued* function if its behavior at any particular point z_0 is independent of the path one chooses to reach the point in an analytic continuation. There is only one function value at the point z_0. This attribute does not exist for *multiple-valued* functions, for which different analytic continuations used to reach a point z_0 may result in different function values at the point z_0. The function has several "branches" with different function values. Furthermore it can happen that the same point may be regular in one continuation and singular in the other. For multiple-valued functions it is important to distinguish between the various function values. In particular, for the description of physical problems with multiple-valued functions, an identification of the correct answer to the question is crucial.

The conventional method to bring order in the multiple branches of solutions of a function is the application of Riemann surfaces. Exceptional points are typically square root branch points. Roots $\sqrt[n]{z}$ of higher orders n can also appear but follow the same mechanisms. Hence, the discussion of the Riemann surface of the square root is the best starting point to consider the properties of exceptional points.

In general, Riemann surfaces can be constructed with the following method [63]. In the vicinity of a point z_1 in a certain region of the complex plain the multiple-valued analytic function $F(z)$ is expressed as a power series around z_1. The expansion with its radius of convergence defines a "functional element" and describes one part of the function

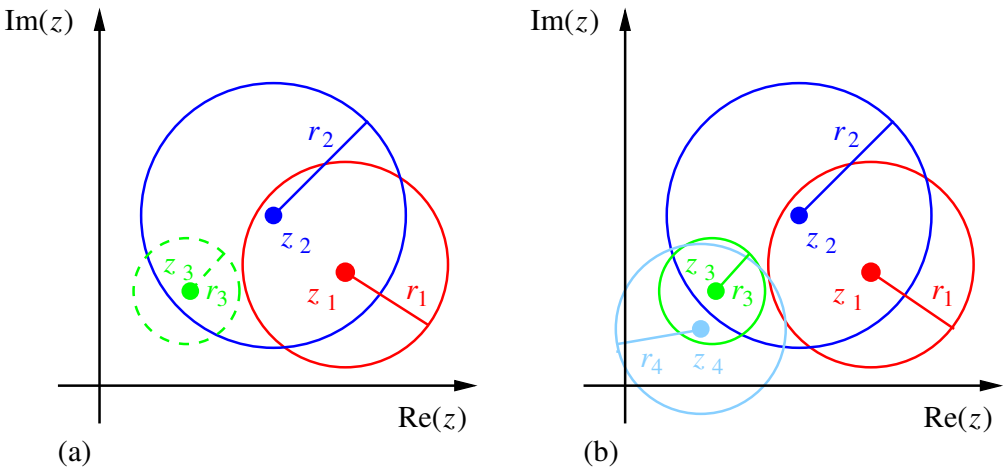

Figure 2.1: Construction of a Riemann surface with power series expansions. (a) If the areas within the radii of convergence of the different expansions are pasted together such that identical points are bearers of the same function value in each expansion, one gets a unique representation of one branch of a multiple-valued function. (b) The fourth circle intersects with all preceding circles.

$F(z)$ on one branch. The points within the circle of convergence are bearers of one unique function value because the branch of the multiple-valued function is determined by the expansion coefficients chosen. The first functional element can now be continued by a second one which consists of a second power series around a point z_2 of the first continuation. It has its own radius of convergence (see figure 2.1(a)). The two parts are pasted together such that they are bearers of the same unique function values in the overlap region. The procedure can be continued with further power series in the same manner and one gets a covering of the z-plane similar to the one shown in figure 2.1(a) where only unique function values of one branch appear. If after repeated application of the continuation a new functional element represented by its circle of convergence intersects with one of the former disks which is not its direct predecessor (see, e.g., figure 2.1 (b)), two possible situations can appear. The first possibility is that the new and the old disk can be bearers of the same function value. In this case the new circle can be considered as a part of the single-valued continuation and can be pasted together with the former ones. In the second possible case the continuation of the functional elements with the method described above leads to different function values on the "old" and the "new" disk. Now, the two overlapping disks are not pasted together. They represent two different sheets of which each bears one of the multiple function values at the same points z. On each sheet the function values are unique. Note that the borders between different sheets are not defined absolutely. They depend on the initial point z_1 that was chosen for the first power series expansion.

The square root of z, $f(z) = \sqrt{z}$ has two function values for every $z \neq 0$ and can

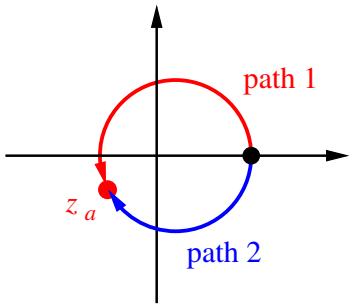

Figure 2.2: Two possible paths for the analytic continuation starting at a point on the axis of positive reals with the end point z_a.

be considered as the simplest multiple-valued function. With the procedure described above, the Riemann surfaces can be constructed by starting at a point on the axis of positive reals. Then the entire complex plane can be covered with subsequent continuations of the first expansion if the axis of negative reals is avoided. The result is one of the two sheets which bears unique function values, i.e., it represents one branch of the two solutions. If, for example, the border given by the axis of negative reals is traversed during a complex continuation as depicted in figure 2.2 (path 1), the point z_a bears a different function value as after the continuation which does no cross the border (path 2). The two function values differ by the factor of $\mathrm{e}^{\frac{1}{2}\cdot 2\mathrm{i}\pi} = -1$. The second sheet which bears the function values of the second branch, i.e., the function values of the first branch with opposite sign, covers the complex plane a second time. However, the point $z = 0$ has to be excluded because it has only one function value. Figure 2.3(a) shows both sheets marked by red and green surfaces connected at a border. In the example used here, this border was introduced as the axis of negative reals, however as denoted above depending on the first covering of the complex plane, whose starting point can be chosen arbitrarily, other locations of the border are possible. Again, one can proceed the analytic continuation of the power series expansions (now on the second sheet) such that the axis of negative reals is crossed, which corresponds to the open boundary in the upper sheet in figure 2.3(a). The results are values which are multiplied with an additional factor of -1 and, therefore, are identical with those on the first sheet. Thus, both sheets are not only connected at the dashed line of figure 2.3(a), but a second connection between the two open boundaries has to be done by penetrating the intermediate sheet. Figure 2.3(b) shows the result of the completed landscape of the two Riemann surfaces of $f(z) = \sqrt{z}$.

Branch point singularities are points at which two or more branches coalesce, that is, the function values of the different branches have the same value. At the branch points the different sheets, which bear the unique function values of one branch, are connected. As mentioned above, the function $f(z) = \sqrt{z}$ has only one function value at $z = 0$ and this point, indeed, is a branch point. Here, the upper and the lower sheet of the

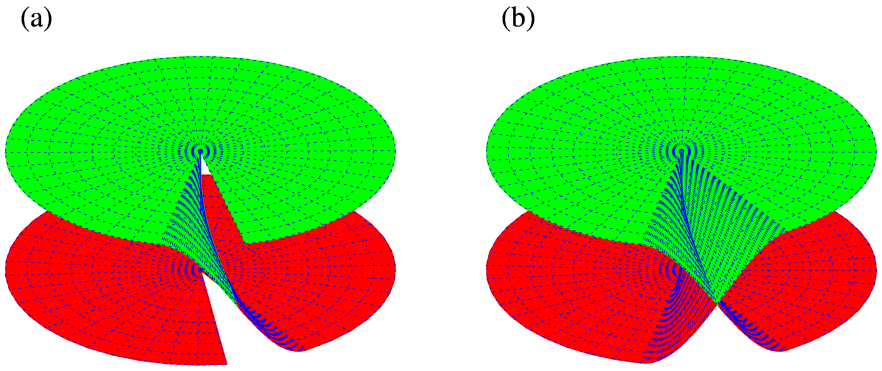

Figure 2.3: Construction of the Riemann surface for the function $f(z) = \sqrt{z}$. (a) An analytic continuation shows that two sheets whose function values differ by a factor of $e^{\frac{1}{2}\cdot 2i\pi} = -1$ exist. Starting at the first sheet (marked by the red surface) one crosses the border to the second sheet (green surface) when the point $z = 0$ is encircled. (b) A second circle around $z = 0$ leads back to the first sheet (cf. reference [64]).

representation displayed in figure 2.3(b) are connected.

2.2 Appearance and properties of exceptional points

The term "exceptional" points is used for branch points which appear in eigensystems that depend on a parameter [1]. For example, let the linear map $\boldsymbol{y} = \boldsymbol{T}(\kappa)\boldsymbol{x}$ represented by a matrix $\boldsymbol{T}(\kappa)$ depend holomorphically on a scalar complex parameter κ in a domain D_0 of the complex plane. The eigenvalues λ of $\boldsymbol{T}(\kappa)$ satisfy the characteristic equation

$$\det\left(\boldsymbol{T}(\kappa) - \lambda\mathbf{1}\right) = 0\,, \tag{2.1}$$

which is an algebraic equation whose degree is identical with the dimension of the vector space and whose coefficients are holomorphic in κ. In the complex domain D_0 the solutions λ are analytic functions of κ or branches of analytic functions which have only algebraic singularities [63].

If two (or more) eigenvalues belong to two (or more) branches of the same analytic function, exceptional points can appear. Exceptional points are the branch point singularities of the analytic functions. They appear at isolated points in the two-dimensional parameter space of the scalar complex parameter κ. The name exceptional points has its origin in the fact that the number of different eigenvalues s of the linear map $\boldsymbol{T}(\kappa)$ is normally a constant s_0 and is independent of the parameter κ with the exception of

some special points, at which two (or more) eigenvalues are identical and the number s of *different* eigenvalues is less than s_0 [1][1].

The branch point singularity structure of the exceptional points leads to important consequences for the associated eigenvalues and eigenvectors.

1. If one encircles the exceptional point in the parameter space, a permutation of the eigenvalues can be observed [1]. Generalized one can trace the path of the eigenvalues for a closed curve in the parameter space, which encircles the exceptional point in a domain of the parameter space including a small disk around the exceptional point but excluding the branch point $\kappa = \kappa^{(\mathrm{EP})}$. Then one observes groups of eigenvalues

$$\{\lambda_1(\kappa), \ldots, \lambda_p(\kappa)\}, \quad \{\lambda_{p+1}(\kappa), \ldots, \lambda_{p+q}(\kappa)\}, \quad \ldots \tag{2.2}$$

   in such a way that each group undergoes a cyclic permutation by a revolution of the parameter κ. In the most common case in physical systems where two eigenvalues form a square root branch point singularity, there is one group of two permuting eigenvalues and all further eigenvalues do not undergo a permutation. The two eigenvalues which represent the two branches of one analytic function with the singularity at $\kappa = \kappa^{(\mathrm{EP})}$ are interchanged after the circle around the exceptional point. This can directly be seen in figure 2.3(b). Starting at an arbitrarily chosen parameter value κ_0 one crosses the border between both sheets exactly one time for one turn around $\kappa^{(\mathrm{EP})} = 0$ and an analytic continuation of the eigenvalue $\lambda_1(\kappa_0)$ ends at the starting point of the second $\lambda_2(\kappa_0)$.

2. For $\kappa \neq \kappa^{(\mathrm{EP})}$ the eigenvalues belonging to the exceptional points are different and each of them belongs to a distinct eigenvector. Accordingly these eigenvectors undergo the same permutation as the eigenvalues, and, at the exceptional points they likewise pass through a branch point singularity [1]. Note that this means that there is only one linearly independent eigenvector for the two degenerate eigenvalues. At an exceptional point, the dimension of the space of eigenvectors is less than its dimension in the rest of the parameter space (without further exceptional points which may exist). In the matrix, the eigenvalues and eigenvectors form a normal block [65, 66]. This is a further important property of exceptional points, which distinguishes them from "normal" degeneracies where two eigenvalues belonging to two different analytic functions have the same value.

[1] It should be mentioned that the original definition of an exceptional point by Kato [1] includes all possibilities at which two eigenvalues are identical and the number s of *different* eigenvalues is less than the constant value s_0. Next to the branch point singularities, at which this is always the case, e.g., two different single-valued analytic functions with each of them describing an eigenvalue may become identical at an isolated point in the parameter space. Following Kato these points are also called "exceptional points". However, in the context of resonances in physical systems, the term "exceptional points" is *exclusively* used for *branch point singularities* of two (or more) eigenvalues (see, e.g., the introductions of [4, 9, 65]).

3. Connected with the permutation of the eigenvectors is the appearance of a geometric phase. In the most common physical situation of a square root branch point resulting from a complex symmetric matrix, the geometric phase becomes manifest in the change of sign of one of the two eigenvectors [2] and can be written in the form
$$[\boldsymbol{x}_1, \boldsymbol{x}_2] \overset{\text{circle}}{\longrightarrow} [\boldsymbol{x}_2, -\boldsymbol{x}_1] \,, \tag{2.3}$$
where $\boldsymbol{x}_1$ and $\boldsymbol{x}_2$ are the eigenvectors permuted during the loop around the exceptional point. A more detailed description of the geometric phase is given in section 2.4.

Up to now exceptional points were only considered in two-dimensional parameter spaces, but the effect is not restricted to two dimensions. In higher-dimensional parameter spaces of complex matrices, an exceptional "point" is always an object of codimension 2 [66]. That is, in two dimensions an exceptional point, indeed, appears as a point, whereas it is a one-dimensional object (or line) in three dimensions and has the form of a two-dimensional "exceptional surface" in a four-dimensional parameter space.

2.3 A simple example in a non-Hermitian linear map

One of the most simple examples in which an exceptional point occurs in linear maps is described by the two-dimensional matrix [1]
$$\boldsymbol{M}(\kappa) = \begin{pmatrix} 1 & \kappa \\ \kappa & -1 \end{pmatrix} \tag{2.4}$$
with the complex parameter κ. The two eigenvalues of the matrix are given by
$$\lambda_1 = \sqrt{1+\kappa^2} \,, \tag{2.5a}$$
$$\lambda_2 = -\sqrt{1+\kappa^2} \tag{2.5b}$$
and are obviously two branches of the same analytic function in κ. There are two exceptional points in the system, which appear at the complex conjugate values $\kappa_\pm = \pm\mathrm{i}$ as can be seen immediately. The eigenvectors, which belong to the two eigenvalues are
$$\boldsymbol{x}_1(\kappa) = \begin{pmatrix} -\kappa \\ 1-\sqrt{1+\kappa^2} \end{pmatrix} \,, \tag{2.6a}$$
$$\boldsymbol{x}_2(\kappa) = \begin{pmatrix} -\kappa \\ 1+\sqrt{1+\kappa^2} \end{pmatrix} \,. \tag{2.6b}$$
They also depend on the parameter κ and pass through a branch point singularity at the exceptional points $\kappa_\pm = \pm\mathrm{i}$, where the only linearly independent eigenvector reads
$$\boldsymbol{x}(\pm\mathrm{i}) = \begin{pmatrix} \mp\mathrm{i} \\ 1 \end{pmatrix} \,. \tag{2.7}$$

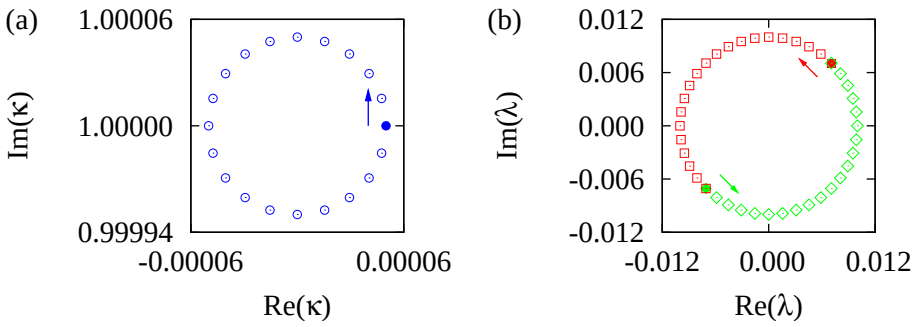

Figure 2.4: (a) Circle in the parameter space κ with the exceptional point $\kappa_+ = \mathrm{i}$ as center point for the simple model (2.4). (b) Eigenvalues $\lambda_{1,2}$ calculated for the parameter values from (a) indicated by red squares and green diamonds, respectively. In this case each of the two eigenvalues traverses a semicircle. In (a) and (b) the filled symbols represent the first parameter value κ_0 and the corresponding eigenvalues $\lambda_{1,2}(\kappa_0)$, respectively. The arrows point in the direction of progression.

The branch point singularity leads to a characteristic behavior of the corresponding eigenvalues under changes of the parameters. If one chooses a closed loop in the parameter space and calculates the eigenvalues for a set of parameters on this loop, the permutation of the eigenvalues can be seen by plotting the paths of the two eigenvalues in the complex energy plane. Such a situation is displayed in figure 2.4. Here, one circle

$$\kappa(\varphi) = \mathrm{i} + \varrho \mathrm{e}^{\mathrm{i}\varphi} \tag{2.8}$$

around the singularity $\kappa_+ = \mathrm{i}$ is passed in the parameter space, which is shown in figure 2.4(a). After one revolution, the first eigenvalue, which is marked by red squares, will travel to the starting point of the second one marked by green diamonds and vice versa. As a consequence, the path of one eigenvalue is not closed if one traversal of the loop in parameter space is performed. But the path is closed if the parameter space loop is traversed twice. Of course, for the simple model it is also possible to demonstrate the half circle structure analytically. If the parameter space curve (2.8) is applied to the eigenvalues (2.5a) and (2.5b) one obtains for $\varrho \ll 2$ the expansion

$$\lambda_{1,2} = \pm\sqrt{1 + (\mathrm{i} + \varrho \mathrm{e}^{\mathrm{i}\varphi})^2} = \pm\sqrt{\varrho}\mathrm{e}^{\mathrm{i}\varphi/2}\sqrt{2\mathrm{i} + \varrho \mathrm{e}^{\mathrm{i}\varphi}} \approx \pm\sqrt{2\varrho}\mathrm{e}^{\mathrm{i}\pi/4}\mathrm{e}^{\mathrm{i}\varphi/2} \tag{2.9}$$

or

$$\lambda_1 = \sqrt{2\varrho}\mathrm{e}^{\mathrm{i}(\pi/4+\varphi/2)}\,, \tag{2.10a}$$

$$\lambda_2 = \sqrt{2\varrho}\mathrm{e}^{\mathrm{i}(5\pi/4+\varphi/2)}\,, \tag{2.10b}$$

which reproduces the half circles shown in figure 2.4 for a full parameter space loop $\varphi = 0 \ldots 2\pi$ correctly.

2.4 Geometric phases of exceptional points

2.4.1 Geometric phases in quantum systems

If the Hamiltonian of a quantum system depends on a set of parameters, e.g., represented by the vector $\boldsymbol{\kappa}$, and the parameters are changed adiabatically, the stationary states will, at any instance during the change, be in an eigenstate of the Hamiltonian $H(\boldsymbol{\kappa})$. After a closed loop is traversed the original state will be restored up to a phase factor. In this case, a circuit-dependent component $\mathrm{e}^{\mathrm{i}\xi}$ is accumulated in addition to the familiar time-dependent part $\mathrm{e}^{-\mathrm{i}Et/\hbar}$ as was demonstrated and calculated by Berry [17]. A special case of the geometric phase is the sign change of an eigenstate for a loop around a conical intersection [67].

In his treatment of the geometric phase Berry [17] considered its appearance in Hermitian quantum systems. Here, the time evolution of a state initially prepared in the $\boldsymbol{\kappa}$-dependent stationary eigenstate $|\psi_n(\boldsymbol{\kappa})\rangle$ has the form

$$|\psi(t)\rangle = \exp\left\{-\frac{\mathrm{i}}{\hbar}\int_0^t \mathrm{d}t'\, E_n(\boldsymbol{\kappa}(t')) + \mathrm{i}\beta_n(t)\right\}|\psi_n(\boldsymbol{\kappa}(t))\rangle \ , \tag{2.11}$$

where the parameter $\boldsymbol{\kappa}$ is changed with time. Additional to the familiar dynamical phase factor

$$\exp\left\{-\frac{\mathrm{i}}{\hbar}\int_0^t \mathrm{d}t'\, E_n(\boldsymbol{\kappa}(t'))\right\} \ ,$$

the geometric phase $\beta_n(t)$ is taken into account. The requirement that $|\psi(t)\rangle$ satisfies the Schrödinger equation yields

$$\dot{\beta}_n(t) = \mathrm{i}\langle\psi_n(\boldsymbol{\kappa}(t))|\nabla_{\boldsymbol{\kappa}}\psi_n(\boldsymbol{\kappa}(t))\rangle \cdot \dot{\boldsymbol{\kappa}}(t) \ , \tag{2.12}$$

which determines $\beta_n(t)$. After a closed loop C of $\boldsymbol{\kappa}$, the complete phase change of the state $|\psi(t)\rangle$ can be expressed with

$$|\psi(T)\rangle = \exp\{\mathrm{i}\beta_n(C)\}\exp\left\{-\frac{\mathrm{i}}{\hbar}\int_0^T \mathrm{d}t'\, E_n((\boldsymbol{\kappa}(t'))\right\}|\psi(0)\rangle \tag{2.13}$$

and the geometric phase

$$\beta_n(C) = \mathrm{i}\oint_C \langle\psi_n(\boldsymbol{\kappa})|\nabla_{\boldsymbol{\kappa}}\psi_n(\boldsymbol{\kappa})\rangle \cdot \mathrm{d}\boldsymbol{\kappa} \ . \tag{2.14}$$

The case of an Hermitian Hamiltonian discussed above is very descriptive but needs some extensions for non-Hermitian systems [68], which are of essential interest for the discussion of exceptional points. In this case, one has to take into account both the right hand $|\psi_n\rangle$ and the left hand eigenvectors $\langle\tilde{\psi}_m|$, which form a complete bi-orthonormal set with

$$\langle\tilde{\psi}_m|\psi_n\rangle = \delta_{mn} \ . \tag{2.15}$$

The time evolution of the right hand and left hand states is now determined by the two time-dependent Schrödinger equations

$$\mathrm{i}\hbar\frac{\partial}{\partial t}|\psi\rangle = H(t)|\psi\rangle \;, \tag{2.16a}$$

$$\mathrm{i}\hbar\frac{\partial}{\partial t}|\tilde{\psi}\rangle = H^{+}(t)|\tilde{\psi}\rangle \;, \tag{2.16b}$$

respectively and yields the conserved inner product

$$\langle\tilde{\psi}(t)|\psi(t)\rangle = \langle\tilde{\psi}(0)|\psi(0)\rangle \;. \tag{2.17}$$

When the evolution equations (2.16a) and (2.16b) are combined with the bi-orthogonality properties (2.15), the phase change of a state initially prepared in the right hand eigenstate $|\psi_n\rangle$ has the form (2.13) already obtained in the Hermitian case but with the different geometric phase term

$$\beta_n(C) = \mathrm{i}\oint_C \langle\tilde{\psi}_n(\boldsymbol{\kappa})|\nabla_{\boldsymbol{\kappa}}\psi_n(\boldsymbol{\kappa})\rangle\cdot\mathrm{d}\boldsymbol{\kappa} \tag{2.18}$$

instead of the Hermitian result (2.14). That is, the geometric phase also depends on the left hand eigenvector $\langle\tilde{\psi}_n(\boldsymbol{\kappa})|$.

2.4.2 Geometric phases at branch point singularities

Since the eigenstates are permuted for a loop around an exceptional point, the relation (2.13) is not reasonable for a single loop. There are two approaches used to discuss the geometric phases appearing in connection with exceptional points. On the one hand it is possible to use the relation (2.13) for a twofold circle around the exceptional point. After the second circle both eigenstates differ only in a phase factor from their initial values and the relation (2.13) is applicable. On the other hand one can take into account the permutation and investigate the relation of the first eigenstate $|\psi_1(T)\rangle$ after one circle around the degeneracy with the original value $|\psi_2(0)\rangle$ of the second state and vice versa.

The evaluation of the integral (2.18) for a double circle, which was performed by Mailybaev et al. [69] can be used to calculate the geometric phase in different cases. In particular, this is possible for exceptional points which appear in matrices beyond two dimensions, a case which is important to take into account because of couplings of many quantum states typically appearing in physical Hamiltonians. For the evaluation the norm $\langle\tilde{\psi}_n(\boldsymbol{\kappa})|\psi_n(\boldsymbol{\kappa})\rangle$ which was assumed to be unity in equation (2.18) is explicitly written in the extended geometric phase integral (2.18) for a twofold loop, viz.

$$\beta_n^{(2)}(C) = \beta_{n+1}^{(2)}(C) = \mathrm{i}\oint_{2C}\frac{\langle\tilde{\psi}_n(\boldsymbol{\kappa})|\mathrm{d}\psi_n(\boldsymbol{\kappa})\rangle}{\langle\tilde{\psi}_n(\boldsymbol{\kappa})|\psi_n(\boldsymbol{\kappa})\rangle} \;. \tag{2.19}$$

Note that due to the permutation of the eigenstates the geometric phases $\beta_n(C)$ and $\beta_{n+1}(C)$ of both eigenstates involved must be identical for a double cycle. The superscript (2) indicates the two turns around the exceptional point. In the case of a complex symmetric Hamiltonian the left hand and right hand eigenvectors are complex conjugate, i.e., $\langle\tilde{\psi}_n(\boldsymbol{\kappa})| = \langle\psi_n^*(\boldsymbol{\kappa})|$ and the integral can be brought in the form

$$\beta_n^{(2)}(C) = \beta_{n+1}^{(2)}(C) = \frac{\mathrm{i}}{2}\oint_{2C} \mathrm{d}\ln\left(\langle\psi_n^*(\boldsymbol{\kappa})|\psi_n(\boldsymbol{\kappa})\rangle\right) \ , \tag{2.20}$$

which demonstrates that the value of the integral only depends on the number of turns made by the integral kernel around the branch point of the complex logarithm at the exceptional point. According to the calculation by Mailybaev et al. [69] there is, for the path $2C$, exactly one turn around the branch point independently of the number of dimensions of the Hamiltonian matrix. Hence, the complex logarithm function changes by $\pm 2\pi\mathrm{i}$ and the geometric phase term is $\beta_n^{(2)}(C) = \pm\pi$. Since the geometric phase has its origin in the degeneracies it is zero if the exceptional point is not located within the area enclosed by the path of integration. However, it does not depend on the explicit choice of the shape of the path and, therefore, it belongs to the so called topological phases like Berry's phase which appears for a turn around a conical intersection. A phase factor of $e^{\pm\pi\mathrm{i}}$ means that after two circles around the exceptional point passed adiabatically both eigenstates have changed their sign. The result can be formulated by

$$[\psi_n, \psi_{n+1}] \overset{2 \text{ circles}}{\rightarrow} [-\psi_n, -\psi_{n+1}] \ . \tag{2.21}$$

A similar procedure for non-symmetric complex matrix representations of the Hamiltonian shows that deviations from the geometric phase $\pm\pi$ may appear. In particular, the geometric phase $\beta_n^{(2)} = \beta_{n+1}^{(2)}$ can be determined with the calculation of [69]

$$\beta_n^{(2)} = \beta_{n+1}^{(2)} = \pm\pi + \mathrm{i}\oint_C \left(\langle\tilde{\psi}_0(\boldsymbol{\kappa})|\mathrm{d}\psi_1(\boldsymbol{\kappa})\rangle + \langle\tilde{\psi}_1(\boldsymbol{\kappa})|\mathrm{d}\psi_0(\boldsymbol{\kappa})\rangle\right) \ . \tag{2.22}$$

In this expression, $\psi_0(\boldsymbol{\kappa})$ and $\psi_1(\boldsymbol{\kappa})$ represent two vectors which span the $\boldsymbol{\kappa}$-dependent linear invariant subspace of the two eigenvectors belonging to the branching solutions. The integral expression in equation (2.22) describes the deviation from the geometric phase $\pm\pi$ appearing in the case of complex symmetric matrices. As can be shown [69] this integral vanishes for 2×2 matrices and the geometric phase does not differ from the symmetric case.[2] However, for higher-dimensional systems the integral is in general nonzero. An approximation for a small loop

$$C = \left\{\boldsymbol{\kappa}(t) = \boldsymbol{\kappa}^{(\mathrm{EP})} + \epsilon\hat{\boldsymbol{\kappa}}(t) \mid 0 \leq t \leq T\right\} \tag{2.23}$$

[2]Note that the geometric phase $\pm\pi$ for a two-dimensional non-symmetric matrix is not a topological property. As was recently discussed [70], this result depends on the choice to go two times along the *same* path around the exceptional point, which was assumed for the derivation of equation (2.22). If any other path $\tilde{C}$ which encircles the exceptional point twice is used, the geometric phase is sensitive to its shape even for a 2×2 matrix.

around the exceptional point $\boldsymbol{\kappa}^{(\mathrm{EP})}$ leads to the result

$$\beta_n^{(2)} = \beta_{n+1}^{(2)} = \pm\pi + \mathrm{i}a\epsilon^2 + \mathrm{O}(\epsilon^3) \,, \tag{2.24}$$

where the correction term a depends on the information about the system at the exceptional point including the eigenvectors and the first derivatives of the Hamiltonian with respect to the parameter $\boldsymbol{\kappa}$ as well as on the shape of the loop $\hat{\boldsymbol{\kappa}}(t)$. It can be written in the form [69]

$$\begin{aligned} a = \sum_{k\neq n,n+1} \oint_C \Bigg(& 2\frac{\langle\tilde{\psi}_0^{(\mathrm{EP})}|H_1|\psi_k^{(\mathrm{EP})}\rangle\langle\tilde{\psi}_k^{(\mathrm{EP})}|\mathrm{d}H_1|\psi_0^{(\mathrm{EP})}\rangle}{(E_k^{(\mathrm{EP})} - E_n^{(\mathrm{EP})})^3} \\ & + \frac{\langle\tilde{\psi}_1^{(\mathrm{EP})}|H_1|\psi_k^{(\mathrm{EP})}\rangle\langle\tilde{\psi}_k^{(\mathrm{EP})}|\mathrm{d}H_1|\psi_0^{(\mathrm{EP})}\rangle}{(E_k^{(\mathrm{EP})} - E_n^{(\mathrm{EP})})^2} + \frac{\langle\tilde{\psi}_0^{(\mathrm{EP})}|H_1|\psi_k^{(\mathrm{EP})}\rangle\langle\tilde{\psi}_k^{(\mathrm{EP})}|\mathrm{d}H_1|\psi_1^{(\mathrm{EP})}\rangle}{(E_k^{(\mathrm{EP})} - E_n^{(\mathrm{EP})})^2} \Bigg) \,, \end{aligned} \tag{2.25}$$

where the derivatives

$$H_1 = \sum_{j=1}^{m} \frac{\partial H}{\partial \kappa_j}\kappa_j \,, \tag{2.26a}$$

$$\mathrm{d}H_1 = \sum_{j=1}^{m} \frac{\partial H}{\partial \kappa_j}\mathrm{d}\kappa_j \tag{2.26b}$$

with respect to the m parameters appear and the superscript (EP) always indicates that the quantities are taken at the exceptional point $\boldsymbol{\kappa}^{(\mathrm{EP})}$. Equation (2.25) shows that the deviation of the geometric phase from $\pm\pi$ is due to the influence of the energy levels $k \neq n, n+1$ not involved in the degeneracy.

2.4.3 Direct determination of the geometric phase for complex symmetric matrices

For complex symmetric matrices the geometric phase can be revealed and observed by continuously tracking the eigenvectors during the parameter space path around the exceptional point. This is possible if the eigenvectors are chosen such that the orthogonality relation (2.15) is fulfilled for all parameter values $\boldsymbol{\kappa}$ on the circle, where the right hand and left hand eigenvectors are complex conjugate, i.e.,

$$\langle\psi_n^*|\psi_m\rangle = \delta_{mn} \,. \tag{2.27}$$

This was discussed for the most general form of a two-dimensional matrix of the type $H_0 + \kappa H_1$ with real H_0 and H_1 and a complex parameter κ by Heiss [2]. An especially descriptive illustration is possible for a small circle around one of the exceptional points in

the simple model introduced in section 2.2, whose appropriately normalized eigenvectors can be obtained from equations (2.6a), (2.6b) and read

$$\boldsymbol{x}_1(\kappa) = \frac{1}{\sqrt{\kappa^2 + \left(1 - \sqrt{1+\kappa^2}\right)^2}} \begin{pmatrix} -\kappa \\ 1 - \sqrt{1+\kappa^2} \end{pmatrix} , \tag{2.28a}$$

$$\boldsymbol{x}_2(\kappa) = \frac{1}{\sqrt{\kappa^2 + \left(1 + \sqrt{1+\kappa^2}\right)^2}} \begin{pmatrix} -\kappa \\ 1 + \sqrt{1+\kappa^2} \end{pmatrix} . \tag{2.28b}$$

For a small circle around the exceptional point at $\kappa_+ = \mathrm{i}$, i.e.,

$$\kappa(\varphi) = \mathrm{i} + \varrho \mathrm{e}^{\mathrm{i}\varphi} , \tag{2.8}$$

only the leading order of a fractional power series expansion in $\varrho^{1/4}$ is important. In this approximation the vectors can be written in the form

$$\boldsymbol{x}_1(\varphi) = 2^{-3/4}\varrho^{-1/4} \begin{pmatrix} e^{\mathrm{i}7\pi/8} e^{-\mathrm{i}\varphi/4} \\ e^{\mathrm{i}11\pi/8} e^{-\mathrm{i}\varphi/4} \end{pmatrix} , \qquad \boldsymbol{x}_2(\varphi) = 2^{-3/4}\varrho^{-1/4} \begin{pmatrix} e^{\mathrm{i}11\pi/8} e^{-\mathrm{i}\varphi/4} \\ e^{\mathrm{i}15\pi/8} e^{-\mathrm{i}\varphi/4} \end{pmatrix} . \tag{2.29}$$

Now the analytic continuation of the eigenvectors for one full circle, i.e., $\varphi = 0 \ldots 2\pi$ leads to the phase behavior,

$$\boldsymbol{x}_1(0) = 2^{-3/4}\varrho^{-1/4} \begin{pmatrix} e^{\mathrm{i}7\pi/8} \\ e^{\mathrm{i}11\pi/8} \end{pmatrix} \quad \longrightarrow \quad \boldsymbol{x}_1(2\pi) = 2^{-3/4}\varrho^{-1/4} \begin{pmatrix} e^{\mathrm{i}3\pi/8} \\ e^{\mathrm{i}7\pi/8} \end{pmatrix} = -\boldsymbol{x}_2(0) , \tag{2.30a}$$

$$\boldsymbol{x}_2(0) = 2^{-3/4}\varrho^{-1/4} \begin{pmatrix} e^{\mathrm{i}11\pi/8} \\ e^{\mathrm{i}15\pi/8} \end{pmatrix} \quad \longrightarrow \quad \boldsymbol{x}_2(2\pi) = 2^{-3/4}\varrho^{-1/4} \begin{pmatrix} e^{\mathrm{i}7\pi/8} \\ e^{\mathrm{i}11\pi/8} \end{pmatrix} = \boldsymbol{x}_1(0) . \tag{2.30b}$$

The typical notion used for this consequence of the geometric phase is the expression

$$[\boldsymbol{x}_1, \boldsymbol{x}_2] \overset{\text{circle}}{\rightarrow} [-\boldsymbol{x}_2, \boldsymbol{x}_1] \qquad \text{or} \qquad [\psi_1, \psi_2] \overset{\text{circle}}{\rightarrow} [-\psi_2, \psi_1] , \tag{2.31}$$

which includes both the permutation during the traversal of a single closed loop around the exceptional point and the phase change of one of the eigenvectors. This phase change continues with every additional loop. After the second revolution both eigenvectors have changed their sign and the double revolution of the exceptional point reproduces the geometric phase result of equation (2.21). Thus, the method described here offers a further possibility to determine the geometric phase in the case of complex symmetric matrices. The behavior in equations (2.30a) and (2.30b) also reveals the structure that the normalized eigenvectors pass through a fourth root branch point [2] at the exceptional point, whereas the eigenvalues are the two branches of a square root function. Four circles are required to restore the original situation $[\boldsymbol{x}_1, \boldsymbol{x}_2]$ or $[\psi_1, \psi_2]$.

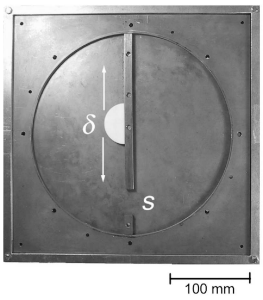

Figure 2.5: Photograph of the microwave cavity used in the experiments by Dembowski et al. (taken from refrence [11]). The geometry consists of two semicircles. Two parameters are introduced by the position δ of a Teflon stub and the opening s of the slit, which influence the positions and widths of the resonances.

The method described here contains one considerable advantage for the determination of the geometric phase in numerical simulations. The adiabatic change of the parameter is not essential. The phase can be determined by varying the parameter in small steps and considering the eigenvectors normalized accordingly to equation (2.27). If one pays attention to the continuity of the phase, the behavior (2.31) can directly be observed and an explicit calculation of the geometric phase integral (2.20) is not required.

A similar correspondence can be found for two-dimensional non-symmetric matrices if the eigenvectors are normalized according to the bi-orthonormal relation (2.15) instead of equation (2.27). However, as was mentioned in section 2.4.2 the behavior of the geometric phase is much more complicated in this case.

2.4.4 Experimental studies in microwave cavities

The most systematic experimental investigation of exceptional points was performed for the resonances of microwave cavities [8–12]. Here, flat microwave cavities are used as a model for two-dimensional quantum systems. Due to the mathematical equivalence of the Helmholtz equation of electrodynamics with the two-dimensional Schrödinger equation for a particle in a box with infinitely high walls, microwave cavities are a common model used to simulate quantum systems [71]. The electric field distribution is analogous to the wave function and the eigenenergies are represented by the frequencies. The experiments are very illustrative and, therefore, shall be recapitulated briefly. In particular, the measurement of the field distribution allows for the reconstruction of the wave functions, which opens the possibility to investigate the phase behavior of the two coupled resonances in the vicinity of the exceptional point.

The experiments accomplished by Dembowski et al. [9–11] allow for the observation of two resonances near an exceptional point, which are well separated in frequency from other eigenmodes and can be described with a two-level model. A microwave cavity which consisted of two semicircular parts was used. The geometry can be seen in the

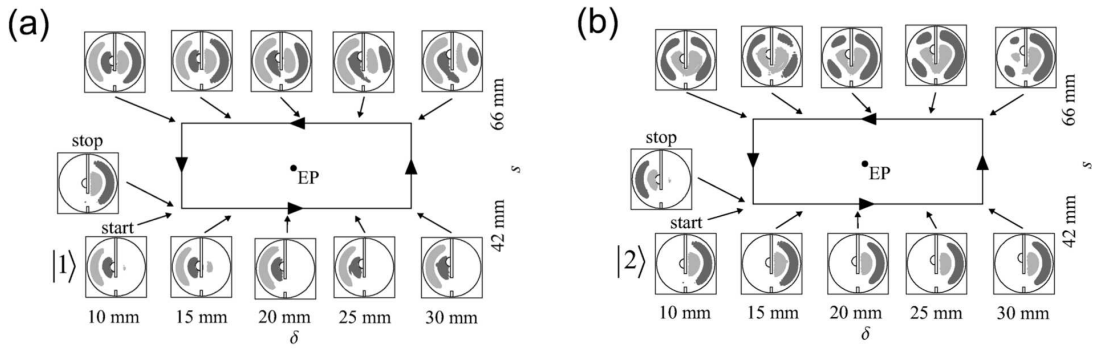

Figure 2.6: The reconstructed electrical field distributions of two resonances associated with the exceptional point are shown in figures (a) and (b) (taken from reference [11]). They demonstrate the behavior of the wave functions. For each resonance the nodal lines are followed from a "start" configuration to a "stop" value of the parameters chosen on a closed path around the exceptional point. An observation of the wave functions leads to the result that the first wave function in (a) develops after the loop into the initial field distribution of the second one. (b) The second wave function develops into the negative of the first, and thus proves experimentally the existence of the geometric phase expected at an exceptional point.

photograph in figure 2.5. A Teflon stub, whose position δ can be changed, and a slit with variable opening s are used to influence the resonances. The (real) variables δ and s span the two-dimensional parameter space required for the investigation of exceptional points and, with a subsequent change of δ and s, a circle around the degeneracy can be traversed. The sign change of the wave functions cannot be observed directly because only the squared field distributions are accessible in the measurements. To reconstruct the phase relations, the nodal lines of the wave functions are followed for small changes of the parameters and the development of the signs, which are arbitrarily chosen in the beginning, is observed. Figure 2.6(a) shows the evolution of the first wave function ψ_1 which develops after a full loop around the exceptional point into the second one ψ_2, whereas figure 2.6(b) demonstrates that the wave function ψ_2 evolves into a field distribution which is the negative of the first wave function. This behavior proves experimentally the existence of the sign change of *one* of the wave functions, which is the result expected for the geometric phase of an exceptional point. It can be written in the form

$$[\psi_1, \psi_2] \overset{\text{circle}}{\rightarrow} [\psi_2, -\psi_1] \,, \tag{2.32}$$

and is equivalent to the one given in equation (2.31).

2.5 Chiral states

In systems that can be described by a complex symmetric matrix or a complex symmetric matrix representation of an Hamiltonian the eigenfunctions of the coalescing states show an additional feature directly at the exceptional point, viz. they specify a chirality [72]. As is stated above, the two eigenstates fulfill the orthogonality relation

$$\langle \psi_n^* | \psi_m \rangle = \delta_{mn} \ . \tag{2.27}$$

At the exceptional point both states have to be identical and orthogonal simultaneously. With a short calculation it can be shown immediately that for a two-dimensional matrix the non-normalized eigenstates must have the form

$$|\psi^{(\mathrm{EP})}\rangle = |\psi_1(\boldsymbol{\kappa}^{(\mathrm{EP})})\rangle = |\psi_2(\boldsymbol{\kappa}^{(\mathrm{EP})})\rangle \propto \begin{pmatrix} \pm \mathrm{i} \\ 1 \end{pmatrix} , \tag{2.33}$$

which is true for any particular basis since the vector is invariant under all transformations which conserve the complex symmetry of the Hamiltonian [72]. However, one of the two possibilities for the wave function $|\psi^{(\mathrm{EP})}\rangle$ at the exceptional point cannot be transferred into the other and, hence, the wave function is either proportional to $(+\mathrm{i}, 1)$ or to $(-\mathrm{i}, 1)$. In a quantum system, the two possible superpositions of the two basis states

$$|\psi^{(\mathrm{EP})}\rangle = |\psi_2\rangle \pm \mathrm{i}|\psi_1\rangle \tag{2.34}$$

represent solutions rotating either clockwise or counterclockwise because each of them is oscillating in time with the same frequency (due to the degeneracy) and they follow each other with a phase difference of either $\Delta\phi = +\pi/2$ or $\Delta\phi = -\pi/2$. This is the typical manifestation of chirality. The sign of the chirality is unambiguously defined by the positive direction of time, which is clearly given by the decay of the resonances.

Again an experimental verification in microwave cavities was performed and directly demonstrated the existence of the chirality in real physical systems [10]. The phase difference between two modes which were excited via two antennas in a cavity with a geometry similar to the one shown in figure 2.5 was measured. The microwave signal was fed into the antennas with a fixed frequency but controllable phase shift. For appropriately chosen parameters defining the exceptional point, a clear identification of a chirality of the superimposed eigenstates was observed.

The considerations done in this section are not restricted to two-dimensional systems. The generalization to higher-dimensional systems is also possible and can be expressed with the expansion coefficients $c_k(\kappa)$ of the vector

$$|\psi^{(\mathrm{EP})}\rangle = \sum_k c_k(\boldsymbol{\kappa}) |\psi_k(\boldsymbol{\kappa})\rangle \tag{2.35a}$$

where

$$c_k(\boldsymbol{\kappa}) = \langle \tilde{\psi}_k(\boldsymbol{\kappa}) | \psi^{(\mathrm{EP})}\rangle \tag{2.35b}$$

and $\langle\tilde{\psi}_k(\boldsymbol{\kappa})|$ are the left hand eigenvectors which are normalized such that they form a basis which fulfills the bi-orthogonality relation (2.15) for $\boldsymbol{\kappa} \neq \boldsymbol{\kappa}^{(\mathrm{EP})}$. Let c_1 and c_2 be the coefficients which belong to the branching states. Then, the ratio c_1/c_2 is either $c_1/c_2 = +\mathrm{i}$ or $c_1/c_2 = -\mathrm{i}$ and, thus, each exceptional point is associated with a chirality [72] even if it is embedded in a higher-dimensional matrix.

2.6 Diabolical points

Diabolical points [67, 73] are degeneracies between two energy levels of a real symmetric (or in an extension Hermitian) parameter-dependent Hamiltonian. They have some similar properties as exceptional points and are sometimes confused with the branch point singularities of non-Hermitian Hamiltonians. In this section diabolical points are introduced and their differences to exceptional points are pointed out.

If a system depends on a set of parameters $\boldsymbol{\kappa}$, degeneracies can be systematically searched and adjusted with appropriately chosen parameter values $\boldsymbol{\kappa}^{(\mathrm{d})}$. For example, let the two eigenstates $|\psi_1^{(\mathrm{d})}\rangle$ and $|\psi_2^{(\mathrm{d})}\rangle$ be two degenerate eigenvalues with [73]

$$H(\boldsymbol{\kappa}^{(\mathrm{d})})|\psi_1^{(\mathrm{d})}\rangle = E^{(\mathrm{d})}|\psi_1^{(\mathrm{d})}\rangle\,, \qquad H(\boldsymbol{\kappa}^{(\mathrm{d})})|\psi_2^{(\mathrm{d})}\rangle = E^{(\mathrm{d})}|\psi_2^{(\mathrm{d})}\rangle\,. \tag{2.36}$$

Near the degeneracy $\boldsymbol{\kappa}^{(\mathrm{d})}$, the difference of the energies

$$\Delta E(\boldsymbol{\kappa}) = \sqrt{\left[H_{11}(\boldsymbol{\kappa}) - H_{22}(\boldsymbol{\kappa})\right]^2 + 4|H_{12}(\boldsymbol{\kappa})|^2} \tag{2.37}$$

depends to lowest order in $\boldsymbol{\kappa} - \boldsymbol{\kappa}^{(\mathrm{d})}$ on the matrix elements

$$H_{ij}(\boldsymbol{\kappa}) = \langle\psi_i^{(\mathrm{d})}|H(\boldsymbol{\kappa}) - H(\boldsymbol{\kappa}^{(\mathrm{d})})|\psi_j^{(\mathrm{d})}\rangle\,. \tag{2.38}$$

The requirement for a degeneracy of a real Hamiltonian is

$$H_{11}(\boldsymbol{\kappa}^{(\mathrm{d})}) = H_{22}(\boldsymbol{\kappa}^{(\mathrm{d})})\,, \qquad H_{12}(\boldsymbol{\kappa}^{(\mathrm{d})}) = 0 \tag{2.39}$$

and at least two parameters are needed to satisfy them. Because of the two conditions the degeneracies in real symmetric Hamiltonians have co-dimension two. For exactly two parameters they are isolated points. In an $M > 2$-dimensional parameter space they describe an $M-2$-dimensional manifold.

The term diabolical point has its origin in the form of the energy surfaces in the space spanned by the energy difference ΔE and the two parameters κ_1 and κ_2 of the system. Close to the degeneracy the matrix elements H_{ij} depend linearly on the components of $\boldsymbol{\kappa} - \boldsymbol{\kappa}^{(\mathrm{d})}$ and according to equation (2.37) the energy separation will have the from

$$\Delta E(\boldsymbol{\kappa}) = \sqrt{A\left(\kappa_1 - \kappa_1^{(\mathrm{d})}\right)^2 + B\left(\kappa_2 - \kappa_2^{(\mathrm{d})}\right)^2 + C\left(\kappa_1 - \kappa_1^{(\mathrm{d})}\right)\left(\kappa_2 - \kappa_2^{(\mathrm{d})}\right)}\,, \tag{2.40}$$

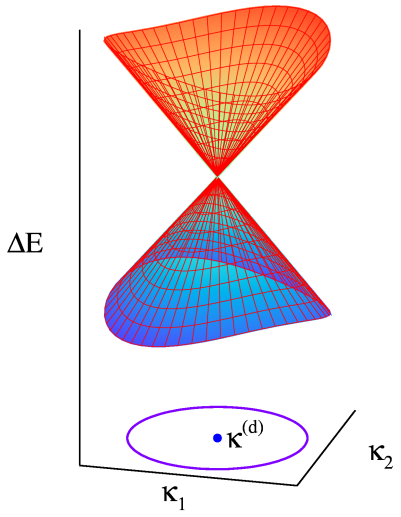

Figure 2.7: Conical intersection of a real symmetric Hamiltonian depending on the two parameters κ_1 and κ_2 according to equation (2.40). The blue circle marks a closed loop in the parameter space around the diabolical point $\boldsymbol{\kappa}^{(\mathrm{d})}$.

where the quadratic form is positive definite and A, B, and C depend on $\nabla\boldsymbol{\kappa}|_{\boldsymbol{\kappa}=\boldsymbol{\kappa}^{(\mathrm{d})}}$. Equation (2.40) represents a double cone and leads to the commonly used expression of a "conical intersection" or a "diabolical point". An illustration of the conical structure is given in figure 2.7. For a path in the parameter space around diabolical points a geometric phase factor occurs. Each of the two states involved in the degeneracy experiences a sign change. As was already pointed out by Longuet-Higgins [74] this sign change is a test for diabolical points of real symmetric Hamiltonians. It appears if and only if the parameter space curve encloses an odd number of diabolical points.

The most important difference between exceptional points and diabolical points is that diabolical points are degeneracies of real symmetric or Hermitian Hamiltonians whereas exceptional points are branch point singularities of non-Hermitian Hamiltonians. There are some important consequences.

- At a diabolical point the eigenvectors of the degenerate states are always orthogonal contrary to exceptional points at which a coalescence of the eigenvectors occurs.

- For a parameter space loop around an exceptional point a permutation of the branching eigenvalues is observed. Such a behavior does not appear at diabolical points.

- The geometric phase which appears in connection with an exceptional point, where one of the two eigenstates interchanged alters its sign, is different from the geometric phase of an diabolical point, where *both* associated eigenstates change their sign for a *single* loop around the degeneracy.

For Hermitian Hamiltonians the condition $H_{12}(\boldsymbol{\kappa}^{(\mathrm{d})}) = 0$ in equation (2.39) splits into its real and imaginary part, viz.

$$\mathrm{Re}(H_{12}(\boldsymbol{\kappa}^{(\mathrm{d})})) = 0 \,, \qquad \mathrm{Im}(H_{12}(\boldsymbol{\kappa}^{(\mathrm{d})})) = 0 \,. \tag{2.41}$$

Thus, compared with the real case one additional condition must be fulfilled and a diabolical point of Hermitian Hamiltonians has co-dimension three. The structure is extended to a hyperbolical intersection in a four-dimensional space spanned by ΔE, κ_1, κ_2, and κ_3. Here also a geometric phase is involved for closed paths in the parameter space. Since the diabolical points are of co-dimension three, the phase factor (2.18) must be explicitly evaluated with equation (2.14). As was demonstrated by Berry [73] for a three-dimensional parameter space the geometric phase is determined by the flux of a vector field

$$V_n(\boldsymbol{\kappa}) = \mathrm{Im}\left(\sum_{m \neq n} \frac{\langle \psi_n(\boldsymbol{\kappa}) | \nabla_{\boldsymbol{\kappa}} H(\boldsymbol{\kappa}) | \psi_m(\boldsymbol{\kappa}) \rangle \times \langle \psi_m(\boldsymbol{\kappa}) | \nabla_{\boldsymbol{\kappa}} H(\boldsymbol{\kappa}) | \psi_n(\boldsymbol{\kappa}) \rangle}{[E_m(\boldsymbol{\kappa}) - E_n(\boldsymbol{\kappa})]^2} \right) \,, \tag{2.42}$$

which is obviously singular at the points of degeneracy, through any surface bounded by the parameter space loop.

3 Complex rotation

A crucial step for the investigation of exceptional points in quantum resonance spectra is the calculation of the resonances. It is the purpose of this chapter to connect the resonances with complex energies and to present a method to calculate them.

The time evolution of resonances of open quantum systems, i.e., decaying unbound states with a lifetime can – in a simple approach – be described by a wave function [75]

$$\psi(t) = \mathrm{e}^{-\mathrm{i}\tilde{E}t/\hbar}\psi(0) \;, \tag{3.1a}$$

whose complex energy eigenvalue

$$\tilde{E} = E - \mathrm{i}\Gamma/2 \tag{3.1b}$$

can be divided into a real part $E = \mathrm{Re}(\tilde{E})$ which represents the energy and a decay rate or width given by the imaginary part $\mathrm{Im}(\tilde{E}) = -\Gamma/2$. However, complex energies cannot appear as eigenvalues of a Hamiltonian which is normally Hermitian since Hermitian operators have always real eigenvalues. The complex rotation method is one possible technique to uncover the complex energies (3.1b). One of its major purposes is to construct the non-Hermitian operators which include the resonance eigenvalues. Further names which have been used for the complex rotation are "complex coordinate-rotation", "complex coordinates", "complex scaling", "dilation analyticity" [15]. Here a summary of the results and consequences of the method is presented. Further details and a description of the rigorous theory can be found in review articles by Reinhardt [15], Ho [16], Moiseyev [14], and the references therein.

In section 3.1 the complex scaling is introduced with a method to perform the transformation of the Hamiltonian and the wave functions. The influence of the scaling on the energy spectrum and the exposure of resonances is discussed in section 3.2. For the scaled eigenstates special care has to be taken of the correct calculation of inner products, which is mentioned in section 3.3. The direct method used usually in numerical determinations by means of matrix diagonalizations is introduced in section 3.4. The chapter ends with a short discussion of the connection of the complex energy eigenvalues with the poles of the scattering matrix in section 3.5 and the manifestations of exceptional points in resonance spectra in section 3.6.

3.1 Introduction of complex scaled wave functions and operators

The complex scaling can be introduced with a unitary operator $U(\theta)$, which acts on the wave functions and the Hamiltonian of the system,

$$(U(\theta)HU^{-1}(\theta))(U(\theta)\psi_n) = E_n(U(\theta)\psi_n)\ . \tag{3.2}$$

Several forms of similarity transformations have been used to produce the complex rotated Schrödinger equations. A discussion of some possibilities can be found in reference [14]. For the discussion required here, one can concentrate on an operator with the action

$$U(\theta)\psi(\boldsymbol{r}) = \mathrm{e}^{\mathrm{i}3\theta/2}\psi(\boldsymbol{r}\mathrm{e}^{\mathrm{i}\theta}) \tag{3.3a}$$

on the wave function and

$$\bar{H}(\theta) = (U(\theta)HU^{-1}(\theta)) = -\frac{1}{2}\mathrm{e}^{-2\mathrm{i}\theta}\Delta + V(\boldsymbol{r}\mathrm{e}^{\mathrm{i}\theta}) \tag{3.3b}$$

on the Hamilton operator. In principle, it performs the complex rotation or complex scaling

$$\boldsymbol{r} \to \mathrm{e}^{\mathrm{i}\theta}\boldsymbol{r} \tag{3.4}$$

on all occurrences of the relative coordinate $\boldsymbol{r}$ in the wave function and the Hamiltonian. The equations (3.3a) and (3.3b) are presented for a two-body Hamiltonian. An extension for a N-body system is done by the application of the complex scaling for all independent center of mass coordinates $\boldsymbol{r}_i$.

A considerable advantage of the representation of the complex rotation in the form (3.3a) and (3.3b) is the close relation with the integration variable in the evaluation of energy expectation values. For example, in the case of a radially symmetric normalized wave function which is the solution of a Hamilton operator with a radially symmetric potential $V(r)$, the energy expectation value has the form

$$\langle E\rangle = \int_0^\infty R(r)\left(-\frac{1}{2}\frac{1}{r^2}\frac{\mathrm{d}}{\mathrm{d}r}r^2\frac{\mathrm{d}}{\mathrm{d}r} + V(r)\right)R(r)\,r^2\mathrm{d}r \tag{3.5}$$

and the complex rotation (3.3a) and (3.3b) leads to the integral

$$\begin{aligned}\langle E\rangle &= \int_0^\infty \mathrm{e}^{\mathrm{i}3\theta/2}R(\mathrm{e}^{\mathrm{i}\theta}r)\left(-\frac{1}{2}\mathrm{e}^{-2\mathrm{i}\theta}\frac{1}{r^2}\frac{\mathrm{d}}{\mathrm{d}r}r^2\frac{\mathrm{d}}{\mathrm{d}r} + V(\mathrm{e}^{\mathrm{i}\theta}r)\right)\mathrm{e}^{\mathrm{i}3\theta/2}R(\mathrm{e}^{\mathrm{i}\theta}r)\,r^2\mathrm{d}r \\ &= \int_0^\infty R(\mathrm{e}^{\mathrm{i}\theta}r)\left(-\frac{1}{2}\frac{1}{(\mathrm{e}^{\mathrm{i}\theta}r)^2}\frac{\mathrm{d}}{\mathrm{d}(\mathrm{e}^{\mathrm{i}\theta}r)}(\mathrm{e}^{\mathrm{i}\theta}r)^2\frac{\mathrm{d}}{\mathrm{d}(\mathrm{e}^{\mathrm{i}\theta}r)} + V(\mathrm{e}^{\mathrm{i}\theta}r)\right)R(\mathrm{e}^{\mathrm{i}\theta}r)\,(\mathrm{e}^{\mathrm{i}\theta}r)^2\mathrm{d}(\mathrm{e}^{\mathrm{i}\theta}r)\ ,\end{aligned} \tag{3.6}$$

which is identical with the integration of the variable $\rho = \mathrm{e}^{\mathrm{i}\theta}r$ on the complex contour $C = \{\rho = r\mathrm{e}^{\mathrm{i}\theta}\,|\,0 \le r < \infty\}$,

$$\langle E\rangle = \int_C R(\rho)\left(-\frac{1}{2}\frac{1}{\rho^2}\frac{\mathrm{d}}{\mathrm{d}\rho}\rho^2\frac{\mathrm{d}}{\mathrm{d}\rho} + V(\rho)\right)R(\rho)\,\rho^2\mathrm{d}\rho\ . \tag{3.7}$$

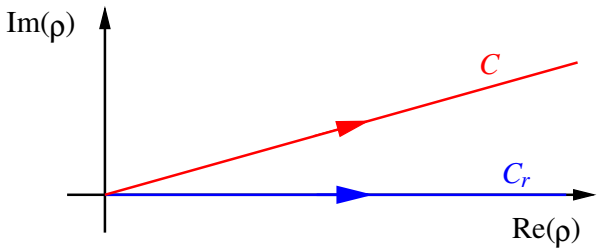

Figure 3.1: Two different contours for the evaluation of the integral (3.7). The path C_r goes along the real axis and corresponds to the direct evaluation of the expectation value integral (3.5) for a bound state, whereas the contour C is equivalent to the integration of the expectation value for a complex rotated Hamiltonian and scaled wave functions as in equation (3.6).

Thus, one can easily see that the procedure (3.3a) and (3.3b) has the same effect on the energy expectation value as an evaluation of the same integral on a different contour in the space of complex coordinates. This relation points out how the complex rotation influences the calculation of energies discussed in the next section.

3.2 Influence of the complex rotation on the energy spectrum

The energies of bound states are invariant under the complex rotation. This can be seen particularly clear in the formulation of the contour integral (3.7) [15]. As was discussed above the complex rotation corresponds to the evaluation of the energy expectation value (3.5) on the complex contour $C = \{\rho = re^{i\theta} \,|\, 0 \leq r < \infty\}$ instead of the real axis. Both contours are plotted in figure 3.1. According to Cauchy's theorem two different contours which connect the same two points in the complex plane lead to the same values of the line integral if the integrated function is holomorphic in between the two contours. Normally, the integral kernel is holomorphic. For bound state wave functions which vanish for large values of r, the path which connects the contours C and C_r at "infinite" distance from the origin does not contribute to a line integral and the continuation of the path C can be established such that it is connected with the path C_r without changing the value of the integral. Then, the two contours C and C_r lead to the same value of the expectation value.

For scattering states the energy spectrum changes when the complex rotation is applied. The continuum is rotated by an angle of 2θ into the lower half of the complex plane. This can be demonstrated especially easy for interaction potentials which are not too long ranged [14, 15]. Here, the asymptotic behavior of radial scattering solutions is

given by linear combinations

$$\psi_{\text{scatt}} = A(k)\frac{\mathrm{e}^{\mathrm{i}kr}}{r} + B(k)\frac{\mathrm{e}^{-\mathrm{i}kr}}{r} \tag{3.8a}$$

as $r \to \infty$ with the energy

$$E = \frac{k^2}{2} \tag{3.8b}$$

in appropriate units. After introducing the complex rotation, the wave functions have the form

$$\psi_{\text{scatt}} = A(k)\frac{\mathrm{e}^{\mathrm{i}k\mathrm{e}^{\mathrm{i}\theta}r}}{\mathrm{e}^{\mathrm{i}\theta}r} + B(k)\frac{\mathrm{e}^{-\mathrm{i}k\mathrm{e}^{\mathrm{i}\theta}r}}{\mathrm{e}^{\mathrm{i}\theta}r} \ , \tag{3.9}$$

where one of the exponentials diverges for real values of k as $r \to \infty$. The only possibility to keep the wave functions non-divergent bounded is to introduce a complex k of the form [14]

$$k \to k\mathrm{e}^{-\mathrm{i}\theta} \tag{3.10}$$

when the complex rotation is applied. In any other case one obtains non-physical divergent wave functions. The consequence for the energy is that it becomes

$$E \to \bar{E} = \frac{k^2\mathrm{e}^{-2\mathrm{i}\theta}}{2} \ , \tag{3.11}$$

which describes the rotation of the continuum into the lower half of the complex plane by the angle 2θ.

The most incisive effect of the complex rotation on the energy spectrum concerns resonances. They appear as *new* discrete eigenvalues on the lower half of the energy plane, which in contrast to the continuum do not depend on the rotation angle. The complex rotated eigenfunctions of the resonant states are square integrable. A simple analytic example which contains this effect is given by the inverted harmonic oscillator [14], which is in appropriately chosen units represented by the Hamiltonian

$$H = -\frac{1}{2}\frac{\mathrm{d}^2}{\mathrm{d}x^2} - \frac{1}{2}x^2 \ . \tag{3.12}$$

This potential has no bound states, i.e., no square integrable wave functions belonging to discrete real valued energy eigenvalues appear. However, discrete energy eigenvalues connected with square integrable wave functions can be found with the complex rotation method. The complex scaled wave functions

$$\psi_n(\mathrm{e}^{\mathrm{i}\theta}x) = cH_n(\mathrm{e}^{\mathrm{i}\theta}x/\sqrt{\mathrm{i}})\mathrm{e}^{\mathrm{i}\mathrm{e}^{2\mathrm{i}\theta}x^2/2} \ , \tag{3.13a}$$

where $H_n(x)$ are the Hermite polynomials [76] and c is a normalization constant, solve the transformed Hamiltonian

$$\bar{H} = -\frac{1}{2}\mathrm{e}^{-2\mathrm{i}\theta}\frac{\mathrm{d}^2}{\mathrm{d}x^2} - \mathrm{e}^{2\mathrm{i}\theta}\frac{1}{2}x^2 \ . \tag{3.13b}$$

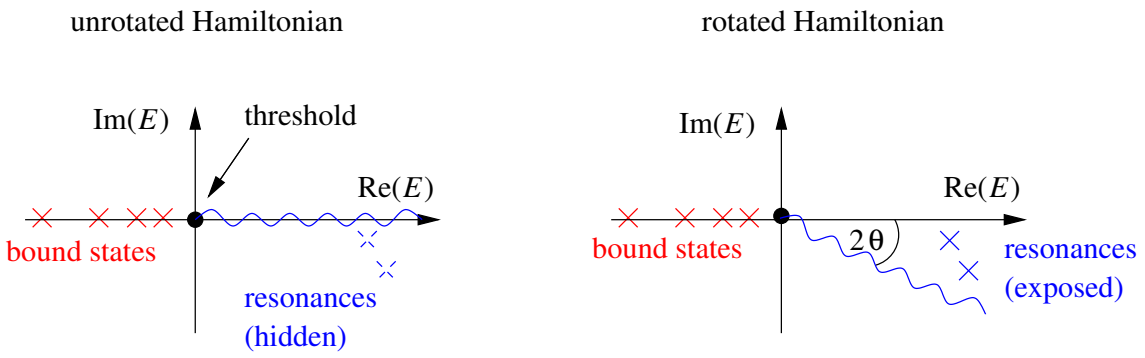

Figure 3.2: Illustration of the effects of the complex rotation. In the rotated Hamiltonian the continua are rotated by the angle 2θ into the lower half of the complex plane and resonances are exposed as discrete complex energy eigenvalues (cf. reference [15]).

The energy eigenvalues have the form

$$\tilde{E}_n = -\mathrm{i}(n + \frac{1}{2}) \tag{3.13c}$$

and are purely imaginary. According to equation (3.1b) they correspond to an infinite number of resonances which have all the same position $E = 0$ but different widths $\Gamma = 2n + 1$. For an appropriately chosen rotation angle θ the wave functions (3.13a) are square integrable, i.e., the energy expectation value exists for the complex rotated wave functions. The example points out that the resonance eigenfunctions which do not belong to the Hilbert space *without* the complex rotation can become square integrable *with* the complex rotation and thus become part of the Hilbert space.

The above results can be summarized with the following statements [15, 16], which are illustrated in figure 3.2:

1. The real valued bound state energies remain unchanged under the complex scaling transformation.

2. The energy values that represent continuum states are rotated downward into the complex plane such that they enclose an angle of 2θ with the real axis.

3. The resonances are "exposed" by the rotated continuum states for arguments of the complex energies in the range

$$-2\theta \leq \arg(\tilde{E} - E_{\mathrm{thresh}}) < 0 \;, \tag{3.14}$$

where E_{thresh} is the lowest scattering threshold and $\tilde{E} = E - \mathrm{i}\Gamma/2$ is the complex resonance energy with the position E and width Γ.

3.3 Complex rotation and inner products

In inner products one has to pay regard to the fact that the complex scaled variables $\boldsymbol{r}\mathrm{e}^{\mathrm{i}\theta}$ are not an intrinsic complex part of the wave functions. The scaled wave functions are not associated with an Hermitian Hamiltonian[1] and therefore need further consideration. In particular, it was argued above that the expectation value of the energy for bound states does not change by the complex scaling. The contour integral (3.7) can be understood as the complex scaled integral expectation value (3.5). This is only true and the form of the scaled expectation value (3.6) is only valid if no complex conjugation of the scaled coordinates $\boldsymbol{r}\mathrm{e}^{\mathrm{i}\theta}$ is performed. There may be no complex conjugation of the terms $\mathrm{e}^{\mathrm{i}\theta}$ which were introduced during the scaling [15]. By contrast, the conjugation behavior of the intrinsically complex parts of a wave function may not be changed because they are not connected with the scaling. For example, if a wave function is given by a radially part $R(r)$ multiplied with a complex spherically harmonic $Y_{l,m}(\vartheta,\varphi)$, the complex scaled wave function $\psi(r,\vartheta,\varphi) = R(\mathrm{e}^{\mathrm{i}\theta}r)Y_{l,m}(\vartheta,\varphi)$ has the form

$$\psi^*(r,\vartheta,\varphi) = R(\mathrm{e}^{\mathrm{i}\theta}r)Y^*_{l,m}(\vartheta,\varphi)\ , \tag{3.15}$$

where the factor $\mathrm{e}^{\mathrm{i}\theta}r$ remains unchanged and only the spherical harmonic $Y_{l,m}(\vartheta,\varphi)$ experiences a complex conjugation.

As a consequence the Hermitian inner product of quantum mechanics must be generalized in the presence of complex scaled variables. The generalized form, which is often called c-product, must be defined in such a way that the complex conjugate is only taken for the terms of a function which are complex not as a result of the complex scaling [14].

3.4 Direct approach

In explicit numerical computations of complex energy eigenvalues with the diagonalization of real matrices a procedure called *direct approach* by Reinhardt [15] is of considerable advantage. It is possible if a real valued matrix representation

$$H_{ij} = \langle\chi_i(\boldsymbol{r})|H(\boldsymbol{r})|\chi_j(\boldsymbol{r})\rangle \tag{3.16}$$

of the usual unrotated Hamiltonian in the unrotated basis exists and if only (positive and negative) powers of the coordinates $\boldsymbol{r}$ appear in the potential V of H. Then, the Hamiltonian can be divided into parts $V^{(n)}$ which contain one power r^n of $r = |\boldsymbol{r}|$ and the kinetic energy T. A complex scaled Hamiltonian according to equation (3.4) can be achieved with

$$\bar{\boldsymbol{H}} = \mathrm{e}^{-2\mathrm{i}\theta}\boldsymbol{T} + \sum_n \mathrm{e}^{\mathrm{i}n\theta}\boldsymbol{V}^{(n)}\ , \tag{3.17}$$

[1] One has to keep in mind, that $\bar{H}$ becomes non-Hermitian by the complex scaling.

where the sum runs over all powers of r emerging in the potential. $\boldsymbol{T}$ and $\boldsymbol{V}^{(n)}$ are the same real matrices which appear in the original Hamiltonian (3.16). Due to the complex factors $\mathrm{e}^{\mathrm{i}n\theta}$ the original matrix $\boldsymbol{H}$ has been transformed to a complex symmetric one and is *not* Hermitian. The solution of the eigensystem

$$\bar{\boldsymbol{H}}\bar{\boldsymbol{c}}_i = \tilde{E}_i\bar{\boldsymbol{c}}_i \tag{3.18}$$

yields the complex eigenvalues $\tilde{E}_i$ and leads to complex vectors $\bar{\boldsymbol{c}}_i$ of expansion coefficients. With this method the representation of a complex rotated wave function is referred to the vectors $\bar{\boldsymbol{c}}_i$ [15] and no new matrix element calculated with complex rotated wave functions is required. As can be seen above, only the real matrices $\boldsymbol{T}$ and $\boldsymbol{V}^{(n)}$ are needed to build the transformed representation (3.17). As a consequence of the non-Hermitian structure of the matrix representation of the Hamiltonian one has to distinguish between left hand and right hand eigenvectors.

3.5 Connection of resonances with poles of the scattering matrix

The scattering matrix S describes transition probabilities from an incoming wave into outgoing waves after a scattering process [77]. In large distances the asymptotic behavior of an elastic scattering process for an incoming wave can be written as [14]

$$\psi = A(k)\mathrm{e}^{-\mathrm{i}\boldsymbol{k}\cdot\boldsymbol{r}} + B(k)\mathrm{e}^{\mathrm{i}kr} \propto \mathrm{e}^{-\mathrm{i}\boldsymbol{k}\cdot\boldsymbol{r}} + S(k)\mathrm{e}^{\mathrm{i}kr} \ . \tag{3.19}$$

The incoming plane wave describes a free particle and $S(k)$ is the scattering matrix representing the ratio between the outgoing and the incoming wave. As can be shown with a short calculation, the resonances of a scattering system are constituted by the poles of the scattering matrix $S(k)$ [14]. A simple pole of the scattering matrix has the form

$$S(k) \propto \frac{1}{k - k_n} \tag{3.20}$$

and resonances appear as complex poles k_n with $\mathrm{Re}(k_n) > 0$ and $\mathrm{Im}(k_n) < 0$. With the help of the residue theorem the number N of poles can be determined by the integral

$$N = \frac{1}{2\pi\mathrm{i}} \oint_C \frac{\partial \ln S(k)}{\partial k}\,\mathrm{d}k \ , \tag{3.21}$$

where the path C has to be a closed contour around the fourth quarter of the complex plane as shown in figure 3.3 and

$$\frac{\partial \ln S(k)}{\partial k} = \frac{-1}{k - k_n} \tag{3.22}$$

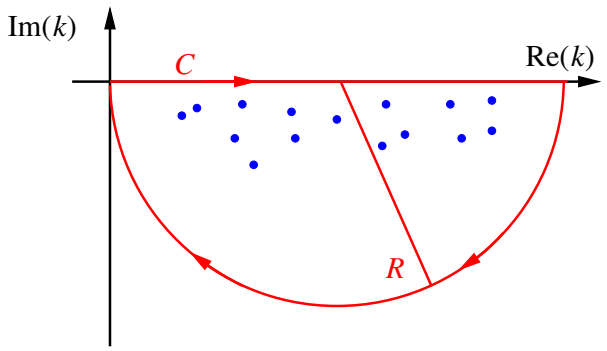

Figure 3.3: The red line marks a possible contour C in the fourth quarter of the complex plane around the poles of the scattering matrix, which are represented by blue dots. If all poles are located within a bounded region, the contour integral can be replaced with an integral along the axis of positive reals for $R \to \infty$.

according to equation (3.20). If all poles are located within a bounded region in the complex plane, the contour integral can be replaced by a path along the axis of real k with $0 \leq k < \infty$ (see figure 3.3). Then, the energy density of states

$$\varrho(E) = \frac{\partial N}{\partial E} = \frac{\partial N}{\partial k}\frac{\partial k}{\partial E} \tag{3.23}$$

can be determined with

$$\frac{\partial N}{\partial k} = \frac{1}{2\pi \mathrm{i}}\frac{\partial \ln S(k)}{\partial k} \tag{3.24}$$

from equation (3.22) together with the energy

$$E = \frac{\hbar^2 k^2}{2} \,. \tag{3.25}$$

Local maxima of the density of states on the axis of real k appear at the positions $k = \mathrm{Re}(k_n)$ and have the values

$$\varrho_{\max} = -\frac{1}{2\pi\hbar^2}\frac{1}{\mathrm{Re}(k_n)\mathrm{Im}(k_n)} \,, \tag{3.26}$$

which correspond to the complex energies

$$E_n = \frac{\hbar^2 k_n^2}{2} \,. \tag{3.27}$$

Hence, the complex energies, where the resonances occur in the form of Lorentz-shaped peaks, are connected with the poles of the scattering matrix.

3.6 Exceptional points in quantum resonance spectra

As is discussed in the introduction the occurrence of exceptional points in quantum mechanics is a typical phenomenon in resonance spectra. The complex scaled Hamiltonians are non-Hermitian which is necessary for the possibility of coalescing eigenstates, where two wave functions or eigenvectors become identical. Exceptional points are parameter values for which two of the complex energies obtained as eigenvalues of the rotated Hamiltonian pass through a branch point singularity. At the exceptional point both the energies (real part) and the widths (imaginary part) of both solutions have the same value.

Exceptional points represent a special kind of poles of the scattering matrix. At the critical parameter values, two resonances coalesce completely, i.e., the real and the imaginary part of the complex energies are identical and also the values k_n become identical.[2] As a consequence exceptional points appear as *double* poles of the scattering matrix. The scattering matrix has the form

$$S_{\text{double}}(k) \propto \frac{1}{(k-k_n)^2} \tag{3.28}$$

instead of equation (3.20) and the derivative

$$\frac{\partial \ln S_{\text{double}}(k)}{\partial k} = \frac{-2}{k-k_n} \tag{3.29}$$

immediately shows that the double poles are correctly counted as two resonances "on top of each other." The peak height is

$$\varrho_{\text{max,double}} = -\frac{1}{\pi\hbar^2}\frac{1}{\text{Re}(k_n)\text{Im}(k_n)} \ . \tag{3.30}$$

[2] One has to keep in mind that only k_n in the fourth quarter of the complex plane are allowed, i.e., only one of the two square roots $k_n \propto \sqrt{E_n}$ is a valid result.

4 Numerical diagonalization of matrices

In the numerical calculation of the eigenenergies of a quantum system, the diagonalization of a matrix representation of the Hamiltonian has become one possible standard technique. For problems appearing in atomic physics often *infinite*-dimensional basis sets appear and the accuracy of numerically computed eigenvalues depends critically on the size of the matrix. Therefore, very efficient methods for the diagonalization are required, to include as many basis states as possible in the *finite*-dimensional matrix representation which is used in the calculation. The most efficient methods are developed for the most common cases, namely Hermitian or real symmetric matrices. However, the calculation of resonances with the complex rotation method requires the solution of non-Hermitian complex symmetric eigenvalue problems. For this class of matrices usually algorithms for general non-symmetric problems must be used which are numerically more expensive.

The extension of fast algorithms for real symmetric matrices to complex numbers just by introducing complex variables in the program and using the linear algebra for real matrices may seem to be the most efficient way to compute the eigenvalues of large non-Hermitian complex symmetric matrices. This chapter addresses the question whether this procedure, already successfully used in the absence of branch point singularities [30, 31], works reliably in the presence of exceptional points. An application of algorithms for real symmetric matrices requires that the real Euclidean norm $||\boldsymbol{x}||_{\mathrm{r}} = \boldsymbol{x}^T\boldsymbol{x}$ of a vector without complex conjugation is retained after the extension to complex numbers. There can appear difficulties, which are discussed in this chapter. Some of the diagonalization methods rely on the fact that every eigenvector of the matrix can be normalized with the real Euclidean norm or that the eigenvectors are pairwise orthogonal. Both conditions are always fulfilled for real symmetric matrices but not for complex symmetric ones. In particular, at an exceptional point two eigenvectors become linearly dependent (see section 2.2) and the conditions are not fulfilled. In addition to this effect, which is directly connected with exceptional points, further vanishing real Euclidean norms without relation to branch point singularities can lead to problems. Both cases are studied.

The influences of complex valued variables in algorithms for real symmetric matrices can be best understood in simple direct algorithms, which are discussed in section 4.1. In section 4.1.1 the possible failure of the Jacobi algorithm for complex matrices and its divergent terms at exceptional points are analyzed. The discussion in section 4.1.2 shows

that the Householder transformation for real symmetric matrices is normally capable to tridiagonalize a complex symmetric matrix even in the presence of exceptional points since it refers the calculation of the eigenvalues to a second step, which is investigated for the example of the QL method in section 4.1.3. The results for the direct methods are summarized in section 4.1.4. In section 4.2 iterative methods for large matrices with several thousand basis states are covered. In particular, the Lanczos method for real symmetric matrices and the more general Arnoldi iteration are examined in sections 4.2.1 and 4.2.2, respectively. Suitable implementations of both algorithms are briefly introduced in section 4.2.3. In this chapter the term "exceptional points" is used synonymously for a square root branch point, where two linearly dependent eigenvectors appear. This is the typical case in the physical systems considered in this thesis.

4.1 Simple generalizations of direct methods for real symmetric matrices

There are several direct methods for the diagonalization of real symmetric matrices. Here, it is investigated whether it is possible to extend some of the methods to complex symmetric matrices and to calculate the eigenvalues even in the presence of exceptional points.

4.1.1 Jacobi transformation

The Jacobi transformation is a method which uses a sequence of orthogonal similarity transformations of the type

$$\boldsymbol{P}_{pq} = \begin{pmatrix} 1 & & & & & & \\ & \ddots & & & & & \\ & & \cos\alpha & \cdots & \sin\alpha & & \\ & & \vdots & 1 & \vdots & & \\ & & -\sin\alpha & \cdots & \cos\alpha & & \\ & & & & & \ddots & \\ & & & & & & 1 \end{pmatrix} \tag{4.1}$$

for different rows and columns p and q to diagonalize a real symmetric matrix $\boldsymbol{A}$ [78]. The rotation angle α is chosen such that the two off-diagonal elements $a_{pq} = a_{qp}$ of the real symmetric matrix $\boldsymbol{A}$ are set to zero with the similarity transformation

$$\boldsymbol{A}' = \boldsymbol{P}_{pq}^T \boldsymbol{A} \boldsymbol{P}_{pq} \tag{4.2}$$

in the current step. Successive transformations are carried out. These undo previously set zeros but the sum of the squares of the off-diagonal elements

$$S = \sum_{r \neq s} a_{rs}^2 \tag{4.3}$$

decreases monotonically. To achieve convergence it is, in general, necessary to perform several passes of cycles going through all combinations of rows p and columns q.

A simple extension of the Jacobi algorithm to complex numbers, where only the functions $\sin\alpha$ and $\cos\alpha$ are allowed to become complex and no further consideration for the diagonalization of complex matrices are done, corresponds to the procedure mentioned above. For the Jacobi transformation there are two crucial consequences.

The first consequence is connected with exceptional points. If during the application of the algorithm in the rows and columns p and q a matrix of the form

$$\boldsymbol{A} = \begin{pmatrix} \ddots & \cdots & \cdots & \cdots & \cdots \\ \cdots & a_{pp} & \cdots & \mp\frac{a_{qq}-a_{pp}}{2\mathrm{i}} & \cdots \\ \cdots & \vdots & \ddots & \vdots & \cdots \\ \cdots & \mp\frac{a_{qq}-a_{pp}}{2\mathrm{i}} & \cdots & a_{qq} & \cdots \\ \cdots & \cdots & \cdots & \cdots & \ddots \end{pmatrix} \tag{4.4}$$

appears, no "orthogonal" transformation with complex extended sine and cosine functions, which transform the off-diagonal elements to zero, exists. The situation in equation (4.4) may always appear in a complex symmetric matrix. It occurs in particular always at an exceptional point, which forms a normal block and cannot be brought into diagonal form with a similarity transformation. Consequently the Jacobi algorithm must fail. An exceptional point leads to diverging terms.

In practice, it is very unlikely that the Jacobi transformation tries to diagonalize the exceptional point elements shown in equation (4.4) in the last step if the branch point is embedded in a higher-dimensional matrix. In the previous steps the exceptional point is "mixed" with further eigenvalues and these contributions of other eigenvalues avoid diverging terms. If the algorithm now stops due to numercial convergence criteria before it returns to the normal block representing the exceptional point, a form which is "sufficiently" diagonal may appear. Thus, it is possible that the algorithm converges due to numerical convergence criteria.

The second consequence of the simple complex extension is related with the decrease of the off-diagonal elements. It can be shown that the sum S of the squares of the off-diagonal elements (4.3) changes by the amount [78]

$$\Delta S = -2a_{pq}^2 \,. \tag{4.5}$$

For real matrices it is evident that this corresponds to a monotonic decrease of the norm of the off-diagonal elements, whereas this is not fulfilled in the case of complex

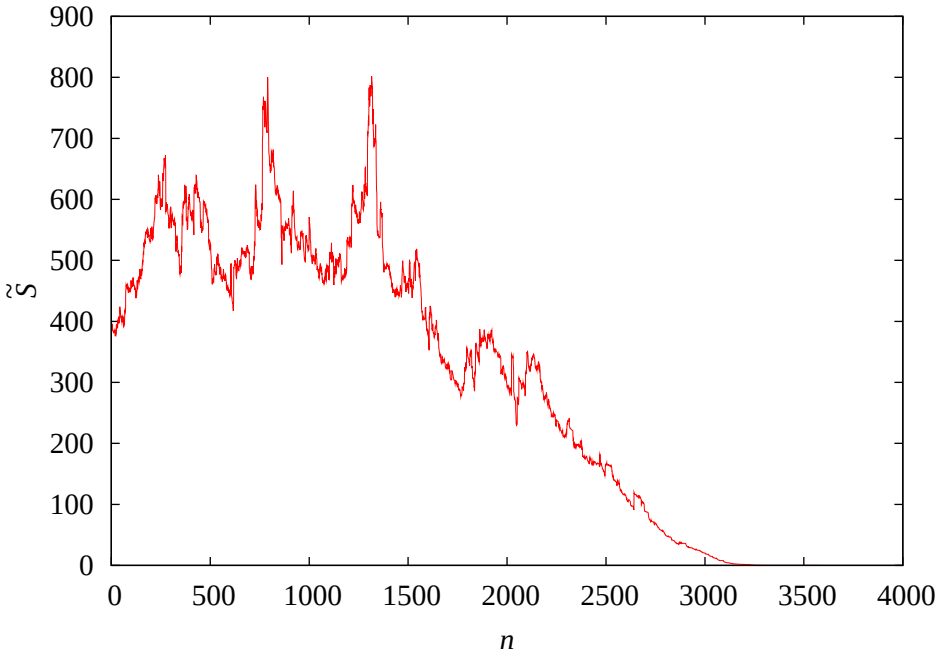

Figure 4.1: The sum of the norm $\tilde{S} = \sum_{r \neq s} |a_{rs}|^2$ of the off-diagonal elements is shown for a number of successive Jacobi rotations applied to a complex symmetric matrix. As can be seen $\tilde{S}$ does not monotonically decrease as in the real symmetric case.

matrix elements. An adequate quantity to measure the progress of the diagonalization for complex matrices is the sum of the square modulus of the off-diagonal elements

$$\tilde{S} = \sum_{r \neq s} |a_{rs}|^2 \,, \tag{4.6}$$

which can both increase and decrease. Indeed, it happens that the sum $\tilde{S}$ increases during a run of the algorithm. Figure 4.1 shows the norm $\tilde{S}$ for the diagonalization of a square matrix of dimension 20. For successive Jacobi rotations one can observe alternating increases and decreases of $\tilde{S}$. Finally, the algorithm succeeds and the matrix is diagonalized. However, this does not always happen. A similar diagonalization attempt for a second matrix of dimension 50 is presented in figure 4.2. Here the algorithm is not successful and the norm of the off-diagonal elements diverges. Because of this convergence behavior one can conclude that the Jacobi rotation is not applicable for complex symmetric matrices.

4.1.2 Householder reduction

Often it is the best choice to start an iterative elimination of off-diagonal elements after the matrix has been reduced to a simple form. For real symmetric matrices an efficient

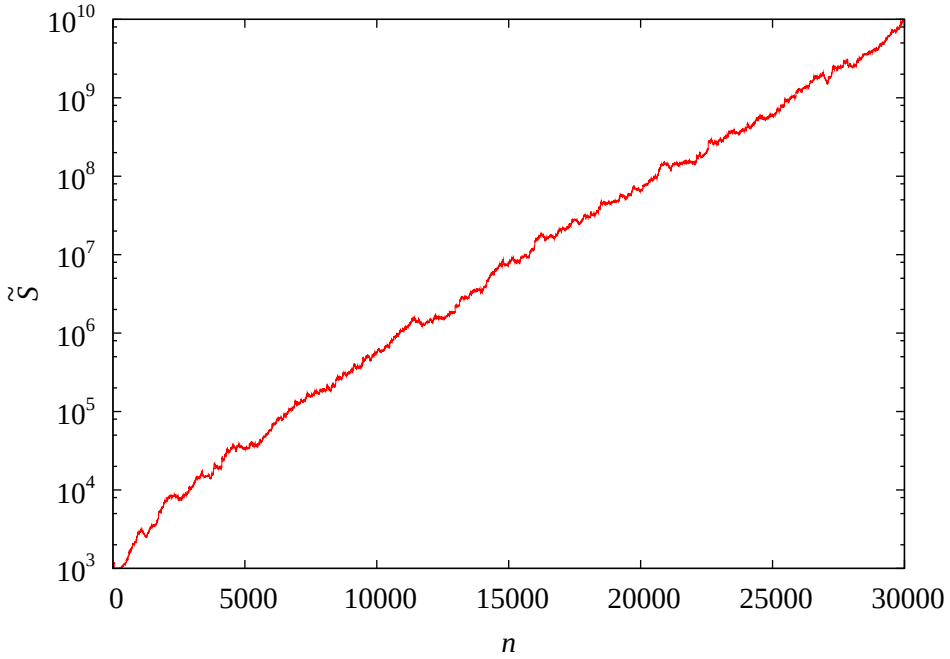

Figure 4.2: In this example for a complex symmetric matrix the sum $\tilde{S}$ of the off-diagonal elements increases until it diverges. The Jacobi algorithm fails in the attempt to diagonalize the matrix.

method is the reduction to tridiagonal form with the Householder method and successive diagonalization of the tridiagonal matrix.

The Householder algorithm [78] uses orthogonal matrices of the form

$$\boldsymbol{P} = \mathbf{1} - \frac{\boldsymbol{u}\boldsymbol{u}^{\mathrm{T}}}{C} \,, \tag{4.7}$$

where the vector $\boldsymbol{u}$

$$\boldsymbol{u} = \boldsymbol{x} \mp ||\boldsymbol{x}||_{\mathrm{R}} \hat{\boldsymbol{e}}_1 \tag{4.8}$$

contains a column vector $\boldsymbol{x}$ of the matrix $\boldsymbol{A}$ to be diagonalized and C is a normalization based on the real Euclidean norm

$$C = \frac{1}{2}||\boldsymbol{u}||_{\mathrm{R}}^2 = \frac{1}{2}\boldsymbol{u}^{\mathrm{T}}\boldsymbol{u} \tag{4.9}$$

of the vector $\boldsymbol{u}$. For example one can start the reduction by choosing $\boldsymbol{x}$ to be the $n-1$ lower components of the first column of the matrix $\boldsymbol{A}$. With a short calculation it can be shown that now the lower $n-2$ components of the first column are set to zero. Since the matrix is symmetric this also holds for the $n-2$ right components of the first row

and the transformed matrix $\boldsymbol{A}'$ reads

$$\boldsymbol{A}' = \boldsymbol{PAP} = \begin{pmatrix} a_{11} & k & 0 & \cdots & 0 \\ k & & & & \\ 0 & & & & \\ \vdots & & & \text{(remaining submatrix)} & \\ 0 & & & & \end{pmatrix} . \tag{4.10}$$

A successive application on the remaining submatrices yields a tridiagonal matrix with $n-2$ steps.

The simple extension to complex symmetric matrices by introducing complex variables without changing the algorithm now can lead to one difficulty. The scalar C can become zero due to its definition (4.9). If the normalization is written explicitly,

$$\boldsymbol{u}^{\mathrm{T}}\boldsymbol{u} = 2||\boldsymbol{x}||_{\mathrm{R}}^2 \mp 2x_1||\boldsymbol{x}||_{\mathrm{R}} , \tag{4.11}$$

one immediately sees that this happens for the two cases $||\boldsymbol{x}||_{\mathrm{R}} = 0$ and $x_1 = \pm||\boldsymbol{x}||_{\mathrm{R}}$, where x_1 is the first component of the vector $\boldsymbol{x}$. The latter case is not critical because the sign of $\mp 2x_1||\boldsymbol{x}||_{\mathrm{R}}$ can be chosen arbitrarily and, in particular, the choice used in numerical calculations to lessen roundoff errors [78] (The largest possible value of $\boldsymbol{u}^{\mathrm{T}}\boldsymbol{u}$ is chosen.) always avoids a divergence.

The first possibility for a divergence, viz. $||\boldsymbol{x}||_{\mathrm{R}} = 0$, is always possible for complex symmetric matrices but can be avoided with an adequate permutation of columns and rows. In contrast to the Jacobi rotation, exceptional points do not necessarily lead to diverging terms in the complex extended Householder transformation. This can directly be shown for the simplest possibility of an exceptional point embedded in a non-tridiagonal matrix, namely a 3×3-matrix,

$$\boldsymbol{A} = \begin{pmatrix} a & 0 & \frac{a-b}{2\mathrm{i}} \\ 0 & e & 0 \\ \frac{a-b}{2\mathrm{i}} & 0 & b \end{pmatrix} , \tag{4.12a}$$

where the first and the third rows and columns contain the exceptional point and e is the third eigenvalue. The two-dimensional vector

$$\boldsymbol{u} = \begin{pmatrix} \frac{a-b}{2\mathrm{i}} \\ \frac{a-b}{2\mathrm{i}} \end{pmatrix} \tag{4.12b}$$

and the scalar

$$C = -\frac{(a-b)^2}{4} \tag{4.12c}$$

behave completely regular and lead to the permutation matrix

$$\boldsymbol{P} = \begin{pmatrix} 1 & 0 & 0 \\ 0 & 0 & -1 \\ 0 & -1 & 0 \end{pmatrix} \tag{4.12d}$$

for the sole Householder step required to obtain the tridiagonal matrix

$$\boldsymbol{A}' = \begin{pmatrix} a & -\frac{a-b}{2\mathrm{i}} & 0 \\ -\frac{a-b}{2\mathrm{i}} & b & 0 \\ 0 & 0 & e \end{pmatrix} . \tag{4.12e}$$

The example illustrates directly why the tridiagonalization does not conflict with the existence of exceptional points. Square root branch points form a two-dimensional normal block, which can be embedded in a tridiagonal structure. The tridiagonalization postpones the difficult task to gain the eigenvalues from the normal block to the subsequent algorithm applied to the simplified matrix.

The example considered here can be generalized to more complicated matrices. In particular, the investigation of the Householder transformation for a general three-dimensional complex symmetric matrix shows that only the vanishing real Euclidean norm $||\boldsymbol{x}||_{\mathrm{R}} = 0$ leads to a failure of the algorithm, which has no connection to the appearance of an exceptional point. Hence, the simple extension to complex variables may result in diverging terms but in contrast to the Jacobi transformation exceptional points do not raise a problem.

Applied to Hermitian matrices with the correct complex Euclidean norm one also achieves a tridiagonalization of the matrix. If the algorithm with the complex Euclidean norm is used for general matrices, one accomplishes a reduction to Householder form, which is still a good starting point for a consecutive eigenvalue calculation [79]. However a tridiagonal matrix makes the eigenvalue calculation more efficient. For example, the numerical effort for the QL algorithm mentioned in the next section is of order $\mathrm{O}(n^2)$ per iteration for a Hessenberg matrix and $\mathrm{O}(n)$ for a tridiagonal matrix, where n is the dimension of the square matrix. By ignoring the complex Euclidean norm for complex symmetric matrices one gains the optimal tridiagonal structure but bears the risk of a failure due to diverging terms for $C = 0$ in equation (4.7).

4.1.3 QL algorithm for the eigenvalues of a real tridiagonal matrix

As mentioned above the tridiagonalization of a complex symmetric matrix succeeds in general for matrices containing exceptional points but postpones the problem of the calculation of the eigenvalues to a subsequent algorithm. For tridiagonal or Hessenberg matrices very efficient methods are the QR and QL algorithms, which are based on the fact that any matrix $\boldsymbol{A}$ can be decomposed in the form

$$\boldsymbol{A} = \boldsymbol{Q}\boldsymbol{R} \qquad \text{or} \qquad \boldsymbol{A} = \boldsymbol{Q}\boldsymbol{L} , \tag{4.13}$$

where $\boldsymbol{Q}$ is unitary and $\boldsymbol{R}$ and $\boldsymbol{L}$ are upper and lower triangular, respectively. With the help of this relation a series of unitary transformations

$$\boldsymbol{A}_{i+1} = \boldsymbol{Q}_i^+ \boldsymbol{A}_i \boldsymbol{Q}_i \tag{4.14}$$

can be constructed which has the following convergence properties [78, 79].

- The sequence of matrices $\boldsymbol{A}_i$ converges to a lower triangular form as $i \to \infty$ if all eigenvalues have different absolute value, which is not the interesting case for exceptional points.
- If degenerate eigenvalues λ_d of multiplicity p appear, which is exactly the case for an exceptional point ($p = 2$ for a square root branch point), the sequence $\boldsymbol{A}_i$ converges to lower triangular form except for a diagonal block matrix of dimension p. The eigenvalues of the block matrix converge to λ_d.

Thus, the QL algorithm for general matrices again does not completely solve the problem. The normal blocks representing the exceptional point remain and their eigenvalues must be determined with another method. However, the normal blocks are of very low dimension. For the most common case of an exceptional point corresponding to a square root branch point singularity, the matrix has dimension two and can be calculated easily. It should be noted that the normal blocks often are diagonalized due to numerical convergence criteria. Numerically, an "exact" normal block is a rare case. In most cases the eigenvalues of exceptional points can be found.

In the case of real matrices, $\boldsymbol{Q}$ is orthogonal and, again, for a simple complex extension without the additional numerical costs of complex algorithms, "orthogonal" matrices with complex coefficients can be used. For many examples the algorithm succeeds but a loss in numerical accuracy is possible.

4.1.4 Possibilities for the application of algorithms for real matrices

Based on the discussions above one can conclude that it is often possible to use algorithms for real symmetric matrices with complex-valued coefficients for the diagonalization of complex symmetric matrices. There is no guarantee that the modified methods will succeed but in most cases they do. In particular, the following results can be given for the algorithms under consideration.

- One can implement a test in the Jacobi iteration, which prevents the algorithm to perform a rotation if the program tries to diagonalize a normal block, which is impossible. Then no diverging terms will appear. However, as was mentioned above, the algorithm can fail completely for complex symmetric matrices. The diverging norm of the off-diagonal elements shown in figure 4.2 forbids the use of the algorithm.

- A feasible possibility is provided by a combination of the tridiagonalization with the Householder method and successive application of the QR or QL algorithm. The result will be a matrix which is diagonal or block diagonal. The normal blocks of exceptional points can remain and their eigenvalues must be calculated analytically. In the QR or QL step, unitary rotation matrices can be used which works stable for complex symmetric matrices. Thus, the only possible point of failure appears in the first step. If in one of the Householder transformations a column vector with vanishing real Euclidean norm emerges, the tridiagonalization cannot be carried out, but this is a rare case and not connected with the occurrence of branching eigenvalues.

4.2 Iterative methods for large matrices

4.2.1 Lanczos algorithm for Hermitian matrices

The direct algorithms considered so far have in common that they are simple enough to discuss the influence of complex extensions but that they are too expensive for the diagonalization of large matrices with up to several thousand basis states usually required in atomic physics. Here, often variants of the iterative Lanczos algorithm are used which allow for the efficient and fast calculation of *some* of the eigenvalues of a Hermitian or real symmetric matrix. The Lanczos method is based on an orthonormal set of basis vectors $\boldsymbol{q}_1, \boldsymbol{q}_2, \ldots, \boldsymbol{q}_m$ of the Krylov space

$$K_m(\boldsymbol{q}, \boldsymbol{A}) = \mathrm{span}[\boldsymbol{q}, \boldsymbol{A}\boldsymbol{q}, \ldots, \boldsymbol{A}^{m-1}\boldsymbol{q}] \;, \tag{4.15}$$

which are built of a starting vector $\boldsymbol{q}$ and the sequence of its multiplications with the matrix $\boldsymbol{A}$ to be diagonalized [79]. In general, the maximum dimension m of the space spanned according to equation (4.15) with the highest index for which $\dim K_m(\boldsymbol{q}, \boldsymbol{A}) = m$ is satisfied, is lower than the dimension n of the matrix $\boldsymbol{A}$. Beginning with a starting vector $\boldsymbol{q}$ the orthonormal basis can be constructed with the recursion

$$\boldsymbol{q}_1 = \boldsymbol{q} \;, \tag{4.16a}$$

$$\gamma_1 \boldsymbol{q}_0 := 0 \;, \tag{4.16b}$$

$$\boldsymbol{A}\boldsymbol{q}_i = \gamma_i \boldsymbol{q}_{i-1} + \delta_i \boldsymbol{q}_i + \gamma_{i+1} \boldsymbol{q}_{i+1} \qquad \text{for} \quad i \geq 1 \;, \tag{4.16c}$$

where

$$\delta_i = \boldsymbol{q}_i^+ \boldsymbol{A}\boldsymbol{q}_i \;, \tag{4.16d}$$

$$\gamma_{i+1} = \sqrt{\boldsymbol{r}_i^+ \boldsymbol{r}_i} \;, \qquad \text{with} \quad \boldsymbol{r}_i = \boldsymbol{A}\boldsymbol{q}_i - \delta_i \boldsymbol{q}_i - \gamma_i \boldsymbol{q}_{i-1} \;, \tag{4.16e}$$

$$\boldsymbol{q}_{i+1} = \frac{\boldsymbol{r}_i}{\gamma_{i+1}} \;, \qquad \text{if} \quad \gamma_{i+1} \neq 0 \;. \tag{4.16f}$$

From the recursion equations one can read that the procedure stops for the index i with $\gamma_{i+1} = 0$, which is $i = m$.

The Lanczos algorithm provides the tridiagonalization of a matrix, which becomes clear if one writes the recursion equations (4.16a)–(4.16f) in the matrix form

$$\boldsymbol{A}\boldsymbol{Q}_i = \boldsymbol{Q}_i\boldsymbol{J}_i + \gamma_{i+1}\boldsymbol{q}_{i+1}\hat{\boldsymbol{e}}_i^T \ , \tag{4.17}$$

where $\hat{\boldsymbol{e}}_i$ is the i-th axis vector $\hat{\boldsymbol{e}}_i^T = (0, 0, \ldots, 1)$ and the matrices

$$\boldsymbol{Q}_i = (\boldsymbol{q}_1, \boldsymbol{q}_2, \ldots, \boldsymbol{q}_i) \ , \tag{4.18a}$$

$$\boldsymbol{J}_i = \begin{pmatrix} \delta_1 & \gamma_2 & & 0 \\ \gamma_2 & \delta_2 & \ddots & \\ & \ddots & \ddots & \gamma_i \\ 0 & & \gamma_i & \delta_i \end{pmatrix} \tag{4.18b}$$

appear. In particular, for $i = m$ equation (4.17) reduces to

$$\boldsymbol{A}\boldsymbol{Q}_m = \boldsymbol{Q}_m\boldsymbol{J}_m \tag{4.19}$$

and a simple calculation reveals that each eigenvalue of the *symmetric tridiagonal* matrix $\boldsymbol{J}_m$ is also an eigenvalue of $\boldsymbol{A}$. Thus, the calculation of the eigenvalues with the Lanczos algorithm starts with the determination of the coefficients γ_i and δ_i in the recursion equations (4.16a)–(4.16f). Then, the symmetric tridiagonal matrix $\boldsymbol{J}_i$ is built up, which has a much simpler form than $\boldsymbol{A}$ and whose eigenvalues can be calculated efficiently with, e.g, one of the methods described above. As was already mentioned the recursion (4.16a)–(4.16f) can stop for $m \leq n$. Thus, the matrix has in general less eigenvalues than $\boldsymbol{A}$. But it is not the aim of the Lanczos algorithm to calculate all eigenvalues of the matrix $\boldsymbol{A}$. It is especially efficient if only the largest and smallest eigenvalues of the matrix are searched. The extremal eigenvalues of $\boldsymbol{J}_i$ converge very fast to the extremal eigenvalues of $\boldsymbol{A}$ and, hence, often a small number of iterations (4.16a)–(4.16f) is sufficient to calculate the largest and smallest eigenvalues. Spectral transformations, which shift and invert the eigenvalue problem, allow for the calculation of a specified number of eigenvalues in any part of the spectrum [80].

In the Lanczos algorithm for real symmetric matrices, the recursion equations (4.16a)–(4.16f) are valid but the Hermitian conjugate vectors $\boldsymbol{q}_i^+$ in equation (4.16d) and $\boldsymbol{r}_i^+$ in equation (4.16e) are identical with the transpose vectors $\boldsymbol{q}_i^T$ and $\boldsymbol{r}_i^T$, respectively. The simple extension to complex symmetric matrix elements now consists in using the transpose of the complex vectors $\boldsymbol{q}_i^T$ and $\boldsymbol{r}_i^T$, which means that the real Euclidean norm of the vector $\boldsymbol{r}_i$ is used in equation (4.16e). This can result in a vanishing coefficient γ_{i+1} before the desired convergence for the eigenvalues is reached. The vector $\boldsymbol{r}_i$ is not an eigenvector of the matrix $\boldsymbol{A}$ and, therefore, this problem of convergence for complex symmetric matrices is not directly connected with exceptional points. As stated above

for the Householder method the tridiagonalization with the Lanczos algorithm can in general also succeed for complex symmetric matrices which contain a square root branch point. However, the algorithm can fail due to the case of $\gamma_{i+1} = 0$ in an early step.

The crucial step for an exceptional point is the consecutive calculation of the eigenvalues from the tridiagonal matrix $\boldsymbol{J}_i$. Here, normally the QL method which assumes a Hermitian (or real symmetric) tridiagonal matrix is used. As is discussed in section 4.1.3 the algorithm can succeed but may also fail because normally no care is taken of exceptional points in implementations of the Lanczos method. Alternatively a reduction to the Schur normal form may be applied, which is always possible and avoids problems with exceptional points.

4.2.2 Arnoldi algorithm

The Arnoldi algorithm finds the eigenvalues of general matrices and is not restricted to Hermitian or real symmetric cases. It is similar to the Lanczos method and is based on a sequence of orthonormal vectors $\boldsymbol{q}_1, \boldsymbol{q}_2, \ldots, \boldsymbol{q}_m$ which span the Krylov subspace $K_m(\boldsymbol{q}, \boldsymbol{A})$, where now the complex Euclidean norm based on the Hermitian inner product $\boldsymbol{q}^+\boldsymbol{q}$ is used for the orthonormalization. Again, a recursion equation builds up the sequence $\boldsymbol{q}_1, \boldsymbol{q}_2, \ldots, \boldsymbol{q}_m$. It has the form [81]

$$\boldsymbol{q}_1 = \frac{\boldsymbol{q}}{\sqrt{\boldsymbol{q}^+\boldsymbol{q}}} \,, \tag{4.20a}$$

$$h_{j,i} = \boldsymbol{q}_j^+ \boldsymbol{A}\boldsymbol{q}_i \,, \quad j = 1, 2, \ldots, i \,, \tag{4.20b}$$

$$\boldsymbol{r}_{i+1} = \boldsymbol{A}\boldsymbol{q}_i - \sum_{j=1}^{i} h_{j,i}\boldsymbol{q}_j \,, \tag{4.20c}$$

$$h_{i+1,i} = \sqrt{\boldsymbol{r}_{i+1}^+ \boldsymbol{r}_{i+1}} \,, \tag{4.20d}$$

$$\boldsymbol{q}_{i+1} = \frac{\boldsymbol{r}_{i+1}}{h_{i+1,i}} \,. \tag{4.20e}$$

The similarity with the Lanczos method becomes especially clear if the iteration is written in the matrix form

$$\boldsymbol{A}\boldsymbol{Q}_i = \boldsymbol{Q}_i\boldsymbol{H}_i + h_{i+1,i}\boldsymbol{q}_{i+1}\hat{\boldsymbol{e}}_i^T \tag{4.21}$$

or in the case $i = m$

$$\boldsymbol{A}\boldsymbol{Q}_m = \boldsymbol{Q}_m\boldsymbol{H}_m \,, \tag{4.22}$$

where $\boldsymbol{Q}_i$ has the shape (4.18a). The elements $h_{i,j}$ replace the coefficients δ_i and γ_i of the Lanczos method and form the upper Hessenberg matrix

$$\boldsymbol{H}_i = \begin{pmatrix} h_{1,1} & h_{1,2} & h_{1,3} & \cdots & h_{1,n} \\ h_{2,1} & h_{2,2} & h_{2,3} & \cdots & h_{2,n} \\ 0 & h_{3,2} & h_{3,3} & \cdots & h_{3,n} \\ \vdots & \ddots & \ddots & \ddots & \vdots \\ 0 & \cdots & 0 & h_{n,n-1} & h_{n,n} \end{pmatrix} . \tag{4.23}$$

The extremal eigenvalues of $\boldsymbol{H}_i$ converge to the extremal eigenvalues of $\boldsymbol{A}$. Similar to the Lanczos algorithm it is now the aim of the method to compute the coefficients $h_{i,j}$ with the help of the recursion equations (4.20a)–(4.20e) and to transform the matrix to a simpler shape, which is an upper Hessenberg matrix. A consecutive QL sequence for non-symmetric Hessenberg matrices can be used to gain the eigenvalues reliably.

4.2.3 Suitable implementations for high-dimensional matrices

There are powerful implementations of Lanczos and Arnoldi algorithms which allow for fast and numerically efficient eigenvalue calculations of high-dimensional matrices. The "spectral transformation Lanczos method" (STLM) algorithm by Ericsson and Ruhe [80] is intended to solve real symmetric generalized eigenvalue problems. It uses a transformation of the underlying matrices to shift and invert the problem and computes a specified number of eigenvalues in a user-defined part of the spectrum. A powerful implementation of the Arnoldi method is provided by the Arnoldi package ARPACK [82]. It uses the "implicitly restarted Arnoldi method" (IRAM) to solve symmetric, non-symmetric, and generalized eigenvalue problems in large systems and works especially efficient for sparse matrices.

The discussion in section 4.2.1 shows, that it is in principle possible to introduce complex variables in the Lanczos algorithm such that it can calculate the eigenvalues of complex symmetric matrices. Far from exceptional points in the parameter space one can find very good results. Tests with complex symmetric matrices have shown that the eigenvalues are determined with an accuracy comparable with the accuracy of algorithms for general complex symmetric matrices. This has in particular been checked for the STLM implementation mentioned above. The procedure can even succeed in the calculation of the degenerate eigenvalues at an exceptional point. This case has been observed. However, there were also cases in which the STLM routines failed completely to produce converged eigenvalues in the presence of an exceptional point. They use a variant of the QL algorithm with implicit shifts that is not able to extract the eigenvalues of the normal blocks appearing for the exceptional points in the tridiagonalized matrix. Thus, the convergence is not reliable.

The implicitly restarted Arnoldi method works efficiently and stable in the presence of exceptional points for the complex generalized eigenvalue problem appearing in the

calculations for the hydrogen atom required in chapter 5 and it is in general well suited for large sparse eigenvalue problems of general complex matrices. In particular, because of its stability at the branch point singularities of interest in this thesis it is the method of choice.

Since it ignores the complex structure of symmetric matrices with complex elements and performs the transformation to a tridiagonal form, the spectral transformation Lanczos method can solve large sparse complex symmetric eigenvalue problems faster than Arnoldi algorithms. As has been tested vectors $\boldsymbol{r}_i$ with vanishing real Euclidean norm in equation (4.16e) are rare events and, therefore, do normally not disturb the tridiagonalization. If special care is taken of the occurrence of exceptional points in the consecutive solution of the eigenvalue problem for the tridiagonal matrix, the Lanczos method may be a fruitful alternative. For example a QL algorithm which assumes a complex Hessenberg matrix may be used to get the eigenvalues reliably. Alternatively, the reduction to the Schur normal form may be applied to the much smaller matrices obtained after the Lanczos iteration. However, numerical roundoff errors are always possible during the Lanczos iteration due to small real Euclidean norms of the vectors $\boldsymbol{r}_i$ (cf. equations (4.16e) and (4.16f)) and one has to check if one can trust the results.

5 Detection of exceptional points in spectra of the hydrogen atom

The detection of exceptional points in spectra of the hydrogen atom in external fields is a nontrivial task in numerical calculations as well as in experimental observations. In numerical calculations one has to find degeneracies of complex eigenvalues in the form of branch point singularities, where a high-dimensional matrix representation is used. Experiments appropriate to find exceptional points demand the detailed analysis of photoionization cross sections for several dedicated combinations of external fields to extract the positions and widths of the resonances measured. It is the purpose of this section to elaborate and present methods to detect exceptional points in numerical data and to present typical results. Furthermore, a method which allows for finding exceptional points in experimental spectra is proposed. A more detailed discussion of the properties of exceptional points found numerically will be given in chapter 6.

In section 5.1 the Hamiltonian of the hydrogen atom in crossed external electric and magnetic fields is introduced and a short description of the matrix representation used for the numerical calculations is given. A powerful method for the search for the branch point singularities in spectra of the hydrogen atom is developed and discussed in section 5.2. Examples of exceptional points found in spectra of the hydrogen atom are given in section 5.3. Finally, a method which opens the possibility to detect exceptional points in experimental photoionization spectra is elaborated in section 5.4.

5.1 Hamiltonian and matrix representation

In this chapter the hydrogen atom in static crossed electric and magnetic fields is investigated and the following Hamiltonian is used. The electric field shall point in the x-direction and the magnetic field is orientated along the z-axis,

$$\boldsymbol{E} = E\hat{\boldsymbol{e}}_x \ , \qquad \boldsymbol{B} = B\hat{\boldsymbol{e}}_z \ . \tag{5.1}$$

The Hamiltonian without relativistic corrections and finite nuclear mass effects [83] reads

$$H = \frac{1}{2\mathrm{m_e}}\boldsymbol{p}^2 - \frac{1}{4\pi\varepsilon_0}\frac{e^2}{r} + \frac{1}{2}\frac{\mathrm{e}}{\mathrm{m_e}}BL_z + \frac{1}{8}\frac{\mathrm{e}^2}{\mathrm{m_e}}B^2(x^2+y^2) + \mathrm{e}Ex \ , \tag{5.2}$$

where $\boldsymbol{p}$ is the momentum of the electron, r its distance to the nucleus, and L_z the z-component of the angular momentum. It contains the Coulomb potential $\propto 1/r$, the

paramagnetic term $\propto BL_z$, the diamagnetic term $\propto B^2(x^2+y^2)$, and the potential due to the external electric field $\propto Ex$. After the introduction of atomic Hartree units (see appendix A.1.1), the Hamiltonian has the much simpler form

$$H = \frac{1}{2}\boldsymbol{p}^2 - \frac{1}{r} + \frac{1}{2}\gamma L_z + \frac{1}{8}\gamma^2(x^2+y^2) + fx \tag{5.3}$$

with the electric and magnetic field strengths $f = E/\mathrm{E}_0$ and $\gamma = B/\mathrm{B}_0$, respectively, where $\mathrm{E}_0 = 5.14 \times 10^{11}\,\mathrm{V/m}$ and $\mathrm{B}_0 = 2.35 \times 10^5\,\mathrm{T}$. The energy is measured in units of Hartree $\mathrm{E_h} = 4.36 \times 10^{-18}\,\mathrm{J} = 27.2\,\mathrm{eV}$.

For the numerical calculation of the energy eigenvalues in a matrix representation of the Hamiltonian (5.3) it is advantageous to transform the respective Schrödinger equation into dilated semiparabolic coordinates. This transformation is presented in detail in appendix B.1. The regularized form has the shape

$$\begin{aligned}\Big\{\Delta_\mu + \Delta_\nu - \left(\mu^2+\nu^2\right) + b^4\gamma\left(\mu^2+\nu^2\right)\mathrm{i}\frac{\partial}{\partial\varphi} - \frac{1}{4}b^8\gamma^2\mu^2\nu^2\left(\mu^2+\nu^2\right) \\ - 2b^6 f\mu\nu\left(\mu^2+\nu^2\right)\cos\varphi + 4b^2\Big\}\psi = \lambda\left(\mu^2+\nu^2\right)\psi\end{aligned} \tag{5.4}$$

with the dilated semiparabolic coordinates μ, ν, φ, and the free dilation parameter b. The corresponding matrix equation is a generalized eigenvalue problem with the eigenvalue

$$\lambda = -(1 + 2b^4 E)\ . \tag{5.5}$$

The form (5.4) with the term

$$\begin{aligned}\Delta_\mu + \Delta_\nu - \left(\mu^2+\nu^2\right) &= \frac{1}{\mu}\frac{\partial}{\partial\mu}\mu\frac{\partial}{\partial\mu} + \frac{1}{\mu^2}\frac{\partial^2}{\partial\varphi^2} + \frac{1}{\nu}\frac{\partial}{\partial\nu}\nu\frac{\partial}{\partial\nu} + \frac{1}{\nu^2}\frac{\partial^2}{\partial\varphi^2} - \left(\mu^2+\nu^2\right) \\ &= -2H_0\end{aligned} \tag{5.6}$$

already suggests that an adequate basis for the matrix representation is given by the eigenstates of the two-dimensional harmonic oscillator (see appendix B.2). Due to the appearance of the coordinates μ and ν a well suited complete basis set is given by the states

$$|n_\mu, n_\nu, m\rangle = |n_\mu, m\rangle \otimes |n_\nu, m\rangle\ , \tag{5.7}$$

where each of $|n_\mu, m\rangle$ and $|n_\nu, m\rangle$ represents an eigenstate of the two commuting operators

$$N = a_1^+ a_1 + a_2^+ a_2\ , \tag{5.8a}$$

$$L = \mathrm{i}(a_1 a_2^+ - a_1^+ a_2) = (q_1 p_2 - q_2 p_1) \tag{5.8b}$$

of the two-dimensional isotropic harmonic oscillator [84] with common eigenvalue m of L. The operators a_i and a_i^+ are the familiar ladder operators of the one-dimensional harmonic oscillator.

To calculate the resonances of the system the complex rotation method is used, which has proven to be a powerful method for the calculation of atomic resonance spectra [30, 31, 85]. Here, the direct approach introduced in section 3.4 can be applied to the matrix representation of the Schrödinger equation (5.4). The complex scaling is included via the dilation parameter b, where the transformation

$$b^2 = |b^2|\mathrm{e}^{\mathrm{i}\theta} \tag{5.9}$$

performs the complex rotation

$$\boldsymbol{r} \rightarrow \mathrm{e}^{\mathrm{i}\theta}\boldsymbol{r} \tag{3.4}$$

and leads to the complex scaled Schrödinger equation

$$\begin{aligned}\Big\{ &-2H_0 + |b|^4\mathrm{e}^{\mathrm{i}2\theta}\gamma\left(\mu^2+\nu^2\right)\mathrm{i}\frac{\partial}{\partial\varphi} - \frac{1}{4}|b|^8\mathrm{e}^{\mathrm{i}4\theta}\gamma^2\mu^2\nu^2\left(\mu^2+\nu^2\right) \\ &-2|b|^6\mathrm{e}^{\mathrm{i}3\theta}f\mu\nu\left(\mu^2+\nu^2\right)\cos\varphi + 4|b|^2\mathrm{e}^{\mathrm{i}\theta} + \left(\mu^2+\nu^2\right)\Big\}\mathrm{e}^{-\mathrm{i}2\theta}\psi = 2|b|^4E\left(\mu^2+\nu^2\right)\psi\end{aligned} \tag{5.10}$$

with a non-Hermitian matrix representation in the form

$$\boldsymbol{A}(\gamma, f)\Psi = 2b^4E\boldsymbol{C}\Psi\ , \tag{5.11}$$

where $\boldsymbol{A}(\gamma, f)$ is a complex symmetric matrix and $\boldsymbol{C}$ is real symmetric positive definite. Above the ionization threshold, resonances are uncovered as complex energies E, where the real and imaginary parts represent the positions and widths of the resonances as discussed in chapter 3.

The Hamiltonian has two constants of motion, namely the energy and the parity with respect to the ($z = 0$)-plane. The latter symmetry opens the possibility to separate eigenstates by their z-parity and to consider the associated subspaces separately. If one uses basis states with defined z-parity the matrix representation decomposes in two independent blocks. If not stated otherwise, the examples discussed in this thesis are given for even z-parity.

The computation of the eigenvalues was performed by applying the ARPACK library (cf. section 4.2.3 and reference [82]). For typical calculations used, the number of basis states was in the order of 10,000 to 12,300. The exact determination of the positions of exceptional points up to four valid digits often required larger matrices with up to 17,300 states. If the matrices $\boldsymbol{A}$ and $\boldsymbol{C}$ are built up appropriately, they have a band structure. Typical matrix sizes and band widths used in the calculations are listed in table 5.1 in dependence of the oscillator quantum numbers $n = n_\mu + n_\nu$.

5.2 Procedure for the search for exceptional points

The Hamiltonian in the Schrödinger equation (5.10) is non-Hermitian. Two parameters, viz. the strengths of the external electric and magnetic fields, are available to influence

Table 5.1: Typical matrix sizes used in the calculations for the hydrogen atom in crossed external fields. $n = n_\mu + n_\nu$ is the highest oscillator level included. The lowest oscillator level was always 0. The band width obtained for the matrix structure realized in the program is measured for the complete band, i.e., all states left and right from the diagonal are counted.

n	basis states	band width
30	5 456	577
37	9 880	839
40	12 341	967
45	17 296	1 199

the values of the resonances and, thus, it should be possible to produce degeneracies of the complex resonance energies. Exceptional points do exist in atomic spectra if the fields can be chosen in such a way that a coalescence of two states occurs. The crossed fields hydrogen system fulfills all necessary conditions for the appearance of exceptional points, however, one has to find them in the spectrum to proof their existence. It is a nontrivial task to search for these degeneracies. The variation of the parameter values γ and f does not lead to clear indications for degeneracies, and, it is not known in advance which parameter values are a good choice for starting the search.

Examples for two different parameter regions are shown in figures 5.1 and 5.2. In the first example one can see resonances which behave obviously very regularly under changes of the two field strengths. Each symbol type belongs to one parameter set. The paths of the resonances in the complex energy plane are almost parallel to each other and do not indicate intersections. In the second example a more irregular behavior can be observed. The resonances move in different directions and it is even hardly possible to track the paths of some of the resonances and to relate the resonances of consecutive steps. Here, branch point degeneracies are expected to occur more likely.

A direct search by minimizing the distance between two arbitrary resonances did not lead to the discovery of exceptional points, however, exploiting the properties of the branch point singularities has been very successful. In particular, the permutation of the two eigenvalues involved in the singularity provides a clear signature which can be used to detect exceptional points and to scan a larger area of the parameter space, namely the complete circular surface, at once. A good choice for a closed loop is a "circle" in the parameter space of the two field strengths with a radius $\delta < 1$ chosen relative to the center (γ_0, f_0),

$$\gamma(\varphi) = \gamma_0(1 + \delta\cos\varphi)\ , \tag{5.12a}$$

$$f(\varphi) = f_0(1 + \delta\sin\varphi)\ . \tag{5.12b}$$

A fundamental advantage of the method is the possibility to automatize the procedure up to a certain extent. If the steps on the circle are chosen small enough, the resonances

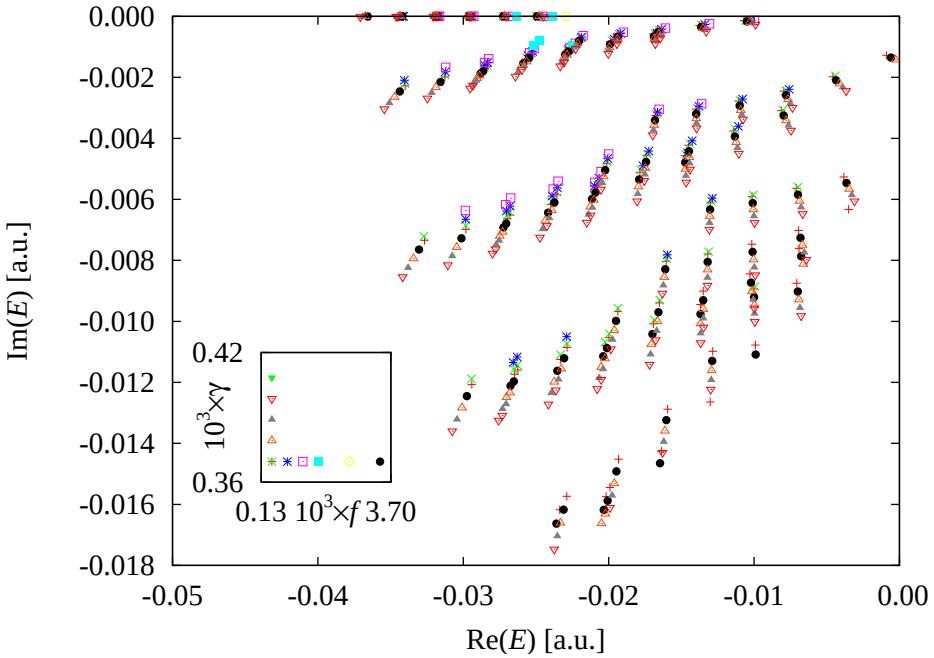

Figure 5.1: Resonances in spectra of the hydrogen atom in crossed external fields for a regular part of the parameter space. Each symbol type represents converged resonances in the energy range shown for a given parameter set. The parameters were chosen on two lines. First, γ was varied in the range $4.3\times10^{-4} < \gamma < 3.4\times10^{-3}$ for fixed $f = 3.7\times10^{-4}$, then f was chosen $3.7 \times 10^{-4} < f < 4.1 \times 10^{-4}$ for fixed $\gamma = 4.3 \times 10^{-4}$ (see inset).

of two consecutive steps can be mapped unambiguously and their motion in the complex energy plane can be followed. A successful sequence for the detection of exceptional points consists of four steps.

1. A parameter region with resonances close to each other must be searched to have a high probability to find exceptional points. Then, the parameter space region of interest must be divided such that circles of the type (5.12a), (5.12b) can be traversed with a reasonable radius. A partitioning as shown in figure 5.3 has turned out to be a good choice. The circle form (5.12a), (5.12b) represents the best method to avoid abrupt changes in the behavior of the resonances when one crosses over from the variation of one of the field strengths to the other. In the parameter region shown in figure 5.2 typically between 20 and 30 steps on a radius $\delta \approx 10^{-2}$ have proven to provide a good filtering.

2. Eigenvalues which do not return to their starting point after the parameter space circle is closed, are marked. In a second step one has to decide if they are good candidates for exceptional points or if they do not return due to effects at the border of the energy range considered for the calculation. In particular, an unambiguous

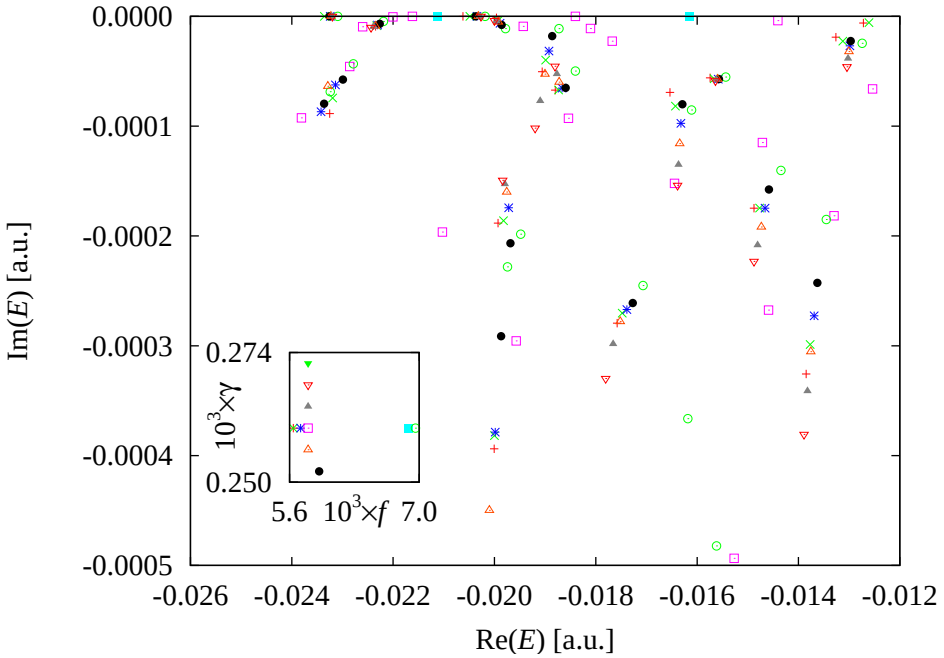

Figure 5.2: Resonances in spectra of the hydrogen atom in crossed external fields for a part of the parameter space with irregular motions of the resonances. As in figure 5.1 each symbol type represents converged resonances of one parameter set. The parameters were varied in the ranges $5.64\times10^{-3} < \gamma < 6.92\times10^{-3}$ and $2.52\times10^{-4} < f < 2.72\times10^{-4}$ (see inset).

permutation of two eigenvalues is a proof for the existence of an exceptional point.

3. If two eigenvalues which (can) belong to an exceptional point have been found, the degeneracy must be determined by minimizing the distance of the two complex energies. This can be performed with a two-dimensional root search when the two eigenvalues have clearly been identified and are sufficiently separated from other eigenvalues.

4. After the degeneracy has been found numerically a last circle with a small radius (typically $\delta \approx 10^{-12}$) around the parameter point at which the degeneracy occurs, is used to decide whether the branch point singularity structure is present and whether the degeneracy found is really an exceptional point.

5.3 Examples for exceptional points

With the method described above, exceptional points have been found for the first time in spectra of the hydrogen atom in static external fields [86]. Figure 5.4(a) shows a typical

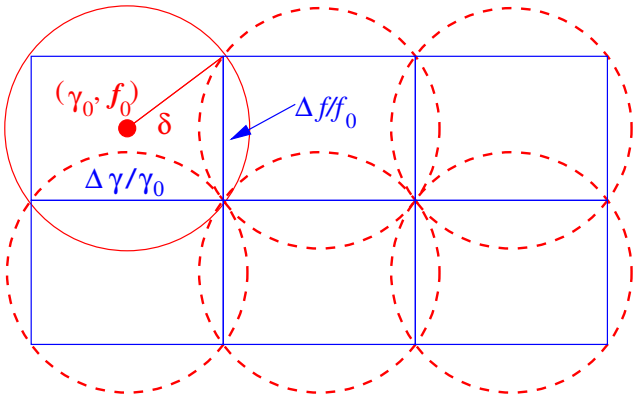

Figure 5.3: Partitioning of the (γ, f) parameter space used for the search for exceptional points. The parameter space region is divided such that the radii of the circles are in the range $\delta \approx 10^{-2}$, which leads to a sufficiently clear identification of the resonances.

result obtained in a numerical calculation. The squares and the diamonds represent one of the eigenvalues at different field strengths, respectively. In this example, using 20 steps on the circle in parameter space has been sufficient to obtain a clear signature of the branch point singularity. The "radius" of the circle according to equations (5.12a) and (5.12b) was $\delta = 0.01$. This value is sufficiently large to have an exceptional point inside the circular surface with a high probability and is small enough to track the paths of the eigenvalues with a low number of calculations. Figure 5.4(b) shows the position of the degenerate eigenvalues (marked by the blue arrow) in the complex energy plane among the resonances in their vicinity.

Examples for parameter values of exceptional points and the position of the degenerate eigenvalues in the complex energy plane are given in table 5.2. The values were obtained by minimizing the distance of two eigenvalues which indicated a branch point singularity. The degeneracy of the two eigenvalues, the existence of only one eigenvector, and the permutation of eigenvalues were used to identify the exceptional points. In the calculations the relative difference $|E_1 - E_2|/|E_1|$ of the two eigenvalues could be reduced down to 10^{-13}. However, this is only the result for a single matrix representation. More critical is the influence of the complex rotation on the matrix with finite size. Using oscillator levels up to 45 (see table 5.1) the convergence of typically three to four valid digits in the parameters as well as in the energies can be achieved. The convergence was checked with the stability of the results against changes in the matrix size and the complex parameter b.

5.4 Exceptional points in experimental data

In experiments the complex eigenvalues cannot be obtained directly. But it is possible to measure the photoionization cross section and to extract the energy (real part of a com-

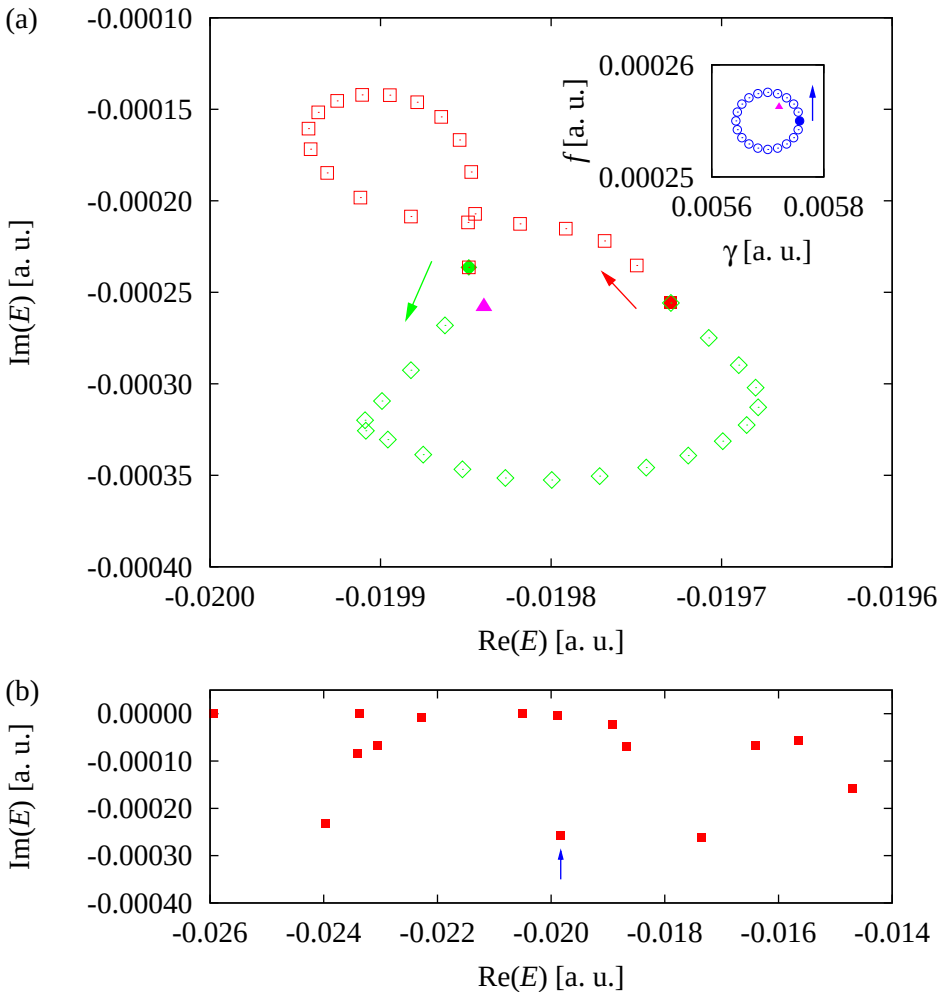

Figure 5.4: (a) Paths of the two eigenvalues which degenerate at the exceptional point in the complex energy plane. The squares and the diamonds represent one of the eigenvalues, respectively. Each point of one eigenvalue belongs to a different set of parameters. The path in the field strength parameter space is a circle defined in equations (5.12a) and (5.12b) with $\delta = 0.01$ (see inset). The first set of parameters and the corresponding eigenvalues are represented by filled symbols. The arrows indicate the direction of progression. The filled triangle marks the position of the exceptional point in the parameter space and the corresponding complex energy of the degenerate resonances. (b) Resonances in the complex energy plane for the parameter values $\gamma = 0.00572$ and $f = 0.000256$ (atomic units) at the exceptional point. The position of the two degenerate eigenvalues is marked by the blue arrow.

Table 5.2: Examples for exceptional points in spectra of the hydrogen atom in crossed magnetic (γ) and electric (f) fields. All values in atomic units. The numbers are used as labels to identify the exceptional points.

Number	γ	f	Re(E)	Im(E)
1	0.002335	0.0001177	−0.01767	−0.000103
2	0.002575	0.000117114	−0.015067	−0.0000823
3	0.002752	0.0001298	−0.015714	−0.00022637
4	0.0030152	0.0001231	−0.01209	−0.000099
5	0.003045	0.0001332	−0.015812	−0.0001896
6	0.0030460	0.000127302	−0.017624	−0.000087
7	0.0037915	0.0001535	−0.01240	−0.000164
8	0.004604	0.0002177	−0.022135	−0.00006878
9	0.004714	0.00021529	−0.01394	−0.00010
10	0.00483	0.000213	−0.01255	−0.00030
11	0.00529	0.0002011	−0.0150	−0.000136
12	0.00537	0.000214	−0.01884	−0.0000679
13	0.005388	0.0002619	−0.02360	−0.00015
14	0.00572	0.000256	−0.01984	−0.000258
15	0.00611	0.000256	−0.01593	−0.00024
16	0.00615	0.000265	−0.0158	−0.000374
17	0.00776	0.000301	−0.0179	−0.000756

plex eigenvalue) and width (imaginary part) of the resonances, which then can be used to search for exceptional points in experimental data. Due to the lack of experimental data suitable for the investigation of exceptional points, numerical photoionization cross sections are applied to demonstrate the applicability of the method. First the numerical determination of the photoionization cross section is performed before the signal is used to extract the complex energies and to verify the existence of exceptional points.

5.4.1 Photoionization cross section

Since the complex energy eigenvalues were obtained using the complex rotation technique it is straightforward to calculate the photoionization cross section with the same method. The procedure presented by Rescigno and McKoy [87] is based on the evaluation of the polarizability

$$P(E) = \langle \psi_0 | D(\boldsymbol{r}) | \psi_E \rangle \ , \tag{5.13}$$

where D is the dipole operator in atomic units for a given direction of polarization of the unit electric radiation field $\boldsymbol{E}_r$,

$$D(\boldsymbol{r}) = \boldsymbol{E}_r \cdot \boldsymbol{r} \ , \tag{5.14}$$

with the position $\boldsymbol{r}$ of the electron. Here, ψ_0 is the stationary state with energy E_0 and ψ_E is the ionized state. Formally ψ_E can be calculated as first-order perturbation wave function of an atom in the presence of an electric field,

$$(H - E)\psi_E = D(\boldsymbol{r})\psi_0 \,, \tag{5.15}$$

by inverting the operator $(H - E)$, which yields

$$P(E) = \left\langle \psi_0 \,\middle|\, D(\boldsymbol{r})\frac{1}{H - E}D(\boldsymbol{r}) \,\middle|\, \psi_0 \right\rangle . \tag{5.16}$$

With the complex energy eigenvalues E_i and the corresponding eigenfunctions ψ_i already calculated in the resonance search the evaluation of equation (5.16) can be done using the substitution

$$\frac{1}{H - E} = \sum_j \frac{\psi_j(\theta)\psi_j^+(\theta)}{E_j - E} \,. \tag{5.17}$$

Then, the photoionization cross section can be written in the form

$$\sigma(E) = 4\pi\alpha(E - E_0)\mathrm{Im}\left(\sum_j \frac{\langle\Psi_0|D|\Psi_j(\theta)\rangle^2}{E_j - E}\right) \,, \tag{5.18}$$

since $\sigma(E) = 4\pi\alpha(E-E_0)\mathrm{Im}(P(E))$. In equation (5.18), α is the fine-structure constant. It is important to note that the rotated eigenfunctions calculated with the complex rotation method are used in equation (5.18), where the rotation angle θ is compensated during the calculation. In converged spectra, the result is independent of the rotation angle θ.

5.4.2 Extracting complex energies from experimental data

Due to the form (5.18) of the photoionization cross section, in which the resonance states $\Psi_j(\theta)$ contribute, a first assumption can be that they lead, at a branch point singularity, to a strong signal dominating the photoionization cross section. For a correct application of equation (5.18) the resonance eigenvectors $\Psi_j(\theta)$ have to be normalized with a c-product, which leads to a diverging behavior at the exceptional point. However, as can be shown this diverging behavior of the eigenvectors does not carry over to the photoionization cross section and does not directly lead to a characteristic signal applicable to verify exceptional points. A more detailed discussion of the properties of the cross section in the vicinity of exceptional points will be given in section 6.5. Here, a method based on the permutation behavior, which can be used to identify exceptional points reliably, is presented.

The form (5.18) of the photoionization cross section can be used to find the complex energy eigenvalues. In particular, one can exploit the Fourier transform, i.e., the time signal

$$c(t) = \int_{-\infty}^{\infty} \sigma(E)\mathrm{e}^{\mathrm{i}Et}\,\mathrm{d}E \,, \tag{5.19}$$

which has the dominant structure

$$c(t) = \sum_j a_j \exp(\mathrm{i}E_j t) \ . \tag{5.20}$$

The form (5.20) is well suited for the application of the harmonic inversion method [88], which allows for the calculation of the complex energies E_j with a high precision. The key idea of the method is to determine the time signal on K values located on an equidistant grid $c_n = c(t_n)$. Then, the nonlinear set of equations

$$c_n = \sum_j a_j \exp(\mathrm{i}E_j t) \ , \quad n = 0, 1, \ldots, 2K-1 \tag{5.21}$$

is solved to extract the complex energies E_j and the amplitudes a_j of the sum (5.20). There are several methods to solve these equations efficiently [89].

With this knowledge, a search for exceptional points in an experiment starts with the measurement of the photoionization cross section for different field strengths, which are located on a closed loop in the (γ, f)-space, e.g., on a circle of the type defined in equations (5.12a) and (5.12b). For each measurement, one obtains a spectrum whose time signal is calculated with a Fourier transform. Then the Harmonic inversion method is applied to extract the complex energies of the resonances. The energy values are drawn in a diagram. After these steps, the same method which is used to search for branch point singularities in numerical calculations can be applied to the experimental results. The diagrams can be used to look for the characteristic open curves of single eigenvalues. Figure 5.5(a) shows an example of a typical result for the photoionization cross section with the bound state energy $E_0 = -0.125$ ($n = 2$, p-orbital) for different field strengths which are located on a closed loop in the parameter space. The loop encircles an exceptional point. Although not experimental but theoretical photoionization spectra have been used as input for the calculations, it is obvious that it is possible to extract the complex energies from a typical cross section as it is obtained in an experiment. In figure 5.5(b) one can see the paths of complex eigenvalues extracted from the spectra. In the example 16 cross sections were used. This number is sufficient to give a clear indication of an exceptional point as shown in figure 5.5(b). That is, with the harmonic inversion method, it is possible to extract the complex eigenvalues of resonances from experimental photoionization cross sections and to detect branch points of resonances in experimental data. This opens the way for the experimental observation of exceptional points in atomic spectra.

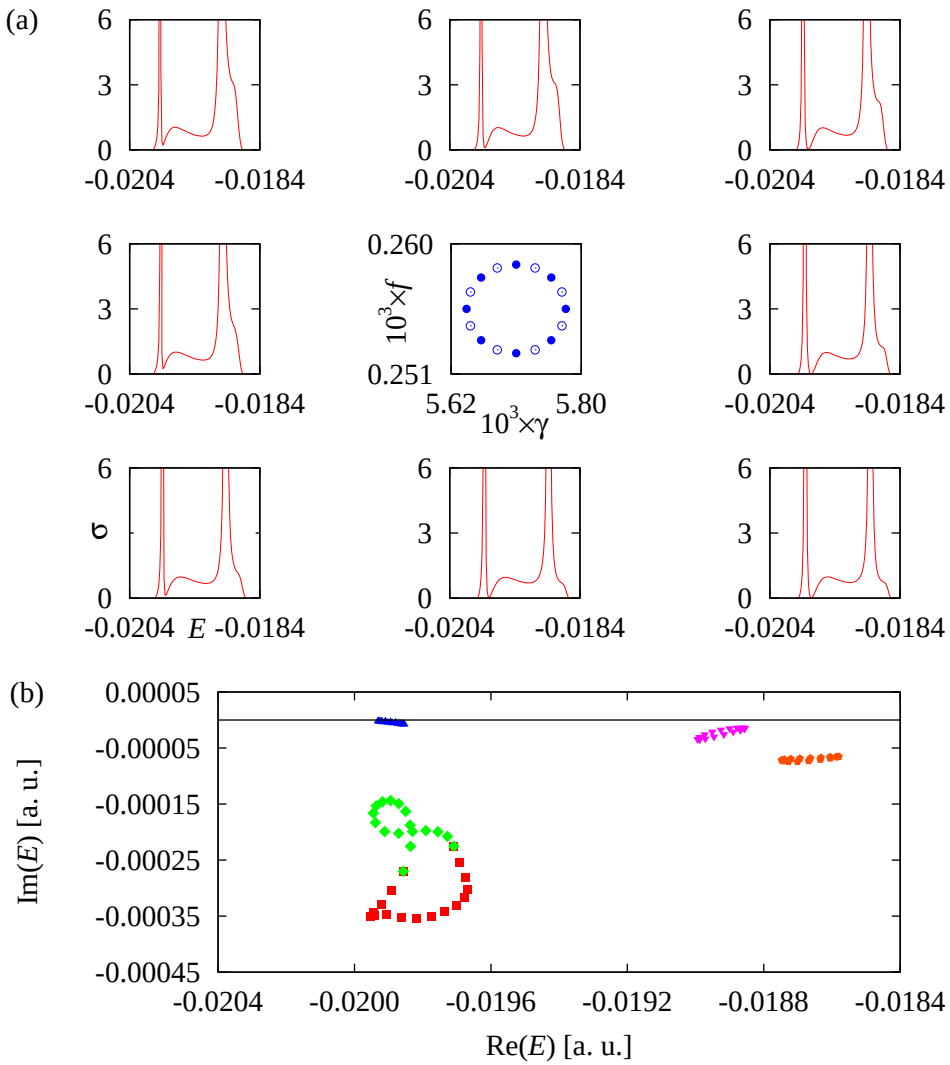

Figure 5.5: (a) Photoionization cross section of the energy range in which two eigenvalues connected with an exceptional point appear. The cross section is shown for eight different pairs of parameter values γ and f located on a circle around the exceptional point. (b) Complex energy eigenvalues extracted from the cross sections with the harmonic inversion method. Each eigenvalue is drawn with a different symbol. Altogether, 16 pairs of parameter values were used. In (a), every second cross section is shown. The signature of a branch point singularity connected with the two eigenvalues labeled with squares and diamonds, respectively, is clearly visible.

6 Properties of exceptional points in spectra of the hydrogen atom

After a method to detect exceptional points in numerical calculations has been presented in chapter 5, this chapter is devoted to a more detailed discussion of some properties found for the exceptional points in spectra of the hydrogen atom. An analysis of the eigenvalues is presented as well as the investigation of the phase behavior of the wave functions in the vicinity of the branch point singularities.

A matrix model adequate to describe two resonances in the vicinity of an exceptional point is presented in section 6.1. Section 6.2 starts with the properties of the complex energy eigenvalues. The local structure at the exceptional points (section 6.2.1), the shape of the eigenvalue loops for circles in the parameter space (section 6.2.2), and the rare case of structures which include three resonances (section 6.2.3) are discussed. In section 6.3 it is demonstrated that the geometric phase typical for exceptional points can be found for the eigenvectors determined in the numerical calculations. Furthermore, it will be shown that the exceptional points in the spectra of the hydrogen atom are closely related with avoided level crossings in section 6.4. The diverging behavior of dipole matrix elements and the regular shape of the observable photoionization cross section at exceptional points is discussed in section 6.5.

6.1 Matrix model for the description of two resonances close to an exceptional point

Two-dimensional matrix models with a complex parameter have proven to give a good description of the two complex eigenvalues in the vicinity of exceptional points and can also provide good results for the resonances of the hydrogen atom in external fields. However, for some effects they are not sufficient and the actual influence of the two real parameters γ and f must be taken into account. A more adequate description is given by

$$\boldsymbol{M} = \begin{pmatrix} a_0 + a_\gamma(\gamma-\gamma_0) + a_f(f-f_0) & b_0 + b_\gamma(\gamma-\gamma_0) + b_f(f-f_0) \\ b_0 + b_\gamma(\gamma-\gamma_0) + b_f(f-f_0) & c_0 + c_\gamma(\gamma-\gamma_0) + c_f(f-f_0) \end{pmatrix} . \tag{6.1}$$

This two-dimensional matrix is still a very simple model because it includes only the two states involved in the exceptional point and ignores couplings with other levels.

Furthermore, a linear dependence of the matrix elements on the two field strengths is assumed, which is certainly only true for small distances to the center point (γ_0, f_0). In contrast to the simple model used in section 2.3, however, it includes two real parameters with complex prefactors $a_{\gamma,f}$, $b_{\gamma,f}$, $c_{\gamma,f}$ and correctly reproduces the matrix shape of the full Hamiltonian to lowest order. In a power series expansion its eigenvalues fulfill the relations

$$\lambda_1 + \lambda_2 = \mathrm{tr}(\boldsymbol{M}) = A + B(\gamma - \gamma_0) + C(f - f_0) \,, \tag{6.2a}$$

$$\begin{aligned}(\lambda_1 - \lambda_2)^2 = \mathrm{tr}(\boldsymbol{M}) - 4\mathrm{det}(\boldsymbol{M}) = D + E(\gamma - \gamma_0) + F(f - f_0) + G(\gamma - \gamma_0)^2 \\ + H(\gamma - \gamma_0)(f - f_0) + I(f - f_0)^2\end{aligned} \tag{6.2b}$$

with new coefficients $A, B, C, D, E, F, G, H, I$. Since the eigenvalues do not change for a similarity transformation of the matrix $\boldsymbol{M}$ and the explicit choice of the matrix is not relevant, the representation (6.2a) and (6.2b) is more suitable than equation (6.1), in which more coefficients appear. The coefficients can be determined with a fit of the exact quantum energies to equations (6.2a) and (6.2b) in a region of the parameter space in which only two resonances are relevant. A fit for 6 different parameter sets[1] yields the 9 coefficients A, B, C, D, E, F, G, H, I and, thus, determines completely the two eigenvalues of the model (6.1) in dependence of the deviations from the center point (γ_0, f_0).

6.2 Properties of the eigenvalues

6.2.1 Local structure of the degeneracies

Exceptional points are square root branch points and the local structure of the eigenvalues around an exceptional point should be reflected in the dependence of the complex energy eigenvalues on the parameters. In particular, in a close vicinity of the exceptional point the energies should to lowest order depend on the parameters γ and f in the form of a square root function. An illustration of this behavior is given in figure 6.1, where the real and the imaginary part of two coalescing eigenvalues in the vicinity of the exceptional point labeled 12 in table 5.2 is drawn. In the figure, δ represents a parameter which defines a line via equations (5.12a) and (5.12b), where now the angle φ is set to a fixed value, δ is varied and the "center" is set to $(\gamma_0, f_0) = (\gamma^{(\mathrm{EP})}, f^{(\mathrm{EP})})$, i.e., $\delta^{(\mathrm{EP})} = 0$ corresponds to the exceptional point. Square root functions were fitted to the data points and lead to a good correspondence very near to the exceptional point. They are drawn with blue lines in figure 6.1. For larger distances deviations are visible, however, the *local* square root shape of the energies is clearly demonstrated.

[1] Six differences $\lambda_1 - \lambda_2$ are required to determine D, E, F, G, H, and I. Three of the same parameter sets can be used to set A, B, and C with the sum $\lambda_1 + \lambda_2$.

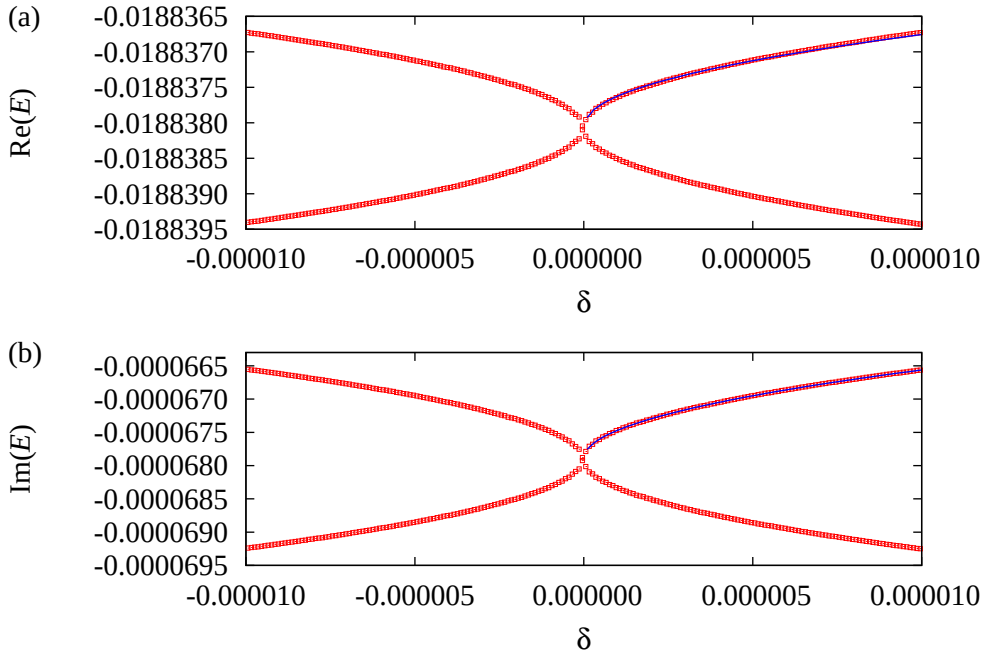

Figure 6.1: Local structure of two complex eigenvalues in the vicinity of the exceptional point labeled 12 in table 5.2. The real (a) and the imaginary (b) part of the complex energy (red squares) are shown for a line represented by the parameter δ, a constant angle φ, and $(\gamma_0, f_0) = (\gamma^{(\mathrm{EP})}, f^{(\mathrm{EP})})$ in equations (5.12a) and (5.12b), i.e., $\delta^{(\mathrm{EP})} = 0$. Square root functions fitted to the data points and drawn with blue lines demonstrate the local square root branch point structure.

6.2.2 Shapes of the eigenvalue loops

As can be seen in figure 5.4(a) the shape of the paths covered by the two energy eigenvalues differs considerably from the semicircle form obtained for a small loop in the simple two-dimensional matrix model in figure 2.4(b) on page 25. For the parameter space circle used in figure 5.4 the form of the representation of the Hamiltonian must be taken into account. A good description of the complicated behavior is possible with the model (6.2a), (6.2b). Using this matrix, a more detailed investigation of the phenomenon is done in figure 6.2. Here a circle around the exceptional point, which is always located exactly in the center, is performed for three different radii. For radii $\delta = 0.03$ and $\delta = 0.01$ (see figures 6.2(a) and (b)) the complicated structure already known from figure 5.4(a) appears. The deformations of the eigenvalue paths can be reproduced with the matrix (6.1). The lines in figures 6.2(a) and (b) represent the positions of the two model eigenvalues λ_1 and λ_2 for the same parameter space circle which was used for the exact quantum resonances. The very good agreement demonstrates that it is possible to describe the local structure of the resonances at an exceptional point with a simple two-

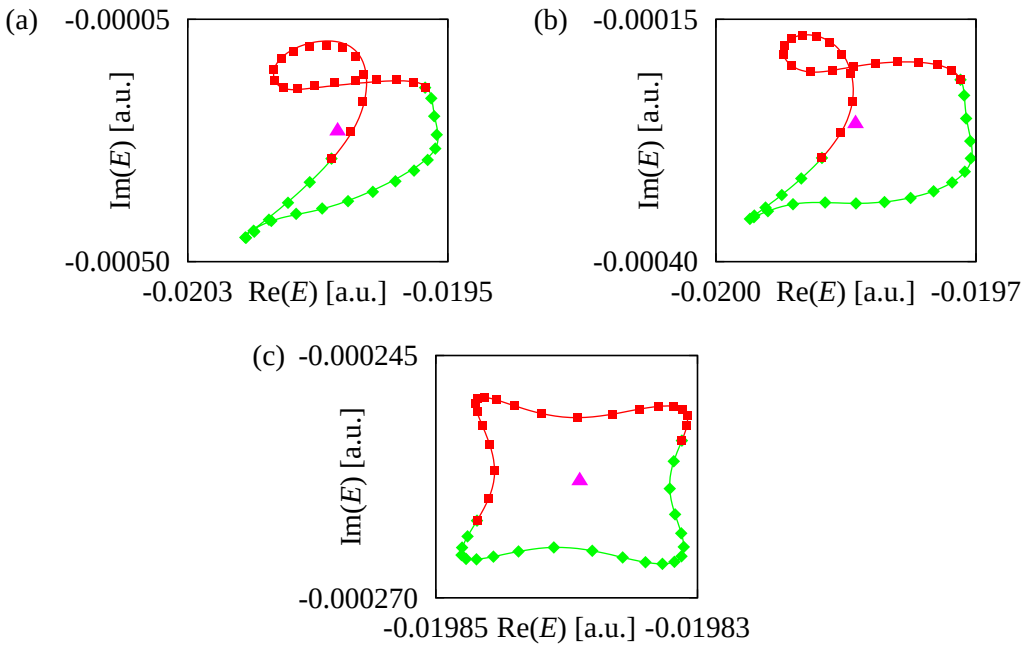

Figure 6.2: Paths of the two eigenvalues considered in figure 5.4 for different radii of the parameter space circle (5.12a), (5.12b), where the center (γ_0, f_0) was always chosen to be exactly the exceptional point. (a) $\delta = 3 \times 10^{-2}$, (b) $\delta = 10^{-2}$, (c) $\delta = 10^{-4}$. The position of the resonances at (γ_0, f_0) is marked by a triangle in each figure. The squares and diamonds represent the exact quantum resonances. The lines represent the eigenvalues of the two-dimensional matrix model (6.1), whose coefficients have been fitted to the numerical results of the exact quantum calculations.

dimensional model that ignores the influence of further resonances even if complicated structures of the eigenvalue paths appear.

Figure 6.2(c) shows a circle around the same exceptional point for the much smaller radius $\delta = 10^{-4}$, where the shape of the paths becomes more similar to the semicircle known from figure 2.4(b). The position of the degenerate eigenvalues for the parameters chosen at the exceptional point, which is marked by the triangle in figure 6.2(c), now is located in the center of the enclosing eigenvalue trajectories. However, it is not a perfect semicircle. This effect is a result of the dependence on two real parameters with two complex prefactors as introduced in the model (6.1). While the models using one complex parameter (cf. section 2.3) lead to a perfect semicircle as is demonstrated with the power series expansion (2.9) on page 25, this is not true for the description (6.1). With a short calculation it can be shown that a fractional power series expansion similar

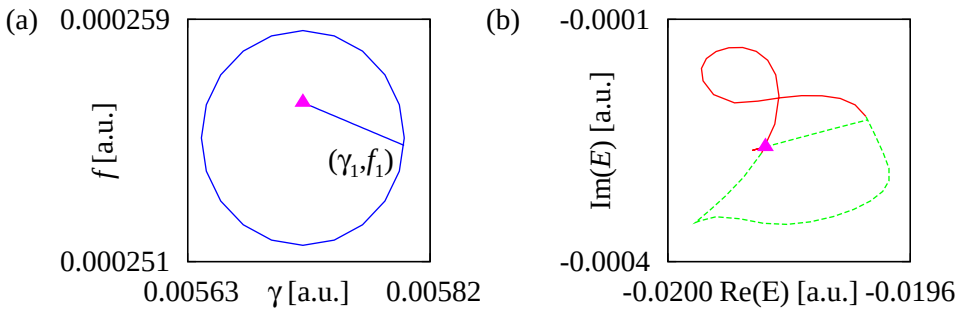

Figure 6.3: (a) A circle in the parameter space is chosen such that it goes through the parameter set (γ_1, f_1) at which one of the energy eigenvalues returns to its position at the exceptional point. A straight line connects the exceptional point and the parameter set (γ_1, f_1). (b) Paths of the two numerically exact complex energies for the circle and the straight line described in (a).

to equation (2.9) for the model (6.2a), (6.2b) to lowest order reads

$$\lambda_{1,2} = \frac{A}{2} \pm \frac{1}{2}\sqrt{\frac{E\gamma_0 + Ff_0}{2}\delta}\,\sqrt{1 + \frac{E\gamma_0 - Ff_0}{E\gamma_0 + Ff_0}\mathrm{e}^{-\mathrm{i}2\varphi}}\;\mathrm{e}^{\mathrm{i}\varphi/2} \tag{6.3a}$$

in the case $|E\gamma_0 - Ff_0| < |E\gamma_0 + Ff_0|$ or, if $|E\gamma_0 - Ff_0| > |E\gamma_0 + Ff_0|$,

$$\lambda_{1,2} = \frac{A}{2} \pm \frac{1}{2}\sqrt{\frac{E\gamma_0 - Ff_0}{2}\delta}\,\sqrt{1 + \frac{E\gamma_0 + Ff_0}{E\gamma_0 - Ff_0}\mathrm{e}^{\mathrm{i}2\varphi}}\;\mathrm{e}^{-\mathrm{i}\varphi/2} \tag{6.3b}$$

where the second term under the second square root normally is large enough to have a considerable influence and leads to the modulation of the "radius" during the traversal of the semicircle which can be seen in figure 6.2(c). Again, the model fitted to the numerical data and shown with the lines in the figure perfectly reproduces the behavior.

Intersections of an eigenvalue path with itself are observed, which means that the eigenvalue can have the same complex energy for two different parameter sets. In figure 6.2(a) one can even see that the position of the exceptional point lies outside the area enclosed by the two eigenvalue paths. This is possible if *one* of the two eigenvalues (in this example obviously the resonance denoted by red squares) has the same complex energy as at the exceptional point for a second parameter set and the line "crosses" the exceptional point. The crossing of an eigenvalue line with the position of an exceptional point in the complex energy plane is drawn in figure 6.3. The parameter space circle plotted in figure 6.3(a) is chosen such that it goes directly through the point (γ_1, f_1) at which one of the resonances returns to its position at the exceptional point, which can be seen in figure 6.3(b). Additionally, the straight line shown in figure 6.3(a) is performed. For this line one observes one of the resonances (denoted by the dashed green line in

figure 6.3(b)) which leaves the position of the exceptional point. The second resonance (solid red line) also departs from the exceptional point but returns to its original position on the same path.

6.2.3 Structures with three resonances

In the high-dimensional matrix representation of the hydrogen atom also connections between different exceptional points can be observed. An example is given in figure 6.4, where a structure with three resonances is shown. In figure 6.4(a) obviously a permutation of three eigenvalues can be observed for a closed loop in the parameter space. From that behavior one can assume that an exceptional point consisting of three resonances which form a cubic root branch point singularity was detected. However, a more detailed analysis shows that this is not the case, however, there is a close relationship with a triple coalescence as will become clear below. There are two exceptional points located in the circular surface of the parameter space circle of the type (5.12a), (5.12b) used in figure 6.4(a). This can directly be shown if one chooses two different parameter loops with two different center points (γ_0, f_0) and smaller radii δ, which is done in figures 6.4(b) and (c). Then, one can observe that there are two exceptional points at which two of the three resonances form a square root branch point. The resonance denoted by pentagons in figure 6.4 is involved in both exceptional points.

Of course, it is not possible to describe a behavior of this kind with the two-dimensional matrix models used so far. At least a three-dimensional model is required to simulate three energy eigenvalues which are connected with each other. Indeed, it can be shown that it is possible to reconstruct the structures shown in figure 6.4 with a three-dimensional matrix model. In extension of the matrix (6.1) a good choice is a three-dimensional, symmetric matrix, whose elements are given by a power series expansion in the two field strengths γ and f around a center point (γ_0, f_0), viz.

$$\begin{aligned} M_{ij} = M_{i,j}^{(0,0)} &+ M_{i,j}^{(1,0)}(\gamma-\gamma_0) + M_{i,j}^{(0,1)}(f-f_0) + M_{i,j}^{(2,0)}(\gamma-\gamma_0)^2 \\ &+ M_{i,j}^{(1,1)}(\gamma-\gamma_0)(f-f_0) + M_{i,j}^{(0,2)}(f-f_0)^2 + M_{i,j}^{(3,0)}(\gamma-\gamma_0)^3 \\ &+ M_{i,j}^{(2,1)}(\gamma-\gamma_0)^2(f-f_0) + M_{i,j}^{(1,2)}(\gamma-\gamma_0)(f-f_0)^2 + M_{i,j}^{(0,3)}(f-f_0)^3 + \dots \end{aligned} \tag{6.4}$$

with $M_{ji} = M_{ij}$ and $i, j \in \{1, 2, 3\}$. The eigenvalues of this matrix model can, as in the two-dimensional case, be fitted to a matrix of this type. Since a model description for the eigenvalues λ is searched, the best method is to fit the coefficients of the characteristic polynomial

$$\lambda^3 + a\lambda^2 + b\lambda + c = 0 \tag{6.5a}$$

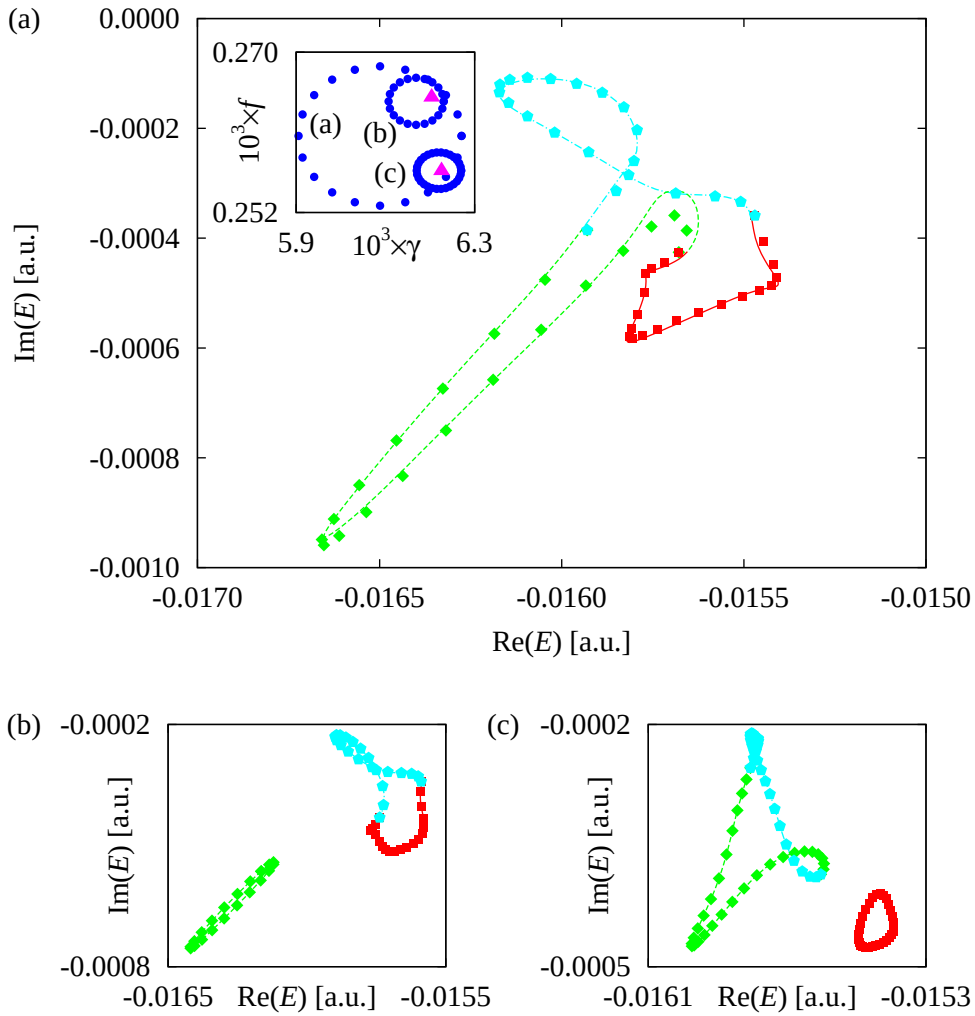

Figure 6.4: Illustration of a structure in the vicinity of two exceptional points in which three resonances are involved. Each of the resonances is denoted by a different symbol. In figure (a) the parameter space loop is chosen such that both exceptional points are located within the circular surface. The resonance marked by pentagons forms a branch point singularity with two further states at two different parameter values, which is shown with two additional parameter space loops in whose circular surface only one of the two exceptional points is located (figures (b) and (c)). The lines mark the eigenvalues of the three-dimensional model (6.4), (6.5a) fitted to the numerical data. The inset of figure (a) shows the three parameter space loops (circles) and the position of the two exceptional points (triangles).

with the familiar relations

$$a = -(\lambda_1 + \lambda_2 + \lambda_3) \ , \tag{6.5b}$$
$$b = \lambda_1\lambda_2 + \lambda_1\lambda_3 + \lambda_2\lambda_3 \ , \tag{6.5c}$$
$$c = -\lambda_1\lambda_2\lambda_3 \tag{6.5d}$$

to the exact numerical results. If the form (6.4) of the matrix is assumed, a, b, and c will also be given by a power series expansion in the two field strengths. For the discussion in figure 6.4 terms up to third order were included. This leads to 10 coefficients (similar to equation (6.4)) for each of the terms a, b, and c, and 10 combinations of field strengths are required to obtain 10 triples of eigenvalues for the relations (6.5b)–(6.5d). The eigenvalues for the three-dimensional matrix model agree very well with the numerically exact resonances and show that it is sufficient to take the three resonances into account to explain their behavior. The influence of further resonances can be ignored in the investigation of the threefold permutation. The model can even be used to predict the positions of the two exceptional points located within the parameter space loop. For the case shown in figure 6.4(a) the model predicts the positions of the two exceptional points labeled 15 and 16 in table 5.2 at ($\gamma_1 = 6.12 \times 10^{-3}, f_1 = 2.53 \times 10^{-4}$) and ($\gamma_2 = 6.15 \times 10^{-3}, f_2 = 2.68 \times 10^{-4}$), respectively, which approximates the results of the full quantum system very well.

The finding of the threefold permutation is especially interesting because it is strongly related to branching solutions beyond the typical square root branch point studied mostly in physical examples. In particular, the possibility for a cubic branch point in a three-dimensional symmetric matrix is the topic of current studies [90]. For a complex symmetric matrix a coalescence of N levels requires $(N^2+N-2)/2$ real parameters. That is, for $N = 3$ coalescing levels in the form of a cubic branch point singularity 5 parameters are necessary. That means for the hydrogen atom that additionally to the two field strengths γ and f three further parameters have to be introduced. This is a very complicated task and it was even difficult to find square root branch points in a two-dimensional parameter space. Already the presence of two closely related exceptional points in which altogether three resonances are involved as shown in figure 6.4 is a remarkable observation. The three additional parameters would be required to form a coalescence of both exceptional points or, in other words, they would be necessary to shift the three resonances such that they form a cubic root branch point in the five-dimensional parameter space.

6.3 Phase of the wave functions

A further property of exceptional points which can be checked in the numerical calculations is the phase change of one of the eigenvectors described with the equation

$$[\boldsymbol{x}_1, \boldsymbol{x}_2] \overset{\text{circle}}{\rightarrow} [\boldsymbol{x}_2, -\boldsymbol{x}_1] \tag{2.3}$$

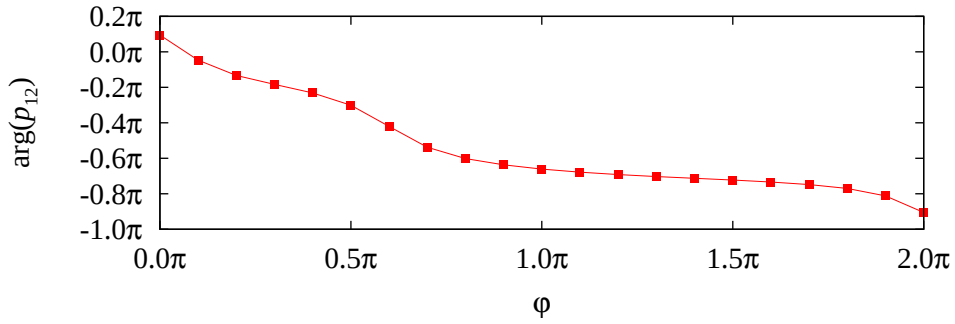

Figure 6.5: Phase of the complex matrix element p_{12} defined in equation (6.8). It changes its value by π during the traversal of the circle in parameter space. The result corresponds to the expected change in sign of *one* of the two eigenvectors.

in section 2.2. To demonstrate this phase change an orthogonality relation of the eigenvectors apart exceptional points can be exploited. In general, but not at the exceptional points, the eigenvectors of the resonances can be normalized such that

$$\langle \Psi_i | \boldsymbol{C} | \Psi_j \rangle = \delta_{ij} \tag{6.6}$$

with the matrix $\boldsymbol{C}$ from equation (5.11). With this relation the phase change of one of the eigenfunctions, when a circle around an exceptional point is performed, can be seen as a change in sign of an arbitrary matrix element

$$p_{12} = \langle \Psi_1 | \, \boldsymbol{M} \, | \Psi_2 \rangle \tag{6.7}$$

for the two eigenvectors $|\Psi_1\rangle$ and $|\Psi_2\rangle$ which describe the resonances associated with the exceptional point. A good choice for the matrix element is given by $\boldsymbol{M} = \mathbf{1}$, i.e.,

$$p_{12} = \langle \Psi_1 | \, \Psi_2 \rangle \, , \tag{6.8}$$

which can be calculated immediately since the eigenvectors are obtained easily in the form (6.6). For this normalization, the matrix element (6.8) is not diagonal and, thus, is adequate to investigate the phase behavior.

For the loop shown in figure 5.4(a), the matrix element p_{12} from equation (6.8) was calculated. The phase of the complex number, plotted in figure 6.5, changes its value by π. This clearly proves the change in sign of *one* of the two eigenstates as mentioned above.

6.4 Connection with avoided level crossings

There is a close relation between avoided level crossings of the real energies of bound states and exceptional points. As was demonstrated, the level repulsions of bound states

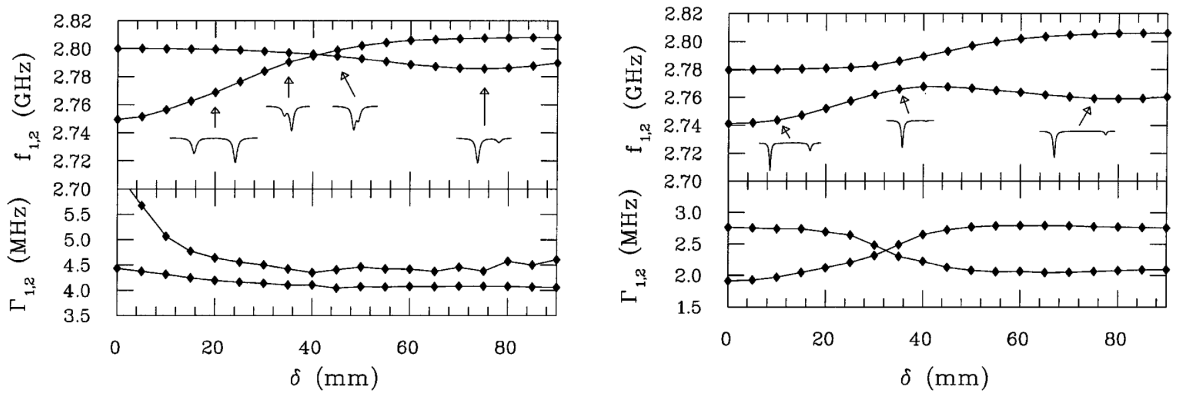

Figure 6.6: Resonances of the microwave experiment introduced in section 2.4.4 for two different fixed slit widths $s \neq s^{(\mathrm{EP})}$ (taken from reference [9]). The position of the Teflon stub, i.e., the second parameter is varied. On the left hand side a crossing of the frequencies $f_{1,2}$ and an avoided crossing of the widths $\Gamma_{1,2}$ can be observed. The opposite case can be seen on the right hand side.

of a Hermitian Hamiltonian which depends on one real parameter are associated with an exceptional point if the parameter is continued into the complex plane [2, 4]. A similar effect appears for the resonances of open quantum systems. Here, one can observe crossings or avoided crossings of the positions and widths of the resonances for lines in the parameter space which do not cross the exceptional point. An example for the microwave experiments introduced in section 2.4.4 is presented in figure 6.6. Here one of the two parameters, viz. the width s of the slit, is held constant at two different values apart from the exceptional point for the measurements displayed on the left hand side and on the right hand side. The position δ of the Teflon stub, which represents the second parameter, is varied. Since the exceptional point is not crossed on the parameter space line, no degeneracy is achieved. However, on the left hand side one can observe a crossing of the frequencies $f_{1,2}$ and an avoided crossing of the widths $\Gamma_{1,2}$. The opposite case can be seen on the right hand side.

Of course avoided level crossings of the energies or widths can also be observed in spectra of the hydrogen atom in external fields. Figure 6.7 shows the real part of the complex energy in dependence of a parameter α which defines a straight line of the form

$$\gamma = 0.80516 \times 10^{-2}\alpha \,, \tag{6.9a}$$

$$f = 0.32169 \times 10^{-3}\alpha \,, \tag{6.9b}$$

$$\gamma/f = 25.03 \tag{6.9c}$$

in the (γ, f)-space. The line is chosen such that it goes directly through the exceptional point labeled 12 in table 5.2. The position of the exceptional point is marked by the

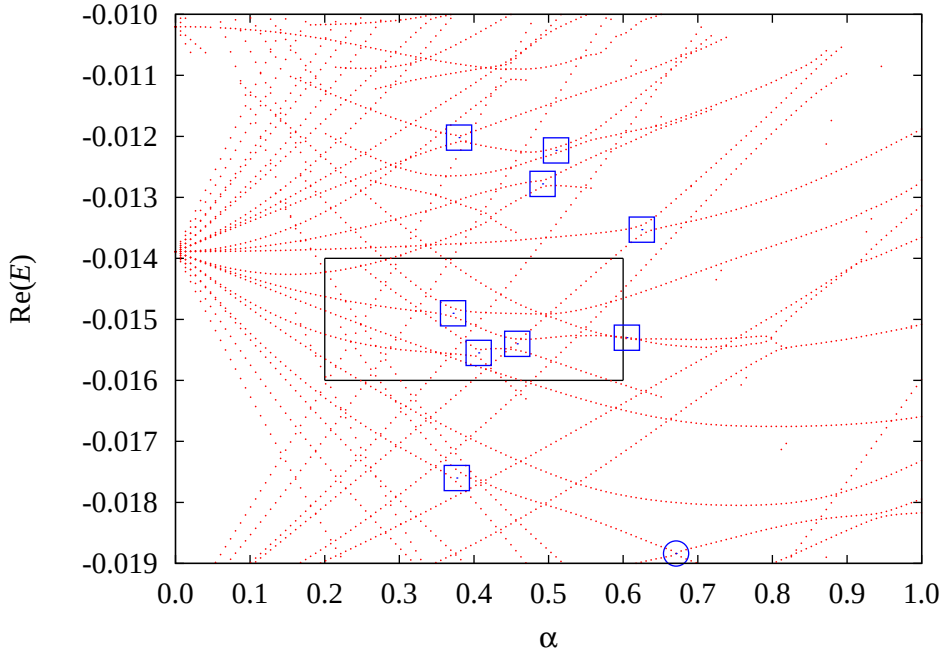

Figure 6.7: Real part of the complex energy as a function of the one-dimensional parameter α, $\gamma = 0.80516 \times 10^{-2}\alpha$, $f = 0.32169 \times 10^{-3}\alpha$, defined with equations (6.9a) and (6.9b). The blue circle marks an exceptional point. Avoided crossings (marked by blue squares) appear, which are connected with exceptional points. Only resonances with $|\mathrm{Im}(E)| < 0.0005$ are drawn to simplify the figure. The black frame marks the region investigated in detail in figure 6.8(a) to demonstrate how an avoided crossing leads to an exceptional point if the parameters are varied.

blue circle in the figure. In the vicinity of the parameter space line further exceptional points are located. Since the line does not cross these critical parameter values, the exceptional points lead to the avoided crossings in the energy or the widths, where the avoided energy (or real part) crossings are shown in the figure. They are marked by blue squares. The close connection between the avoided crossings and branch point singularities of exceptional points can be shown very directly. It is possible in all cases marked in figure 6.7 to vary the parameters γ and f such that a coalescence of the two eigenvalues forming the avoided crossing is achieved. That is, all avoided crossings found in the diagram are associated with exceptional points of the corresponding resonances. In all cases, where the description of the energy range under consideration is possible with the model (6.1), i.e., always if only two resonances are involved, the adjustment of the parameters γ and f leads to a branch point. Thus, exceptional points are the normal origin of narrow avoided level crossings.

A more detailed illustration is given in figure 6.8. The region marked by the black frame in figure 6.7 is magnified in figure 6.8(a). Three of the avoided level crossings are

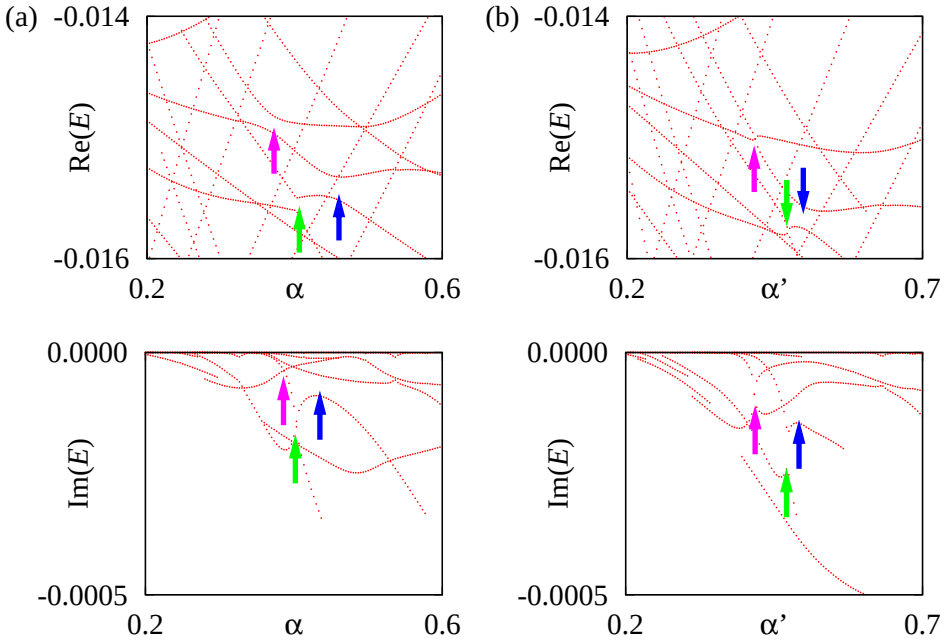

Figure 6.8: (a) Detailed illustration of the region marked by the black frame in figure 6.7. Three of the avoided energy crossings are included. In addition, the imaginary part is shown, which exhibits two crossings (magenta and green arrows) and one avoided crossing (blue arrow). (b) The same region is shown for the field strengths varied on the line $\gamma = 0.65378 \times 10^{-2}\alpha'$, $f = 0.28213 \times 10^{-3}\alpha'$ given by equations (6.10a) and (6.10b). One of the three exceptional points is located on this line and the corresponding avoided energy crossing marked by a magenta arrow in figure (a) has been transformed into a branch point singularity, where both the real and imaginary parts are identical. The other two encounters show at least one avoided crossing in the real or in the imaginary part.

included and, in addition, the imaginary part of the resonances is shown. The encounter of two resonances marked by the green arrow shows an avoided crossing in the real part and a crossing in the imaginary part. The blue arrow exhibits avoided crossings in the real as well as in the imaginary part. The encounter marked by the magenta arrow shows an avoided crossing of the real part which is accompanied by a crossing in the imaginary part. Its behavior changes for a slightly different line in the parameter space defined by

$$\gamma = 0.65378 \times 10^{-2}\alpha' \,, \tag{6.10a}$$

$$f = 0.28213 \times 10^{-3}\alpha' \,, \tag{6.10b}$$

$$\gamma/f = 23.17 \,. \tag{6.10c}$$

Now the avoided energy crossing is changed into a crossing, which can be seen in figure 6.8(b). The line (6.10a), (6.10b) goes exactly through the corresponding exceptional

point. As a consequence the avoided crossing is transformed into a branch point degeneracy at which both the real and imaginary parts are identical, whereas the other two encounters do not form a degeneracy. They belong to different exceptional points which are not crossed by the line. The encounter labeled with the blue arrows forms, again, an avoided crossing both in the real and in the imaginary part. The third encounter, which is marked by green arrows has inverted its behavior. Now, it forms a real part crossing and an avoided crossing of the imaginary part.

The connection between avoided crossings and exceptional points provides an additional possibility to detect the branch point singularities in spectra of the hydrogen atom. Exceptional points can be found if the real part of the complex resonance energies is plotted as a function of *one* parameter similar to α in equations (6.9a) and (6.9b). If avoided crossings of the energy are found, one can apply the method elaborated in section 5.2.

6.5 Dipole matrix elements and the photoionization cross section at exceptional points

The dipole matrix elements used to calculate the photoionization cross section (5.18) depend on the resonance wave functions ψ_E, which lead to a remarkable behavior at exceptional points. The resonances at the branch points are described by eigenstates which cannot be normalized with the c-product required for the complex rotation method (cf. section 3.3). It is a common property of the c-product normalized eigenvectors of complex symmetric matrices that their components diverge at exceptional points (see reference [2] and compare sections 2.4.3 and 2.5). That behavior can be observed directly for the normalized eigenvectors

$$\boldsymbol{x}_1(\kappa) = \frac{1}{\sqrt{\kappa^2 + \left(1 - \sqrt{1+\kappa^2}\right)^2}} \begin{pmatrix} -\kappa \\ 1 - \sqrt{1+\kappa^2} \end{pmatrix} , \tag{2.28a}$$

$$\boldsymbol{x}_2(\kappa) = \frac{1}{\sqrt{\kappa^2 + \left(1 + \sqrt{1+\kappa^2}\right)^2}} \begin{pmatrix} -\kappa \\ 1 + \sqrt{1+\kappa^2} \end{pmatrix} \tag{2.28b}$$

of the simple two-dimensional matrix model introduced in chapter 2 at the exceptional points $\kappa = \pm\mathrm{i}$. The diverging behavior must carry over to the dipole matrix elements and, indeed, the numerical results show that the resonance wave functions obtained with the complex rotation method lead to diverging dipole matrix elements. However, this is not an observable physical property because the single dipole matrix elements of the two identical wave functions at an exceptional point are not accessible. In particular, the photoionization cross section behaves regularly and does not diverge at an exceptional point, as was already mentioned in section 5.4.2 and as will be shown here.

To get a comprehensible explanation of the effects, one can investigate a close vicinity of the exceptional points. There, only the two resonances involved in the branch point singularity are important if they are sufficiently separated from all further resonances, which is in general possible since only a narrow region of the complex energy plane around two (almost) degenerate eigenvalues must be taken into account. In this case, one can restrict the discussion to a two-dimensional subspace spanned by the two relevant eigenvectors close to the exceptional point. To keep the discussion clear, the symmetric matrix model introduced in section 2.3 on page 24 is used,[2] the results, however, are valid for all complex symmetric matrices. The normalized eigenvectors, which correspond to the resonance wave functions ψ_E are given in this model by equations (2.28a) and (2.28b).

The dipole matrix elements have the form $P = \langle\psi_0|D(\boldsymbol{r})|\psi_E\rangle$ and the most general representation is given by a product $P_{1,2} = \boldsymbol{y} \cdot \boldsymbol{x}_{1,2}$ of the eigenvectors $\boldsymbol{x}_{1,2}$ with an arbitrary vector

$$\boldsymbol{y} = \begin{pmatrix} y_1 \\ y_2 \end{pmatrix} . \tag{6.12}$$

If now the squares of the dipole matrix elements, which are required for the photoionization cross section, are calculated for a small complex deviation δ from one of the two exceptional points,

$$\kappa = \mathrm{i} + \delta , \tag{6.13}$$

a fractional power series shows that the single contributions

$$\bar{P}_1^2 = (\boldsymbol{y} \cdot \boldsymbol{x}_1)^2 = \frac{\mathrm{e}^{\mathrm{i}3\pi/4}}{2\sqrt{2}} \frac{(y_1 + \mathrm{i}y_2)^2}{\sqrt{\delta}} + \frac{1}{2}(y_1^2 + y_2^2) + \frac{\mathrm{e}^{\mathrm{i}5\pi/4}}{8\sqrt{2}}(y_1^2 - 6\mathrm{i}y_1y_2 - y_2^2)\sqrt{\delta} + \mathrm{O}(\delta) , \tag{6.14a}$$

$$\bar{P}_2^2 = (\boldsymbol{y} \cdot \boldsymbol{x}_2)^2 = \frac{\mathrm{e}^{\mathrm{i}7\pi/4}}{2\sqrt{2}} \frac{(y_1 + \mathrm{i}y_2)^2}{\sqrt{\delta}} + \frac{1}{2}(y_1^2 + y_2^2) + \frac{\mathrm{e}^{\mathrm{i}\pi/4}}{8\sqrt{2}}(y_1^2 - 6\mathrm{i}y_1y_2 - y_2^2)\sqrt{\delta} + \mathrm{O}(\delta) \tag{6.14b}$$

diverge with $1/\sqrt{\delta}$. It is interesting to note that the sum of both contributions has always the value

$$(\boldsymbol{y} \cdot \boldsymbol{x}_1)^2 + (\boldsymbol{y} \cdot \boldsymbol{x}_2)^2 = y_1^2 + y_2^2 , \tag{6.15}$$

independently of the parameter κ, i.e., of the presence of the exceptional point, and of the matrix used. It is fulfilled for all eigenvectors $\boldsymbol{x}_{1,2}$ of a two-dimensional symmetric matrix. More interesting is, however, the sum

$$\bar{\sigma} = \frac{(\boldsymbol{y} \cdot \boldsymbol{x}_1)^2}{\lambda_1 - E} + \frac{(\boldsymbol{y} \cdot \boldsymbol{x}_2)^2}{\lambda_2 - E} , \tag{6.16}$$

[2] Note that in particular there is no difference in the behavior of the eigenvalues visible between the lowest order power series expansions (2.9) and (6.3a), (6.3b) if only the distance δ (or ϱ) is varied and the angle φ is kept constant.

which describes the contribution of the two resonances to the photoionization cross section with the eigenvalues

$$\lambda_1 = \sqrt{1+\kappa^2}\,, \tag{2.5a}$$

$$\lambda_2 = -\sqrt{1+\kappa^2} \tag{2.5b}$$

and a real variable E representing the energy. Here, one can also look at the contributions of the single eigenvalues and obtains in a fractional power series expansion around the branch point

$$\begin{aligned}\bar{\sigma}_1 = \frac{(\boldsymbol{y}\cdot\boldsymbol{x}_1)^2}{\lambda_1 - E} &= \frac{\mathrm{e}^{\mathrm{i}7\pi/4}}{2\sqrt{2}}\frac{(y_1+\mathrm{i}y_2)^2}{E\sqrt{\delta}} + f_1(E,y_1,y_2) + f_2(E,y_1,y_2)\sqrt{\delta} \\ &\quad + f_3(E,y_1,y_2)\delta + \mathrm{O}(\delta^{3/2})\,,\end{aligned} \tag{6.17a}$$

$$\begin{aligned}\bar{\sigma}_2 = \frac{(\boldsymbol{y}\cdot\boldsymbol{x}_2)^2}{\lambda_2 - E} &= \frac{\mathrm{e}^{\mathrm{i}3\pi/4}}{2\sqrt{2}}\frac{(y_1+\mathrm{i}y_2)^2}{E\sqrt{\delta}} + f_1(E,y_1,y_2) - f_2(E,y_1,y_2)\sqrt{\delta} \\ &\quad + f_3(E,y_1,y_2)\delta + \mathrm{O}(\delta^{3/2})\end{aligned} \tag{6.17b}$$

with rather complicated expressions $f_1(E,y_1,y_2)$, $f_2(E,y_1,y_2)$, and $f_3(E,y_1,y_2)$ which do not depend on δ. These parts diverge, however, $\bar{\sigma}_1$ and $\bar{\sigma}_2$ alone are not observable. The sum contributes to the photoionization cross section. In particular, at the exceptional point ($\delta = 0$) the two resonances overlap. For the sum one finds

$$\bar{\sigma} = 2f_1(E,y_1,y_2) + 2f_3(E,y_1,y_2)\delta + \mathrm{O}(\delta^2)\,, \tag{6.18}$$

that is, the photoionization cross section converges linearly to a constant value at the branch point.

Numerical calculations for the hydrogen spectra discussed in this thesis demonstrate the applicability of the simple model. For this purpose, the square modulus of the dipole matrix elements $\langle\Psi_0|D|\Psi_j(\theta)\rangle$ and the photoionization cross section (5.18) are calculated on a straight line of the form (5.12a), (5.12b) for a constant angle φ and variable distance δ to the exceptional point $(\gamma_0, f_0) = (\gamma^{(\mathrm{EP})}, f^{(\mathrm{EP})})$. The results have been verified for different angles φ.

Figure 6.9 shows the squares of the two isolated dipole matrix elements for the resonances which form the exceptional point labeled 12 in table 5.2. Both matrix elements behave like the approximate equations (6.14a) and (6.14b) of the simple two-dimensional model. The single terms $|P_1|^2$ and $|P_2|^2$ diverge in the form of a reciprocal square root which is shown with a fit of the numerical results to the function

$$P_{\mathrm{fit}}(\delta) = \frac{a}{\sqrt{\delta}} + b\,. \tag{6.19}$$

An excellent agreement can be observed. Additionally, the real and imaginary parts of the sum $P_1^2 + P_2^2$ are plotted. As expected from equation (6.15) for the two-dimensional model, this sum has a constant value.

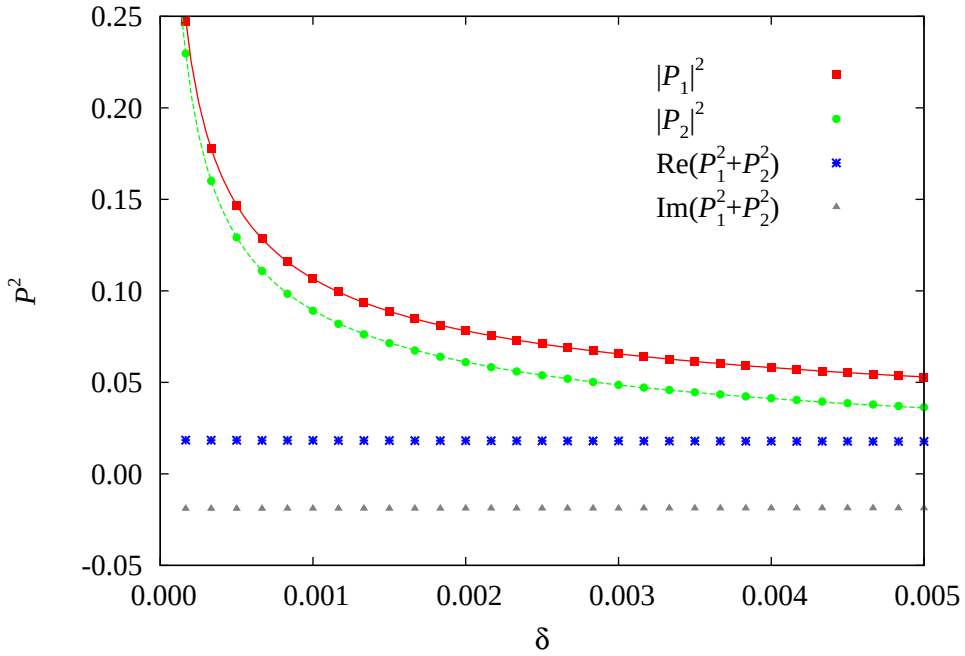

Figure 6.9: Squares P^2 of the dipole matrix elements forming the exceptional point labeled 12 in table 5.2 for a line of the form (5.12a), (5.12a) with the constant angle $\varphi = 0.7$ and $(\gamma_0, f_0) = (\gamma^{(\mathrm{EP})}, f^{(\mathrm{EP})})$. In both cases the square modulus diverges in the form of a reciprocal square root. A fit of the data points to a function of the form $a/\sqrt{\delta} + b$ which is expected from equations (6.14a) and (6.14b) is shown with the solid red and dashed green line. The real and the imaginary part of the sum $P_1^2 + P_2^2$ is also drawn.

The photoionization cross section $\sigma(\mathrm{Re}(E^{(\mathrm{EP})}))$ evaluated at the real part of the energy $E^{(\mathrm{EP})}$ at the exceptional point according to equation (5.18) is shown in figure 6.10 in dependence of the distance parameter δ. As can be seen directly in the figure the numerical data points (red points) converge linearly to a constant value for $\delta \to 0$. The red line represents a fit to the function

$$\sigma_{\mathrm{fit}}(\mathrm{Re}(E^{(\mathrm{EP})})) = a + b\delta \tag{6.20}$$

whose form is expected from the power series expansion (6.18) of the two-dimensional model. The comparison shows a good agreement.

In summary, the results for the hydrogen atom in crossed external fields demonstrate that single dipole matrix elements show a diverging behavior for resonance eigenstates at an exceptional point, however, the photoionization cross section behaves regularly and converges linearly to a constant value. Both observations can be explained with a simple two-dimensional matrix model, which provides an excellent qualitative description of the properties in the local vicinity of the branch point singularity. The lack of a characteristic

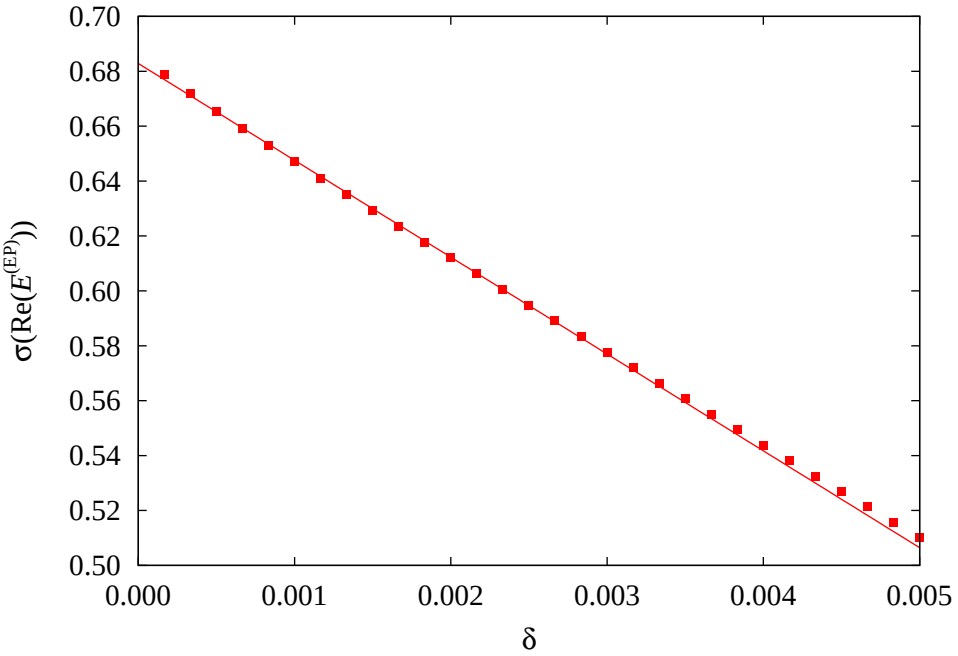

Figure 6.10: Photoionization cross section $\sigma(\mathrm{Re}(E^{(\mathrm{EP})}))$ with the bound state energy $E_0 = -0.125$ ($n = 2$, p-orbital). The numerical data (dots) converge linearly to a constant value as is expected from equation (6.18). Again, the line (5.12a), (5.12b) with constant angle φ and $(\gamma_0, f_0) = (\gamma^{(\mathrm{EP})}, f^{(\mathrm{EP})})$ is used.

signal in the cross section directly at the exceptional point made necessary the method introduced in section 5.4.2 to verify exceptional points in experimental data.

7 Influence of the transition state on the resonances of the hydrogen atom

Exceptional points are a phenomenon which appears for resonances of *open* quantum systems, i.e., they are closely related with the ionization mechanism. The energy range, which has been investigated in the discussions in chapters 5 and 6 exhibits a further property of the ionization process, viz. a close connection with the classical transition state theory. The ionization mechanism of the hydrogen atom in crossed electric and magnetic fields has already been investigated by application of the transition state theory [33–36], however, a complete physical picture is still lacking. In particular, the existence of transition states localized in the vicinity of the Stark saddle point in the quantum spectrum is unclear. It is the purpose of this chapter to demonstrate the connection between the classical motion of an electron confined near the classical transition state and exact quantum resonances.

Section 7.1 describes briefly the basic concept of the transition state theory and its application to the hydrogen atom. The system and an approximation around the saddle point are introduced in section 7.2 and the results presented in section 7.3 uncover the close relation between the classical electron motions near the transition state and exact quantum spectra.

7.1 Transition state of the hydrogen atom in crossed electric and magnetic fields

The transition state theory is a fundamental approach for the description of transformations in dynamical systems that has applications far beyond the ionization of atoms. In particular, it has its main application in the theory of chemical reaction rates (see, e.g. [91]) in which it also has its early origin [92, 93]. The transition state theory can be applied to many dynamical systems which evolve from an initial ("reactants") to a final state ("products"). The key concept is based on trajectories in the classical phase space of a dynamical system. In particular, regions of the phase space which identify the reactant side and such which represent the product side are introduced. Of special interest are trajectories that connect the reactant side with the product side, because they describe the "reaction". The theory postulates the existence of a minimal set of states which is passed by all of these "reactive" trajectories and this set is called the

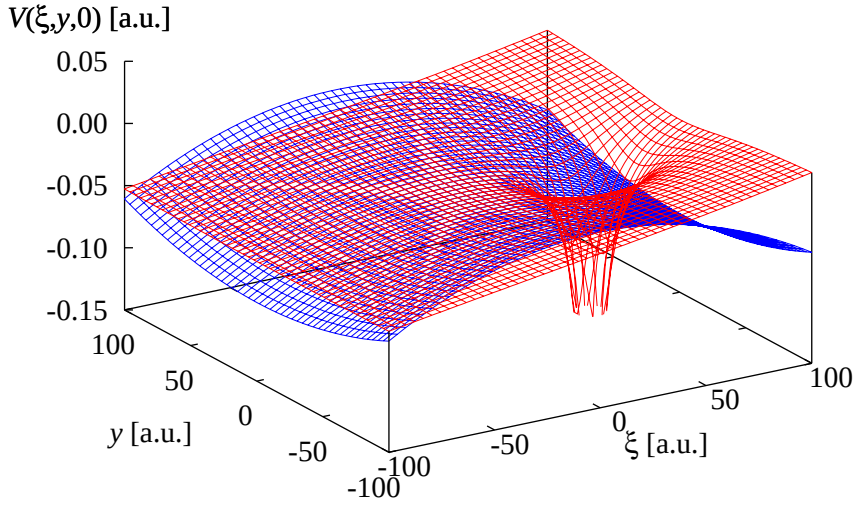

Figure 7.1: Potential of the hydrogen atom in an external electric field in the ξ-y-plane (cf. equation (7.2)) with $\xi = x - x_s$ denoted by the solid red grid. Reactive trajectories must pass the Stark saddle point at $(\xi = 0, y = 0)$ in whose vicinity the transition state is located. The dashed blue grid describes a quadratic approximation around the saddle point (cf. equation (7.3)).

transition state. The transition state has no intersection with a "nonreactive" trajectory and, therefore, it describes a *boundary* between reactants and products in the phase space.

Among the large number of applications of the transition state theory, it has proven to be important for the understanding of the ionization mechanism of atoms. In the case of the hydrogen atom in an external electric field the "reaction" corresponds to the ionization. The potential of the system is plotted in figure 7.1, in which the Stark saddle point can be seen. Classical trajectories describing an ionization must pass the saddle point and, therefore, the transition state must be located in its vicinity. An early work by Clark et al. [37] can be understood as the first step to discuss the ionization mechanism of the hydrogen atom in crossed electric and magnetic fields in this context. Here, a quadratic expansion of the potential around the Stark saddle point (see figure 7.1) was used to calculate quasi bound states confined in the vicinity of the saddle. Further progress was achieved by Jaffé et al. [33, 34] who discussed the transition state theory for systems without time-reversal symmetry and found the transition state of the planar (i.e., two-dimensional) hydrogen atom in crossed external electric and magnetic fields. With the help of methods from nonlinear dynamics the authors of references [33, 34]

discussed the chaotic ionization mechanism and were able to explain the existence of electrons ionizing promptly and electrons which ionize delayed after repeated encounters with the core region. The problem that the practical applicability of the transition state theory was restricted to low-dimensional systems was overcome with an algorithmic procedure to identify the transition state in higher-dimensional systems [35, 36], which is based on a normal form representation of a power series expansion of the Hamiltonian. The quadratic approximation used by Clark et al. is identical with the lowest order in the normal form expansion of the Hamiltonian introduced by Uzer et al. [36].

Since the identification of the transition state for the hydrogen atom in crossed external fields the question, whether the classical trajectories in its vicinity influence the full quantum spectrum, remained open. To find an answer to this question it is advantageous to concentrate on the most simple approximation and use the power series expansion of the potential around the Stark saddle point up to second order introduced by Clark et al. [37]. Higher orders would rapidly lead to a drastic increase of the computational effort and, as can be seen from the results, the agreement of the quantized energy levels of the electron motion with resonances of the quantum mechanically exact spectrum is already very good for the simple expansion. Thus, the expansion is completely sufficient to show the influence of the transition state on the quantum spectrum.

7.2 Hamiltonian and resonances in the vicinity of the Stark saddle point

The Hamiltonian of the hydrogen atom in crossed electric and magnetic fields, which already appeared in equation (5.3) on page 62, is now written in the form

$$H = \frac{1}{2}\left(\boldsymbol{p} + \boldsymbol{A}\right)^2 - \frac{1}{r} + fx \;, \tag{7.1}$$

where $\boldsymbol{A}$ represents the vector potential. Again, the electric field is oriented along the x-axis and the magnetic field is supposed to be parallel to the z-axis. As in section 5.1, usually the symmetric gauge $\boldsymbol{A} = -1/2(\boldsymbol{r} \times \gamma \boldsymbol{e}_z)$ with the magnetic flux density γ is used, whereas, for the the approximated states discussed in this chapter the application of the gauge $\boldsymbol{A} = (-\gamma y, 0, 0)$ is more suitable. As was already mentioned in section 5.1, besides the energy, the parity with respect to the $z = 0$-plane is a constant of motion of the system, which opens the possibility to consider states with even and odd z-parity separately.

The transition state is located in the vicinity of the Stark saddle point, where the net electric force vanishes. For the potential caused by the external electric field and the nucleus,

$$V_f = -\frac{1}{r} + fx \;, \tag{7.2}$$

the saddle point is located on the x-axis at $x_s = -1/\sqrt{f}$ and the saddle point energy has the value $V_f(\boldsymbol{r}_s) = -2\sqrt{f}$. The most simple approximation of the potential V_f which contains the structure of the saddle, is a quadratic expansion. This expansion leads to unbound solutions called "Quasi-Penning resonances" by the authors of reference [37] due to a formal similarity with the Penning trap. Here, the essential results are recapitulated. The expansion of the potential up to second order terms reads

$$V_f(\boldsymbol{r}) = -2\sqrt{f} - \sqrt{f}^3\xi^2 + \frac{1}{2}\sqrt{f}^3\left(y^2+z^2\right) + \mathrm{O}((\boldsymbol{r}-\boldsymbol{r}_s)^3)\,, \tag{7.3}$$

where the abbreviation $\xi = x - x_s$ is used. The saddle structure of the potential is visualized in figure 7.1, where the potential (7.3) (dashed blue grid) is plotted in the ξ-y-plane. The comparison with the exact electric potential (7.2) shows clearly that the approximation is only valid close to the saddle point and can only describe states in its vicinity correctly.

Using the gauge $\boldsymbol{A} = (-\gamma y, 0, 0)$ the Hamiltonian in the vicinity of $\boldsymbol{r}_s$ reads

$$H = \frac{1}{2}\left(p_\xi^2 + p_y^2 + p_z^2\right) - \gamma y p_\xi + \frac{1}{2}\gamma^2 y^2 - 2\sqrt{f} + \frac{1}{2}\sqrt{f}^3\left(y^2+z^2-2\xi^2\right) \tag{7.4}$$

and the eigenvalues of the quadratic potential yield the energy levels

$$E_{n_z,n_1,n_2} = -2\sqrt{f} + \omega_z(n_z+\frac{1}{2}) + \omega_1(n_1+\frac{1}{2}) + \omega_2(n_2+\frac{1}{2})\,, \tag{7.5}$$

where ω_z represents the frequency of the z-motion and is given by $\omega_z = f^{3/4}$. The separation of the coupled equations in ξ- and y-directions with the help of an adequate canonical transformation [36], leads to one real oscillation frequency,

$$\omega_1 = \left\{\frac{1}{2}\left(\gamma^2 - \sqrt{f}^3 + \sqrt{\left(\gamma^2-\sqrt{f}^3\right)^2 + 8f^3}\right)\right\}^{1/2}\,, \tag{7.6}$$

and one imaginary decay rate,

$$\omega_2 = \mathrm{i}\left\{\frac{1}{2}\left(\sqrt{f}^3 - \gamma^2 + \sqrt{\left(\gamma^2-\sqrt{f}^3\right)^2 + 8f^3}\right)\right\}^{1/2}\,, \tag{7.7}$$

which describes the resonance character of the eigenstates. Thus, the resonance energies (real part of the complex eigenvalues) are completely determined by the two quantum numbers n_z, n_1 and read

$$\mathrm{Re}(E)_{n_z,n_1} = -2\sqrt{f} + \omega_z(n_z+\frac{1}{2}) + \omega_1(n_1+\frac{1}{2})\,. \tag{7.8}$$

The aim of this chapter is to present evidence for the occurrence of resonances near the transition state. For this purpose the approximate energy values (7.8) are compared with exact quantum calculations, which are determined with the method described in section 5.1.

7.3 Signatures of the transition state in quantum spectra

To decide whether there is a connection between the classical motion around the saddle point and the exact quantum calculations, the energy eigenvalues (7.8) are compared with the exact quantum resonances. A coincidental agreement between two energies of both approaches for a *single* parameter value is always possible and does not give an answer to the question. However, a connection between the approximation (7.8) and the quantum resonances is certainly present if the two results agree in a *larger region* of the parameter space. To check the connection, calculations on *lines* in the two-dimensional parameter space spanned by the two field strengths are performed, i.e., a parameter α is introduced and field strengths $f(\alpha)$ and $\gamma(\alpha)$ are considered as functions of α, as it was already done for the discussions in section 6.4.

An example for a comparison is presented in figure 7.2 for states with even z-parity. Here, the resonances are calculated for different external field strengths on the line defined by

$$\gamma = 0.008 \times \alpha \,, \tag{7.9a}$$
$$f = 0.0003 \times \alpha \,, \tag{7.9b}$$
$$0 < \alpha < 1 \,, \tag{7.9c}$$

i.e., the ratio γ/f of the two field strengths is always constant. The solid blue lines represent the energy eigenvalues (7.8) of the quadratic approximation around the saddle point and the red points are the numerically exact computed resonances of the Hamiltonian (7.1). The results show that for the lowest quantum numbers n_z, n_1 of the approximation there is a very good agreement between both approaches on a large range of parameters α. The "Quasi-Penning" resonances are accompanied by the quantum mechanically exact states when α is changed. This behavior is stressed by a larger point size for the exact resonances.

Of course, the effect does also appear for odd z-parity, which is shown separately in figure 7.2(b) for the same situation as in figure 7.2(a). As one can see, the agreement of the resonances is, again, very good in a large region of the parameter space.

However, there are parameter values α for which a different behavior between both approaches exists. For low electric field strengths the Coulomb potential becomes to dominant and the expansion of the potential in the vicinity of the Stark saddle point no longer leads to reasonable solutions as can be observed in figure 7.2. Furthermore, avoided level crossings of the numerically exact resonances have no counterpart in the approximate states. Couplings of the states, which are the origin of avoided level crossings, are not included in the simple model. Thus, the deviations in these regions are not surprising. Figure 7.3 shows an example of a region with avoided level crossings of quantum mechanically exact resonances. It can be seen clearly that far from the crossing the agreement between the numerically exact states and the energy value corresponding

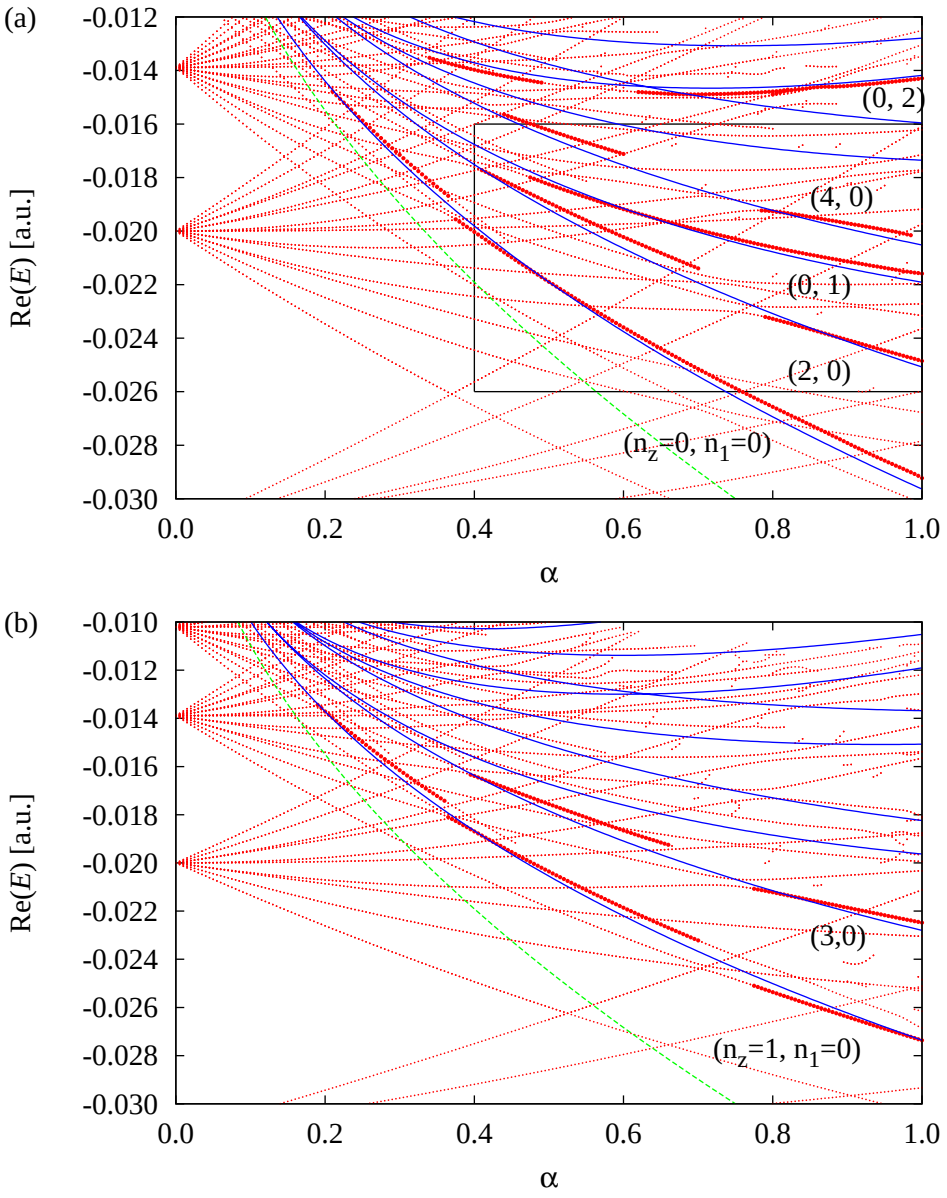

Figure 7.2: (a) Comparison of the quantized energies of the electron motion near the transition state (solid blue lines) with exact quantum calculations (red points) on the line $\gamma = 0.008 \times \alpha$, $f = 0.0003 \times \alpha$ for $0 < \alpha < 1$ as defined in equations (7.9a)–(7.9c) in the (γ,f)-space for even z-parity. Only exact quantum energies with $|\mathrm{Im}(E)| < 0.0006$ are shown. The exact resonances which accompany the approximate energies (7.8) are marked by a larger point size. The lowest (dashed green) line marks the saddle point energy. The black frame marks the region magnified in figure 7.3. (b) Same situation for states with odd z-parity.

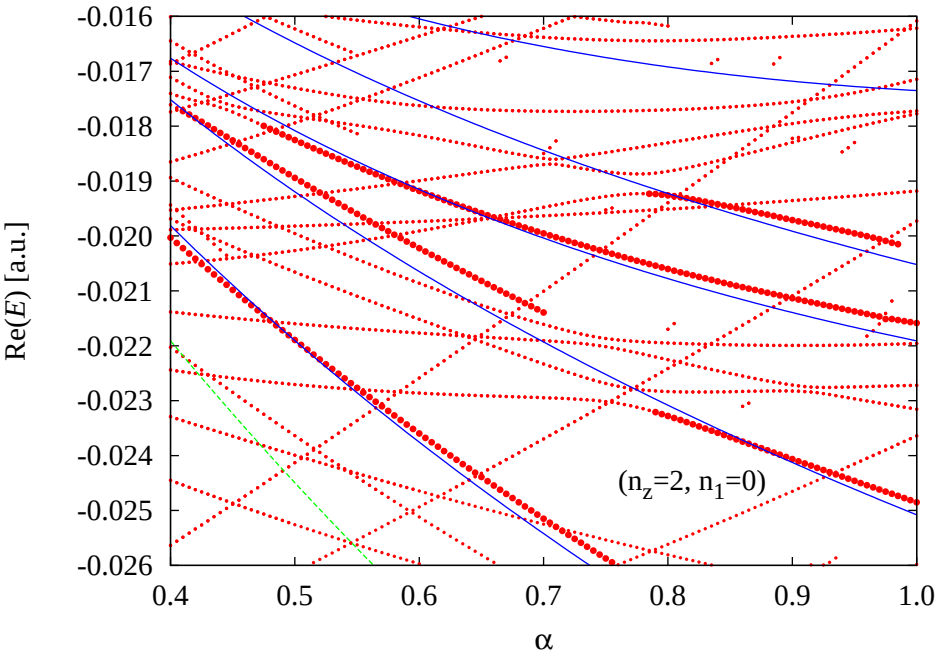

Figure 7.3: Same situation as depicted in figure 7.2. The region around the avoided level crossings near the state with $n_z = 2$, $n_1 = 0$ is magnified.

to $n_z = 2$, $n_1 = 0$ in equation (7.8) is very good, whereas, at the avoided crossings itself the approximate solutions cannot reproduce the results of the full Hamiltonian (7.1).

The calculations shown in figure (7.4) are performed on the line

$$\gamma = 0.01 \times \alpha' \,, \tag{7.10a}$$
$$f = 0.0001 + 0.0002 \times \alpha' \,, \tag{7.10b}$$
$$0 < \alpha' < 1 \,. \tag{7.10c}$$

Now the ratio of the field strengths is not constant. For $\alpha' = 0$ there is still an electric field present but no magnetic field. The important property of this line is the existence of the saddle for all values of α' drawn in figure 7.4. Again, there are exact quantum resonances which behave like the approximate solutions around the Stark saddle point and lead to a good agreement between both approaches on a wide range of parameters values. Also near $\alpha' = 0$, where a pure Stark effect is present, the classical electron motion near the transition state describes the quantum resonances very well.

The results shown here have demonstrated that there is clear evidence for classical motions of electrons which are confined at the Stark saddle point in exact energy spectra. The calculation of the resonances on lines in the parameter space spanned by the strengths of the two external fields have revealed structures which demonstrate the connection of the electron motion near the transition state and numerically exact computed

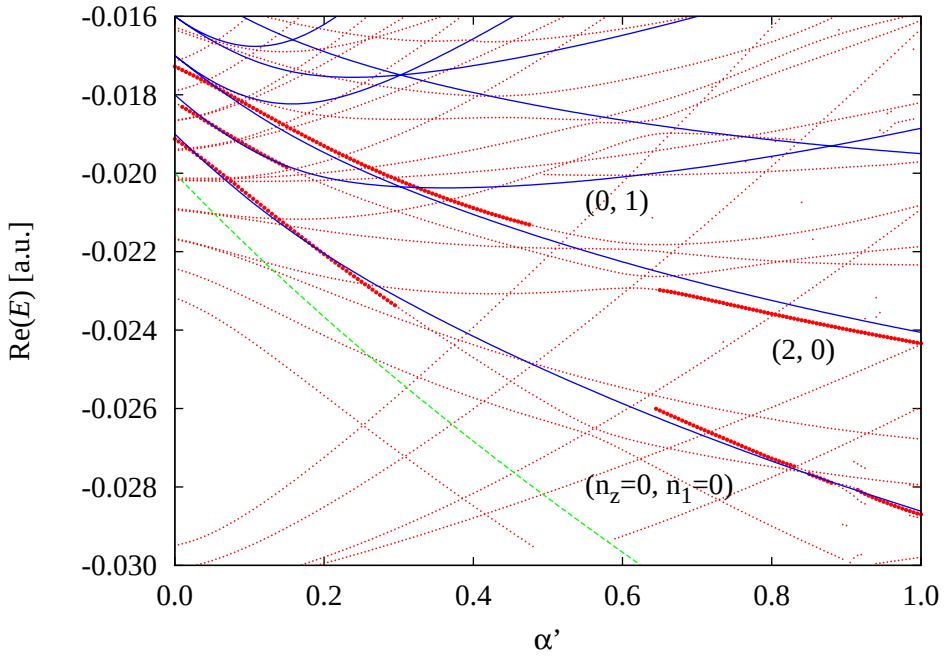

Figure 7.4: Same comparison of the quantized energies of the electron motion near the transition state (solid blue lines) with exact quantum calculations (red points) as in figure 7.2 but on the line $\gamma = 0.01 \times \alpha'$, $f = 0.0001 + 0.0002 \times \alpha'$ for $0 < \alpha' < 1$ defined in equations (7.10a)–(7.10c). Only exact quantum energies with $|\mathrm{Im}(E)| < 0.0002$ are shown. The saddle point energy is marked by the lowest (dashed green) line.

resonances. The agreement of the energies of both approaches is very good. This might be surprising because the most simple expansion of the potential only up to second order was used, i.e., the approximation is only valid in a small region very close to the saddle point. This clearly can be understood as a signal for an eminent influence of the transition state on the exact quantum spectrum and demonstrates the importance of the transition state for the ionization mechanism. It should be noted, however, that the excellent agreement between both methods exists only for the real part of the complex energy eigenvalues. The simple approximation used in the expansion of the potential is not capable to reproduce the correct decay rates or imaginary parts. It seems worthwhile to extend the calculations done here to the normal form procedure developed by Uzer et al. [36] and to check whether higher orders can lead to an even better description of the quantum resonances with the electron motion.

8 Nonlinear exceptional points in Bose-Einstein condensates with $1/r$ interaction

The discussion of exceptional points in quantum systems so far has been devoted only to the resonances which appear in the *linear* Schrödinger equation with a non-Hermitian Hamiltonian. There are situations in which a *nonlinear* Hamiltonian is required to describe the quantum system. In particular, the Gross-Pitaevskii equation [38, 39], which is a mean field description of an interacting Bose gas, where all atoms are in the same state, is of high interest due to the experimental realization of Bose-Einstein condensates. Here, the mean field approximation leads to a nonlinear potential and establishes features not known from ordinary linear Schrödinger equations. For example, the coalescence of two wave functions, which depend on a parameter can occur, a situation which seems to be similar to an exceptional point. It is the purpose of this and the following chapter to show, that such a coalescence, indeed, describes a branch point singularity of the energy eigenvalues and the wave functions. The analysis done here reveals for the first time the existence of exceptional points in quantum systems described by the *nonlinear* Gross-Pitaevskii equation. The system investigated in this chapter is especially dedicated because analytical solutions are on-hand.

The basis for the analysis is the well known property of Bose-Einstein condensates with attractive interatomic interactions that stationary solutions to the Gross-Pitaevskii equation exist only in certain regions of the parameter space governing the physics of the condensates. For example, for the case of an attractive s-wave contact interaction tunable parameters are the number of particles or the s-wave scattering length, which can be varied in the vicinity of Feshbach resonances by adjusting an external magnetic field. It was theoretically predicted [40–42], and experimentally confirmed [43–45], that the condensate collapses when, for given negative scattering length, the number of particles becomes too large. In an alternative experiment [46] the collapse was induced by tuning the scattering length. Huepe et al. [47, 48] have shown that the critical parameter values where a collapse occurs in fact correspond to *bifurcation points* of the solutions to the stationary Gross-Pitaevskii equation, where two solutions appear out of nowhere, and analyzed the linear stability of the states. These bifurcation points are, as will be shown here, branch point singularities and allow for an extension of the term "exceptional point" to nonlinear quantum systems.

The bifurcations are not restricted to condensates, where only an attractive s-wave contact interaction and a trap potential exist. It was demonstrated [49, 50] that similar behavior persists in Bose-Einstein condensates where additionally a long-range "gravity-like", attractive $1/r$ interaction is present. Such "monopolar" quantum gases could be realized according to O'Dell et al. [51] by a combination of 6 appropriately arranged "triads" of intense off-resonant laser beams, however, the experimental realization is a very challenging task.

An important feature of Bose-Einstein condensates with attractive $1/r$ interaction is the case of self-trapping, i.e., condensation without external trap. This system has the great advantage that simple approximate analytic solutions exist, which can be used for the investigation of the exceptional points. The branch point singularity structure can be revealed directly from the analytic terms, which is only possible *without* external harmonic trap. The analytic solutions raise the system to the ideal candidate for the investigation of exceptional points in nonlinear quantum systems, despite the lack of an experimental realization. The results are a basis for more complicated experimentally accessible modifications as dipolar Bose-Einstein condensates, which are discussed in chapter 9.

The system is introduced in section 8.1, where a variational approximation (section 8.1.1) and a numerically exact approach (section 8.1.2) to find solutions are presented. To investigate the properties of exceptional points, a non-symmetric matrix model is required which is given in section 8.2. An analytic continuation of the wave functions done in section 8.3 reveals the existence of exceptional points in the solutions of the Gross-Pitavskii equation by studying the energy eigenvalues (section 8.3.1) and the wave functions (section 8.3.2). The complex solutions obtained with the analytic continuation are interpreted as a decaying condensate in section 8.4. Finally, the stability of the two condensate wave functions emerging at the exceptional point is studied in section 8.5 for the variational (section 8.5.1) and the numerically exact solutions (section 8.5.2).

8.1 Bose-Einstein condensates with $1/r$ interaction

In this section the equations and results for self-trapped Bose-Einstein condensates with attractive $1/r$-interaction which are necessary for the subsequent analysis of exceptional points are briefly reviewed. The extended Gross-Pitaevskii equation without external trap potential reads

$$\left[-\Delta_{\boldsymbol{r}} + N\left(8\pi a\left|\psi(\boldsymbol{r})\right|^2 - 2\int \mathrm{d}^3\boldsymbol{r}'\frac{\left|\psi(\boldsymbol{r}')\right|^2}{\left|\boldsymbol{r}-\boldsymbol{r}'\right|}\right)\right]\psi(\boldsymbol{r}) = \varepsilon\psi(\boldsymbol{r})\ , \tag{8.1}$$

where the natural "atomic" units introduced in references [49, 50] were used (cf. appendix A.2). Lengths are measured in units of a "Bohr radius" a_u and energies in units of a

"Rydberg energy" E_u, which are given by

$$a_u = \frac{\hbar^2}{mu} , \qquad E_u = \frac{\hbar^2}{2ma_u^2} ,$$

respectively, where u determines the strength of the atom-atom-interaction [51], and m is the mass of one boson. In equation (8.1), ε is the chemical potential, a the s-wave scattering length and N the number of bosons. As was pointed out in references [49, 50] with the use of the scaling property of the system, the physics of a self-trapped condensate is only determined by one parameter, namely N^2a, which will be necessary for the identification of the exceptional point. Exploiting the scaling properties and introducing the scaled variables [94]

$$(\tilde{\boldsymbol{r}}, \tilde{a}, \tilde{\varepsilon}, \tilde{E}, \tilde{t}, \tilde{\psi}) = (N\boldsymbol{r}, N^2a, \varepsilon/N^2, E/N^3, N^2t, N^{-3/2}\psi) , \tag{8.2}$$

the system can be brought into the form

$$\left[-\Delta_{\tilde{\boldsymbol{r}}} + 8\pi\tilde{a}|\tilde{\psi}(\tilde{\boldsymbol{r}})|^2 - 2\int \mathrm{d}^3\tilde{\boldsymbol{r}}' \frac{|\tilde{\psi}(\tilde{\boldsymbol{r}}')|^2}{|\tilde{\boldsymbol{r}} - \tilde{\boldsymbol{r}}'|}\right] \tilde{\psi}(\tilde{\boldsymbol{r}}) = \tilde{\varepsilon}\tilde{\psi}(\tilde{\boldsymbol{r}}) , \tag{8.3}$$

where all occurrences of the particle number N have been absorbed in the scaled variables (8.2). The scaled variables are used throughout the rest of the chapter and the tilde is omitted in what follows. A further quantity necessary for the discussions in this chapter is the mean field energy of the self-trapped condensate, whose scaled form reads

$$E[\psi] = \int \mathrm{d}^3\boldsymbol{r}\, \psi^*(\boldsymbol{r}) \left(-\Delta_{\boldsymbol{r}} + 4\pi a\, |\psi(\boldsymbol{r})|^2 - \int \mathrm{d}^3\boldsymbol{r}' \frac{|\psi(\boldsymbol{r}')|^2}{|\boldsymbol{r} - \boldsymbol{r}'|}\right)\psi(\boldsymbol{r}) . \tag{8.4}$$

The solutions one has to be interested in for the discussion of branch point singularities, viz. the two states emerging at the tangent bifurcation, are radially symmetric. One of them is the ground state. Thus, one can concentrate on radially symmetric solutions of equation (8.3), which are now obtained by variational approximations and numerically exact methods.

8.1.1 Variational solutions

An analytic approximation for the two wave functions of the condensate which emerge at the tangent bifurcation can be obtained using a variational principle. Calculations with a Gaussian type orbital were performed by O'Dell et al. [51] and compared with numerically accurate solutions by Papadopoulos et al. [49, 50]. The trial wave function is given by

$$\psi(\boldsymbol{r}) = A \exp\left[-\frac{1}{2}k^2\boldsymbol{r}^2\right] , \tag{8.5}$$

where

$$A = \left(\frac{k}{\sqrt{\pi}}\right)^{3/2} \tag{8.6}$$

is the normalization constant and the variation is performed with respect to the width represented by k. The two stationary values,

$$E_\pm = -\frac{4}{9\pi}\frac{1 \pm 2\sqrt{1+\frac{8}{3\pi}a}}{\left(1 \pm \sqrt{1+\frac{8}{3\pi}a}\right)^2} , \tag{8.7}$$

of the mean field energy (8.4) are obtained at

$$k_\pm = \frac{1}{2}\sqrt{\frac{\pi}{2}}\frac{1}{a}\left(\pm\sqrt{1+\frac{8}{3\pi}a}-1\right) . \tag{8.8}$$

E_+ represents the variational approximation for the ground state of the condensate, the second solution (excited state) is labeled E_-. Furthermore, the analytical expressions for the chemical potentials of the two solutions are given by

$$\varepsilon_\pm = -\frac{4}{9\pi}\frac{5 \pm 4\sqrt{1+\frac{8}{3\pi}a}}{\left(1 \pm \sqrt{1+\frac{8}{3\pi}a}\right)^2} , \tag{8.9}$$

respectively. The tangent bifurcation is obvious from equations (8.7) and (8.9). For negative scattering lengths with $a < -3\pi/8$ there is no (real) result for E and ε, at the critical value $a = -3\pi/8$ both solutions have the same value ($E_+ = E_-$, $\varepsilon_+ = \varepsilon_-$), and above $-3\pi/8$, one obtains two different real solutions. The chemical potential is shown as a function of the scattering length parameter a in figure 8.1.

8.1.2 Exact calculations

In order to be in a position to compare numerically exact calculations with the results of the variational approach, radially symmetric wave functions are assumed. For the search of numerically exact solutions to the integro-differential equation (8.3), the radial part is written in the form of two differential equations [50],

$$\psi''(r) + \frac{2}{r}\psi'(r) = -U(r)\psi(r) + 8\pi\bar{a}|\psi(r)|^2\psi(r) , \tag{8.10a}$$

$$U''(r) + \frac{2}{r}U'(r) = -8\pi|\psi(r)|^2 . \tag{8.10b}$$

The two second order differential equations can be transformed to first order equations and integrated, e.g., with a Runge-Kutta-Merson algorithm starting at, e.g., $\bar{r}_0 = 10^{-19}$ slightly greater than zero with the initial conditions

$$\bar{\psi}(\bar{r}_0) = 1 , \ \bar{\psi}'(\bar{r}_0) = 0 , \ \bar{U}(\bar{r}_0) = u_0 , \ \bar{U}'(\bar{r}_0) = 0 . \tag{8.11}$$

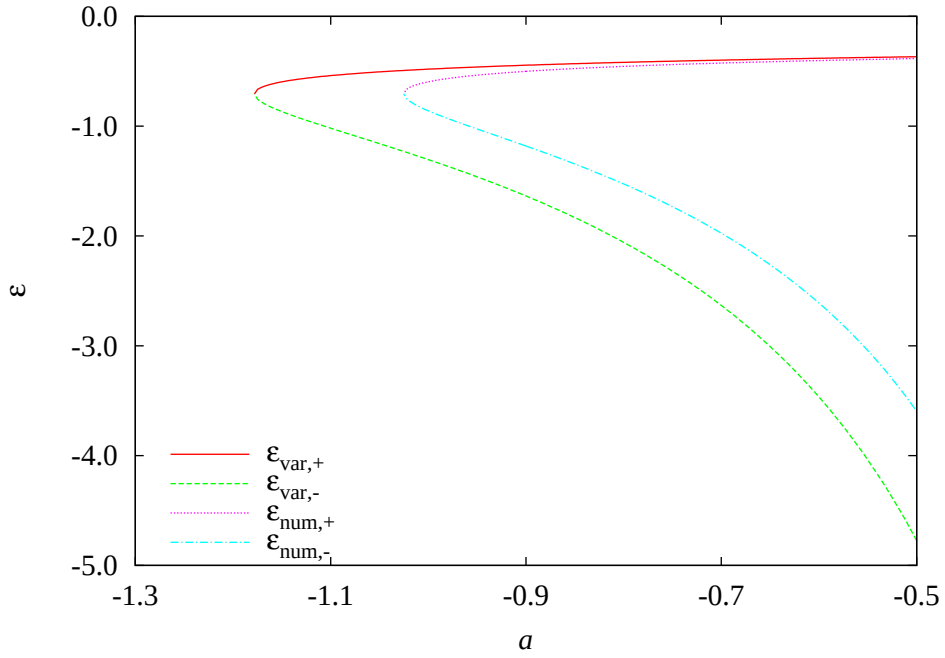

Figure 8.1: Scaled chemical potentials of the two solutions. The results of the variational and the numerical exact calculations are shown. Two solutions emerge in a tangent bifurcation at a critical value of the scaled parameter a. In the variational approximation the critical value is $a = -3\pi/8 = -1.1780$, whereas the numerical exact solutions emerge at $a = -1.0251$ [49, 50]. The "atomic" units introduced above are used.

The value u_0 must be determined such that $\bar{\psi}(\bar{r})$ vanishes in the limit $\bar{r} \to \infty$. Numerically, integration up to $\bar{r}_{\max} \approx 15$ is sufficient. The wave function obtained with the initial condition $\bar{\psi}(\bar{r}_0) = 1$ is not normalized, which is indicated with the bar.

Since the Gross-Pitaevskii equation is a nonlinear differential equation the correct normalization of the numerical wave functions cannot be obtained by a multiplication with a normalization constant. However, again, scaling properties of the system can be exploited to achieve a correct scaling and normalization of the wave functions. As can be seen with a simple calculation, the transformation

$$(\psi, r, \varepsilon, a) \to (\nu^2\psi, \frac{r}{\nu}, \nu^2\varepsilon, \frac{a}{\nu^2}) \tag{8.12}$$

leaves the system (8.10a), (8.10b) of differential equations invariant. With the normalization condition $||\psi||^2 = 1$ and the scaling invariance (8.12), the normalization factor is given by (cf. [94, 95])

$$1/\nu = ||\psi||^2 = 4\pi \int_0^\infty |\psi(r)|^2 r^2 \, \mathrm{d}r \tag{8.13}$$

and the properly scaled and normalized wave function $\psi(r)$ is obtained as

$$\psi(r) = \nu^2 \bar{\psi}(\bar{r}/\nu) \tag{8.14}$$

with the scattering length

$$a = \frac{\bar{a}}{\nu^2} \ . \tag{8.15}$$

An explicit calculation of the integral (8.13) is not required. Using the asymptotic behavior of the numerically computed potential $\bar{U}(\bar{r})$ for large radial coordinates

$$\bar{U}(\bar{r}) \approx \bar{\varepsilon} + \frac{2}{\nu}\frac{1}{\bar{r}} \ , \tag{8.16}$$

the factor ν can be calculated from

$$\nu = \lim_{\bar{r}\to\infty} \frac{-2}{\bar{r}^2 \bar{U}'(\bar{r})} \ . \tag{8.17}$$

The correctly scaled chemical potential can also be determined with the help of approximation (8.16):

$$\varepsilon = \nu^2 \lim_{\bar{r}\to\infty} \left(\bar{U}(\bar{r}) + \bar{r}\bar{U}'(\bar{r})\right) \ . \tag{8.18}$$

Only for the mean field energy a further integral is required. Using the virial theorem [40, 51] one obtains

$$E = -\langle U \rangle = -4\pi\nu^3 \int_0^\infty |\bar{\psi}(\bar{r})|^2 \bar{U}(\bar{r}) \bar{r}^2 \mathrm{d}\bar{r} \ . \tag{8.19}$$

The numerical exact chemical potential is also shown in figure 8.1. It agrees, qualitatively, with the result of the variational approach, however, the tangent bifurcation is shifted to a higher critical scattering length $a = -1.0251$ [49, 50]. It will be shown in section 8.3 that in both the variational approach and the exact calculations the tangent bifurcation at the critical scattering length is a branch point singularity of the wave functions, i.e., an exceptional point.

8.2 Exceptional points in symmetric and non-symmetric matrices

Usually complex symmetric matrices or complex symmetric matrix representations of Hamiltonians are used to investigate exceptional points in quantum systems (see, e.g., [2, 19, 86]). For the discussion of the extension to nonlinear quantum systems it is important to take into account non-symmetric matrices, which show some differences to the symmetric case and which have a correspondence in the nonlinear solutions considered here. Simple non-symmetric matrices have been investigated before [66, 69, 96] also

for systems with time reversal symmetry breaking [97–99]. It is instructive to discuss a simple two-dimensional model which extends the matrix introduced in section 2.3. The example is provided by the 2×2-matrix

$$\boldsymbol{M}(\kappa) = \begin{pmatrix} 1 & \kappa \\ c+\kappa & -1 \end{pmatrix}. \tag{8.20}$$

In (8.20), κ is a complex parameter, and the complex number c is introduced to distinguish between the general non-symmetric case ($c \neq 0$) and a symmetric matrix ($c = 0$) in the discussion below. The eigenvalues read

$$\lambda_{1,2}(\kappa) = \pm\sqrt{1 + c\kappa + \kappa^2} \tag{8.21}$$

and are obviously two branches of one analytic function. Corresponding non-normalized eigenvectors of the two eigenvalues are given by

$$\boldsymbol{x}_{1,2}(\kappa) = \begin{pmatrix} -\kappa \\ 1 \mp \sqrt{1 + c\kappa + \kappa^2} \end{pmatrix}. \tag{8.22}$$

There are two exceptional points for $\kappa_{A,B} = -c/2 \pm \sqrt{c^2/4 - 1}$. At these parameter values, both the eigenvalues $\lambda_{1,2}$ and the eigenvectors $\boldsymbol{x}_{1,2}$ pass through a branch point singularity. For the further discussions it is sufficient to concentrate on the case $\kappa = \kappa_A$. Then, the degenerate eigenvalues have the value $\lambda_{1,2}(\kappa_A) = 0$ and the two eigenvectors $\boldsymbol{x}_{1,2}$ are parallel to

$$\boldsymbol{x}_{1,2}(\kappa_A) = \begin{pmatrix} c/2 - \sqrt{c^2/4 - 1} \\ 1 \end{pmatrix}. \tag{8.23}$$

The important property of exceptional points can, of course, also be seen in non-symmetric matrices. In particular, the permutation of the two eigenvalues if the exceptional point is encircled in the parameter space is present. An illustration in the non-symmetric case $c = 1$ is given in figure 8.2 for the path

$$\kappa_\varrho(\varphi) = -c/2 + \sqrt{c^2/4 - 1} + \varrho\, \mathrm{e}^{\mathrm{i}\varphi} \tag{8.24}$$

around the critical value κ_A. An approximation for small radii $\varrho \ll |2\sqrt{c^2/4 - 1}|$ leads to

$$\begin{aligned} \lambda_1(\kappa_\varrho(\varphi)) &= \sqrt{2\varrho\sqrt{c^2/4 - 1}}\, \mathrm{e}^{\mathrm{i}(\varphi/2 + \pi/4)}, \\ \lambda_2(\kappa_\varrho(\varphi)) &= \sqrt{2\varrho\sqrt{c^2/4 - 1}}\, \mathrm{e}^{\mathrm{i}(\varphi/2 + 5\pi/4)}, \end{aligned} \tag{8.25}$$

which is very similar to the example in section 2.3. If a full circle in the complex parameter space κ is traversed, the paths of the eigenvalues form a semicircle as can be seen from equation (8.25). Neither of the two eigenvalues passes through a closed loop. The first arrives, after the parameter space loop, at the starting point of the second one

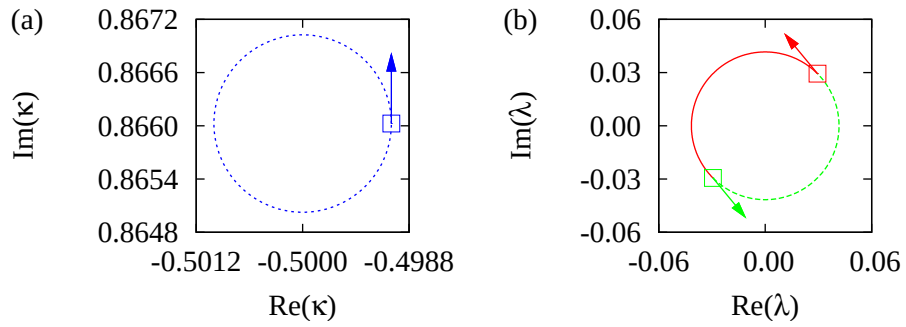

Figure 8.2: Eigenvalues of the two-dimensional model defined in equation (8.20) with $c = 1$ for a circle around the exceptional point. (a) Circle in the parameter space with radius $\varrho = 10^{-3}$. The starting point $\kappa(0)$ is marked by an open square and the direction of progression is indicated with the arrow. (b) Path of the eigenvalues $\lambda_{1,2}$ (denoted by different colors) for the parameter values on the circle. The eigenvalues which belong to the first parameter value $\kappa(0)$ are labeled with open squares and the arrows point in the direction of progression.

and vice versa. Two circles in the κ-space ($\varphi = 0 \ldots 4\pi$) are required to obtain a full circle of *one* of the eigenvalues.

For exceptional points in linear systems there is a noteworthy difference for complex symmetric and non-symmetric matrices. In the first case, which is obtained for $c = 0$ in the model (8.20), was realized experimentally in the resonances investigated in microwave cavities [9], and appears in the hydrogen atom in crossed electric and magnetic fields (cf. chapters 5 and 6), there is always a distinct phase behavior of the eigenvectors. If an exceptional point is encircled, the two eigenvectors are interchanged (as expected from the behavior of the energy eigenvalues) and, additionally, *one* of the two eigenvectors changes its sign. This effect is demonstrated in section 2.4.3 and can be summarized with, e.g.,

$$[\boldsymbol{x}_1, \boldsymbol{x}_2] \overset{\text{circle}}{\longrightarrow} [-\boldsymbol{x}_2, \boldsymbol{x}_1] \,. \tag{2.31}$$

As was discussed in section 2.4.3, the phase behavior can be obtained for the vectors $\boldsymbol{x}_i$ normalized with the Euclidean norm without complex conjugation $N_i = \sqrt{\boldsymbol{x}_i^T \boldsymbol{x}_i}$, where $\boldsymbol{x}_i^T$ is the transpose of the vector $\boldsymbol{x}_i$ (cf. [100]). This normalization fixes the phase and is the method required for the comparison with the nonlinear system studied in this chapter (cf. section 8.3 and appendix C).

For the non-symmetric case the change in sign does not appear for a vector whose phase has been fixed with the *same method*, i.e., the Euclidean norm without complex conjugation. A non-symmetric matrix is obtained in the model (8.20) for $c \neq 0$. Then, there is only a permutation of the eigenvectors, which can be summarized with

$$[\boldsymbol{x}_1, \boldsymbol{x}_2] \qquad \overset{\text{circle}}{\longrightarrow} \qquad [\boldsymbol{x}_2, \boldsymbol{x}_1] \,. \tag{8.26}$$

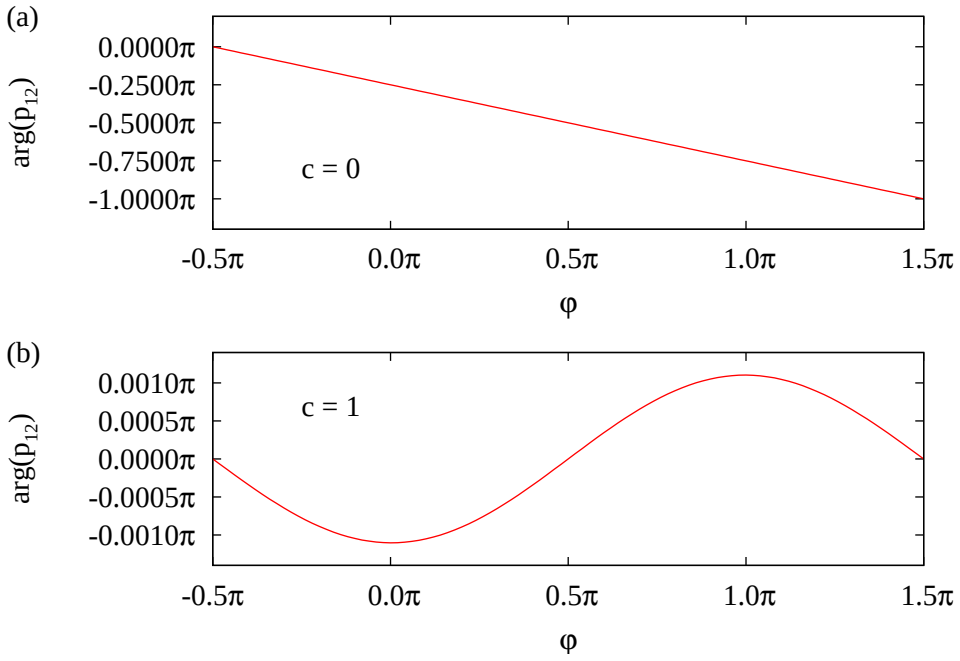

Figure 8.3: Phase of the product p_{12} for a circle in the parameter space of type (8.24) with radius $\varrho = 10^{-3}$ around the exceptional point. (a) Symmetric matrix with $c = 0$. The phase changes by π indicating the change in sign of one of the eigenvectors from (2.31). (b) Non-symmetric matrix with $c = 1$. There is no change in sign as noted in (8.26).

This is shown analytically for a small circle in appendix C. Note that the phase behavior (8.26) does not represent the "geometric phase" of an eigenvector during the circle around an exceptional point. As is mentioned in section 2.4.2, the geometric phase in the case of a non-symmetric matrix differs from 0.

A demonstration of the phase behavior is possible with the product

$$p_{12} = \boldsymbol{x}_1^T \begin{pmatrix} 0 & 1 \\ 1 & 0 \end{pmatrix} \boldsymbol{x}_2 \; . \tag{8.27}$$

The non-diagonal matrix ensures, that the product p_{12} does not vanish in the symmetric case. If the change in sign is present, the phase of p_{12} changes its value by π when a full circle around the exceptional point is traversed. In figure 8.3 the behavior of the product is shown for the example (8.20). The change in sign is obvious in the symmetric case $c = 0$ and does not appear for the non-symmetric choice $c = 1$.

8.3 Analytic continuation of the Gross-Pitaevskii system

In the extended Gross-Pitaevskii equation (8.3), both the variational and the numerical calculations suggest the existence of an exceptional point at the tangent bifurcation. For the critical parameter value, one obtains two identical states. The chemical potentials, the mean field energies and the wave functions are identical. In contrast to exceptional points in linear systems described in section 8.2 the coalescence of the two states of the nonlinear Gross-Pitaevskii equation (8.3) can appear for a purely real wave function at a real energy in a one-dimensional parameter space. This is a consequence of the nonlinearity of the Gross-Pitaevskii equation. If one wants to check whether or not the degeneracy in the nonlinear system has the same branch point singularity structure as exceptional points in open quantum systems described by the linear Schrödinger equation, one has to extend the parameter a to complex values and to investigate the complex vicinity of the degeneracy.

The analytic continuation of the Gross-Pitaevskii system is a nontrivial task. The Gross-Pitaevskii equation (8.3) contains the square modulus of the wave function ψ and is therefore a non-analytic function of ψ. It has been argued that the tempting simple replacement of $|\psi|^2$ with ψ^2 is valid only with the assumption that the entire wave function is real valued [101]. Here, the following procedure for complex wave functions is suggested.

Any complex wave function can be written as

$$\psi(\boldsymbol{r}) = \mathrm{e}^{\alpha(\boldsymbol{r})+\mathrm{i}\beta(\boldsymbol{r})} \,, \tag{8.28}$$

where the real functions $\alpha(\boldsymbol{r})$ and $\beta(\boldsymbol{r})$ determine the amplitude and phase of the wave function, respectively. The complex conjugate and the square modulus of $\psi(\boldsymbol{r})$ read

$$\psi^*(\boldsymbol{r}) = \mathrm{e}^{\alpha(\boldsymbol{r})-\mathrm{i}\beta(\boldsymbol{r})} \,, \; |\psi(\boldsymbol{r})|^2 = \mathrm{e}^{2\alpha(\boldsymbol{r})} \,. \tag{8.29}$$

Using the ansatz (8.28) the Gross-Pitaevskii system can be written as two coupled nonlinear differential equations for $\alpha(\boldsymbol{r})$ and $\beta(\boldsymbol{r})$, however, without any complex conjugate or square modulus. These equations can now be continued analytically by allowing for complex valued functions $\alpha(\boldsymbol{r})$ and $\beta(\boldsymbol{r})$. This implies that equation (8.29) *without* complex conjugate of $\alpha(\boldsymbol{r})$ and $\beta(\boldsymbol{r})$ is formally used for the calculation of ψ^* and $|\psi(\boldsymbol{r})|^2$, and thus the square modulus of ψ can become complex. The physical interpretation of a complex absorbing potential in the Gross-Pitaevskii system will be discussed below in section 8.4.

It should be noted that the above procedure is analogous to the complex scaling method introduced in chapter 3, viz. the replacement $r \to r\mathrm{e}^{\mathrm{i}\theta}$ in the Hamiltonian, used for the calculation of resonances in open quantum systems. For states on the left hand side of operators there is no complex conjugation of the $r\mathrm{e}^{\mathrm{i}\theta}$ arising from the scale transformation but complex conjugation is applied to the intrinsically complex part of the function.

In the following the branch point singularity at the tangent bifurcation will be encircled. For the variational approach discussed in section 8.1.1 the equations (8.7), (8.8), and (8.9) are straightforwardly extended to complex values of the parameter a, yielding complex results for the chemical potential, the mean field energy, and the wave functions. The situation is more complicated for the exact calculations in section 8.1.2 because the differential equations (8.10a) and (8.10b) do not directly depend on the scaled scattering length a but on the unscaled (or un-normalized) parameter $\bar{a}$. For complex $\bar{a}$ the differential equations (8.10a) and (8.10b) can be continued analytically resulting in complex wave functions. Then, the two complex parameters u_0 and $\bar{a}$ are determined in a multidimensional root search problem, to fulfill the condition of vanishing wave functions in the limit $r \to \infty$, and to achieve the given value of a.

8.3.1 Branch point singularity structure of the energies

The variational solutions (8.7) for the mean field energy, and (8.9) for the chemical potential show a branch point singularity at the bifurcation point. For a circle around the critical value of the complex parameter a the typical permutation of the two solutions is expected and found, as is shown in figure 8.4 for the variational approximation as well as for the numerical exact calculations. The circle in the parameter space is defined by

$$a = a_\mathrm{c} + \varrho\, \mathrm{e}^{\mathrm{i}\varphi} \,, \qquad \varphi = 0 \ldots 2\pi \,, \tag{8.30}$$

where a_c is set to the critical value $a_\mathrm{var} = -3\pi/8 = -1.1780$ in the variational and to $a_\mathrm{num} = -1.0251$ in the numerical exact calculations, respectively. The radius $\varrho = 10^{-3}$ was used. Both cases are shown in figures 8.4 (a) and (b). In figures 8.4 (c) and (d) the variational and numerical solutions for the chemical potential are drawn. The results were obtained for different parameter values located on the circle. As can be seen in the figures, the permutation of the two values of the chemical potential appears very clearly. Each of the two solutions ε_+ and ε_- traverses a path in the complex energy plane similar to a semicircle. A fractional power series expansion of the variational result (8.9) for small radii,

$$\varepsilon_\pm = -\frac{20}{9\pi} \pm \frac{8}{3\pi}\sqrt{\varrho}\, \mathrm{e}^{\mathrm{i}\varphi/2} - \left(\frac{4}{3\pi} + \frac{128}{27\pi^2}\right) \sqrt{\varrho}^2\, \mathrm{e}^{\mathrm{i}\varphi} \pm \left(\frac{8}{9\pi} - \frac{64}{9\pi^2}\right) \sqrt{\varrho}^3\, \mathrm{e}^{(3/2)\mathrm{i}\varphi} + \mathrm{O}\left(\sqrt{\varrho}^4\right) \,, \tag{8.31}$$

confirms this finding. The term $\frac{8}{3\pi}\sqrt{\varrho}\, \mathrm{e}^{\mathrm{i}\varphi/2}$, which dominates the path of the eigenvalue for $\varrho \ll 1$, leads to a semicircle.

For the mean field energy the permutation is also present but the structure of the paths of the two solutions is different. As can be seen from the fractional power series expansion of the analytic solution (8.7),

$$E_\pm = -\frac{4}{9\pi} + 0\sqrt{\varrho}\, \mathrm{e}^{\mathrm{i}\varphi/2} + \frac{32}{27\pi^2}\sqrt{\varrho}^2\, \mathrm{e}^{\mathrm{i}\varphi} \pm \left(\frac{4}{9\pi} - \frac{32}{9\pi^2}\right) \sqrt{\varrho}^3\, \mathrm{e}^{(3/2)\mathrm{i}\varphi} + \mathrm{O}\left(\sqrt{\varrho}^4\right) \,, \tag{8.32}$$

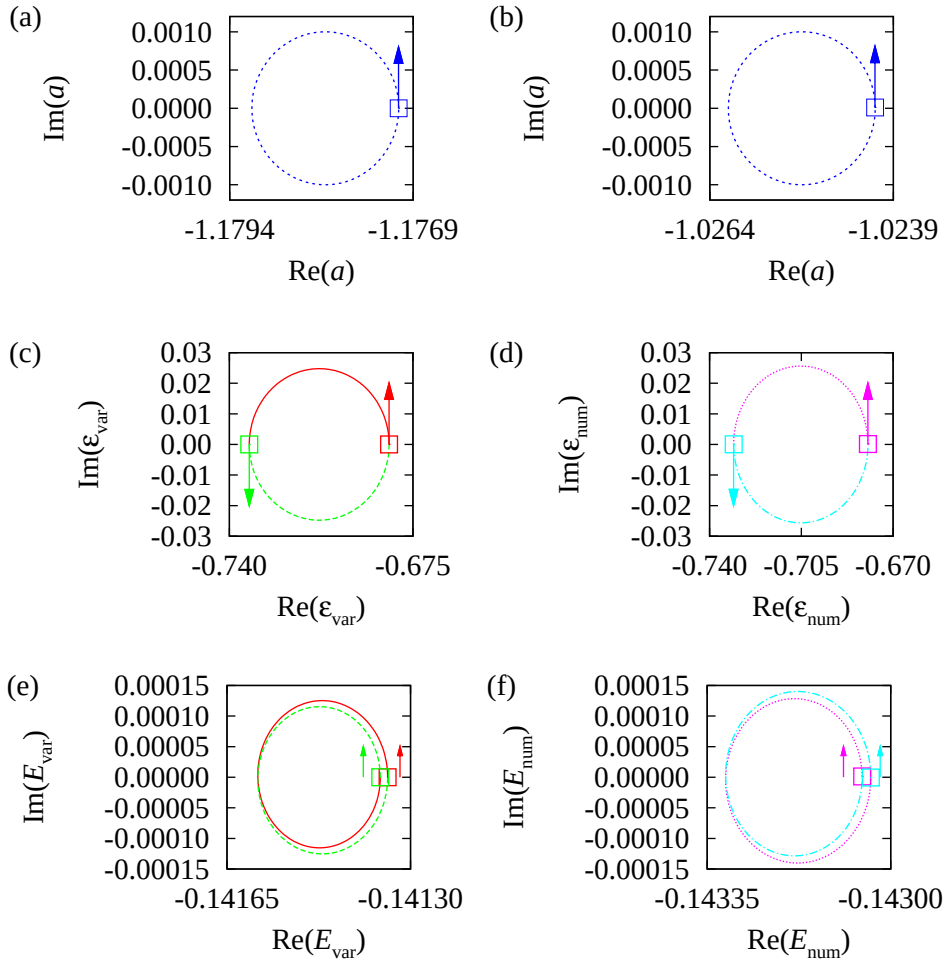

Figure 8.4: Chemical potential and mean field energy for a circle in the complex a parameter space. The first row shows the parameter space circle of type (8.30) with $\varrho = 10^{-3}$ used for the variational (a) and the numerical exact (b) calculations. The starting point is marked by an open square and the direction of progression is indicated with an arrow. In the second row, the chemical potentials ε for the variational (c) and numerical (d) solutions are plotted. The variational (e) and numerical (f) mean field energies E are presented in the third row. Each of the two solutions is drawn with a different line. The results obtained for the first parameter value on the circle are marked by an open square and the arrows point in the direction of progression. A permutation of the two solutions is present for the mean field energy as well as for the chemical potential indicating the existence of an exceptional point. All energies are given in units of the "Rydberg energy" E_u mentioned in section 8.1.

the first order term with the phase $e^{i\varphi/2}$ vanishes. The lowest non-vanishing order has the phase factor $e^{i\varphi}$, which leads to a closed curve for a complete circle in the parameter space ($\varphi = 0 \ldots 2\pi$). The third order term is the lowest order responsible for a permutation. As a consequence, it becomes more and more difficult to see a permutation for decreasing radii ϱ. Nevertheless, the permutation of the two values is present. The same result can be seen in figures 8.4 (e) and (f). The dominating structure is given by the circle following from the second order term but the permutation is clearly visible even for the small radius $\varrho = 10^{-3}$.

The exceptional point discussed here was discovered for a real value of the parameter a. This fact raises the question whether it is an object with co-dimension two as in the linear case. One has to consider that the exceptional point is still an isolated point in the two-dimensional parameter space spanned by the real and imaginary parts of a, i.e., it is a point in the parameter space which became *two-dimensional* by the complex extension. This finding is in full agreement with non-Hermitian linear systems, in which the co-dimension of exceptional points is two (cf. section 2.2). The analytic continuation is required to confirm the branch point singularity structure. As mentioned above, the appearance on the real axis is possible because of the nonlinearity of the Gross-Pitaevskii equation.

8.3.2 Behavior of the wave functions

The eigenfunctions of the extended stationary Gross-Pitaevskii equation (8.1) are not orthogonal. They behave more like the eigenstates of a non-symmetric linear system and the phase behavior (8.26) without a change in sign is expected. A possibility to check this is to calculate the complex overlap integral for the two non-orthogonal normalized states

$$O_{12} = 4\pi \int_0^\infty \psi_1(r)\psi_2(r)\, r^2 \mathrm{d}r \tag{8.33}$$

for parameter values located on a circle of the type (8.30). For this calculation it is important to note that the numerical wave functions calculated with the method described above have a phase which is fixed by the normalization factor ν determined by equation (8.13) without complex conjugation for the analytic continuation of the extended Gross-Pitaevskii model (cf. equation (8.29)). A similar procedure is used for the variational result, where the normalization constant A in (8.6) is calculated with a normalization integral without complex conjugation.

If one of the two states changes its sign during the traversal of the loop, the phase of the complex value O_{12} changes its value by π similarly to the phase behavior of the product p_{12} from equation (8.27). If this is not the case, the phase returns to its original value at the end of the loop.

In figure 8.5 the phase of the integral (8.33) is plotted for the circle defined in equation (8.30) with radius $\varrho = 10^{-3}$. The result shows clearly that the phase of O_{12} returns to its initial value after one circle around the exceptional point, demonstrating that no change

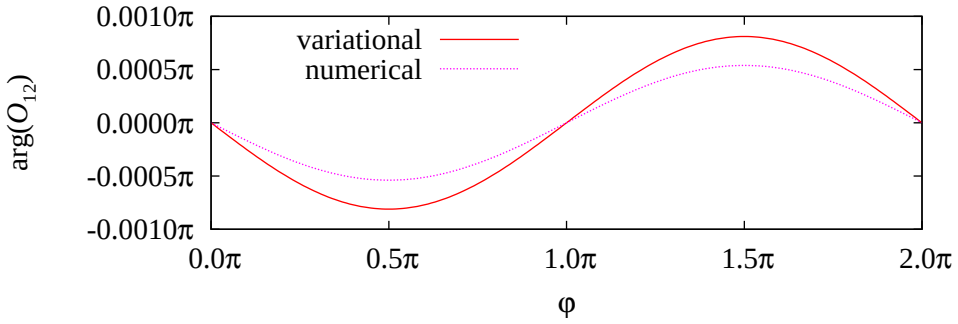

Figure 8.5: Phase $\arg(O_{12})$ of the overlap integral O_{12} defined in equation (8.33). The path in the parameter space a is a circle with the critical value as center point and $\varrho = 10^{-3}$. The angle on the circle is denoted by φ. Both the variational and the numerical results show that the phase of O_{12} returns to its initial value at the end of the circle and that the change in sign from (2.31) is not present as expected for exceptional points in linear systems described by a non-symmetric matrix.

in sign of the eigenvectors occurs. Thus, the wave functions behave in the same way as for exceptional points in linear systems described by a non-symmetric matrix (cf. section 8.2).

8.4 Decay of the condensate

The Gross-Pitaevskii equation (8.1) depends on the scattering length a of the contact potential. In section 8.3 that parameter has been extended to complex values, although the physical scattering length is always real, to investigate the complex vicinity of the branch point. There is, however, a physical situation where complex continuation is needed for real a, viz. when the scattering length is below the critical value at the tangent bifurcation. For $a < -3\pi/8 = -1.1780$ the variational solutions (8.7) and (8.9) for the mean field energy and the chemical potential become complex although a itself is real. Those parameters become complex also for the analytically continued numerically exact calculations at $a < -1.0251$. A complex chemical potential as a signature of a decaying condensate has already been discussed in reference [102].

The standard physical interpretation of complex eigenenergies is that they describe decaying resonances in open systems or systems with absorbing potentials, as is discussed in chapter 3 for the complex scaling method. The imaginary part of the energy E is related to the width Γ, decay rate λ, and lifetime T of the resonance by $\Gamma = \hbar\lambda = \hbar/T = -2\,\mathrm{Im}(E)$. Both the real and complex wave function of the Bose-Einstein condensate above and below the tangent bifurcation vanishes at large radius r and, thus, the wave function cannot describe a decay of the condensate by outgoing particles. However, with

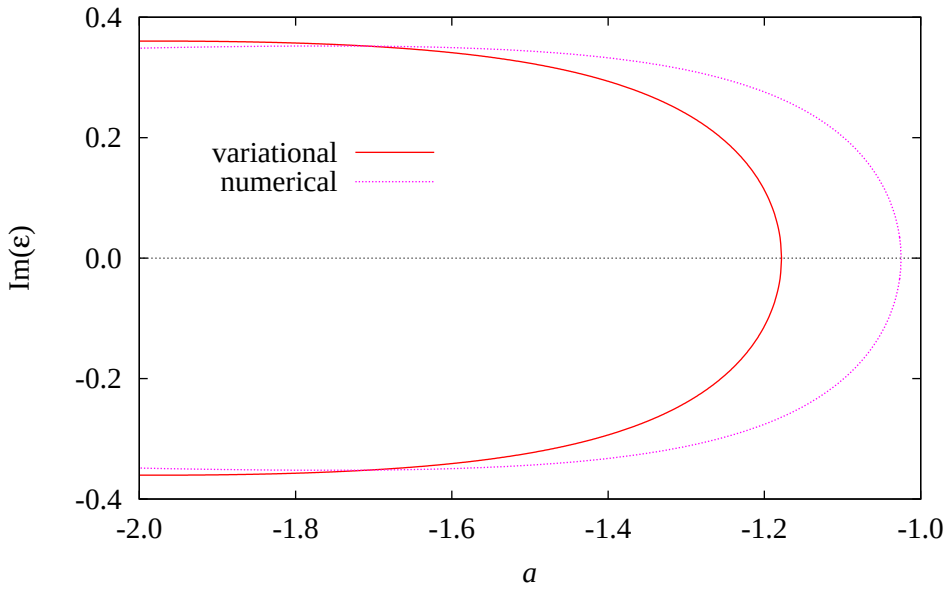

Figure 8.6: Imaginary part of the chemical potential for real a below the bifurcation point obtained with the variational and the numerical calculations. Both the continuation of the ground state and the continuation of the excited state are plotted. One is the complex conjugate of the other.

a complex wave function $\psi(\boldsymbol{r})$, the effective potential

$$V_{\text{eff}}(\boldsymbol{r}) = 8\pi a|\psi(\boldsymbol{r})|^2 - 2\int \mathrm{d}^3\boldsymbol{r}'\,\frac{|\psi(\boldsymbol{r}')|^2}{|\boldsymbol{r}-\boldsymbol{r}'|} \tag{8.34}$$

becomes complex and, therefore, contains an absorbing part. The decay is now an internal collapse of the condensate. The physical interpretation might be that at large negative scattering lengths the contact potential is so attractive that the atoms of the condensate form molecules or clusters as discussed, e.g., in references [46, 102, 103]. The decreasing number of atoms means the decay of the condensate. The imaginary part of the chemical potential as a function of the scattering length is presented in figure 8.6 for the variational as well as for the exact calculation. As was the case for parameter values above the critical point, there are two solutions. Below the critical a one is the complex conjugate of the other.

8.5 Linear stability of the bifurcating states

The two eigenstates discussed in this chapter are the solutions of a nonlinear differential equation, namely the Gross-Pitaevskii equation and it is important to know the stability properties of the eigenstates under small perturbations to get a complete picture of

the vicinity of the exceptional point studied here. This is done in this section for the variational solutions, and then it is demonstrated how the essential features carry over to the analysis of the numerically exact solutions.

To discuss the stability properties one has to investigate the time behavior of small perturbations of the stationary solutions with the linearized equations of motion. Thus, the time-dependent version of the Gross-Pitaevskii equation (8.3) is required. With the scaled variables introduced above it reads

$$\mathrm{i}\frac{\partial}{\partial t}\psi(\boldsymbol{r},t) = H\psi(\boldsymbol{r},t) = \left[-\Delta_{\boldsymbol{r}} + V_c + V_u\right]\psi(\boldsymbol{r},t)\ , \tag{8.35}$$

with the two nonlinear potentials

$$V_c = 8\pi a|\psi(\boldsymbol{r},t)|^2\ , \tag{8.36a}$$

$$V_u = -2\int \mathrm{d}^3\boldsymbol{r}'\frac{|\psi(\boldsymbol{r}',t)|^2}{|\boldsymbol{r}-\boldsymbol{r}'|}\ . \tag{8.36b}$$

8.5.1 Stability of the variational solutions

The time evolution of Gaussian wave packets consistent with the stationary time-independent ansatz (8.5) can be determined with the time-dependent variational principle

$$||\mathrm{i}\dot{\psi}(t) - H\psi(t)|| \stackrel{!}{=} \min \tag{8.37}$$

and a radially symmetric Gaussian wave packet of the form

$$\psi(r,t) = \mathrm{e}^{\mathrm{i}(Ar^2+\gamma)} = \mathrm{e}^{-(A_i r^2+\gamma_i)+\mathrm{i}(A_r r^2+\gamma_r)} \tag{8.38}$$

which is the test function. The minimization of the term (8.37) with respect to the time-dependent variational parameters $\{A(t),\gamma(t)\} = \{A_r(t)+\mathrm{i}A_i(t),\gamma_r(t)+\mathrm{i}\gamma_i(t)\}$ yields their equations of motion. These have been calculated in references [94, 104] and read

$$\dot{A} = -4A^2 + 2\sqrt{2}\pi e^{-2\gamma_i}\left(aA_i - \frac{1}{6}\right)\ , \tag{8.39a}$$

$$\dot{\gamma} = 6\mathrm{i}A + \frac{\pi e^{-2\gamma_i}}{2\sqrt{2}\,A_i}\left(5 - 14aA_i\right)\ . \tag{8.39b}$$

The imaginary part of equation (8.39b) can be integrated analytically,

$$\gamma_i(t) = -\frac{3}{4}\ln\frac{2A_i(t)}{\pi}\ , \tag{8.40}$$

and guarantees the normalization condition $||\psi||^2 = 1$. The final form of the equations of motion split into their real and imaginary parts is given by

$$\dot{A}_r = -4(A_r^2 - A_i^2) + \frac{8}{\sqrt{\pi}} A_i^{3/2} \left(a A_i - \frac{1}{6} \right) , \tag{8.41a}$$

$$\dot{A}_i = -8 A_r A_i , \tag{8.41b}$$

$$\dot{\gamma}_r = -6 A_i + \frac{1}{\sqrt{\pi}} \sqrt{A_i} \, (5 - 14 a A_i) , \tag{8.41c}$$

where the phase term (8.41c) has no influence on the stability and does not influence the width terms (8.41a) and (8.41b).

In the time-dependent variational approach, the two stationary states of the time-dependent Gross-Pitaevskii equation (8.35) appear as the time-independent solutions (fixed points) of the equations of motion (8.41a) and (8.41b). Requiring $\dot{A}_i = 0$ and $\dot{A}_r = 0$ immediately leads to

$$\hat{A}_r = 0 , \tag{8.42a}$$

$$\hat{A}_i = \frac{1}{6a} + \frac{\pi}{8a^2} \left(1 \pm \sqrt{1 + \frac{8a}{3\pi}} \right) . \tag{8.42b}$$

The vanishing real part of $\hat{A}$ implies that the state indeed is a stationary Gaussian. The scaled chemical potentials ε are given by the negative time derivative $-\dot{\gamma}_r$ of the phase of the wave function in equation (8.41c),

$$\varepsilon_{\pm}^{(\mathrm{var})} = -\dot{\gamma}_r = -\frac{4}{9\pi} \frac{5 \pm 4\sqrt{1 + \frac{8a}{3\pi}}}{\left(1 \pm \sqrt{1 + \frac{8a}{3\pi}} \right)^2} \tag{8.43}$$

and correctly reproduce the result (8.9).

The linearization of the equations of motion (8.41a) and (8.41b) around the stationary solutions $\hat{A}_r$, $\hat{A}_i$ are given by

$$\delta \dot{A}_{r\pm} = \pm \frac{8}{9\pi} \frac{\sqrt{1 + \frac{8a}{3\pi}}}{\left(\sqrt{1 + \frac{8a}{3\pi}} \pm 1 \right)^2} \delta A_{i\pm} , \tag{8.44a}$$

$$\delta \dot{A}_{i\pm} = -\frac{32}{9\pi} \frac{1}{\left(\sqrt{1 + \frac{8a}{3\pi}} \pm 1 \right)^2} \delta A_{r\pm} . \tag{8.44b}$$

The eigenmodes with the eigenvalues $\xi^{(\mathrm{var})}$ of equations (8.44a) and (8.44b) are calculated with the usual ansatz $\delta A_{r,i}(t) = \delta A_{r,i}^{(0)} \mathrm{e}^{\xi^{(\mathrm{var})} t}$. For the stationary ground state one finds

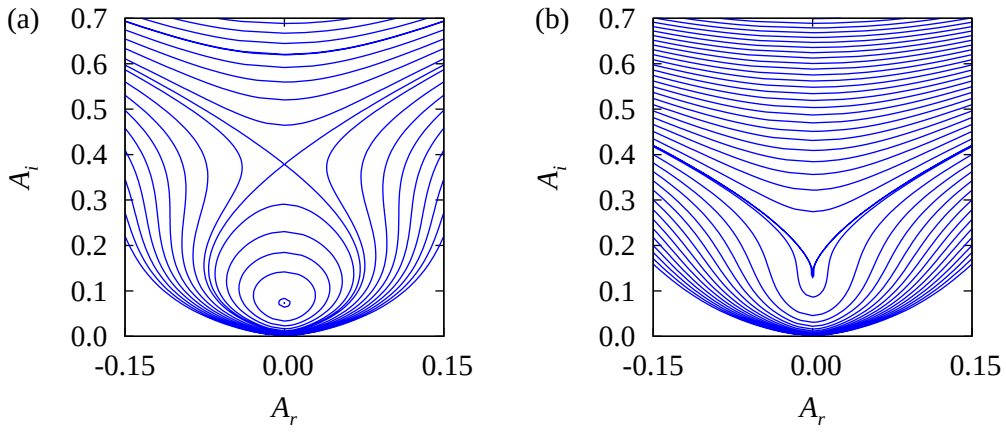

Figure 8.7: Equipotential lines according to equation (8.46) in the vicinity of the two stationary states. (a) For $a = -1.0$ the elliptic and the hyperbolic fixed points are clearly visible. (b) For $a = -3\pi/8 = -1.1780$ at the exceptional point the stationary states coalesce and the stable motion near the elliptic fixed point vanishes.

the two eigenvalues

$$\xi_+^{(\mathrm{var})} = \pm\frac{16\mathrm{i}}{9\pi}\frac{\sqrt[4]{1+\frac{8a}{3\pi}}}{\left(\sqrt{1+\frac{8a}{3\pi}}+1\right)^2}\,, \tag{8.45}$$

which are always imaginary for $a > -3\pi/8$ (i.e., above the bifurcation point). They describe an *elliptic fixed point*, which is stable and can be seen in figure 8.7(a), where equipotential lines

$$E = \frac{3\,(A_i^2 + A_r^2)}{A_i} + \frac{2\sqrt{A_i}(2aA_i - 1)}{\sqrt{\pi}} \tag{8.46}$$

for fixed mean field energy E are drawn. Due to the conservation of the mean field energy for a motion in the (A_r,A_i)-space they correspond to "phase portraits" in these variables. The two eigenvalues of the excited stationary state,

$$\xi_-^{(\mathrm{var})} = \pm\frac{16}{9\pi}\frac{\sqrt[4]{1+\frac{8a}{3\pi}}}{\left(\sqrt{1+\frac{8a}{3\pi}}-1\right)^2}\,, \tag{8.47}$$

are always real for negative scattering lengths $a > -3\pi/8$, and one eigenvalue is positive. Hence, the eigenstate is unstable and belongs to a *hyperbolic fixed point*, whose structure can also be seen in figure 8.7(a). At the exceptional point both stationary states coalesce and the stable motions around the elliptic fixed point vanish as is demonstrated in figure 8.7(b).

8.5.2 Stability of the numerically exact solutions

Numerically exact stationary eigenstates of the Gross-Pitaevskii equation (8.3) which are the counterpart of the variational solutions described above are already known from section 8.1.2. Here, the stability of these states is investigated and compared with the eigenvalues (8.45) and (8.47). For the stability analysis, the procedure applied by Huepe et al. [48] for condensates without $1/r$ interaction in a harmonic trap is extended to the scaled integro-differential equation (8.35). The extended Gross-Pitaevskii equation is linearized with the Fréchet derivative, once the wave function has been decomposed in its real $\psi^R(\boldsymbol{r},t)$ and imaginary $\psi^I(\boldsymbol{r},t)$ part. The derivative is evaluated at the real-valued stationary states $\hat{\psi}_\pm(\boldsymbol{r})$ introduced in section 8.1.2, which leads to two coupled equations, viz.

$$\frac{\partial}{\partial t}\delta\psi^R(\boldsymbol{r},t) = \left(-\Delta - \varepsilon + 8\pi a\hat{\psi}_\pm(\boldsymbol{r})^2 - 2\int \mathrm{d}^3\boldsymbol{r}'\,\frac{\hat{\psi}_\pm(\boldsymbol{r}')^2}{|\boldsymbol{r}-\boldsymbol{r}'|}\right)\delta\psi^I(\boldsymbol{r},t)\;, \tag{8.48a}$$

$$\begin{aligned}\frac{\partial}{\partial t}\delta\psi^I(\boldsymbol{r},t) = &\left(-\Delta - \varepsilon + 24\pi a\hat{\psi}_\pm(\boldsymbol{r})^2 - 2\int \mathrm{d}^3\boldsymbol{r}'\,\frac{\hat{\psi}_\pm(\boldsymbol{r}')^2}{|\boldsymbol{r}-\boldsymbol{r}'|}\right)\delta\psi^R(\boldsymbol{r},t)\\ &+ 4\hat{\psi}_\pm(\boldsymbol{r})\int \mathrm{d}^3\boldsymbol{r}'\frac{\hat{\psi}_\pm(\boldsymbol{r}')\,\delta\psi^R(\boldsymbol{r}',t)}{|\boldsymbol{r}-\boldsymbol{r}'|}\;.\end{aligned} \tag{8.48b}$$

For the calculation of the numerical eigenmodes perturbations in the form $\delta\psi^R(\boldsymbol{r},t) = \delta\psi_0^R(\boldsymbol{r})\mathrm{e}^{\xi^{(\mathrm{num})}t}$, and $\delta\psi^I(\boldsymbol{r},t) = \delta\psi_0^I(\boldsymbol{r})\mathrm{e}^{\xi^{(\mathrm{num})}t}$ are used. Note that $\delta\psi_0^R(\boldsymbol{r})$ and $\delta\psi_0^I(\boldsymbol{r})$ are not always real-valued. As solutions of the linearized equations (8.48a) and (8.48b) they can become complex wave functions.

The numerical solution of the linearized wave equations is done with an extension of the method described in section 8.1.2. With the "linearized potential"

$$U_1(\boldsymbol{r}) = 4\int \mathrm{d}^3\boldsymbol{r}'\frac{\hat{\psi}_\pm(\boldsymbol{r}')\,\delta\psi^R(\boldsymbol{r}',t)}{|\boldsymbol{r}-\boldsymbol{r}'|} \tag{8.49}$$

the equations (8.48a) and (8.48b) can be transformed into a system of three second order ordinary differential equations, which can be solved together with the stationary extended Gross-Pitaevskii equation. The ordinary differential equations which have to be solved are the Bogoliubov equations of the system and read

$$\xi\delta\psi_0^R(r) = -\delta\psi_0^I(r)'' - \frac{2}{r}\delta\psi_0^I(r)' + \left(8\pi a\hat{\psi}_\pm(r)^2 - U(r)\right)\delta\psi_0^I(r)\;, \tag{8.50a}$$

$$\xi\delta\psi_0^I(r) = -\delta\psi_0^R(r)'' - \frac{2}{r}\delta\psi_0^R(r)' + \left(24\pi a\hat{\psi}_\pm(r)^2 - U(r)\right)\delta\psi_0^R(r) - U_1(r)\hat{\psi}_\pm(r)\;, \tag{8.50b}$$

$$U_1(r)'' = -\frac{2}{r}U_1(r)' - 16\pi\,\hat{\psi}_\pm(r)\,\delta\psi^R(r,t)\;. \tag{8.50c}$$

The wave functions $\delta\psi_0^R(r)$ and $\delta\psi_0^I(r)$ are only determined up to a complex (normalization) constant, which they have in common. Therefore only two real variables are required to set the initial value $(\delta\psi_0^R(0), \delta\psi_0^I(0)) = (\cos\alpha, \sin\alpha\, \mathrm{e}^{\mathrm{i}\beta})$ for the integration. The real angles α and β, the complex eigenvalue ξ, and the complex initial value $U_1^{(0)} = U_1(0)$ are the parameters which have to be searched to find the solutions of the system (8.50a)–(8.50c). The initial conditions for the first derivatives are $(\delta\psi^R)' = (\delta\psi^I)' = U_1' = 0$. The correct solutions are found when square integrable wave functions are obtained and the value of $U_1^{(0)}$ initially assumed is identical with the integral

$$U_1(0) = 16\pi \int_0^\infty \mathrm{d}r'\, r' \hat{\psi}_\pm(r')\, \delta\psi_0^R(r') \;, \tag{8.51}$$

which can be calculated once the numerical wave function has been determined.

As can be seen from the system (8.50a)–(8.50c), the differential equations are invariant if in addition to the transformations (8.12) the time and the eigenvalue are scaled by $t \to t/\nu^2$ and $\xi \to \nu^2\xi$, respectively. Thus, it is possible to solve the system of differential equations (8.50a)–(8.50c) with the unscaled and non-normalized stationary solutions $\hat{\psi}_\pm(r)$ of the nonlinear extended Gross-Pitaevskii equation computed numerically if a subsequent scaling of the eigenvalues is performed.

When the solution of the linearized system is carried out for the stationary ground state, a pair $\xi_1 = -\xi_2$ of purely imaginary eigenvalues is found. These are plotted as a function of the scaled scattering length a in figure 8.8. The same calculation for the nodeless stationary state yields a pair of purely real eigenvalues. The qualitative agreement between the eigenvalues calculated numerically and the results obtained analytically in the variational approach is very good, but there are significant quantitative differences on the a-axis. Such behavior is known from previous studies of the system [49, 50, 95]. Similar to the case discussed in reference [48], there exist neutral modes with the eigenvalue $\xi^{(\mathrm{num})} = 0$, and additional imaginary eigenvalues are found for both stationary solutions. Altogether, the numerically exact results confirm the stability analysis performed using the analytical eigenvalues of the variational approach.

In summary, one can note that at the exceptional point two solutions to the Gross-Pitaevskii equation are born in a tangent bifurcation. One of the states is a stable ground state. The second is an unstable excited state.

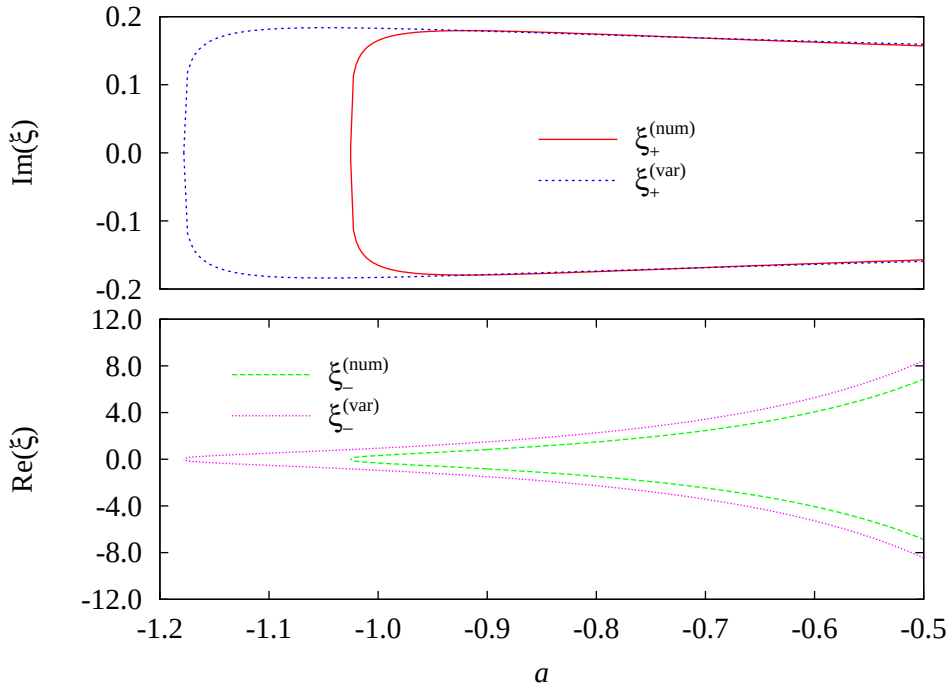

Figure 8.8: Eigenvalues of the linearization of the extended Gross-Pitaevskii system (8.35) for the two stationary solutions emerging at the tangent bifurcation. Both the variational (var) and the numerically exact (num) solutions are shown. The two eigenvalues ξ_+ of the stationary ground state are purely imaginary demonstrating that the state is an elliptic fixed point. In contrast to this finding, the two eigenvalues ξ_- of the nodeless excited state are purely real. One is positive, the other is negative. The state is an hyperbolic fixed point. Vanishing real or imaginary parts are not shown.

9 Dipolar Bose-Einstein condensates

As mentioned in the previous chapter, the self-trapping case of a Bose-Einstein condensate with attractive $1/r$ interaction is of high interest for the investigation of exceptional points due to the analytic variational solutions. However, the realization in experiments remains a challenging task. Experimental realization has been achieved for a similar system with a long-range interaction, viz. dipolar Bose-Einstein condensates [52]. Here, the long-range dipole-dipole interaction appears next to the short-range contact term. The system has attracted much attention in recent years [53–57] and the condensation has been achieved in a gas of chromium atoms [58], which have the large dipole moment of six Bohr magnetons. Recently, very promising experiments have been carried out [59, 60, 62]. For example, the experimental observation of the dipolar collapse of a quantum gas has been reported by Koch et al. [61], which sets in when the contact interaction is reduced below some critical value.

It is the purpose of this chapter to demonstrate that exceptional points also exist in dipolar Bose-Einstein condensates and that the results obtained in chapter 8 can be used to interpret the behavior found here. The investigation of dipolar Bose-Einstein condensates allow for the discussion of exceptional points in cases which are close to experiments. In particular, the examples used here are chosen at parameter values used in the experiments by Koch et al. [61].

The system is investigated within the framework of a variational approach introduced in section 9.1. The variational solutions are used to discuss the branch point singularity structure of the energy eigenvalues in section 9.2 and to analyze the stability properties of the branching solutions in section 9.3.

9.1 Variational mean field approximation

The Gross-Pitaevskii equation for the system [52] includes the dipole-dipole interaction potential

$$V(\boldsymbol{r}-\boldsymbol{r}') = \frac{\mu_0}{4\pi}\frac{\boldsymbol{\mu_1}(\boldsymbol{r})\cdot\boldsymbol{\mu_2}(\boldsymbol{r}') - 3\left(\boldsymbol{\mu}_1(\boldsymbol{r})\cdot\frac{\boldsymbol{r}-\boldsymbol{r}'}{|\boldsymbol{r}-\boldsymbol{r}'|}\right)\left(\boldsymbol{\mu}_2(\boldsymbol{r}')\cdot\frac{\boldsymbol{r}-\boldsymbol{r}'}{|\boldsymbol{r}-\boldsymbol{r}'|}\right)}{|\boldsymbol{r}-\boldsymbol{r}'|^3}\,, \tag{9.1}$$

where $\boldsymbol{\mu}_{1,2}$ are the dipole moments of the interacting particles at places $\boldsymbol{r}$ and $\boldsymbol{r}'$ and μ_0 is the permeability. The potential contributes via its mean field approximation

$$V_{\mathrm{dd}}(\boldsymbol{r}) = N\int|\psi(\boldsymbol{r}')|^2 V(\boldsymbol{r}-\boldsymbol{r}')\,\mathrm{d}^3\boldsymbol{r}' = N\frac{\mu_0\mu^2}{4\pi}\int|\psi(\boldsymbol{r}')|^2\frac{1-3\cos^2\vartheta'}{|\boldsymbol{r}-\boldsymbol{r}'|^3}\,\mathrm{d}^3\boldsymbol{r}'\,, \tag{9.2}$$

where ϑ' is the angle between $\boldsymbol{r}$ and $\boldsymbol{r}'$. As in the monopolar system, appropriate atomic units can be introduced [105, 106]. They are based on the "dipole length" (cf. appendix A.3)

$$a_\mathrm{d} = \frac{\alpha^2}{2}\frac{m}{\mathrm{m_e}}\left(\frac{\mu}{\mu_\mathrm{B}}\right)^2 \mathrm{a}_0 \,, \tag{9.3}$$

with the mass m of one boson, the fine-structure constant α, the electron mass $\mathrm{m_e}$, the Bohr magneton μ_B, and the Bohr radius a_0. These units included, the dimensionless form of the Gross-Pitaevskii equation can be written as [105, 106]

$$\left[-\Delta_{\boldsymbol{r}} + \gamma_\varrho^2\varrho^2 + \gamma_z^2 z^2 + N8\pi a|\psi(\boldsymbol{r})|^2 + N\int |\psi(\boldsymbol{r}')|^2 \frac{1-3\cos^2\vartheta'}{|\boldsymbol{r}-\boldsymbol{r}'|^3}\mathrm{d}^3\boldsymbol{r}'\right]\psi(\boldsymbol{r}) = \varepsilon\psi(\boldsymbol{r}) \,. \tag{9.4}$$

In contrast to the attractive $1/r$ interaction, an external trap is always required for stable dipolar condensates and the anisotropic dipole-dipole interaction demands at least two coordinates (ϱ and z in equation (9.4)) for ordered dipoles to be used in the wave function. Therefore, two additional parameters, namely the two frequencies γ_ϱ and γ_z of the harmonic trap are present. Again, scaling properties can be introduced which reveal that the physics of equation (9.4) is completely determined by three parameters. Using the relations [105, 106]

$$(\tilde{\boldsymbol{r}}, \tilde{\gamma}, \tilde{\varepsilon}, \tilde{E}, \tilde{t}, \tilde{\psi}) = (\boldsymbol{r}/N, N^2\gamma, N^2\varepsilon, NE, t/N^2, N^{3/2}\psi) \,, \tag{9.5}$$

one can bring the Gross-Pitaevskii equation in the scaled form

$$\left[-\Delta_{\tilde{\boldsymbol{r}}} + \tilde{\gamma}_\varrho^2\tilde{\varrho}^2 + \tilde{\gamma}_z^2\tilde{z}^2 + 8\pi a|\tilde{\psi}(\tilde{\boldsymbol{r}})|^2 + \int |\tilde{\psi}(\tilde{\boldsymbol{r}}')|^2 \frac{1-3\cos^2\vartheta'}{|\tilde{\boldsymbol{r}}-\tilde{\boldsymbol{r}}'|^3}\mathrm{d}^3\tilde{\boldsymbol{r}}'\right]\tilde{\psi}(\tilde{\boldsymbol{r}}) = \tilde{\varepsilon}\tilde{\psi}(\tilde{\boldsymbol{r}}) \,, \tag{9.6}$$

where the tilde will be omitted in what follows. The case of ordered dipoles will always be assumed such that a three-dimensional parameter space spanned by the scattering length a and the two scaled trap frequencies γ_ϱ^2 and γ_z^2 is used. Equivalently one can express the two trap frequencies by their geometric mean

$$\bar{\gamma} = \gamma_\varrho^{2/3}\gamma_z^{1/3} \tag{9.7a}$$

and the aspect ratio

$$\zeta = \gamma_z/\gamma_\varrho \,, \tag{9.7b}$$

which allow for the distinction of repulsive and attractive behaviors of the dipole-dipole interaction. For $\zeta > 1$ the condensate will adjust to the pancake like form imposed by the trap geometry. The dipoles will be ordered mainly side by side and their interaction is repulsive. In the opposite case of $\zeta < 1$ the trap imposes a cigar like shape of the condensate and the magnetic dipoles are mainly orientated in a row, which results in an effective attractive dipole-dipole force.

The familiar variational Gaussian ansatz, which has proven to provide good results for condensates with laser induced $1/r$ interaction, is used to study the effects appearing in the Gross-Pitaevskii equation (9.6). The normalized Gaussian (8.5) introduced for the monopolar $1/r$ system is extended to two dimensions,

$$\psi(\boldsymbol{r}) = A \exp\left[-(A_\varrho \varrho^2 + A_z z^2)\right] \ . \tag{9.8}$$

In this approximation the scaled mean field functional $E[\psi]$ and the scaled chemical potential ε read [106]

$$\begin{aligned} E[\psi] &= 2A_\varrho + A_z + \frac{\gamma_\varrho^2}{2A_\varrho} + \frac{\gamma_z^2}{4A_z} + \frac{4}{\sqrt{\pi}} a A_\varrho \sqrt{A_z} \\ &\quad + \frac{2}{\sqrt{\pi}} A_\varrho \sqrt{A_z} \frac{1}{3(\varkappa^2-1)} \left(1 + 2\varkappa^2 - \frac{3\varkappa^2 \arctan\sqrt{\varkappa^2-1}}{\sqrt{\varkappa^2-1}}\right) , \end{aligned} \tag{9.9a}$$

$$\begin{aligned} \varepsilon &= 2A_\varrho + A_z + \frac{\gamma_\varrho^2}{2A_\varrho} + \frac{\gamma_z^2}{4A_z} + \frac{8}{\sqrt{\pi}} a A_\varrho \sqrt{A_z} \\ &\quad + \frac{4}{\sqrt{\pi}} A_\varrho \sqrt{A_z} \frac{1}{3(\varkappa^2-1)} \left(1 + 2\varkappa^2 - \frac{3\varkappa^2 \arctan\sqrt{\varkappa^2-1}}{\sqrt{\varkappa^2-1}}\right) , \end{aligned} \tag{9.9b}$$

where

$$\varkappa = \frac{A_z}{A_\varrho} \ . \tag{9.9c}$$

Stationary solutions to the Gross-Pitaevskii equation are now obtained for the values A_ϱ and A_z which are extrema of the mean field functional.

9.2 Branch points of the energy eigenvalues

It is not possible to get analytic expressions for the stationary states of the Gross-Pitaevskii equation. The extrema are only accessible numerically. Accordingly, exceptional points cannot be confirmed with an analytic expression for the energy eigenvalues as it was possible with the variational solution (8.9) in the self-trapped case of condensates with attractive $1/r$ interaction. The properties of exceptional points, e.g., the permutation of the eigenvalues has to be used to prove their existence as it was done for the hydrogen atom in chapter 5.

The bifurcation scenario at which two solutions to the Gross-Pitaevskii equation appear at a certain value of the scattering length persists in the presence of the dipole-dipole interaction but exhibits a complete three-dimensional structure. Whereas there was only one bifurcation point in the self-trapped case of a Bose-Einstein condensate with attractive $1/r$ interaction, now the scattering length at which the collapse sets in

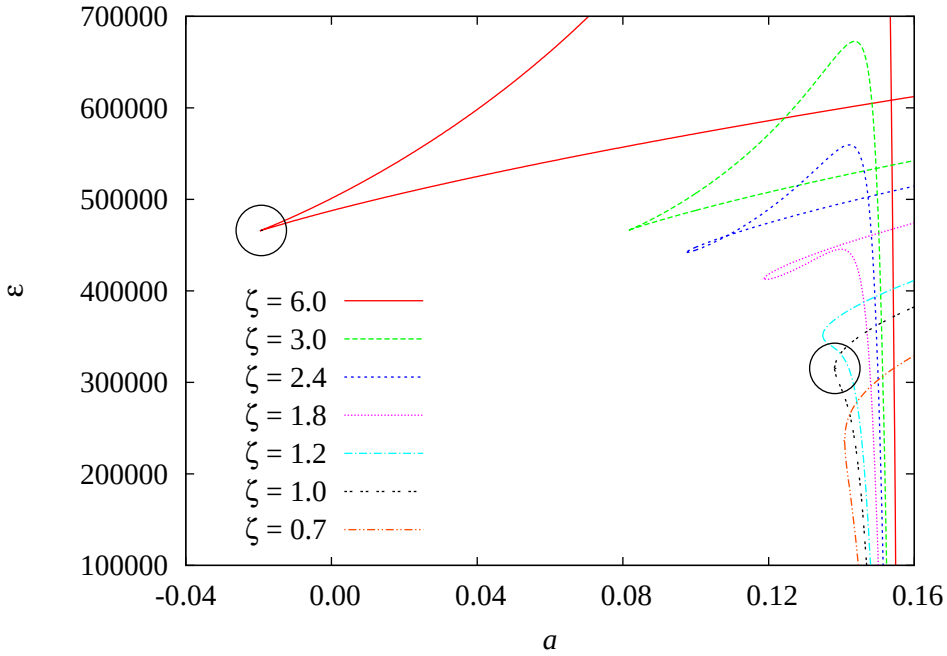

Figure 9.1: Chemical potential (9.9b) of the two stationary states emerging in the tangent bifurcation for several values of the aspect ratio ζ and constant mean trap frequency $\bar{\gamma} = 3.4 \times 10^4$. The two circles mark the bifurcation points investigated in figures 9.3 and 9.4 with respect to exceptional points.

(point of bifurcation) depends on the two further parameters $\bar{\gamma}$ and ζ. Examples are given in figure 9.1 for several aspect ratios ζ. One can find two solutions which emerge together at a critical value of the scattering length, which depends on ζ. If one analyzes the vicinity of the energy functional around the two stationary solutions one can find that one of them corresponds to a minimum in the two-dimensional landscape of the mean field energy spanned by A_ϱ and A_z, and represents the ground state whereas the second one belongs to a saddle point and is an excited state. The mean field energy of the saddle point solution which belongs to the branches diverging for $a \to 1/6$ is always higher than that of the ground state. By contrast, the chemical potential is not adequate to distinguish the ground and the excited state due to the intersections of both branches visible in figure 9.1.

A similar behavior can be found for a variation of the mean frequency $\bar{\gamma}$. One can calculate the bifurcation point for every combination of $\bar{\gamma}$ and ζ and finally obtains a "critical surface," where the collapse of the condensate sets in, in the three-dimensional parameter space. This surface is plotted in figure 9.2. For large values of $\bar{\gamma}$ the dipole-dipole interaction is dominant and determines the collapse behavior which has been proven experimentally [61]. Here, an attractive dipole-dipole interaction can produce a collapse of the condensate which occurs for repulsive scattering lengths $a > 0$. A

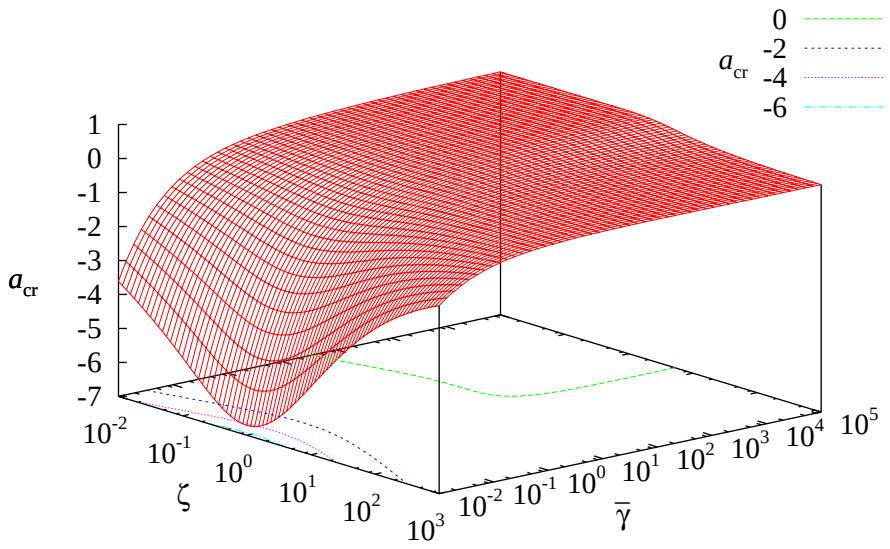

Figure 9.2: Critical surface, where a collapse of the condensate within the mean field approximation (9.9a) is predicted or, in other words, the two stationary states emerge in a tangent bifurcation. Parameters are the aspect ratio ζ and the mean trap frequency $\bar{\gamma}$. Contour lines of constant a_{cr} are drawn at the base of the graph.

repulsive dipole-dipole interaction ($\zeta > 1$) can stabilize the condensate against collapse such that the collapse only sets in for a negative scattering length. For $\bar{\gamma} < 1$ the contact interaction is dominant and the dipole-dipole interaction is only a small perturbation.

After the bifurcation point in the much simpler case of the attractive $1/r$ interaction has turned out to be a branch point singularity of the energy eigenvalues the question arises if this property survives in the dipolar case and if the bifurcation points on the surface 9.2 are exceptional points. One can prove that this is the case if the complex vicinity of the points of bifurcation is investigated. For this purpose the scattering length a is, again, extended to complex numbers. Results are shown in figure 9.3 for $\bar{\gamma} = 3.4 \times 10^4$ and $\zeta = 6$. This configuration is one of the examples realized in the experiment of Koch et al. [61]. A circle of the form (8.30) is used. The results show that the typical permutation of the energy eigenvalues is present, and, thus that they form a branch point singularity. That is, also the collapse points of dipolar condensates are exceptional points. This behavior is, in particular, present in the regime $\bar{\gamma} \gg 1$, where the "dipolar" collapse exists. This means that the experiments by Koch et al. are experimental realizations of a quantum system near an exceptional point.

A more detailed analysis of the permutation property reveals an influence of the aspect ratio on the behavior of the two chemical potentials. Figures 9.3(a), (b), and (c) depict

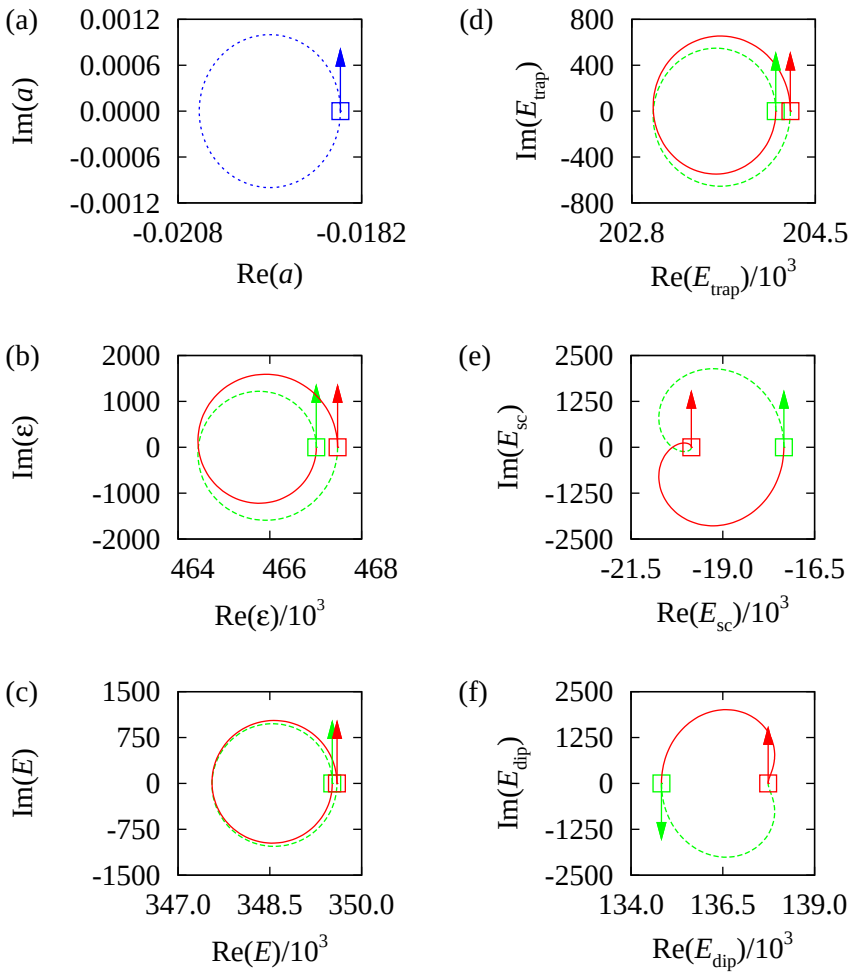

Figure 9.3: (a) Circle in the complex extended space of the scattering length a, (b) chemical potential ε, (c) mean field energy E, (d) trap energy E_{trap}, (e) energy E_{sc} of the scattering term, (f) energy E_{dip} of the dipole-dipole interaction. The trap parameters are $\bar{\gamma} = 3.4 \times 10^4$ and $\zeta = 6$. For all energies a permutation proving the existence of an exceptional point is present.

the complex extended scattering length a, the chemical potential ε, and the mean field energy E. The permutation of the two energy eigenvalues ε of the Gross-Pitaevskii equation is present. The same permutation can also be observed for the mean field energy E, however, the starting and end points of the two energies are very close to each other and their single paths in the complex energy plane are almost closed. Nevertheless, the permutation is present. This behavior of the mean field energy is already known from the Gross-Pitaevskii equation of condensates with attractive $1/r$ interaction, which was discussed with the fractional power series expansion (8.32). There are, however, differ-

ences between both systems for the chemical potential, which has a clear semicircle like structure in the $1/r$ case and which has more similarity with the permutation behavior of the mean field energy in the dipolar case. An analysis of the parts of the energy reveals that the energy E_{trap} of the harmonic trap drawn in figure 9.3(d) already has the shape of the eigenvalue paths of the mean field energy. The scattering term E_{sc} (figure 9.3(e)) and the energy E_{dip} (figure 9.3(f)) alone have a semicircle structure but they almost cancel each other. Both have a difference between the two energy eigenvalues in the same order of magnitude but with opposite order of the eigenvalues on the energy axis. The contribution from the kinetic energy in the Gross-Pitaevskii equation has the smallest influence on the energy difference and is not shown.

As was discussed in section 8.3.1 for the comparison of the chemical potential and the mean field energy, the half circle structure appears if the first order in a fractional power series expansion which is proportional to $\sqrt{\varrho}\mathrm{e}^{\mathrm{i}\varphi/2}$ for a circle of the type

$$a = a_{\mathrm{c}} + \varrho\,\mathrm{e}^{\mathrm{i}\varphi}\,, \qquad \varphi = 0\ldots 2\pi \tag{8.30}$$

around the branch point does not vanish. Obviously this first order is small or does vanish in the cases discussed above. But this is not always the case for dipolar condensates. Figure 9.4 presents the complex vicinity of the bifurcation point for the trap parameters $\bar{\gamma} = 3.4 \times 10^4$ and $\zeta = 1$. Again, a permutation of all eigenvalues can be observed, which proves that the point of bifurcation is an exceptional point. The structure here is more similar to the $1/r$ case than it was for the example at $\zeta = 6$ discussed previously. The chemical potential (figure 9.4(b)) has a half circle structure as all the single components shown in figures 9.4(d), (e), and (f). Only the combination of all components to the mean field energy (figure 9.4(c)) obviously leads to the cancellation of the first order $\sqrt{\varrho}\mathrm{e}^{\mathrm{i}\varphi/2}$ in the small circle.

With the complex extension of the scattering length a, the parameter space in which the exceptional points have been found is four-dimensional. It consists of the real and imaginary parts of a and the two trap parameters $\bar{\gamma}$ and ζ. There are no longer isolated exceptional points. Each bifurcation scenario exhibits one exceptional point at different combinations a, $\bar{\gamma}$, and ζ. The critical surface shown in figure 9.2 represents exactly the sum of all exceptional points and can be called an "exceptional surface." It is a two-dimensional object in the four-dimensional parameter space. This is in accordance with the property of generalized exceptional points which have the co-dimension two.

9.3 Linear stability of the two branches

Since one of the stationary solutions corresponds to a minimum of the mean field functional it should be dynamically stable. The solution which corresponds to the saddle point of the functional should be dynamically stable in one direction and unstable in the other. Both properties can be confirmed with a linear stability analysis similar to

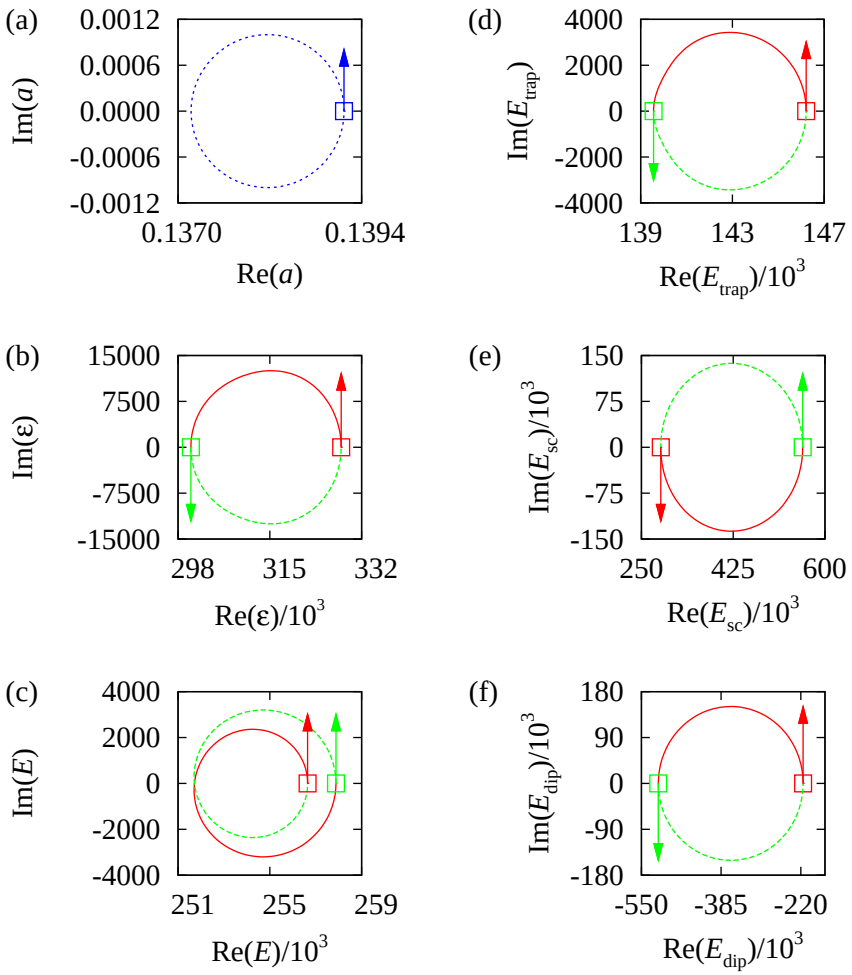

Figure 9.4: Same illustration as in figure 9.3 but for a circle around the bifurcation point appearing for $\bar{\gamma} = 3.4 \times 10^4$ and $\zeta = 1$. Again, the permutation of the energy values proves the existence of an exceptional point. (a) Complex extended scattering length, (b) chemical potential, (c) mean field energy, (d) trap energy, (e) energy of the scattering term, (f) energy of the dipole-dipole interaction.

section 8.5. For this purpose the time-dependent Gross-Pitaevskii equation

$$\mathrm{i}\frac{\partial}{\partial t}\psi(\boldsymbol{r}) = \left[-\Delta_{\boldsymbol{r}} + \gamma_\varrho^2\varrho^2 + \gamma_z^2 z^2 + 8\pi a|\psi(\boldsymbol{r})|^2 + \int |\psi(\boldsymbol{r}')|^2 \frac{1-3\cos^2\vartheta'}{|\boldsymbol{r}-\boldsymbol{r}'|^3}\mathrm{d}^3\boldsymbol{r}'\right]\psi(\boldsymbol{r}) \tag{9.10}$$

is required which is solved with the variational principle (8.37) and the time-dependent version

$$\psi(\boldsymbol{r}) = \exp\left[\mathrm{i}(A_\varrho(t)\varrho^2 + A_z(t)z^2 + \gamma(t))\right] \tag{9.11}$$

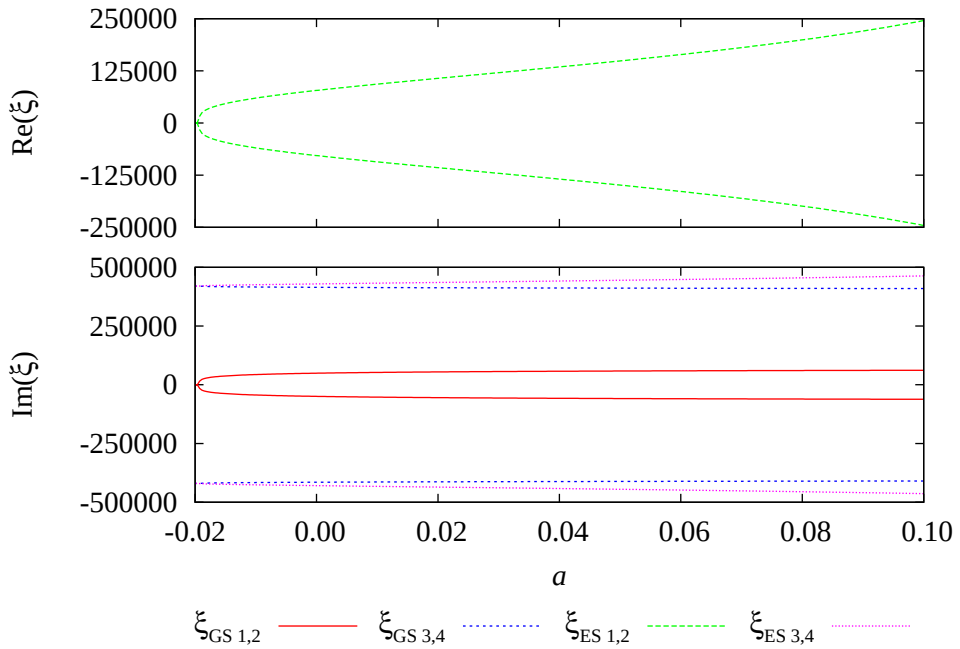

Figure 9.5: Eigenvalues of the linearized equations of motion for the extended Gross-Pitaevskii system (9.10) and the two stationary solutions emerging at the exceptional point. All four eigenvalues ξ_{GS} of the ground state are purely imaginary and demonstrate its stability. By contrast, two eigenvalues ξ_{ES} of the excited state are purely real with one of them positive. This state is dynamically unstable. Vanishing real or imaginary parts are not shown.

of the ansatz (9.8), where A_ϱ, A_z, and γ are now complex variational coefficients. The application of the time-dependent variational principle leads to four coupled equations of motion for the width parameters A_ϱ and A_z which have been presented in reference [104]. Their linearization around the two stationary states leads to the equations of motion for the deviations $\delta A_{\varrho,z}(t) = \delta A^{(0)}_{\varrho,z} \mathrm{e}^{\xi t}$. Since A_ϱ and A_z are complex altogether four eigenvalues ξ are obtained. The stationary solutions are only available numerically and, thus, one can find no analytic expression for the eigenvalues ξ of the linearized equations of motion. A numerical analysis provides the results displayed in figure 9.5, in which all four eigenvalues for both stationary states are drawn. The example is given for the trap parameters $\bar{\gamma} = 3.4 \times 10^4$ and $\zeta = 6$ but is qualitatively identical for all other cases in which both solutions are present. The ground state (labeled GS in the figure) which corresponds to the minimum in the energy functional turns out to be dynamically stable as expected. Its four eigenvalues appear in pairs $\lambda_{\mathrm{GS},1} = -\lambda_{\mathrm{GS},2}$ and $\lambda_{\mathrm{GS},3} = -\lambda_{\mathrm{GS},4}$ and are all purely imaginary. The linearized motions of a condensate wave function in the vicinity of the ground state describe oscillations around the stationary solution. By contrast the eigenvalues of the excited state (labeled ES in the figure) do

not indicate a stable motion. As expected from a saddle point one direction (described by $\lambda_{\mathrm{ES},3} = -\lambda_{\mathrm{ES},4}$) is stable with two purely imaginary eigenvalues and the other exhibits two real eigenvalues $\lambda_{\mathrm{ES},1} = -\lambda_{\mathrm{ES},2}$ with one of them positive. The positive eigenvalue leads to an exponential increase of the one coefficient δA which points in the direction of the corresponding eigenvector in the four-dimensional $(\delta A_\varrho, \delta A_z)$-space. Hence, the excited state is unstable.

The four eigenvalues obtained here for each branch of the solutions to the Gross-Pitaevskii equation reveal a more complicated structure as the two eigenvalues in the radially symmetric case investigated for condensates with attractive $1/r$ interaction in section 8.5 but the main result is the same. At the exceptional point two solutions emerge in a tangent bifurcation. One of them corresponds to a dynamically stable ground state and the other to a dynamically unstable excited stationary solution.

10 Conclusion and outlook

Exceptional points are a feature that can emerge in parameter-dependent open quantum systems with decaying unbound states. They are branch point singularities at which two eigenstates of a non-Hermitian Hamiltonian coalesce. It was the topic of this thesis to investigate these exceptional points in the spectra of atoms in external fields and the Gross-Pitaevskii equations describing Bose-Einstein condensates with long-range interatomic interactions.

The numerical investigation of the resonances of the hydrogen atom required the diagonalization of large complex symmetric matrices with several thousand basis states. The possibility to extend effective algorithms for real symmetric matrices has been analyzed. Even in the case of exceptional points these algorithms often succeed in calculating the eigenvalues. However, without taking care of branch point singularities the success is not reliable. The Arnoldi method for general complex eigenvalue problems was used for the calculations in this thesis. It works sufficiently fast and stable in the presence of exceptional points. If higher-dimensional matrices are required, e.g., to calculate resonances in a higher energy region, which can be influenced by field strengths available in a laboratory, the application of the spectral transformation Lanczos method with a consecutive application of a QL algorithm for non-symmetric Hessenberg matrices is a promising faster alternative.

One of the main results of this thesis is the first detection of exceptional points in numerically exact spectra of an atom in static external fields. It was shown, that the branch point singularities can be found by the permutation of two eigenvalues when an exceptional point is encircled in the parameter space. Further properties can be used to verify their existence. In particular, it was demonstrated that the eigenvectors calculated for the two branching eigenstates exhibit the geometric phase of an exceptional point, where (only) one of the eigenstates changes its sign for a circle in the parameter space around the exceptional point. In addition, it was shown that it is possible to extract the complex eigenvalues of resonances from experimental photoionization cross sections with the harmonic inversion method. This opens the possibility to search for exceptional points in experimental data with the methods developed in this thesis.

The properties of exceptional points in spectra of the hydrogen atom have been analyzed in detail. The local square root branch point structure could be revealed. In a close region around the branch points, it is possible to describe the two branching eigenstates by 2×2-matrix models. Beyond the typical square root branch points the spectra of the hydrogen atom exhibit structures which include three resonances forming two exceptional points close to each other in the parameter space, i.e., one of the three

resonances is involved in both branch points. This finding is especially important because it is closely related with a cubic root branch point, at which all three resonances coalesce. The direct adjustment of such a cubic root branch point would require five external parameters and, therefore, is not possible in the system investigated here. Furthermore, the close relation of avoided level crossings and exceptional points could be found in the resonances of the hydrogen atom. The behavior of dipole matrix elements in the vicinity of branch points has revealed interesting properties. While single dipole matrix elements diverge in the presence of exceptional points this is not the case for observable physical quantities as the photoionization cross section.

An investigation of the resonances in spectra of the hydrogen atom with respect to the classical transition state theory has lead to a deeper insight into the ionization mechanism. The comparison of the resonances in the energy range under consideration has exposed close similarities between the exact quantum resonances and the classical electron motion near the Stark saddle point. The results give clear evidence for the existence of an eminent influence of the classical transition state in quantum spectra. The agreement of the quantized energies of the classical electron motion with the full quantum calculations was extremely good although the lowest nontrivial order in a power series expansion of the potential was used. The results indicate that it may be worthwhile to extend the calculations done here to the normal form procedure developed by Uzer et al. [36]. It will be interesting to analyze whether higher orders can lead to an even better description of the quantum resonances with the electron motion.

A further major topic of this thesis was the extension of the concept of exceptional points to nonlinear quantum systems. In particular, it could be shown that the tangent bifurcation at which two solutions to the Gross-Pitaevskii equation are created at a critical value of the scattering length can be identified as a "nonlinear version" of an exceptional point. For this purpose, the complex vicinities of the tangent bifurcations appearing in the extended Gross-Pitaevskii equations for self-trapped Bose-Einstein condensates with attractive $1/r$ interaction and dipolar quantum gases were investigated. The chemical potentials and the mean field energies show the typical behavior of energies at an exceptional point. Both quantities pass through a branch point singularity at the critical value of the system's parameter. An analysis of the phase behavior of the corresponding wave functions revealed a correspondence with exceptional points of non-Hermitian non-symmetric matrices. For the investigation of the bifurcation points analytic continuations of the Gross-Pitaevskii systems were used. As was discussed, an analytic continuation of the wave functions is not only required for complex values of the scattering length but is necessary for real parameter values below the bifurcation point. Then, a complex absorbing effective potential is obtained indicating an internal collapse of the condensate.

The studies presented in this thesis have shown that exceptional points have important consequences for quantum systems. In particular, it was possible to demonstrate that they exist and can be verified in real physical situations which are accessible both with theoretical and experimental methods. Their manifestations in the resonance spectra

of atoms, viz. the permutation of the eigenvalues, the branch point structure, and the geometric phase are observable features. In the nonlinear Gross-Pitaevskii equation they appear as bifurcation points at which two stationary states are born in a tangent bifurcation.

A Atomic units and atomic-like units for Bose-Einstein condensates

It is a common procedure to introduce appropriate units for the theoretical investigation of physical problems. They are used to eliminate various universal constants or to avoid high powers of 10, which is especially important for numerical computations. In atomic physics mainly so called *atomic units* are used. There are, of course, several possibilities to fix the units of the required quantities in a reasonable way and, indeed, there are at least two important definitions of atomic units in use, viz. *atomic Hartree units* [107] and *atomic Rydberg units*. The close similarities between both systems and their notation can sometimes lead to ambiguities [108]. Therefore, it is very important to clearly state which system of units is used. In this thesis atomic Hartree units are applied for all sections concerning the hydrogen atom in external fields.

Because of the formal similarity between the atom-atom interaction in Bose-Einstein condensates with a laser-induced gravity-like interaction and the Coulomb potential of the hydrogen atom, an adequate description of the system is possible with units defined analogously to atomic units. Here, Rydberg-like units have become accepted [49, 50].

In section A.1.1 the atomic Hartree units are introduced. To enable a comparison with atomic Rydberg units, they are briefly described in section A.1.2. The units used for the investigation of Bose-Einstein condensates with long-range interactions are presented in sections A.2 and A.3.

A.1 Atomic units

A.1.1 Atomic Hartree units

To fix the atomic Hartree units one has to introduce four definitions, which can be achieved with several choices. One possibility is given by the following quantities:

1. The unit of mass is the electron mass $\mathrm{m_e}$.
2. Charges are measured in units of the elementary charge e.
3. The unit of angular momentum is Planck's constant $\hbar = \mathrm{h}/(2\pi)$.
4. Lengths are measured in units of the Bohr radius $\mathrm{a_0} = 4\pi\varepsilon_0\hbar^2/(\mathrm{m_e e^2})$.

Table A.1: Atomic Hartree units

quantity	atomic Hartree unit	Value in SI units [109]
angular momentum	$\hbar = \mathrm{h}/(2\pi)$	$1.054571628(53) \times 10^{-34}\,\mathrm{Js}$
charge	e	$1.602176487(40) \times 10^{-19}\,\mathrm{C}$
electric field	$\mathrm{E_h}/(\mathrm{e\,a_0})$	$5.14220632(13) \times 10^{11}\,\frac{\mathrm{V}}{\mathrm{m}}$
energy	$\mathrm{E_h} = \alpha^2 \mathrm{m_e c^2}$	$4.35974394(22) \times 10^{-18}\,\mathrm{J}$
length	$\mathrm{a_0} = 4\pi\varepsilon_0\hbar^2/(\mathrm{m_e e^2})$	$0.52917720859(36) \times 10^{-10}\,\mathrm{m}$
magnetic flux density	$\hbar/(\mathrm{e\,a_0^2})$	$2.350517382(59) \times 10^{5}\,\mathrm{T}$
mass	$\mathrm{m_e}$	$9.10938215(45) \times 10^{-31}\,\mathrm{kg}$
momentum	$\hbar/\mathrm{a_0}$	$1.992851565(99) \times 10^{-24}\,\frac{\mathrm{kg\,m}}{\mathrm{s}}$
time	$\hbar/\mathrm{E_h}$	$2.418884326505(16) \times 10^{-17}\,\mathrm{s}$

Table A.2: Comparison between atomic Hartree units and atomic Rydberg units

quantity	atomic Hartree unit	atomic Rydberg unit
angular momentum	$\hbar = \mathrm{h}/(2\pi)$	$\hbar$
charge	e	$\mathrm{e}/\sqrt{2}$
electric field	$\mathrm{E_h}/(\mathrm{e\,a_0})$	$\sqrt{2}\,\mathrm{E_\infty}/(\mathrm{e\,a_0}) = \mathrm{E_h}/(\sqrt{2}\,\mathrm{e\,a_0})$
energy	$\mathrm{E_h} = \alpha^2 \mathrm{m_e c^2}$	$\mathrm{E_\infty} = \mathrm{E_h}/2$
length	$\mathrm{a_0} = 4\pi\varepsilon_0\hbar^2/(\mathrm{m_e e^2})$	$\mathrm{a_0}$
magnetic flux density	$\hbar/(\mathrm{e\,a_0^2})$	$\sqrt{2}\,\hbar/(\mathrm{e\,a_0^2})$
mass	$\mathrm{m_e}$	$2\,\mathrm{m_e}$
momentum	$\hbar/\mathrm{a_0}$	$\hbar/\mathrm{a_0}$
time	$\hbar/\mathrm{E_h}$	$\hbar/\mathrm{E_\infty} = 2\hbar/\mathrm{E_h}$

Originally, Hartree [107] mentioned only three of these values to define atomic units, viz. the units of length, charge, and mass, however, the assumption $\alpha = \mathrm{e}^2/(4\pi\varepsilon_0\hbar c)$ was exploited, which is equivalent to the additional determination of the unit of length mentioned above. The definition of the units is often done by formally setting $\hbar = \mathrm{a_0} = \mathrm{m_e} = \mathrm{e} = 1$ or equivalently $\hbar = 4\pi\varepsilon_0 = \mathrm{m_e} = \mathrm{e} = 1$. To indicate the use of atomic Hartree units, numerical values are generally provided with the symbol a.u., e.g. $E = -0.5\,\mathrm{a.u.}$ for the ground state energy of the hydrogen atom in atomic Hartree units.

A.1.2 Atomic Rydberg units

Similarly to the Hartree units, atomic Rydberg units can be introduced with the formal definition $\hbar = \mathrm{a_0} = 2\,\mathrm{m_e} = \mathrm{e}^2/2 = 1$. The most important consequence is that the energy unit is now the Rydberg energy $\mathrm{E_\infty} = \mathrm{E_h}/2$. A comparison between Hartree and Rydberg units is given in table A.2.

A.2 Atomic-like units for Bose-Einstein condensates with attractive $1/r$ interaction

Due to the analogy with the Coulomb interaction the theoretical description of Bose-Einstein condensates with attractive $1/r$ interaction is especially expedient if "atomic" units are used, whose construction is based on the analogy of the $1/r$ interaction term with the Coulomb potential. Rydberg-like units have been introduced [49, 50].

The monopolar atom-atom interaction is described by

$$V_u = -\frac{u}{\boldsymbol{r} - \boldsymbol{r}'} \,, \tag{A.1}$$

where

$$u = \frac{11}{4\pi} \frac{I k^2 \alpha^2}{\mathrm{c}\varepsilon_0^2} \tag{A.2}$$

determines the interaction strength [51]. Here, I represents the intensity of the lasers used to induce the gravity-like interaction and α is the isotropic, dynamic polarizability of the atoms at frequency $\mathrm{c}k$. The analogy

$$u \Leftrightarrow \frac{\mathrm{e}^2}{4\pi\varepsilon_0} \tag{A.3}$$

can then be exploited to construct a "Bohr radius"

$$\mathrm{a}_u = \frac{\hbar^2}{mu} \tag{A.4}$$

with the mass m of one Boson, which is a reasonable choice for the unit of mass. Altogether, the "atomic Rydberg units" for Bose-Einstein condensates can be introduced with the definitions listed in table A.3. Of course, only four of them are required for the definition. Note that these units depend on the strength of the atom-atom interaction and therefore on all quantities listed in equation (A.2).

A.3 Atomic-like units for Bose-Einstein condensates with dipole-dipole interaction

Similarly to the $1/r$ case, it is possible to construct Rydberg-like units for dipolar Bose-Einstein condensates, where the dipole-dipole interaction is the starting point of the introduction of new units. The major step is the specification of a "dipole length" as unit of length with

$$a_\mathrm{d} = \frac{\alpha^2}{2} \frac{m}{\mathrm{m_e}} \left(\frac{\mu}{\mu_\mathrm{B}} \right)^2 \mathrm{a}_0 \,, \tag{A.5}$$

Table A.3: Important "atomic Rydberg units" for Bose-Einstein condensates with long-range interactions.

	units for BECs with	
quantity	$1/r$ interaction	dipole-dipole interaction
angular momentum	$\hbar$	$\hbar$
energy	$E_u = \hbar^2/(2ma_u^2)$	$E_\mathrm{d} = \hbar^2/(2ma_\mathrm{d}^2)$
frequency	$E_u/\hbar$	$E_\mathrm{d}/\hbar$
length	$a_u = \hbar^2/(mu)$	$a_\mathrm{d} = \frac{\alpha^2}{2}\frac{m}{\mathrm{m_e}}\left(\frac{\mu}{\mu_\mathrm{B}}\right)^2 \mathrm{a}_0$
mass	mass m of one Boson	mass m of one Boson
time	$\hbar/E_u$	$\hbar/E_\mathrm{d}$

which depends on the mass m and the magnetic moment μ of the bosons and, therefore, is only fixed for a particular atom. Here, α is the fine-structure constant, a_0 the Bohr radius, $\mathrm{m_e}$ the electron mass, and μ_B the Bohr radius. Combined, the "atomic Rydberg units" for dipolar Bose-Einstein condensates are given with the definitions listed in A.3, where they are compared with the corresponding units for Bose-Einstein condensates with attractive $1/r$ interaction.

B Matrix representation of the hydrogen atom in crossed external fields

As mentioned in section 5.1 the Hamiltonian of the hydrogen atom in static crossed external fields is given by

$$H = \frac{1}{2}\boldsymbol{p}^2 - \frac{1}{r} + \frac{1}{2}\gamma L_z + \frac{1}{8}\gamma^2(x^2 + y^2) + fx, \tag{5.3}$$

with the atomic units presented in appendix A.1.1. For the matrix representation a transformation to dilated semiparabolic coordinates is used. With this transformation a good basis is given by the two-dimensional harmonic oscillator, whose complete basis set of energy eigenstates is well known [84]. With an optimal ordering of the basis states the matrix representation of the Hamiltonian (5.3) leads to a small banded matrix whose bandwidth is between 8.5% and 10% of the matrix sizes used. If all parts of the Hamiltonian (5.3) are expressed in terms of creation and annihilation operators, a very fast matrix setup is possible.

The transformation from Cartesian to dilated semiparabolic coordinates is presented in section B.1 and a reasonable choice for the basis is given in section B.2.

B.1 Hamiltonian in dilated semiparabolic coordinates

The dilated semiparabolic coordinates are defined by

$$\mu = \frac{1}{b}\sqrt{r + z}\,, \tag{B.1a}$$

$$\nu = \frac{1}{b}\sqrt{r - z}\,, \tag{B.1b}$$

$$\varphi = \arctan\frac{y}{x} \tag{B.1c}$$

with

$$r = \sqrt{x^2 + y^2 + z^2}\,, \tag{B.1d}$$

and a free convergence parameter b. The inverse transformation to Cartesian coordinates reads

$$x = b^2 \mu\nu \cos\varphi \ , \tag{B.2a}$$
$$y = b^2 \mu\nu \sin\varphi \ , \tag{B.2b}$$
$$z = \frac{b^2}{2}(\mu^2 + \nu^2) \ , \tag{B.2c}$$

the Laplacian has the form

$$\Delta = \frac{1}{b^4} \frac{1}{\mu^2 + \nu^2} \left(\Delta_\mu + \Delta_\nu\right) \ , \tag{B.3a}$$

where

$$\Delta_\varrho = \frac{1}{\varrho} \frac{\partial}{\partial \varrho} \varrho \frac{\partial}{\partial \varrho} + \frac{1}{\varrho^2} \frac{\partial^2}{\partial \varphi^2} \ , \qquad \varrho \in \{\mu, \nu\} \ , \tag{B.3b}$$

and the z-component of the angular momentum can be expressed with

$$L_z = -\mathrm{i} \frac{\partial}{\partial \varphi} \ . \tag{B.4}$$

Then the Schrödinger equation can be written in the regularized form

$$\Big\{ \Delta_\mu + \Delta_\nu - \left(\mu^2 + \nu^2\right) + b^4 \gamma \left(\mu^2 + \nu^2\right) \mathrm{i} \frac{\partial}{\partial \varphi} - \frac{1}{4} b^8 \gamma^2 \mu^2 \nu^2 \left(\mu^2 + \nu^2\right) - 2 b^6 f \mu\nu \left(\mu^2 + \nu^2\right) \cos\varphi \Big\} \psi = \left\{ -4b^2 + \lambda \left(\mu^2 + \nu^2\right) \right\} \psi \ , \tag{5.4}$$

where the generalized eigenvalue

$$\lambda = -(1 + 2b^4 E) \tag{5.5}$$

appears, which is connected with the energy E. The dilation parameter b is used for the numerical calculations as convergence parameter and has a second important role. As can be seen from the transformations (B.2), the complex rotation performed for the computation of resonances can be achieved with a complex parameter b. A complex phase of $\mathrm{e}^{\mathrm{i}\theta}$ in the square of b, i.e.,

$$b^2 = |b^2| \mathrm{e}^{\mathrm{i}\theta} \tag{B.5}$$

corresponds to a complex rotation (3.4) of the coordinates by the angle θ.

B.2 Basis set

The form of the Schrödinger equation (5.4) suggests the application of a harmonic oscillator basis for the matrix setup and the structure (B.3b), which is identical with the structure of the Laplacian in plane polar coordinates, requires the expression of each of the variables μ and ν in terms of a two-dimensional harmonic oscillator with the Hamiltonian

$$H = \frac{1}{2}(p_1^2 + p_2^2) + \frac{1}{2}(q_1^2 + q_2^2) \ , \tag{B.6}$$

where q_1, q_2, p_1, and p_2 are Cartesian coordinates and their conjugate momenta, respectively. The familiar creation and annihilation operators are given by

$$a_i = \frac{1}{\sqrt{2}}(q_i + \mathrm{i}p_i) \ , \tag{B.7a}$$

$$a_i^+ = \frac{1}{\sqrt{2}}(q_i - \mathrm{i}p_i) \ , \qquad i \in \{1, 2\} \ , \tag{B.7b}$$

which can be used to form a complete set of commuting operators. Here, the most reasonable choice for a set of commuting operators is given by

$$N = A_+^+ A_+ + A_-^+ A_- \ , \tag{B.8a}$$

$$L = A_+^+ A_+ - A_-^+ A_- \ , \tag{B.8b}$$

where

$$A_\pm = \frac{1}{\sqrt{2}}(a_1 \mp \mathrm{i}a_2) \ , \tag{B.8c}$$

$$A_\pm^+ = \frac{1}{\sqrt{2}}(a_1^+ \pm \mathrm{i}a_2^+) \ . \tag{B.8d}$$

Important commutator relations of these operators are

$$[A_r, A_s] = [A_r^+, A_s^+] = 0 \ , \tag{B.9a}$$

$$[A_r, A_s^+] = \delta_{rs} \ , \tag{B.9b}$$

$$[L, A_\pm] = \mp A_\pm \ , \tag{B.9c}$$

$$[L, A_\pm^+] = \pm A_\pm^+ \ , \tag{B.9d}$$

$$[N, A_\pm] = -A_\pm \ , \tag{B.9e}$$

$$[N, A_\pm^+] = A_\pm^+ \ . \tag{B.9f}$$

The eigenstates of the two commuting operators N and L are labeled $|n, m\rangle$ with the eigenvalues

$$N\,|n, m\rangle = n\,|n, m\rangle \ , \tag{B.10a}$$

$$L\,|n, m\rangle = m\,|n, m\rangle \tag{B.10b}$$

and the application of the operators $A_\pm$ and $A_\pm^+$ yields

$$A_\pm |n, m\rangle = \pm\sqrt{\frac{n \pm m}{2}}\, |n-1, m \mp 1\rangle \ , \tag{B.11}$$

$$A_\pm^+ |n, m\rangle = \pm\sqrt{\frac{n \pm m}{2} + 1}\, |n+1, m \pm 1\rangle \ . \tag{B.12}$$

Now the action of the operators appearing in the Schrödinger equation on a basis state can be calculated. In doing so one has to have in mind that *each* of the coordinates μ and ν has the structure of a radial part in plane polar coordinates but that they have the "angle" φ in common (cf. equations (B.3a) and (B.3b)). Consequently, for the matrix representation a basis state of the form

$$|n_\mu, n_\nu, m\rangle = |n_\mu, m\rangle \otimes |n_\nu, m\rangle \tag{5.7}$$

is required. Here, $|n_\mu, m\rangle$ and $|n_\nu, m\rangle$ are eigenstates of the type (B.10), which have a common quantum number m. Furthermore, it is important for the numerical calculations to exploit the mirror symmetry with respect to the $(z = 0)$-plane. Using basis states with defined z-parity the Hamiltonian decomposes in a block diagonal structure with one block for each parity. For $n_\nu \neq n_\mu$, the basis states with defined z-parity can be constructed from equation (5.7) by

$$|n_\mu, n_\nu, m\rangle_\mathrm{e} = \frac{1}{\sqrt{2}} \left(|n_\mu, m\rangle \otimes |n_\nu, m\rangle + |n_\nu, m\rangle \otimes |n_\mu, m\rangle \right) \ , \tag{B.13a}$$

$$|n_\mu, n_\nu, m\rangle_\mathrm{o} = \frac{1}{\sqrt{2}} \left(|n_\mu, m\rangle \otimes |n_\nu, m\rangle - |n_\nu, m\rangle \otimes |n_\mu, m\rangle \right) \ , \tag{B.13b}$$

where $|n_\mu, n_\nu, m\rangle_\mathrm{e}$ and $|n_\mu, n_\nu, m\rangle_\mathrm{o}$ represent states with even an odd z-parity, respectively.

C Phase of the eigenvectors on a parameter space circle

In section 8.2 the phase behavior of the two permuted eigenvectors is compared for symmetric and non-symmetric matrices. Here, the permutation rules are proven for a small circle around the branch point. This is done in extension of the simple symmetric model used in section 2.4.3.

To be able to compare the phase behavior of the wave functions of the nonlinear Gross-Pitaevskii system with the eigenvectors of a matrix, the phase of the vectors is fixed with the same method as is discussed in section 8.3 for the wave functions of the analytic continuation of the extended Gross-Pitaevskii model. This is done with the Euclidean norm without complex conjugation $N_i = \sqrt{\boldsymbol{x}_i^T \boldsymbol{x}_i}$ of the eigenvectors, which is the adequate counterpart of the normalization factors ν from equation (8.13) and A from equation (8.6), where (formally) the complex conjugation is ignored. Then, the normalized eigenvectors have the form

$$\boldsymbol{x}_{1,2}(\lambda) = \frac{1}{N_{1,2}} \begin{pmatrix} -\lambda \\ 1 \mp \sqrt{1 + c\lambda + \lambda^2} \end{pmatrix}$$

with

$$N_{1,2} = \sqrt{\lambda^2 + \left(1 \mp \sqrt{1 + c\lambda + \lambda^2}\right)^2}\,.$$

For a small circle around the exceptional point $\lambda_A = -c/2 + \sqrt{c^2/4 - 1}$ the fractional power series expansion in $\varrho^{1/4}$ of the normalized vectors reads in the non-symmetric case ($c \neq 0$)

$$\begin{aligned} \boldsymbol{x}_1(\varphi) &= \begin{pmatrix} \frac{1}{c}\sqrt{\eta/2} + \frac{2}{c}\sqrt{\kappa/\eta}\sqrt{\varrho}\mathrm{e}^{\mathrm{i}\varphi/2} + \mathrm{O}(\varrho^{3/4}) \\ \sqrt{2/\eta} - \frac{1}{c^2}\sqrt{\kappa\eta}\sqrt{\varrho}\mathrm{e}^{\mathrm{i}\varphi/2} + \mathrm{O}(\varrho^{3/4}) \end{pmatrix}, \\ \boldsymbol{x}_2(\varphi) &= \begin{pmatrix} \frac{1}{c}\sqrt{\eta/2} - \frac{2}{c}\sqrt{\kappa/\eta}\sqrt{\varrho}\mathrm{e}^{\mathrm{i}\varphi/2} + \mathrm{O}(\varrho^{3/4}) \\ \sqrt{2/\eta} + \frac{1}{c^2}\sqrt{\kappa\eta}\sqrt{\varrho}\mathrm{e}^{\mathrm{i}\varphi/2} + \mathrm{O}(\varrho^{3/4}) \end{pmatrix} \end{aligned}$$

with $\kappa = \sqrt{c^2/4 - 1}$, and $\eta = c^2 - 2c\kappa$.

The traversal of a single circle ($\varphi = 0 \ldots 2\pi$) obviously leads to a permutation of the eigenvectors as summarized in (8.26).

In the symmetric case ($c = 0$), a fractional power series expansion of the two normalized eigenvectors looks different. The result is

$$\boldsymbol{x}_1(\varphi) = \begin{pmatrix} \frac{\mathrm{e}^{\mathrm{i}7\pi/8}}{2^{3/4}} \frac{\mathrm{e}^{-\mathrm{i}\varphi/4}}{\varrho^{1/4}} + \frac{\mathrm{e}^{\mathrm{i}9\pi/8}}{2^{5/4}} \varrho^{1/4} \mathrm{e}^{\mathrm{i}\varphi/4} + \mathrm{O}(\varrho^{3/4}) \\ \frac{\mathrm{e}^{\mathrm{i}11\pi/8}}{2^{3/4}} \frac{\mathrm{e}^{-\mathrm{i}\varphi/4}}{\varrho^{1/4}} + \frac{\mathrm{e}^{\mathrm{i}5\pi/8}}{2^{5/4}} \varrho^{1/4} \mathrm{e}^{\mathrm{i}\varphi/4} + \mathrm{O}(\varrho^{3/4}) \end{pmatrix},$$

$$\boldsymbol{x}_2(\varphi) = \begin{pmatrix} \frac{\mathrm{e}^{\mathrm{i}11\pi/8}}{2^{3/4}} \frac{\mathrm{e}^{-\mathrm{i}\varphi/4}}{\varrho^{1/4}} + \frac{\mathrm{e}^{\mathrm{i}5\pi/8}}{2^{5/4}} \varrho^{1/4} \mathrm{e}^{\mathrm{i}\varphi/4} + \mathrm{O}(\varrho^{3/4}) \\ \frac{\mathrm{e}^{\mathrm{i}15\pi/8}}{2^{3/4}} \frac{\mathrm{e}^{-\mathrm{i}\varphi/4}}{\varrho^{1/4}} + \frac{\mathrm{e}^{\mathrm{i}\pi/8}}{2^{5/4}} \varrho^{1/4} \mathrm{e}^{\mathrm{i}\varphi/4} + \mathrm{O}(\varrho^{3/4}) \end{pmatrix}.$$

With a circle around the exceptional point ($\varphi = 0 \ldots 2\pi$) it can be seen directly that $\boldsymbol{x}_1(2\pi) = -\boldsymbol{x}_2(0)$, and $\boldsymbol{x}_2(2\pi) = \boldsymbol{x}_1(0)$, i.e., the permutation rule (2.31) for a symmetric matrix is reproduced in this picture.

Bibliography

[1] T. Kato. *Perturbation theory for linear operators*. Springer, Berlin (1966).

[2] W. D. Heiss. Phases of wave functions and level repulsion. *The European Physical Journal D – Atomic, Molecular, Optical and Plasma Physics* 7, 1–4 (1999).

[3] W. D. Heiss. Repulsion of resonance states and exceptional points. *Physical Review E (Statistical, Nonlinear, and Soft Matter Physics)* 61, 929–932 (2000).

[4] W. D. Heiss and A. L. Sannino. Avoided level crossing and exceptional points. *Journal of Physics A: Mathematical and General* 23, 1167–1178 (1990).

[5] M. V. Berry and D. H. J. O'Dell. Diffraction by volume gratings with imaginary potentials. *Journal of Physics A: Mathematical and General* 31, 2093–2101 (1998).

[6] Pavel Cejnar, Stefan Heinze, and Michal Macek. Coulomb Analogy for Non-Hermitian Degeneracies near Quantum Phase Transitions. *Physical Review Letters* 99, 100601 (2007).

[7] Shachar Klaiman, Uwe Günther, and Nimrod Moiseyev. Visualization of Branch Points in $\mathcal{PT}$-Symmetric Waveguides. *Physical Review Letters* 101, 080402 (2008).

[8] M. Philipp, P. von Brentano, G. Pascovici, and A. Richter. Frequency and width crossing of two interacting resonances in a microwave cavity. *Physical Review E (Statistical, Nonlinear, and Soft Matter Physics)* 62, 1922–1926 (2000).

[9] C. Dembowski, H.-D. Gräf, H. L. Harney, A. Heine, W. D. Heiss, H. Rehfeld, and A. Richter. Experimental Observation of the Topological Structure of Exceptional Points. *Physical Review Letters* 86, 787–790 (2001).

[10] C. Dembowski, B. Dietz, H.-D. Gräf, H. L. Harney, A. Heine, W. D. Heiss, and A. Richter. Observation of a Chiral State in a Microwave Cavity. *Physical Review Letters* 90, 034101 (2003).

[11] C. Dembowski, B. Dietz, H.-D. Gräf, H. L. Harney, A. Heine, W. D. Heiss, and A. Richter. Encircling an exceptional point. *Physical Review E (Statistical, Nonlinear, and Soft Matter Physics)* 69, 056216 (2004).

[12] B. Dietz, T. Friedrich, J. Metz, M. Miski-Oglu, A. Richter, F. Schäfer, and C. A. Stafford. Rabi oscillations at exceptional points in microwave billiards. *Physical Review E (Statistical, Nonlinear, and Soft Matter Physics)* 75, 027201 (2007).

[13] T. Stehmann, W. D. Heiss, and F. G. Scholtz. Observation of exceptional points in electronic circuits. *Journal of Physics A: Mathematical and General* 37, 7813–7819 (2004).

[14] Nimrod Moiseyev. Quantum theory of resonances: calculating energies, widths and cross-sections by complex scaling. *Physics Reports* 302, 212–293 (1998).

[15] W. P. Reinhardt. Complex Coordinates in the Theory of Atomic and Molecular Structure and Dynamics. *Annual Review of Physical Chemistry* 33, 223–255 (1982).

[16] Y. K. Ho. The method of complex coordinate rotation and its applications to atomic collision processes. *Physics Reports* 99, 1–68 (1983).

[17] M. V. Berry. Quantal Phase Factors Accompanying Adiabatic Changes. *Proceedings of the Royal Society of London. Series A, Mathematical and Physical Sciences* 392, 45–57 (1984).

[18] O. Latinne, N. J. Kylstra, M. Dörr, J. Purvis, M. Terao-Dunseath, C. J. Joachain, P. G. Burke, and C. J. Noble. Laser-Induced Degeneracies Involving Autoionizing States in Complex Atoms. *Physical Review Letters* 74, 46–49 (1995).

[19] H. J. Korsch and S. Mossmann. Stark resonances for a double δ quantum well: crossing scenarios, exceptional points and geometric phases. *Journal of Physics A: Mathematical and General* 36, 2139–2153 (2003).

[20] E Hernández, A Jáuregui, and A Mondragón. Non-Hermitian degeneracy of two unbound states. *Journal of Physics A: Mathematical and General* 39, 10087–10105 (2006).

[21] P. von Brentano and M. Philipp. Crossing and anticrossing of energies and widths for unbound levels. *Physics Letters B* 454, 171–175 (1999).

[22] Markus K. Oberthaler, Roland Abfalterer, Stefan Bernet, Jörg Schmiedmayer, and Anton Zeilinger. Atom Waves in Crystals of Light. *Physical Review Letters* 77, 4980–4983 (1996).

[23] A. L. Shuvalov and N. H. Scott. On singular features of acoustic wave propagation in weakly dissipative anisotropic thermoviscoelasticity. *Acta Mechanica* 140, 1–15 (2000).

[24] S. Pancharatnam. The Propagation of Light in Absorbing Biaxial Crystals – I. Theoretical. *Proceedings of the Indian Academy of Sciences, Section A* 42, 86–110 (1955).

[25] M. V. Berry. Pancharatnam, virtuoso of the Poincaré sphere: an appreciation. *Current Science* 67, 220–223 (1994).

[26] S. Freund, R. Ubert, E. Flöthmann, K. Welge, D. M. Wang, and J. B. Delos. Absorption and recurrence spectra of hydrogen in crossed electric and magnetic fields. *Physical Review A (Atomic, Molecular, and Optical Physics)* 65, 053408 (2002).

[27] Jianguo Rao, D. Delande, and K. T. Taylor. Quantum manifestations of closed orbits in the photoexcitation scaled spectrum of the hydrogen atom in crossed fields. *Journal of Physics B: Atomic, Molecular and Optical Physics* 34, L391–L399 (2001).

[28] Thomas Bartsch, Jörg Main, and Günter Wunner. Closed orbits and their bifurcations in the crossed-field hydrogen atom. *Physical Review A (Atomic, Molecular, and Optical Physics)* 67, 063410 (2003).

[29] Thomas Bartsch, Jörg Main, and Günter Wunner. Semiclassical quantization of the hydrogen atom in crossed electric and magnetic fields. *Physical Review A (Atomic, Molecular, and Optical Physics)* 67, 063411 (2003).

[30] Jörg Main and Günter Wunner. Ericson fluctuations in the chaotic ionization of the hydrogen atom in crossed magnetic and electric fields. *Physical Review Letters* 69, 586–589 (1992).

[31] J. Main and G. Wunner. Rydberg atoms in external fields as an example of open quantum systems with classical chaos. *Journal of Physics B: Atomic, Molecular and Optical Physics* 27, 2835–2848 (1994).

[32] Gernot Stania and Herbert Walther. Quantum Chaotic Scattering in Atomic Physics: Ericson Fluctuations in Photoionization. *Physical Review Letters* 95, 194101 (2005).

[33] Charles Jaffé, D. Farrelly, and T. Uzer. Transition State Theory without Time-Reversal Symmetry: Chaotic Ionization of the Hydrogen Atom. *Physical Review Letters* 84, 610–613 (2000).

[34] Charles Jaffé, David Farrelly, and T. Uzer. Transition state in atomic physics. *Physical Review A (Atomic, Molecular, and Optical Physics)* 60, 3833–3850 (1999).

[35] S. Wiggins, L. Wiesenfeld, C. Jaffé, and T. Uzer. Impenetrable Barriers in Phase-Space. *Physical Review Letters* 86, 5478–5481 (2001).

[36] T. Uzer, Charles Jaffé, Jesús Palacián, Patricia Yanguas, and Stephen Wiggins. The geometry of reaction dynamics. *Nonlinearity* 15, 957–992 (2002).

[37] Charles W. Clark, Eric Korevaar, and Michael G. Littman. Quasi-Penning Resonances of a Rydberg Electron in Crossed Electric and Magnetic Fields. *Physical Review Letters* 54, 320–322 (1985).

[38] E. P. Gross. Structure of a Quantized Vortex in Boson Systems. *Il Nuovo Cimento* 20, 454–477 (1961).

[39] L. P. Pitaevskii. Vortex Lines in an Imperfect Bose Gas. *Soviet Physics JETP* 13, 451–454 (1961).

[40] F. Dalfovo and S. Stringari. Bosons in anisotropic traps: Ground state and vortices. *Physical Review A (Atomic, Molecular, and Optical Physics)* 53, 2477–2485 (1996).

[41] R. J. Dodd, Mark Edwards, C. J. Williams, C. W. Clark, M. J. Holland, P. A. Ruprecht, and K. Burnett. Role of attractive interactions on Bose-Einstein condensation. *Physical Review A (Atomic, Molecular, and Optical Physics)* 54, 661–664 (1996).

[42] Víctor M. Pérez-García, Humberto Michinel, J. I. Cirac, M. Lewenstein, and P. Zoller. Dynamics of Bose-Einstein condensates: Variational solutions of the Gross-Pitaevskii equations. *Physical Review A (Atomic, Molecular, and Optical Physics)* 56, 1424–1432 (1997).

[43] C. C. Bradley, C. A. Sackett, and R. G. Hulet. Bose-Einstein Condensation of Lithium: Observation of Limited Condensate Number. *Physical Review Letters* 78, 985–989 (1997).

[44] C. A. Sackett, J. M. Gerton, M. Welling, and R. G. Hulet. Measurements of Collective Collapse in a Bose-Einstein Condensate with Attractive Interactions. *Physical Review Letters* 82, 876–879 (1999).

[45] Jordan M. Gerton, Dmitry Strekalov, Ionut Prodan, and Randall G. Hulet. Direct observation of growth and collapse of a Bose–Einstein condensate with attractive interactions. *Nature* 408, 692–695 (2000).

[46] Elizabeth A. Donley, Neil R. Claussen, Simon L. Cornish, Jacob L. Roberts, Eric A. Cornell, and Carl E. Wieman. Dynamics of collapsing and exploding Bose–Einstein condensates. *Nature* 412, 295–299 (2001).

[47] C. Huepe, S. Métens, G. Dewel, P. Borckmans, and M. E. Brachet. Decay Rates in Attractive Bose-Einstein Condensates. *Physical Review Letters* 82, 1616–1619 (1999).

[48] C. Huepe, L. S. Tuckerman, S. Métens, and M. E. Brachet. Stability and decay rates of nonisotropic attractive Bose-Einstein condensates. *Physical Review A (Atomic, Molecular, and Optical Physics)* 68, 023609 (2003).

[49] I. Papadopoulos, P. Wagner, G. Wunner, and J. Main. Bose-Einstein condensates with attractive 1/r interaction: The case of self-trapping. *Physical Review A (Atomic, Molecular, and Optical Physics)* 76, 053604 (2007).

[50] Ioannis Papadopoulos. *Quantum mechanical calculations for Bose-Einstein condensates with electromagnetically induced* $1/r$*-interaction.* Diplomarbeit, Universität Stuttgart (2007).

[51] D. O'Dell, S. Giovanazzi, G. Kurizki, and V. M. Akulin. Bose-Einstein Condensates with $1/r$ Interatomic Attraction: Electromagnetically Induced "Gravity". *Physical Review Letters* 84, 5687–5690 (2000).

[52] Krzysztof Góral, Kazimierz Rzążewski, and Tilman Pfau. Bose-Einstein condensation with magnetic dipole-dipole forces. *Physical Review A (Atomic, Molecular, and Optical Physics)* 61, 051601 (2000).

[53] L. Santos, G. V. Shlyapnikov, P. Zoller, and M. Lewenstein. Bose-Einstein Condensation in Trapped Dipolar Gases. *Physical Review Letters* 85, 1791–1794 (2000).

[54] M. Baranov, L. Dobrek, K. Góral, L. Santos, and M. Lewenstein. Ultracold Dipolar Gases – a Challenge for Experiments and Theory. *Physica Scripta* T102, 74–81 (2002).

[55] K. Góral, L. Santos, and M. Lewenstein. Quantum Phases of Dipolar Bosons in Optical Lattices. *Physical Review Letters* 88, 170406 (2002).

[56] K. Góral and L. Santos. Ground state and elementary excitations of single and binary Bose-Einstein condensates of trapped dipolar gases. *Physical Review A (Atomic, Molecular, and Optical Physics)* 66, 023613 (2002).

[57] Stefano Giovanazzi, Axel Gorlitz, and Tilman Pfau. Ballistic expansion of a dipolar condensate. *Journal of Optics B: Quantum and Semiclassical Optics* 5, S208–S211 (2003).

[58] Axel Griesmaier, Jörg Werner, Sven Hensler, Jürgen Stuhler, and Tilman Pfau. Bose-Einstein Condensation of Chromium. *Physical Review Letters* 94, 160401 (2005).

[59] J. Stuhler, A. Griesmaier, T. Koch, M. Fattori, T. Pfau, S. Giovanazzi, P. Pedri, and L. Santos. Observation of Dipole-Dipole Interaction in a Degenerate Quantum Gas. *Physical Review Letters* 95, 150406 (2005).

[60] Thierry Lahaye, Tobias Koch, Bernd Fröhlich, Marco Fattori, Jonas Metz, Axel Griesmaier, Stefano Giovanazzi, and Tilman Pfau. Strong dipolar effects in a quantum ferrofluid. *Nature* 448, 672–675 (2007).

[61] T. Koch, T. Lahaye, J. Metz, B. Fröhlich, A. Griesmaier, and T. Pfau. Stabilization of a purely dipolar quantum gas against collapse. *Nature Physics* 4, 218–222 (2008).

[62] T. Lahaye, J. Metz, B. Fröhlich, T. Koch, M. Meister, A. Griesmaier, T. Pfau, H. Saito, Y. Kawaguchi, and M. Ueda. d-Wave Collapse and Explosion of a Dipolar Bose-Einstein Condensate. *Physical Review Letters* 101, 080401 (2008).

[63] Konrad Knopp. *Theory of functions, parts I and II.* Dover Publications, Inc., Mineola (1996).

[64] Konrad Knopp. *Funktionentheorie II, Anwendungen und Weiterführung der allgemeinen Theorie.* Walter de Gruyter & Co, Berlin (1971).

[65] Uwe Günther, Ingrid Rotter, and Boris F Samsonov. Projective Hilbert space structures at exceptional points. *Journal of Physics A: Mathematical and Theoretical* 40, 8815–8833 (2007).

[66] A. P. Seyranian, O. N. Kirillov, and A. A. Mailybaev. Coupling of eigenvalues of complex matrices at diabolic and exceptional points. *Journal of Physics A: Mathematical and General* 38, 1723–1740 (2005).

[67] M. V. Berry and M. Wilkinson. Diabolical Points in the Spectra of Triangles. *Proceedings of the Royal Society of London. Series A, Mathematical and Physical Sciences* 392, 15–43 (1984).

[68] J. C. Garrison and E. M. Wright. Complex geometrical phases for dissipative systems. *Physics Letters A* 128, 177–181 (1988).

[69] Alexei A. Mailybaev, Oleg N. Kirillov, and Alexander P. Seyranian. Geometric phase around exceptional points. *Physical Review A (Atomic, Molecular, and Optical Physics)* 72, 014104 (2005).

[70] Hossein Mehri-Dehnavi and Ali Mostafazadeh. Geometric phase for non-Hermitian Hamiltonians and its holonomy interpretation. *Journal of Mathematical Physics* 49, 082105 (2008).

[71] Hans-Jürgen Stöckmann. *Quantum Chaos: An Introduction*. Cambridge University Press, Cambridge (1999).

[72] W. D. Heiss and H. L. Harney. The chirality of exceptional points. *The European Physical Journal D – Atomic, Molecular, Optical and Plasma Physics* 17, 149–151 (2001).

[73] M. V. Berry. Aspects of Degeneracy. In *Chaotic Behavior in Quantum Systems: Theory and Applications*, edited by Giulio Casati, volume 120 of *NATO ASI Series B: Physics*, pp. 123–140. Plenum Press, New York (1985).

[74] H. C. Longuet-Higgins. The Intersection of Potential Energy Surfaces in Polyatomic Molecules. *Proceedings of the Royal Society of London. Series A, Mathematical and Physical Sciences* 344, 147–156 (1975).

[75] V. Weisskopf and E. Wigner. Berechnung der natürlichen Linienbreite auf Grund der Diracschen Lichttheorie. *Zeitschrift für Physik* 63, 54–73 (1930).

[76] I. S. Gradshteyn and I. M. Ryzhik. *Table of Integrals, Series, and Products*. Academic Press, Amsterdam, seventh edition (2007).

[77] L. D. Landau and E. M. Lifschitz. *Quantenmechanik*, volume III of *Lehrbuch der Theoretischen Physik*. Akademie-Verlag, Berlin, ninth edition (1986).

[78] William H. Press, Saul A. Teukolsky, William T. Vetterling, and Brian P. Flannery. *Numerical Recipes in FORTRAN*. Cambridge University Press, Cambridge, second edition (1992).

[79] Josef Stoer and Roland Bulirsch. *Numerische Mathematik 2*. Springer, Berlin, fourth edition (2000).

[80] Thomas Ericsson and Axel Ruhe. The Spectral Transformation Lanczos Method for the Numerical Solution of Large Sparse Generalized Symmetric Eigenvalue Problems. *Mathematics of Computation* 35, 1251–1268 (1980).

[81] Y. Saad. Variations on Arnoldi's Method for Computing Eigenelements of Large Unsymmetric Matrices. *Linear Algebra and Its Applications* 34, 269–295 (1980).

[82] R. B. Lehoucq, D. C. Sorensen, and C. Yang. *ARPACK Users' Guide*. Siam, Philadelphia (1998).

[83] P. Schmelcher and L. S. Cederbaum. Two-body effects of the hydrogen atom in crossed electric and magnetic fields. *Chemical Physics Letters* 208, 548–554 (1993).

[84] Albert Messiah. *Quantenmechanik*, volume 1. De Gruyter, Berlin, second edition (1991).

[85] D. Delande, A. Bommier, and J. C. Gay. Positive-energy spectrum of the hydrogen atom in a magnetic field. *Physical Review Letters* 66, 141–144 (1991).

[86] Holger Cartarius, Jörg Main, and Günter Wunner. Exceptional Points in Atomic Spectra. *Physical Review Letters* 99, 173003 (2007).

[87] Thomas N. Rescigno and Vincent McKoy. Rigorous method for computing photoabsorption cross sections from a basis-set expansion. *Physical Review A (Atomic, Molecular, and Optical Physics)* 12, 522–525 (1975).

[88] Jörg Main. Use of harmonic inversion techniques in semiclassical quantization and analysis of quantum spectra. *Physics Reports* 316, 233–338 (1999).

[89] Dž. Belkić, P. A. Dando, J. Main, and H. S. Taylor. Three novel high-resolution nonlinear methods for fast signal processing. *The Journal of Chemical Physics* 113, 6542–6556 (2000).

[90] W. D. Heiss. Chirality of wavefunctions for three coalescing levels. *Journal of Physics A: Mathematical and Theoretical* 41, 244010 (2008).

[91] James C. Keck. Variational theory of reaction rates. *Advances in Chemical Physics* 13, 85–121 (1967).

[92] H. Eyring and M. Polanyi. Über einfache Gasreaktionen. *Zeitschrift für Physikalische Chemie B* 12, 279 (1931).

[93] M. G. Evans and M. Polanyi. Some applications of the transition state method to the calculation of reaction velocities, especially in solution. *Transactions of the Faraday Society* 31, 875 (1935).

[94] Holger Cartarius, Tomaž Fabčič, Jörg Main, and Günter Wunner. Dynamics and stability of Bose-Einstein condensates with attractive 1/r interaction. *Physical Review A (Atomic, Molecular, and Optical Physics)* 78, 013615 (2008).

[95] Holger Cartarius, Jörg Main, and Günter Wunner. Discovery of exceptional points in the Bose-Einstein condensation of gases with attractive 1/r interaction. *Physical Review A (Atomic, Molecular, and Optical Physics)* 77, 013618 (2008).

[96] W. D. Heiss. Exceptional points of non-Hermitian operators. *Journal of Physics A: Mathematical and General* 37, 2455–2464 (2004).

[97] H. L. Harney and W. D. Heiss. Time reversal and exceptional points. *The European Physical Journal D – Atomic, Molecular, Optical and Plasma Physics* 29, 429–432 (2004).

[98] W. D. Heiss. Time reversal symmetry breaking and exceptional points. *Journal of Physics A: Mathematical and General* 39, 10077–10080 (2006).

[99] M. V. Berry. Proximity of degeneracies and chiral points. *Journal of Physics A: Mathematical and General* 39, 10013–10018 (2006).

[100] F. Keck, H. J. Korsch, and S. Mossmann. Unfolding a diabolic point: a generalized crossing scenario. *Journal of Physics A: Mathematical and General* 36, 2125–2137 (2003).

[101] Peter Schlagheck and Tobias Paul. Complex-scaling approach to the decay of Bose-Einstein condensates. *Physical Review A (Atomic, Molecular, and Optical Physics)* 73, 023619 (2006).

[102] George E. Cragg and Arthur K. Kerman. Complex Chemical Potential: Signature of Decay in a Bose-Einstein Condensate. *Physical Review Letters* 94, 190402 (2005).

[103] N. R. Claussen, E. A. Donley, S. T. Thompson, and C. E. Wieman. Microscopic Dynamics in a Strongly Interacting Bose-Einstein Condensate. *Physical Review Letters* 89, 010401 (2002).

[104] Tomaž Fabčič. *Wave packet dynamics in atomic systems and Bose-Einstein condensates*. Dissertation, Universität Stuttgart (2008).

[105] Patrick Köberle, Holger Cartarius, Tomaž Fabčič, Jörg Main, and Günter Wunner. Bifurcations, order, and chaos in the Bose-Einstein condensation of dipolar gases (2008). Preprint arXiv:0802.4055.

[106] Patrick Wagner. *Bose-Einstein condensates with electromagnetically induced* $1/r$*-interaction*. Diplomarbeit, Universität Stuttgart (2007).

[107] D. R. Hartree. The Wave Mechanics of an Atom with a Non-Coulomb Central Field. Part I. Theory and Methods. *Proceedings of the Cambridge Philosophical Society* 24, 89–132 (1928).

[108] H. Shull and G. G. Hall. Atomic Units. *Nature* 184, 1559–1560 (1959).

[109] Peter J. Mohr, Barry N. Taylor, and David B. Newell. CODATA recommended values of the fundamental physical constants: 2006. *Reviews of Modern Physics* 80, 633 (2008).

Zusammenfassung in deutscher Sprache

Eine bekannte Eigenschaft von Quantensystemen ist, dass bei Energien über der Ionisationsschwelle Resonanzen innerhalb des Kontinuums ungebundener Zustände existieren. Resonanzen sind langlebige, quasi-gebundene Zustände, zu deren Beschreibung üblicherweise ihre Form, ihre Energie (oder Position) und ihre Breite herangezogen werden. Wie bei den gebundenen Zuständen eines Quantensystems gibt es auch bei Resonanzen den Effekt, dass Entartungen auftreten können, wobei diese für Resonanzen bedeuten, dass sowohl die Energien als auch die Breiten zweier Zustände identisch sind. Eine spezielle Form von Entartungen bei Resonanzen, sogenannte „Ausnahmepunkte“ oder „exceptional points“ [1, 2] haben großes theoretisches [3–7] und experimentelles [8–13] Forschungsinteresse auf sich gezogen. Eng verknüpft mit einem Ausnahmepunkt ist das Auftreten einer sogenannten geometrischen Phase [17], die das Ergebnis einer nichttrivialen topologischen Struktur des Parameterraums ist.

Trotz einer hohen Zahl physikalischer Systeme, in denen Ausnahmepunkte gefunden und untersucht wurden [5–13, 18–25], ist es bisher noch nicht gelungen, sie in Atomen in statischen äußeren Feldern nachzuweisen, was hauptsächlich daran liegt, dass Atome in *einem* äußeren magnetischen *oder* elektrischen Feld am ausführlichsten untersucht wurden, für das Aufspüren von Ausnahmepunkten jedoch zwei Parameter zur Verfügung stehen müssen. Diese liegen bei Atomen in gekreuzten elektrischen *und* magnetischen Feldern vor. Als fundamentale Quantensysteme, die sowohl theoretisch in numerischen Rechnungen als auch experimentell zugänglich sind, eignen sie sich ideal zur Untersuchung des Einflusses von Ausnahmepunkten auf Quantensysteme. In dieser Dissertation werden die Resonanzen des Wasserstoffatoms in gekreuzten Feldern unter Zuhilfenahme der Methode der komplexen Rotation [14–16] numerisch berechnet und der erste Nachweis von Ausnahmepunkten in den Spektren eines Atoms in statischen äußeren Feldern erbracht. Auf die dazu erforderlichen numerischen Methoden zur Diagonalisierung komplex-symmetrischer Matrizen wird eingegangen und die Möglichkeit, effektive Algorithmen für reell-symmetrische Eigenwertprobleme anzupassen, wird ausgelotet.

Bisher lag der Blickpunkt bei der Untersuchung von Ausnahmepunkten hauptsächlich auf offenen, linearen Quantensystemen, die durch einen nicht-hermiteschen Hamiltonoperator beschrieben werden. Darüber hinaus kann das Konzept aber auch auf nichtlineare Quantensysteme erweitert werden, zu denen insbesondere die Gross-Pitaevskii-Gleichung [38, 39] zur Beschreibung von Bose-Einstein-Kondensaten gehört. Von dieser ist bekannt, dass stationäre Lösungen nur für bestimmte Bereiche der Parameter, die das

System bestimmen, existieren. Insbesondere gibt es Punkte im Parameterraum, an denen die Wellenfunktion, die das Bose-Einstein-Kondensat beschreibt, kollabiert [40–45]. Es wurde bereits gezeigt, dass diese Kollapspunkte in Wirklichkeit Bifurkationspunkte darstellen, an denen zwei Lösungen der Gross-Pitaevskii-Gleichung in einer Tangentenbifurkation geboren werden [47, 48]. In dieser Dissertation wird nun gezeigt, dass an diesen Bifurkationspunkten Verzweigungssingularitäten der Energieeigenwerte und der Wellenfunktionen beider Lösungen auftreten. Es handelt sich somit um eine „nichtlineare Ausgabe von Ausnahmepunkten," die hier erstmals vorgestellt und ausführlich untersucht wird.

Ausnahmepunkte Ausnahmepunkte können in Systemen gefunden werden, die mindestens von zwei Parametern abhängen. Sie beschreiben Punkte im Parameterraum, an denen (normalerweise) zwei (Energie)-Eigenwerte als Funktionen der Parameter eine Verzweigungssingularität durchlaufen. Die Eigenwerte lassen sich mathematisch als zwei Zweige der selben analytischen Funktion in den Parametern auffassen und der Ausnahmepunkt ist der Verzweigungspunkt. Der einfachste Vertreter einer analytischen Funktion mit einer Verzweigungssingularität ist die Quadratwurzel $f(z) = \sqrt{z}$, die auch den typischen Fall eines Ausnahmepunkts darstellt und mit ihren riemannschen Flächen in Abschnitt 2.1 vorgestellt wird. Ausnahmepunkte, die in physikalischen Systemen diskutiert werden, sind üblicherweise Lösungen der charakteristischen Gleichung (2.1) auf Seite 22, bei denen zwei Eigenwerte von den beiden Zweigen einer Quadratwurzelfunktion abhängen. Ihre Werte sind mit Ausnahme des einzigen Verzweigungspunkts $z = 0$ unterschiedlich. Von dieser Ausnahme leitet sich der Begriff „Ausnahmepunkt" oder „exceptional point" ab. In diesem Beispiel kann z als komplexer Parameter aufgefasst werden.

Drei wichtigen Eigenschaften der Ausnahmepunkte können verwendet werden, um sie in Quantenspektren zu identifizieren. Umrundet man einen Ausnahmepunkt im Parameterraum, kommt es zu einer Permutation der an der Verzweigung beteiligten Eigenwerte, wie sie in Gleichung (2.2) auf Seite 23 angegeben ist. Der typische Fall der Entartung zweier Eigenwerte in einer Quadratwurzelverzweigung hat das Vertauschen der beiden Eigenwerte zur Folge. Eine graphische Darstellung dieses Effekts ist für ein einfaches Modellsystem in Abbildung 2.4 auf Seite 25 gegeben. Während der Parameter κ einen vollständigen Kreis mit kleinem Radius durchläuft, vertauschen beide Eigenwerte λ nachdem sie einen Halbkreis zurückgelegt haben. Die zweite wichtige Eigenschaft ist das Zusammenfallen der Eigenvektoren am Ausnahmepunkt. Dort gibt es zu den beiden entarteten Eigenwerten nur einen linear unabhängigen Vektor [1]. Auch die dritte Eigenschaft ist mit den Eigenvektoren verknüpft. Diese Vertauschen wie die Eigenwerte bei einer Umrundung des Ausnahmepunkts im Parameterraum. Zusätzlich tritt eine geometrische Phase auf. Bei den Eigenvektoren symmetrischer Matrizen führt dies zu einem Vorzeichenwechsel eines der Vektoren. Das Ergebnis lässt sich in der Form $[\boldsymbol{x}_1, \boldsymbol{x}_2] \overset{\text{Umrundung}}{\rightarrow} [\boldsymbol{x}_2, -\boldsymbol{x}_1]$ darstellen [2]. Bei nicht-symmetrischen Matrizen ist die geo-

metrische Phase von der Wahl des Pfades [70] und dem Einfluss weiterer Eigenvektoren, die nicht an der Verzweigungssingularität beteiligt sind, abhängig [69], wie in Abschnitt 2.4 beschrieben wird.

Üblicherweise erfolgt die geometrische Phase über die Integration entsprechend Gleichung (2.18) entlang des gesamtem im Parameterraum zurückgelegten Weges. Können die Eigenzustände eines quantenmechanischen Systems jedoch auf die Eigenvektoren symmetrischer Matrizen zurückgeführt werden, lässt sich die geometrische Phase eines Ausnahmepunkts direkt bestimmen. Durch die Normierung $\langle\psi_m^*|\psi_n\rangle$ wird ihre Phase in einer eindeutigen Weise fixiert. Achtet man nun beim Umrunden des Ausnahmepunkts auf eine stetige Fortsetzung der Phase kann man ihre Änderung direkt ablesen.

Komplexe Rotation Aus der Tatsache, dass am Ausnahmepunkt zwei Eigenzustände des Hamiltonoperators identisch sind, kann man sofort erkennen, dass im Rahmen der linearen Schrödingergleichung die Existenz von Resonanzen notwendig für das Auftreten von Ausnahmepunkten ist, denn das Zusammenfallen zweier Eigenvektoren ist in den Spektren hermitescher Hamiltonoperatoren, die gebundene Zustände beschreiben, unmöglich. Bei diesen existiert immer ein Satz orthogonaler Eigenvektoren, die nie identisch werden können. Bei Resonanzen ist das nicht der Fall, denn sie gehören nicht zum hermiteschen Definitionsbereich der Hamiltonoperatoren [14] und müssen auf eine andere Weise beschrieben werden. Eine Möglichkeit der Beschreibung von Resonanzen stellt die Methode der komplexen Rotation [14–16] dar, die durch die komplexe Skalierung der Koordinaten *nicht*-hermitesche Hamiltonoperatoren konstruiert, in deren Spektrum die Resonanzen aufgedeckt werden. Resonanzen erscheinen als komplexe Energieeigenwerte $\tilde{E} = E - \mathrm{i}\Gamma/2$, deren Real- und Imaginärteile die Energie E und die Breite Γ repräsentieren. Bei nicht-hermiteschen Operatoren entfällt die Bedingung, die identische Eigenvektoren verbietet.

Prinzipiell führt die Methode die komplexe Skalierung $\boldsymbol{r} \to \mathrm{e}^{\mathrm{i}\theta}\boldsymbol{r}$ der Koordinaten im Hamiltonoperator und in den Wellenfunktionen aus. Als Folge wird das Energiespektrum beeinflusst, wie in Abschnitt 3.2 dargestellt wird. Es lassen sich dabei unterschiedliche Einflüsse auf gebundene Zustände, das Kontinuum und Resonanzen unterscheiden. Die Energien der gebundenen Zustände bleiben nach Durchführung der komplexen Rotation unverändert. Energiewerte, die das Kontinuum repräsentieren, werden so in die untere Hälfte der komplexen Ebene gedreht, dass sie mit der reellen Achsen einen Winkel von 2θ einschließen. Der bedeutendste Einfluss ergibt sich für die Resonanzen. Diese werden durch die komplexe Rotation im Energiespektrum aufgedeckt und erscheinen als neue diskrete, komplexe Energieeigenwerte $\tilde{E} = E - \mathrm{i}\Gamma/2$. Im Gegensatz zu den Kontinuumszuständen hängen sie nicht vom Rotationswinkel ab. Die komplex skalierten Wellenfunktionen der Resonanzen sind quadratintegrabel und werden somit Bestandteil des Hilbertraums. Dadurch wird es möglich, ihren Energieerwartungswert zu berechnen.

Bei der Berechnung von Skalarprodukten muss die komplexe Rotation besonders berücksichtigt werden, wie in Abschnitt 3.3 dargestellt ist. Der komplexe Faktor $\mathrm{e}^{\mathrm{i}\theta}$ ist

kein intrinsischer Anteil der Wellenfunktionen. Damit sich die Bedeutung der Energieerwartungswerte nicht verändert, darf keine komplexe Konjugation der komplexen Anteile einer Wellenfunktion, die durch die Skalierung $e^{i\theta}\boldsymbol{r}$ eingehen, erfolgen. In Skalarprodukten darf also nur eine komplexe Konjugation der intrinsisch komplexen Anteile einer Wellenfunktion durchgeführt werden [14].

Für die numerische Berechnung der komplexen Eigenwerte ist es häufig vorteilhaft, einen direkten Zugang zu verwenden, der in Abschnitt 3.4 beschrieben wird. Hier wird der Matrixaufbau des hermiteschen Hamiltonoperators verwendet. Die einzelnen Terme werden nach den auftretenden Potenzen sortiert und jeder einzelne Term wird mit der zugehörigen Potenz des Skalierungsfaktors $e^{i\theta}$ multipliziert, wie es in Gleichung (3.17) auf Seite 42 dargestellt ist. In der Gleichung läuft die Summe über alle auftretenden Potenzen n der Ortskoordinate $\boldsymbol{r}$ im Potential. Das daraus entstehende Eigenwertproblem (3.18) für die komplexen Energien $\tilde{E}_i$ benötigt nun keine komplex skalierten Wellenfunktionen und es müssen keine neuen Matrizen aufgebaut werden. Die Darstellung der skalierten Wellenfunktionen wird von den komplexen Vektoren $\bar{\boldsymbol{c}}_i$, die sich als Eigenvektoren ergeben, übernommen.

Die Abschnitte 3.5 und 3.6 befassen sich mit der Streumatrix, in der Resonanzen als Pole auftreten. In diesem Bild stellt ein Ausnahmepunkt einen doppelten Pol dar, da hier zwei Resonanzen und damit zwei Pole zusammenfallen.

Numerische Diagonalisierung von Matrizen Bei der numerischen Berechnung der Eigenenergien von Quantensystemen hat sich die Diagonalisierung einer Matrixdarstellung eines Hamiltonoperators als eine mögliche Methode etabliert, mit der sich das Kapitel 4 beschäftigt. Die effizientesten Algorithmen wurden dabei für die am häufigsten auftretenden Fälle, nämlich reell-symmetrische oder hermitesche Matrizen, entwickelt. Für komplex-symmetrische Eigenwertprobleme, wie sie z.B. durch das Anwenden der Methode der komplexen Rotation auftreten, muss häufig auf weniger effiziente Algorithmen für allgemeine komplexe Matrizen zurückgegriffen werden. Oft ist es wesentlich besser, Verfahren für den reell-symmetrischen Fall auf komplex-symmetrische zu übertragen, indem einfach komplexe Variablen in die Programme eingeführt werden und die lineare Algebra für reelle Matrizen beibehalten wird. Insbesondere wird die reell-euklidische Norm $||\boldsymbol{x}||_\mathrm{r} = \boldsymbol{x}^T\boldsymbol{x}$ ohne komplexe Konjugation beibehalten. In den meisten Fällen funktioniert dieses Verfahren sehr gut und hat zu exzellenten Ergebnissen geführt [30, 31]. Die Algorithmen erwarten jedoch meist, dass alle Eigenvektoren paarweise orthogonal zueinander stehen und mit der reell-euklidischen Norm normiert werden können. Beide Bedingungen sind jedoch bei komplex-symmetrischen Matrizen nicht garantiert. Insbesondere an Ausnahmepunkten haben die entarteten Eigenwerte nur einen linear unabhängigen Eigenvektor. Aber auch andere Schwierigkeiten, die nicht mit dem Auftreten eines Ausnahmepunkts zusammenhängen, sind möglich. Beide Effekte werden in Kapitel 4 sowohl an direkten Methoden wie der Jacobi-Transformation (Abschnitt 4.1.1), der Tridiagonalisierung mit der Householder-Transformation (Abschnitt 4.1.2) und anschließender

Bestimmung der Eigenwerte durch den QL-Algorithmus (Abschnitt 4.1.3) als auch an iterativen Methoden wie dem Lanczos- (Abschnitt 4.2.1) und dem Arnoldi-Verfahren (Abschnitt 4.2.2) untersucht.

Die Versuche, eine Diagonalgestalt durch Ähnlichkeitstransformationen zu erreichen, muss beim Auftreten eines Ausnahmepunkts zwangsweise scheitern, da dieser einen Normalblock in der Matrix bildet. Es zeigt sich jedoch, dass numerisch meist eine Bestimmung der Eigenwerte gelingt, da ein Normalblock in numerischer Darstellung nicht exakt vorliegt. Die Reduktion einer Matrix auf Tridiagonalgestalt stellt für den typischen Fall eines Ausnahmepunkts, der Quadratwurzelverzweigung von *zwei* Eigenwerten, kein Problem dar. Der zugehörige 2×2-Normalblock lässt sich in die Tridiagonalgestalt einbinden. Ein Scheitern der Algorithmen ist unabhängig vom Auftreten der Ausnahmepunkte aber auch möglich, da die Konvergenzbedingungen nur für reell-symmetrische Matrizen erfüllt sind oder zufällig auftretende verschwindende reell-euklidische Normen $||\boldsymbol{x}||_\mathrm{r}$ benötigter Vektoren zu divergierenden Termen führen.

Als geeignetste Methode für die Berechnung der Resonanzen des Wasserstoffatoms in dieser Arbeit hat sich die „implicitly restarted Arnoldi method“, die in der ARPACK-Bibliothek implementiert ist, erwiesen. Hier ist insbesondere die Stabilität des Verfahrens, das allgemeine komplexe Eigenwertprobleme lösen kann, beim Auftreten von Ausnahmepunkten von Bedeutung. Werden größere Matrizen benötigt, ist die „spectral transformation Lanczos method“ eine vielversprechende Alternative. Das auf komplexe Zahlen erweiterte Programm für reell-symmetrische Matrizen liefert meist gute Ergebnisse. Führt man die Berechnung der Eigenwerte der durch die Lanczos-Iteration entstandenen tridiagonalen Matrix mit einem Verfahren für allgemeine komplexe Matrizen durch, stellen Ausnahmepunkte prinzipiell keine Schwierigkeit dar. Nachträgliche Tests auf numerische Ungenauigkeiten sind jedoch zwingend notwendig, da bei den komplexen Matrizen immer sehr kleine Normen $||\boldsymbol{x}||_\mathrm{r}$, durch die dividiert wird, auftreten können.

Ausnahmepunkte in Spektren des Wasserstoffatoms in gekreuzten Feldern Als atomares System wird in Kapitel 5 der vorliegenden Arbeit das Wasserstoffatom in gekreuzten, statischen elektrischen und magnetischen Feldern untersucht, dessen Hamiltonoperator in atomaren Einheiten in Gleichung (5.3) auf Seite 62 angegeben ist. Seine Basisdarstellung in dilatierten semiparabolischen Koordinaten und das Einführen der komplexen Rotation sind in Abschnitt 5.1 angegeben.

Als erfolgreiche Suchmethode nach Ausnahmepunkten unter den Resonanzen hat sich erwiesen, entsprechend den Gleichungen (5.12a) und (5.12b) auf Seite 64 Kreise im zweidimensionalen Parameterraum, der von den Feldstärken der beiden äußeren Felder aufgespannt wird, zu ziehen. Tritt dabei das charakteristische Vertauschen zweier Eigenwerte auf und kann dies eindeutig identifiziert werden, hat man ganz sicher einen Ausnahmepunkt gefunden. Ein Beispiel für ein typisches Ergebnis ist in Abbildung 5.4(a) auf Seite 68 dargestellt. Während im Feldstärkeraum ein geschlossener Kreis durchlaufen wird, vertauschen die beiden Resonanzen, die durch rote Quadrate und grüne Rauten

dargestellt sind. Abbildung 5.4(b) zeigt die entarteten Eigenwerte am Ausnahmepunkt (markiert durch einen Pfeil) in der komplexen Energieebene neben weiteren Resonanzen. Weitere Beispiele für Ausnahmepunkte, die auf diese Weise gefunden wurden, sind in Tabelle 5.2 aufgelistet.

Darüber hinaus wird in Abschnitt 5.4 ein Vorschlag für ein Experiment präsentiert, das die Beobachtung von Ausnahmepunkten in gemessenen Photoionisationswirkungsquerschnitten ermöglicht. Dazu müssen die Wirkungsquerschnitte für verschiedene Parameterwerte, die auf einer geschlossenen Linie im Parameterraum liegen, gemessen werden. Aus diesen Daten können unter Verwendung der harmonischen Inversion [88, 89] die komplexen Energien der Resonanzen mit einer hohen Präzision extrahiert werden. Anschließend können die Energien in der komplexen Energieebene aufgetragen werden. Das Verfolgen der Wege der Resonanzen ermöglicht wie im numerischen Fall die Suche nach den charakteristischen Vertauschungen.

Kapitel 6 ist der Beschreibung der Ausnahmepunkte, die in Spektren des Wasserstoffatoms auftreten, gewidmet. Viele Effekte treten in einer lokalen Umgebung der Ausnahmepunkte auf, in der nur die beiden beteiligten Resonanzen von Bedeutung sind und alle weiteren komplexen Energieeigenwerte ignoriert werden können. Dort lässt sich das System lokal durch ein 2×2-Matrixmodell beschreiben. Oft ist es aber nicht ausreichend, das in Abschnitt 2.3 eingeführte Modell mit einem komplexen Parameter zu verwenden, da der tatsächliche Einfluss zweier reeller Parameter (Feldstärken) mit komplexen Vorfaktoren entscheidend ist. Eine bessere Beschreibung ist daher durch das Modell aus Gleichung (6.1) auf Seite 73 gegeben, das genau diese Abhängigkeit berücksichtigt.

In einer sehr lokalen Umgebung um einen Ausnahmepunkt bestätigt sich, dass die Energieeigenwerte in einer Quadratwurzelfunktion vom Abstand δ (vergleiche Gleichungen (5.12a) und (5.12b) auf Seite 64) im Parameterraum abhängen. Graphisch ist dies in Abbildung 6.1 auf Seite 75 dargestellt, wobei die blaue Linie die Anpassung einer Quadratwurzelfunktion an die numerischen Daten repräsentiert.

Wie bereits in Kapitel 5 zu sehen war, zeigt auch Abbildung 6.2 auf Seite 76, dass die Pfade der Eigenwerte in der komplexen Energieebene recht kompliziert sein können und sich auch bei sehr kleinen Radien $\delta = 10^{-4}$ (Abbildung 6.2(c)) nicht auf eine perfekte Halbkreisstruktur, wie sie vom einfachen Modellsystem aus Abschnitt 2.3 bekannt ist, zusammenziehen. Diese Effekte lassen sich jedoch durch die Abhängigkeit des Hamiltonoperators von den Feldstärken erklären und durch das Matrixmodell (6.1) wiedergeben. Die in Abbildung 6.2 eingezeichneten Linien sind die Eigenwerte des Modells (6.1), dessen Koeffizienten an einen Teil der numerischen Eigenwerte angepasst wurden.

Von besonderer Bedeutung ist das Auftreten von Strukturen, an denen drei Resonanzen beteiligt sind, wie dies in Abbildung 6.4(a) auf Seite 79 dargestellt ist, in der eine Permutation aller drei Resonanzen auftritt. Ein solches Verhalten deutet auf das Auftreten einer Verzweigungssingularität einer kubischen Wurzel hin, an der drei riemannsche Flächen zusammentreffen. Eine genauere Betrachtung deckt jedoch auf, dass dieser Fall hier nicht exakt erfüllt ist. Es handelt sich um zwei im Parameterraum sehr dicht liegende Ausnahmepunkte. Eine der Resonanzen (in der Abbildung durch Fünfecke

dargestellt) durchläuft an beiden eine Verzweigung mit jeweils einer anderen Resonanz. Die Abbildungen 6.3(b) und 6.3(c) zeigen die gleichen drei Resonanzen für zwei weitere geschlossene Kreise im Parameterraum, die so angelegt sind, dass sie jeweils nur einen der beiden Ausnahmepunkte umrunden, was die Existenz der zwei Ausnahmepunkte belegt. Dreifache Entartungen in der Form einer kubischen Wurzel können im vorliegenden System nicht gezielt gesucht werden, da dafür fünf Parameter zur Verfügung stehen müssen [90], also drei Parameter fehlen. Um so bemerkenswerter ist die Tatsache, dass eine so eng mit diesem Fall verwandte Struktur hier gefunden wurde.

Als weitere Eigenschaft der Ausnahmepunkte lässt sich die geometrische Phase für die numerische berechneten Eigenvektoren der Matrixdarstellung des Hamiltonoperators nachweisen. Dafür wird in Abschnitt 6.3 das Produkt zweier Wellenfunktionen $p_{12} = \langle \Psi_1 | \, \Psi_2 \rangle$ berechnet, das durch die Wahl der Matrixdarstellung abseits der Ausnahmepunkte nicht verschwindet. Wechselt *einer* der beiden Eigenvektoren während der Umkreisung des Ausnahmepunkts sein Vorzeichen, wie es zu erwarten ist, muss dies auch für die komplexe Zahl p_{12} gelten. Genau dieser Fall lässt sich auch beobachten wie Abbildung 6.5 auf Seite 81 zeigt. Die Phase von p_{12} ändert sich genau um den Wert π.

Die Verbindung von Ausnahmepunkten mit vermiedenen Kreuzungen, die bereits von gebundenen Zuständen bekannt ist [2, 4], lässt sich auch bei Resonanzen finden [9]. Hier können vermiedene Kreuzungen der Realteile (Energien) oder Imaginärteile (Breiten) auftreten, während der jeweils andere Teil der komplexen Energie eine Kreuzung aufweist. Dieses Verhalten lässt sich auch in den Spektren des Wasserstoffatoms finden. Abbildung 6.7 auf Seite 83 zeigt Resonanzen des Wasserstoffatoms in gekreuzten Feldern für eine Gerade im Feldstärkeraum, die durch α repräsentiert wird. Es sind deutlich vermiedene Kreuzungen zu erkennen (markiert durch die blauen Quadrate). Die daran beteiligten Resonanzen lassen sich alle durch Variation beider Feldstärken so zur Entartung bringen, dass sie einen Ausnahmepunkt bilden. Dies ist immer dann, wenn nur zwei Resonanzen im lokalen Energiebereich relevant sind und ein zweidimensionales Matrixmodell angesetzt werden kann, auch der Normalfall.

Weiterhin werden in Abschnitt 6.5 das Verhalten der Dipolmatrixelemente und des Photoionisationswirkungsquerschnitts, die für die experimentelle Beobachtung von Bedeutung sind, am Ausnahmepunkt beschrieben. Es zeigt sich, dass einzelne Dipolmatrixelemente für *einen* der beiden entarteten Zustände bei Annäherung an den Ausnahmepunkt in der Form einer reziproken Quadratwurzel $1/\sqrt{\delta}$ divergieren. Dies führt jedoch zu keinem beobachtbaren Effekt, da am Ausnahmepunkte auch beide Wellenfunktionen identisch sind und nicht unterschieden werden können. Die Summe aus beiden Dipolmatrixelementen verhält sich regulär. Insbesondere gilt dies auch für den Photoionisationswirkungsquerschnitt. Dieser konvergiert in einer kleinen Umgebung um den Ausnahmepunkt linear gegen einen endlichen Wert. Beides lässt sich mit einem einfachen Matrixmodell zeigen und wird durch die numerischen Rechnungen am Wasserstoffatom bestätigt.

Einfluss des klassischen Übergangszustands auf die Resonanzen des Wasserstoffatoms Die betrachteten Resonanzen in den Spektren des Wasserstoffatoms bieten über die Existenz von Ausnahmepunkten hinaus noch einen Einblick in eine weitere Eigenschaft des Ionisationsmechanismus. Dieser wurde für das Wasserstoffatom in gekreuzten elektrischen und magnetischen Feldern bereits unter Anwendung der „Theorie der Übergangszustände“ (oder „transition state theory“) untersucht [33–36], allerdings blieb dabei der Einfluss des klassischen Übergangszustands auf das Quantenspektrum unklar.

Die klassische Theorie der Übergangszustände ist ein fundamentaler Zugang zur Beschreibung von Veränderungen in dynamischen Systemen, der immer dann zum Einsatz kommen kann, wenn eine Entwicklung von einem Ausgangszustand auf einen Endzustand stattfindet. Die Theorie gründet auf der Aufteilung des klassischen Phasenraums in Bereiche, die genau diese Anfangs- und Endzustände beschreiben. Da der Übergangszustand seine ursprüngliche Anwendung in der Beschreibung chemischer Reaktionen hatte, spricht man bei der Entwicklung von einem reaktiven Prozess. Der Übergangszustand beschreibt eine Grenze zwischen Anfangs- und Endzustand, die von allen reaktiven Phasenraumbahnen überschritten wird, nicht aber von den nicht-reaktiven Trajektorien. Beim Wasserstoffatom in gekreuzten Feldern muss der Übergangszustand in der Nähe des Stark-Sattelpunktes (siehe Abbildung 7.1 auf Seite 92) liegen, der von ionisierenden klassischen Elektronenbahnen überschritten werden muss. Eine Methode, ihn bis zu einer beliebigen Ordnung in einer Normalformentwicklung zu identifizieren, ist bekannt [36]. Die niedrigste Ordnung in dieser Entwicklung ist eine quadratische Näherung des Potentials in der Nähe des Sattelpunktes [37]. Die zugehörigen Zustände werden wegen einer formalen Analogie mit dem Potential der Penning-Falle Quasi-Penning-Resonanzen genannt.

Berechnet man die quantisierten Energien der genäherten klassischen Hamiltonfunktion, so erhält man Resonanzzustände deren Realteil der Energie in Gleichung (7.8) auf Seite 94 angegeben ist. Diese können mit den numerisch exakten Ergebnissen verglichen werden. Dabei zeigen sich für Geraden im Parameterraum der beiden Feldstärken sehr gute Übereinstimmungen, die nicht zufällig sein können, da sie für einen großen Bereich im Parameterraum gelten und unabhängig von der Wahl der Linien sind. Beispiele sind in den Abbildungen 7.2, 7.3 und 7.4 beginnend auf Seite 96 gegeben. Die blauen Linien beschreiben die quantisierten Energien aus der Elektronenbewegung in der Umgebung des Übergangszustands und die roten Punkte repräsentieren die exakt numerischen Ergebnisse, die eindeutig von den niedrigsten Quasi-Penning-Resonanzen begleitet werden. Abweichungen gibt es nur bei kleinen elektrischen Feldstärken (linker Rand in Abbildung 7.2) und in der Umgebung vermiedener Kreuzungen, die das einfache Modell nicht erfasst. Dies weist eindeutig auf einen hohen Einfluss des klassischen Übergangszustands und der Elektronenbewegung in seiner Nähe auf den Ionisationsprozess hin. Die gute Übereinstimmung wurde bereits für die quadratische Näherung des Potentials gefunden.

Nichtlineare Ausnahmepunkte bei Bose-Einstein-Kondensaten Ausnahmepunkte existieren auch in nichtlinearen Quantensystemen. Insbesondere die Gross-Pitaevskii-Gleichung [38, 39], die bei ausreichend niedrigen Temperaturen die Wellenfunktion eines Bose-Einstein-Kondensats beschreibt, weist diese Eigenschaft auf. Als besonders geeignetes System bieten sich für die Untersuchung Bose-Einstein-Kondensate mit einer laserinduzierten, attraktiven $1/r$-Wechselwirkung an [49–51, 94, 95]. Dieses System weist die herausragende Eigenschaft auf, dass das Kondensat ohne die sonst notwendige äußere Falle stabil existieren kann. Ohne den Term eines äußeren Potentials in der Gross-Pitaevskii-Gleichung lassen sich mit einem Variationsansatz analytische Näherungslösungen finden, die das Auftreten eines Ausnahmepunkts direkt analytisch nachweisen. Weiterhin geht ohne die Falle nur noch ein äußerer Parameter ein, nämlich die s-Wellen-Streulänge, die sich in der Nähe von Feshbach-Resonanzen durch ein äußeres Magnetfeld einstellen lässt. Die zugehörige Gross-Pitaevskii-Gleichung weist zwei stationäre Lösungen auf, die bei Variation des einzigen Systemparameters gemeinsam in einer Tangentenbifurkation geboren werden. Eine Lösung ist der Grundzustand, die andere beschreibt einen knotenlosen angeregten Zustand. Abbildung 8.1 auf Seite 103 zeigt den Energieeigenwert, das chemische Potential ε, für beide Zustände sowohl für den Variationsansatz als auch für eine exakt numerische Lösung der Gross-Pitaevskii-Gleichung. Die Tangentenbifurkation ist deutlich zu erkennen.

Die beiden Lösungen für das chemische Potential aus dem Variationsansatz sind in Gleichung (8.9) auf Seite 102 angegeben. Daraus lässt sich sofort erkennen, dass es zwei Zweige der gleichen analytischen Funktion sind und somit der Bifurkationspunkt einen Ausnahmepunkt bildet. Das Verhalten gilt auch für die Gesamtenergie und die Wellenfunktionen. Mit den exakt numerischen Lösungen kann bestätigt werden, dass das Auftreten eines Ausnahmepunkts keine Eigenschaft des Variationsansatzes ist. Mangels analytischer exakter Lösungen muss hierfür wieder auf die Eigenschaften der Ausnahmepunkte zurückgegriffen werden. Dies ist möglich, indem man den Bifurkationspunkt in einer *komplexen* Umgebung umrundet. Da mit der s-Wellen-Streulänge nur ein reeller Parameter zur Verfügung steht, bietet es sich an diesen analytisch zu erweitern. Das Ergebnis führt auf komplexe Energien und Wellenfunktionen, in denen sich das charakteristische Permutationsverhalten finden lässt. Abbildung 8.4 auf Seite 110 zeigt die komplex erweiterte Streulänge a, das chemische Potential ε und die Gesamtenergie E sowohl im numerisch exakten (num) als auch im Fall der Variationslösung (var).

Für das Phasenverhalten der Wellenfunktionen wird in Abschnitt 8.3.2 gezeigt, dass es mit dem der Eigenvektoren einer nicht-symmetrischen Matrix verglichen werden kann. Bei einer nicht-symmetrischen Matrix kann nicht durch das Festhalten der Phase mit der reell-euklidischen Norm die geometrische Phase an einem Ausnahmepunkt reproduziert werden. Führt man die reell-euklidische Normierung durch, die eine konsistente Analogie zur notwendigen Normierung der komplex erweiterten Wellenfunktionen ist, tritt kein Vorzeichenwechsel auf. Genau dieses Verhalten wird für die Wellenfunktionen gefunden. Die komplexen Wellenfunktionen, die hier betrachtet werden, führen, da sie in das Potential der nichtlinearen Gross-Pitaevskii-Gleichung eingehen (vergleiche Gleichung (8.34)

auf Seite 113), auf ein komplexes Potential, dessen Imaginärteil als absorbierender Anteil interpretiert werden kann. Dies ist insbesondere interessant, da sich die komplexen Wellenfunktionen nicht nur für die komplex erweiterte Streulänge ergeben, sondern auch für reelle Streulängen unterhalb des Bifurkationspunktes auftreten. Das absorbierende Potential bewirkt in der zeitlichen Entwicklung einen Kollaps der Wellenfunktion.

Für ein vollständiges Bild zu den beiden Zuständen, die aus der Tangentenbifurkation entstehen, wird in Abschnitt 8.5 deren Stabilität gegen kleine Störungen untersucht. Dies geschieht mit einer Linearisierung der zeitabhängigen Gross-Pitaevskii-Gleichung. Im numerisch exakten Fall wird die lineare Ordnung mit der Fréchet-Ableitung nach der Wellenfunktion des Kondensats gebildet. Als Ergebnis erhält man, dass der Grundzustand stabil ist. Die beiden Eigenwerte ξ, die für den Ansatz $\delta\psi(\boldsymbol{r},t) = \delta\psi_0(\boldsymbol{r})\mathrm{e}^{\xi^{(\mathrm{num})}t}$ der Abweichung aus der stationären Lösung gefunden werden, sind rein imaginär und beschreiben einen elliptischen Fixpunkt. Im Gegensatz dazu ist der knotenlose angeregte Zustand instabil. Er beschreibt einen hyperbolischen Fixpunkt mit zwei reellen Eigenwerten, von denen einer positiv ist.

Bei dipolaren Bose-Einstein-Kondensaten [52] treten im Prinzip die gleichen Effekte auf, durch die Anisotropie der Dipol-Dipol-Wechselwirkung kommen aber neue Aspekte hinzu. Durch die experimentelle Realisierung eines Bose-Einstein-Kondensats aus Chrom-Atomen [58] mit einem großen Dipolmoment ist das System von besonderem Interesse. Als zusätzliche Eigenschaft tritt hier auf, dass immer eine äußere Falle benötigt wird. Weiterhin erfordert die Anisotropie der Dipol-Dipol-Wechselwirkung, dass mindestens eine zylindersymmetrische, also zweidimensionale, Wellenfunktion angesetzt werden muss. Konsequenterweise setzt man auch eine zylindersymmetrische äußere Falle an, deren beide Fallenfrequenzen zusammen mit der s-Wellen-Streulänge einen dreidimensionalen Parameterraum bilden. Dieser muss zum Nachweis von Ausnahmepunkten wieder komplex erweitert werden, wird also vierdimensional. Da erweiterte Ausnahmepunkte immer ein Objekt der Kodimension zwei darstellen, ist zu erwarten, dass hier eine Fläche im vierdimensionalen Parameterraum vorliegt. Tatsächlich zeigt sich, dass alle Bifurkationspunkte, an denen die zwei stationären Lösungen aus einer Tangentenbifurkation heraus entstehen, auf einer solchen Fläche liegen, die in Abbildung 9.2 auf Seite 125 dargestellt ist. Da alle diese Bifurkationspunkte eine Verzweigungssingularität der Energien und Wellenfunktionen beinhalten, kann sie als „Ausnahmefläche“ bezeichnet werden. Die Möglichkeit durch eine Veränderung der Fallengeometrie zwischen einer attraktiven und einer repulsiven Wirkung der Dipol-Dipol-Kraft zu variieren, kann genutzt werden, um Unterschiede im Verhalten der Energien beim Umkreisen der Ausnahmepunkte aufzudecken, wie ein Vergleich der Abbildungen 9.3 auf Seite 126 (repulsiv) und 9.4 auf Seite 128 (attraktiv) zeigt. Es ist jedoch immer die Eigenschaft eines Ausnahmepunkts vorhanden.

Fazit In der vorliegenden Dissertation wurden Ausnahmepunkte, die sich in parameterabhängigen Quantensystemen als Verzweigungssingularitäten der Energieeigenwerte

und Wellenfunktionen äußern, untersucht. Als ein wichtiges Ergebnis kann festgehalten werden, dass die Ausnahmepunkte erstmals in den Spektren eines Atoms in äußeren Feldern nachgewiesen werden konnten, deren Eigenschaften ausführlich untersucht wurden. Darüber hinaus haben die Rechnungen für die Spektren des Wasserstoffatoms in gekreuzten elektrischen und magnetischen Feldern gezeigt, dass es eine enge Verwandtschaft der quantenmechanischen Ergebnisse mit der klassischen Theorie der Übergangszustand gibt. Ein weiteres bedeutendes Resultat ist die Möglichkeit der Erweiterung des Konzepts des Ausnahmepunkts auf nichtlineare Quantensysteme. Die Untersuchung der Gross-Pitaevskii-Gleichung für Bose-Einstein-Kondensate mit langreichweitigen Wechselwirkungen hat ergeben, dass die dort auftretenden Bifurkationspunkte, an denen bei Variation der Systemparameter zwei Lösungen aus einer Tangentenbifurkation heraus entstehen, als „nichtlineare Ausgabe“ eines Ausnahmepunkts verstanden werden können.

Die Ergebnisse der vorliegenden Arbeit zeigen, dass Ausnahmepunkte bedeutende Konsequenzen für Quantensysteme haben. Insbesondere ist es gelungen, zu zeigen, dass sie in realen physikalischen Situationen, die sowohl theoretisch als auch experimentell zugänglich sind, existieren und nachgewiesen werden können. Ihre Auswirkungen auf atomare Resonanzspektren, nämlich das Vertauschen der Eigenwerte, die Verzweigungsstruktur und die geometrische Phase sind beobachtbare Charakteristiken. In der nichtlinearen Gross-Pitaevskii-Gleichung treten sie als Bifurkationspunkte auf, an denen zwei Zustände aus einer Tangentenbifurkation heraus entstehen.

Lebenslauf

Holger Cartarius

Geboren am 27. Oktober 1978 in Böblingen.

Schulausbildung

Sept. 1985 – Juli 1989	Friedrich-Silcher-Grundschule Böblingen
Aug. 1989 – Juni 1998	Max-Planck-Gymnasium Böblingen
23. Juni 1998	Abschluss: Abitur

Zivildienst

Aug. 1998 – Aug. 1999	Deutsches Rotes Kreuz, Kreisverband Böblingen

Studium

Okt. 1999 – Dez. 2004	Diplomstudiengang Physik an der Universität Stuttgart
11. Oktober 2001	Vordiplom in Physik
Dez. 2003 – Dez. 2004	Diplomarbeit mit dem Titel „$\hbar$-Entwicklungen in semiklassischen Theorien für Systeme mit weichen Potentialen und Anwendung auf das Wasserstoffatom im Magnetfeld“ am 1. Institut für Theoretische Physik der Universität Stuttgart unter der Betreuung von Priv.-Doz. Dr. Jörg Main
10. Dezember 2004	Abschluss: Diplom-Physiker

Berufliche und wissenschaftliche Tätigkeiten, Promotion

Seit Januar 2005	Wissenschaftlicher Mitarbeiter am 1. Institut für Theoretische Physik der Universität Stuttgart
Okt. 2005 – Sept. 2007	Promotionsstipendium nach dem Landesgraduiertenförderungsgesetz des Landes Baden-Württemberg
Nov. 2005 – Juli 2008	Nebenberufliche Dozententätigkeit, Berufsakademie Stuttgart
Jan. 2005 – Dez. 2008	Promotion über das Thema „Exceptional Points in atomic spectra and Bose-Einstein condensates“ unter der Betreuung von Prof. Dr. Jörg Main

Danksagung

An dieser Stelle möchte ich mich bei allen bedanken, die zum Gelingen dieser Dissertation beigetragen haben. Mein besonderer Dank gilt

- Herrn Prof. Dr. Jörg Main für die Möglichkeit, das interessante Thema bearbeiten zu können, für die hervorragende Betreuung und für die Übernahme des Hauptberichts,
- Herrn Prof. Dr. Hans-Rainer Trebin für die Übernahme des Mitberichts und für die vorbildliche Mentorengruppe während des Diplomstudiums,
- Herrn Prof. Dr. Tilman Pfau für die Übernahme des Prüfungsvorsitzes,
- Herrn Prof. Dr. Günter Wunner für die Anstellung am 1. Institut für Theoretische Physik und für das große Interesse an der Arbeit,
- Herrn Dr. Steffen Bücheler und Herrn Dr. Dirk Engel für die perfekte Systemadministration,
- Herrn Dr. Steffen Bücheler, Herrn Dipl.-Phys. Peter Diemand, Herrn Dr. Dirk Engel, Herrn Dr. Tomaž Fabčič, Herrn Dipl.-Phys. Jan Gehrke, Herrn Dipl.-Phys. Patrick Köberle, Herrn Dipl.-Phys. Ioannis Papadopoulos und Herrn Torsten Schwidder für die gute Zusammenarbeit und für die angenehme Atmosphäre in der Arbeitsgruppe,
- allen weiteren Mitarbeitern des 1. Instituts für Theoretische Physik für das gute Arbeitsklima,
- dem Land Baden-Württemberg und der Universität Stuttgart für die Gewährung des Promotionsstipendiums nach dem Landesgraduiertenförderungsgesetz.

Ehrenwörtliche Erklärung

Ich erkläre, dass ich diese Dissertation, abgesehen von den ausdrücklich bezeichneten Hilfsmitteln und den Ratschlägen von den jeweils namentlich aufgeführten Personen, selbständig verfasst habe.

Stuttgart, den 22. September 2008 *Holger Cartarius*